Modernisation of the Philippine Height System

Author:
Sarmiento, Czar Jakiri

Publication Date:
2020

DOI:
https://doi.org/10.26190/unsworks/3944

Modernisation of the Philippine Height System

Czar Jakiri Soriano Sarmiento

A thesis submitted to the University of New South Wales
In partial fulfilment to the requirement for the degree of
Doctor of Philosophy

School of Civil and Environmental Engineering
The University of New South Wales
Sydney NSW, 2052, Australia
February 2020

Thesis/Dissertation Sheet

Surname/Family Name	:	**SARMIENTO**
Given Name/s	:	**CZAR JAKIRI**
Abbreviation for degree as given in the University calendar	:	**Ph.D.**
Faculty	:	**Engineering**
School	:	**Civil and Environmental Engineering**
Thesis Title	:	**Modernisation of the Philippine Height System**

Abstract

The Philippine Height System (PHS) modernisation is driven by recent advances in geodetic technology and the Philippines' need to be geodetically responsive to natural disasters. Aspects of the shift from a levelling-based system to a GNSS and gravimetric geoid-based system, being a cost-effective modernisation strategy for developing countries, were investigated. This thesis expands available scientific literature for the International Height Reference System/Frame (IHRS/F) development of the International Association of Geodesy (IAG), and the PHS modernisation efforts of the National Mapping and Resource Information Authority (NAMRIA). Three elements of a modern PHS were studied. 1. The engineering implications of the new Philippine Geoid Model (PGM). 2. The temporal variability of the geoid and benchmarks with focus on the effects of tropical hydrology. 3. The PHS relationship to the IHRS/F.

An evaluation of the new Technical University of Denmark (DTU-Space) and NAMRIA-developed PGM, was done to provide a quality baseline for managing the progression and limitations of a gravimetric geoid-based height system for the country. Statistical measures show that points clustered in the southern latitudes and eastern longitudes have relatively higher residuals due to geodynamic and hydrologic activity. It is concluded that a localised PGM can be used for third order applications.

Tropical effects on the reference frame and the geoid were examined. Displacements were analysed by estimating tidal and non-tidal loading for selected Philippine active geodetic stations using rain sensor data, local geologic information and ground validation. The mean dynamic topography (MDT) was also investigated. DTU10, VM500-ph and RADS-ph were compared with GNSS-geoid MDTs (GNSS-PGM2016.66, GNSS-EIGENGL05C). A nationwide scale, low-resolution Philippine vertical ground motion map inferred from Sentinel-1A scenes from January 2015 to December 2019 was also produced. Estimations confirm the intensity of land motion in the eastern and southern part of the country. Using Gravity Recovery and Climate Experiment (GRACE) temporal models, large variations for two IHRS/F-proposed Philippine stations were computed and show coincidence with high rainfall records. A causality relationship between high rainfall and geoid variation, however, is inconclusive.

Lastly, a novel way of characterising local height systems relationship for the IHRS/F that takes into account the non-homogenous states of geodetic development within a developing, archipelagic country is introduced. Recommendations for a modernised Philippine Height System were made as a result of this study.

ORIGINALITY STATEMENT

'I hereby declare that this submission is my own work and to the best of my knowledge it contains no materials previously published or written by another person, or substantial proportions of material which have been accepted for the award of any other degree or diploma at UNSW or any other educational institution, except where due acknowledgement is made in the thesis. Any contribution made to the research by others, with whom I have worked at UNSW or elsewhere, is explicitly acknowledged in the thesis. I also declare that the intellectual content of this thesis is the product of my own work, except to the extent that assistance from others in the project's design and conception or in style, presentation and linguistic expression is acknowledged.'

Signed ……………………………………………………..............

Date **15 May 2020** ……………………………………………………..............

COPYRIGHT STATEMENT

Signed ……………………………………………...........................

Date ……………………15 MAY 2020……………………...............................

AUTHENTICITY STATEMENT

'I certify that the Library deposit digital copy is a direct equivalent of the final officially approved version of my thesis.'

Signed ……………………………………………...........................

Date ……………………15 MAY 2020……………………...............................

INCLUSION OF PUBLICATIONS STATEMENT

UNSW is supportive of candidates publishing their research results during their candidature as detailed in the UNSW Thesis Examination Procedure.

Publications can be used in their thesis in lieu of a Chapter if:

- The candidate contributed greater than 50% of the content in the publication and is the “primary author”, ie. the candidate was responsible primarily for the planning, execution and preparation of the work for publication
- The candidate has approval to include the publication in their thesis in lieu of a Chapter from their supervisor and Postgraduate Coordinator.
- The publication is not subject to any obligations or contractual agreements with a third party that would constrain its inclusion in the thesis

Please indicate whether this thesis contains published material or not:

☐ This thesis contains no publications, either published or submitted for publication

☒ Some of the work described in this thesis has been published and it has been documented in the relevant Chapters with acknowledgement

☐ This thesis has publications (either published or submitted for publication) incorporated into it in lieu of a chapter and the details are presented below

CANDIDATE’S DECLARATION

I declare that:

- I have complied with the UNSW Thesis Examination Procedure
- where I have used a publication in lieu of a Chapter, the listed publication(s) below meet(s) the requirements to be included in the thesis.

Candidate’s Name	Signature	Date (dd/mm/yy)
CZAR JAKIRI SARMIENTO		15/05/2020

To God
Anna, the love of my life
my family and friends and colleagues
Dr. Chris Rizos and Dr. Craig Roberts
and our anonymous examiners.

Thank you.

For those who never lost faith.

Abstract

The Philippine Height System (PHS) modernisation is driven by recent advances in geodetic technology and the Philippines' need to be geodetically responsive to natural disasters. Aspects of the shift from a levelling-based system to a GNSS and gravimetric geoid-based system, being a cost-effective modernisation strategy for developing countries, were investigated. This thesis expands available scientific literature for the International Height Reference System/Frame (IHRS/F) development of the International Association of Geodesy (IAG), and the PHS modernisation efforts of the National Mapping and Resource Information Authority (NAMRIA). Three elements of a modern PHS were studied. 1. The engineering implications of the new Philippine Geoid Model (PGM). 2. The temporal variability of the geoid and benchmarks with focus on the effects of tropical hydrology. 3. The PHS relationship to the IHRS/F.

An evaluation of the new Technical University of Denmark (DTU-Space) and NAMRIA-developed PGM, was done to provide a quality baseline for managing the progression and limitations of a gravimetric geoid-based height system for the country. Statistical measures show that points clustered in the southern latitudes and eastern longitudes have relatively higher residuals due to geodynamic and hydrologic activity. A controlled procedure in establishing an evaluation network over a demonstration area was done to eliminate errors resulting from undocumented accuracy assumptions. It is concluded that a localised PGM can be used for third order applications.

Tropical effects on the reference frame and the geoid were examined. Displacements were analysed by estimating tidal and non-tidal loading for selected Philippine active geodetic stations using rain sensor data, local geologic information and ground validation. The mean dynamic topography (MDT) was also investigated. DTU10, VM500-ph and RADS-ph were compared with GNSS-geoid MDTs (GNSS-PGM2016.66, GNSS-EIGENGL05C). A nationwide scale, low-resolution Philippine vertical ground motion map inferred from Sentinel-1A scenes from January 2015 to December 2019 was also produced. Estimations confirm the intensity of land motion in the eastern and southern part of the country. Using Gravity Recovery and Climate Experiment (GRACE) temporal models, large variations for two IHRS/F-proposed Philippine stations were computed and show coincidence with high rainfall records. A causality relationship between high rainfall and geoid variation, however, is inconclusive.

Lastly, a novel way of characterising local height systems relationship for the IHRS/F that takes into account the non-homogenous states of geodetic development within a developing, archipelagic country is introduced. Recommendations for a modernised Philippine Height System were made as a result of this study.

Table of Contents

List of Acronyms

AF	Attached Frame
AIC	Akaike Information Criterion
ASTI	Advanced Science and Technology Institute
CE	Centre-of-Earth
CF	Centre-of-Figure
CGSD	Coast and Geodetic Survey Department
CHAMP	Challenging Minisatellite Payload for Geophysical Research and Application
CM	Centre-of-Mass
CSR	Centre for Space Research
DTM	Digital Terrain Models
DTU Space	National Space Institute of the Technical University of Denmark
EBK	Empirical Bayesian Kriging
ECCO	Estimating the Circulation and Climate Of The Ocean Model
ECMWF	European Centre for Medium-Range Weather Forecasts
EGM	Earth Gravitational Model
EOST	École Et Observatoire des Sciences De La Terre
ESA	European Space Agency
GBVP	Geodetic Boundary Value Problem
GFZ	German Research Centre for Geosciences
GGM	Global Geopotential Models
GGOS	Global Geodetic Observing System
GLDAS	Global Land Data Assimilation System
GLORYS	Global Ocean Reanalysis and Simulation
GNSS	Global Navigation Satellite Systems
GOCE	Gravity Field And Steady-State Ocean Circulation Explorer
GRACE	Gravity Recovery and Climate Experiment
ICGEM	International Centre For Global Earth Models
IAG	International Association Of Geodesy
IDW	Inverse Distance Weighting
IERS	International Earth Rotation and Reference Systems Service
IHRF	International Height Reference Frame
IHRS	International Height Reference System
ITRF	International Terrestrial Reference Frame
ITRS	International Terrestrial Reference System
IUGG	International Union of Geodesy and Geophysics
IW	Interferometric Wide
JPL	Jet Propulsion Laboratory
LSC	Least Squares Collocation
MDT	Mean Dynamic Topography

MERRA	Modern Era Retrospective Analysis for Research And Applications
MHW	Mean High Water
MLW	Mean Low Water
MSL	Mean Sea Level
MSS	Mean Sea Surface
MTL	Mean Tide Level
MTL	Mean Tide
NAMRIA	National Mapping and Resource Information Authority of the Philippines
NOAH	National Operational Assessment of Hazards
NRMDP	Natural Resources Management Development Project
PAGASA	Philippine Atmospheric, Geophysical and Astronomical Services Administration
PAGeNet	Philippine Active Geodetic Network
PGM	Philippine Geoid Model
PHILVOLCS	Philippine Institute of Volcanology And Seismology
PHS	Philippine Height System
PMB	Philippine Mobile Belt
PRS92	Philippine Reference System Of 1992
RADS	Radar Altimeter Database System
RDTC	Range Doppler Terrain Correction
RMS	Root Mean Square
SIRGAS	South American Geocentric Reference System Project
SLC	Single Look Complex
SNAP	Sentinel Application Platform
SRTM	Shuttle Radar Topography Mission
TF	Tide Free
TUGO	Toulouse Unstructured Grid Ocean Model
UP	University of The Philippines
WGS84	World Geodetic System Of 1984
ZT	Zero Tide

List of Figures

List of Tables

24. **Table A.6.** $\widehat{W}_{0i}$ in m^2/s^2 computation using Approach 2 (GOCO05, GGM05, GECO, EIGEN-GL04, PGM2016).
25. **Table A.7.** $\widehat{W}_{0i}$ in m^2/s^2 computation using Approach 3.
26. **Table A.8.** $\widehat{W}_{0i}$ in m^2/s^2 computation using Approach 4.

Chapter One

Primer

1.1. Introduction

The Philippines is one of the most active physical environments in the world (Lagmay et al., 2009). Capturing this activity with sufficient accuracy and cost-effectiveness is enabled by space-borne methods produced by the rapid development of geodetic technology and practice.

Terrestrial measurements can be classified into the horizontal and the vertical. The uniqueness of these two dimensions delivers a degree of independence from each other in establishment, maintenance and update.

The primary objective of this thesis is to develop a methodology for the empirical modelling of the temporal variations of a modern, tropical, and archipelagic Philippine Height System from terrestrial and space-borne geodetic data.

Modernisation of height systems takes different forms from one national setting to another. The shared concern is to make modernisation within reasonable boundaries of development time, resources and national legal and administrative frameworks.

It is imperative to adopt formal definitions of three important concepts: *reference systems*, *reference frames* and *datums*. Clear definitions of these concepts were provided by Hermann Drewes in the 2007 International Association of Geodesy (IAG) General Assembly.

> *"Reference systems define* constants, conventions, models, and parameters, which serve as the necessary basis for the mathematical representation of geometric and physical quantities. An example is a three-dimensional Cartesian system with the origin in the geo-centre, equatorial orientation, metric scale and rotating with the Earth

> *Reference Frames realise* the reference system physically, i.e., by a solid materialization of points, and mathematically, i.e., by the determination of parameters (e.g., geometric coordinates).
>
> The *geodetic datum fixes* unequivocally the relation between the reference frame and a reference system by allocating a set of "given" parameters, e.g., the coordinates of the origin of the system (X_0, Y_0, Z_0), the direction of coordinate axes X, Y, Z and the scale as a unit of length (e.g., metre)." (Drewes H. , 2009)

Redefining the reference system for height measurements and its realisation into a modern reference frame is an exercise that is driven by recent advances in Global Navigation Satellite Systems (GNSS) and satellite gravity missions such as the Gravity Field and Steady-State Ocean Circulation Explorer (GOCE) and the Gravity Recovery and Climate Experiment (GRACE). The shift of emphasis from a levelling-based system to a GNSS and gravimetric geoid-based system as the most practical next generation heighting solution for the Philippines is explored in this thesis.

This thesis attempts to address the following research challenges associated with a modernising, tropical, and archipelagic Philippine Height System (PHS). 1. The engineering implications of the new Philippine Geoid Model (PGM2016.66). 2. The temporal variability of the geoid and benchmarks with focus on the effects of tropical hydrology. 3. The PHS relationship to the International Height Reference System/Frame (IHRS/F).

This thesis provides a supporting study to the development of the next generation Philippine Height System led by the National Mapping and Resource Information Authority of the Philippines (NAMRIA). The next sections define the context, aims, expected contributions and limitations of the research.

1.2. Research Background

1.2.1. The Philippine Context

1.2.1.1. Physical Geography

The Philippines is an archipelagic nation with a territorial area of 343,448.32 square kilometres (National Statistical Coordination Board, 2010) located in the Southeast Asia region. At roughly 36,000 kilometres, it has the world's fifth longest coastline (Smith, 2017). It is positioned between 4^{o} 01' N and 21^{o} 25' N latitude and between 112^{o} 15' E and 127^{o} 00' E longitude (United Nations Economic and Social Commission for Asia and the Pacific, 2009). The country is traditionally clustered into three major island groups: Luzon, which contains the largest landmass, is in the northern part; Visayas is a collection of small islands that covers the central area, and; Mindanao which is located in the southern section of the country (Fig. 1.1).

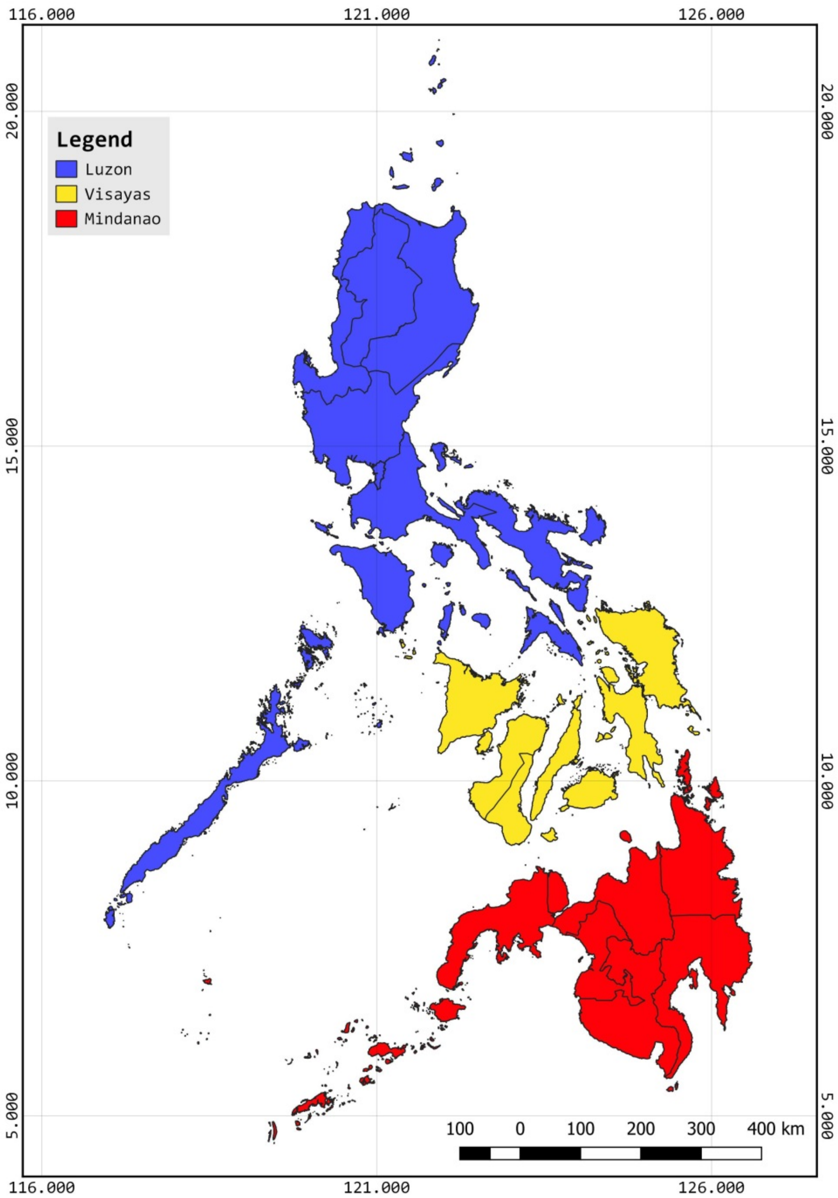

Figure 1.2. Island Groups of the Philippines.

Based on centuries old records, the accepted island count of the Philippines was 7,107 islands, until efforts by NAMRIA to update the number estimates it to 7,641 islands using satellite and airborne datasets in 2016 (CNN Philippines, 2016). The discrepancy is not necessarily due to physical changes. The author notes that the number is just an initial estimate and have yet to be validated on the ground. About 10% of these islands are inhabited.

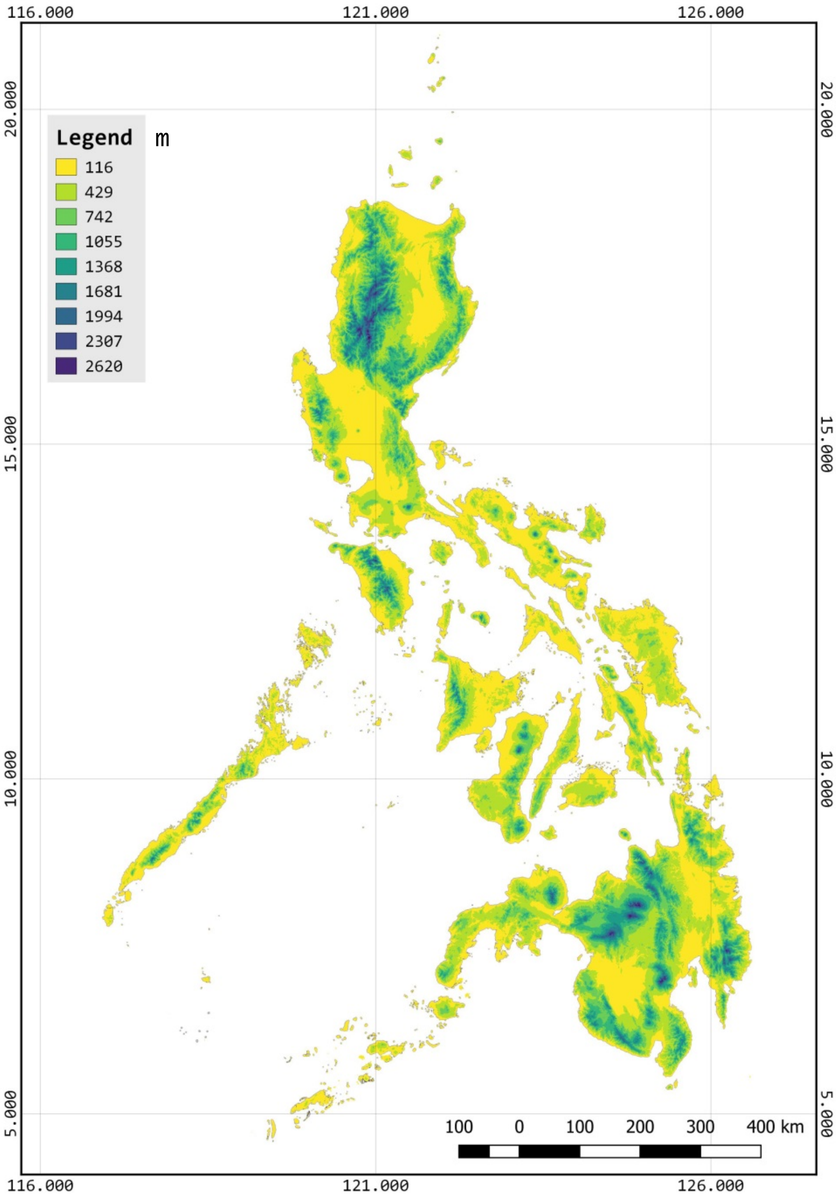

Figure 1.2. Synthetic Aperture Radar-derived Digital Elevation Model of the Philippines (in m) **(National Mapping and Resource Information Authority, 2016).**

Figure 1.2 illustrates the diverse topography of the Philippines. It is divided into 81 provinces. Most of the provinces are coastal, 15 are landlocked, and 16 are island provinces. Luzon is composed of coastal plains and the Cordillera, Zambales and Sierra Madre mountain ranges. In the middle of Cordillera and Sierra Madre is Cagayan Valley, where the nation's largest river flows northward towards the direction of Sta. Ana. Sierra Madre is the Philippines' longest mountain range that stretches over 680 kilometres and reaches elevations of up to 1,915 metres. ~ 80% of the mountain ranges are tropical rainforests. At 22,000 sq.km, Central Luzon is the largest plain in the country. To the south of Central Luzon is Laguna de Bay, Southeast Asia’s largest inland lake. Southwest of the Laguna de Bay is the Taal Volcano complex which hosts the country's third largest lake. The Bicol Peninsula is on the southeast of Luzon. The peninsula is mostly flat and features isolated peaks such as the Mayon and Iriga volcanoes and Mt. Masaraga and Mt. Malinao, Visayas is a collection of island provinces with low to moderately elevated terrain. Mindanao is composed of a complex series of mountain ranges that contains several notable mountains such as the highest point in the Philippines, Mt. Apo, with an elevation of 2,954 metres above mean sea level. Several rivers come from these mountains such as the Rio Grande de Mindanao, Pulangi, and Tagoloan rivers among others.

1.2.1.2. Geology

From 1991 to 2010, the Philippine Institute of Volcanology and Seismology (PHIVOLCS) collaborated with several academic institutions from France, Taiwan, Japan and the USA on a GNSS-aided ground deformation study along the nation’s active crustal structures to examine the kinematics of the archipelago. Results of the study revealed significant internal deformation in the Philippine Mobile Belt (PMB). The PMB is a zone of intense deformation and active seismicity between convergent zones bounding the Philippine archipelago (Gervasio, 1967). In the plate tectonics framework, the PMB represents a zone of deformation between surrounding major plates, namely: the Philippine Plate, Eurasian Plate (Sunda Block) and Indo-Australian Plate (Lagmay et al., 2009). The soil make-up of the Philippines is a combination of low land soils for tilling and upland soils prone to erosion. The classification of the geology and soil composition of the Philippines is summarised in map form through Figure 1.3 and Figure 1.4.

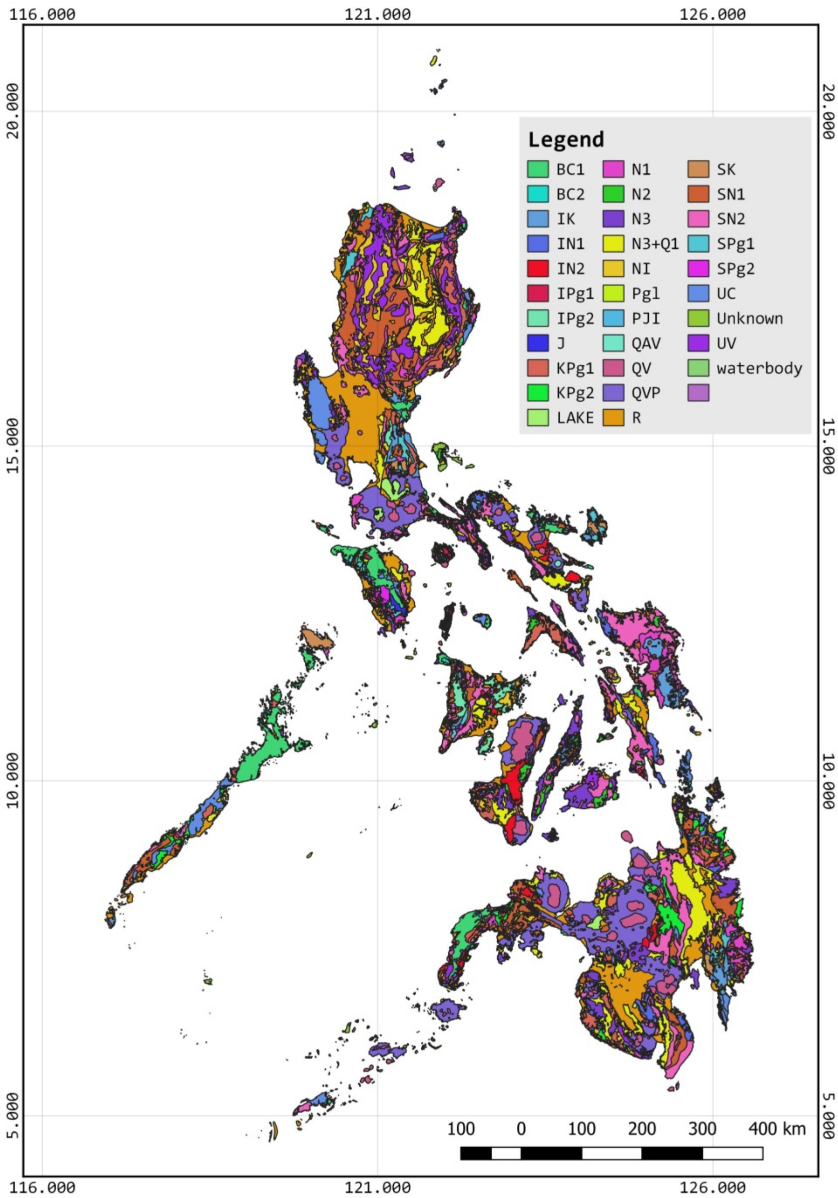

Figure 1.3. Generalised Geology of the Philippines. Data from the United States Geological Survey (USGS) **(United States Geological Survey, 1999)**.

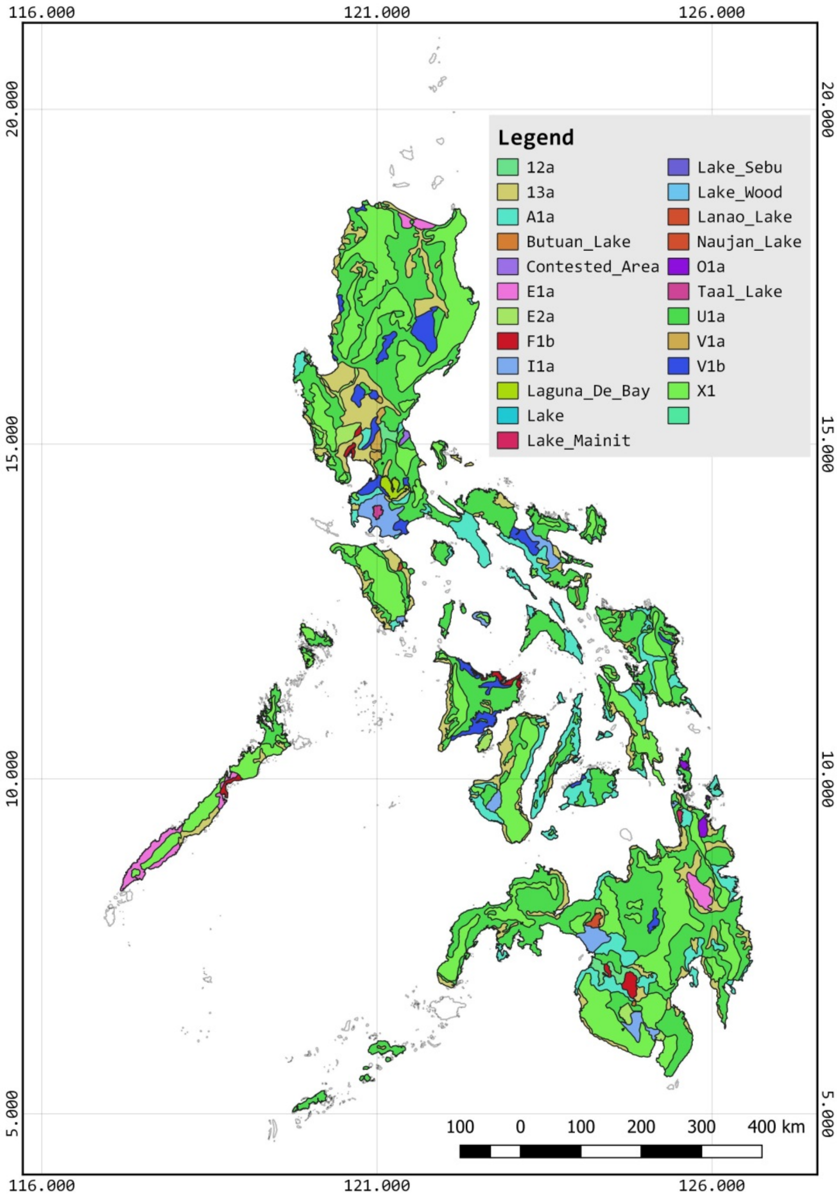

Figure 1.4. Soil Map of the Philippines. Data from the Philippine Department of Agriculture (DA) **(Bato & Nicopior, 2009)**.

1.2.1.3.Weather and Climate

There are many variable factors that characterize a region's climate. The most common of these are rainfall, temperature and humidity (McGuffie & Henderseon-Sellers, 2005). Temperature refers to the "degree of hotness or coldness of a body or environment" (Widerhold, 1997). Humidity is the moisture content of the atmosphere or the "mass of water vapor over mass of air" (Lydolph, 1985). Rainfall is "the amount of liquid precipitation" (Linsley, Kohler, & Paulhus, 1958). It is characterized by frequency, intensity and distribution (Pruppacher & Klett, 1997). Rainfall distribution varies across the Philippine archipelago and is influenced by the direction of the winds and the terrain (Fig. 1.5).

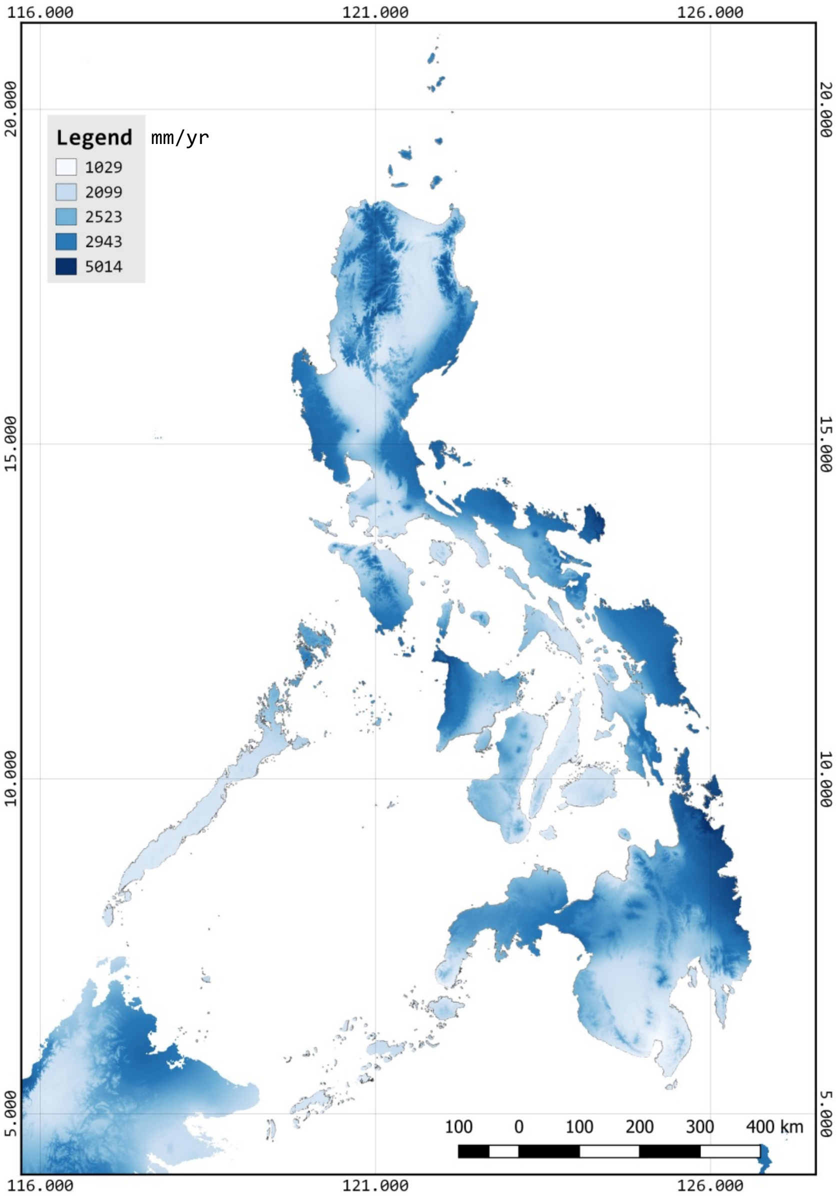

Figure 1.5. Average Annual Precipitation over the Philippines Data from the World Climate Data (mm/yr) **(Hijmans, Cameron, Parra, Jones, & A, 2005)**.

Philippine climate "is influenced by the complex interaction of the country's geography and topography, principal air streams, ocean currents, linear systems such as the intertropical convergence zone, and tropical cyclones which are classified as tropical depression, tropical storm, or typhoon, depending on their intensities." (Philippine Institute for Development Studies, 2005). The Philippine Atmospheric, Geophysical and Astronomical Services Administration (PAGASA), adopted the Modified Coronas Climate Classification Scheme, a rainfall distribution-based climate classification scheme developed by Jose Coronas in 1920 (Juanico, 1987) and modified by Flores et al., (1969) and Kintanar (1984). From this scheme, the climate of the country is divided into two seasons with four types describing the temporal distribution (Table 1.1).

Table 1.1. Climate Types of the Philippines based on rainfall distribution (Modified Corona Classification Scheme).

Type	Dry Season	Wet Season
I	November to April	Rest of the Year
II	No Dry Season	Maximum Rain Period from December to February; Minimum Rainfall from March to May
III	Short Dry Season either from December to February or March to May	No very pronounced maximum rain period
IV	No Dry Season	Rainfall evenly distributed throughout the year.

1.2.1.4. Overview of the Philippine Height System Development

It can be argued that the Philippines never truly had a "national" height system. The old PHS was formed through a collection of *local height systems* (height systems of local coverage and within a national jurisdiction) tied to local tide stations. Officially, the PHS is referred to the MSL of the Manila. However, local MSL surfaces were used in practice. The height datum in northern and southern Luzon originated from the mean sea level (MSL) defined by the series of observation in the Manila South Harbour and Legaspi primary tide station respectively. Mindanao fixed its datum at Davao primary tide station MSL. Other large islands like Cebu, Mindoro and Palawan referred their datums to the MSL defined by their respective local tide gauge stations (Paringit, Ventura, & Isada, 2009). In its current usage, the term Philippine Height System pertains to the reference system, the reference frame and the datum. This is recommended to be addressed in future professional education campaigns of NAMRIA. Officially, the PHS is using orthometric heights. Upon closer investigation of available records, most of the orthometric heights are of the Helmert approximation. There were some instances (usually subcontracted in less developed areas) that recordings of observed/levelled heights were assumed to be orthometric heights.

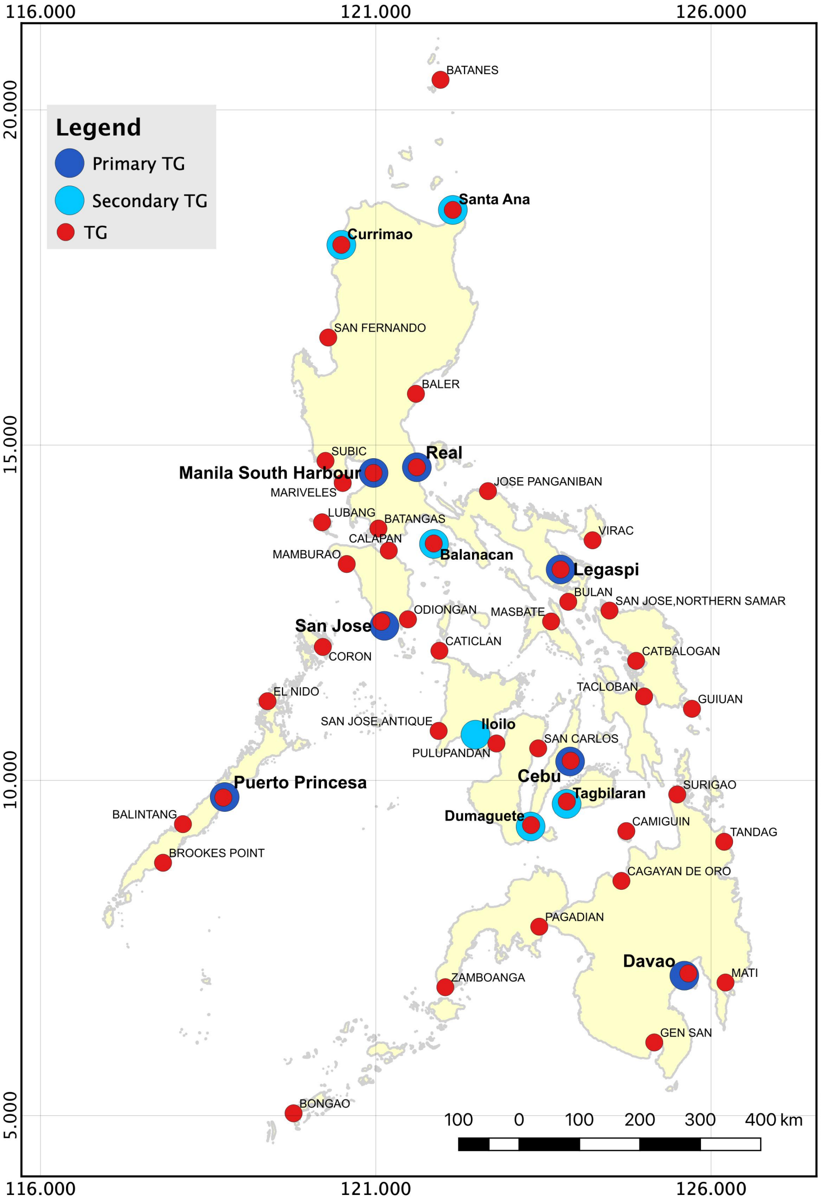

Figure 1.6. Existing Philippine tide gauge stations. Officially, the PHS is tied to Manila. Tide gauge stations in dark and light blue serve as zero levels for levelling locally **(Coast and Geodetic Surveys Department, 2016)**.

The Philippine Geoid Model of 1991 (PGM1991) is the first geoid for the Philippines. PGM1991 was computed using terrestrial gravity data, gravity data from satellite altimetry and the OSU89A (Rapp & Pavlis, 1991) geopotential model. Geoid heights computed from this geoid was projected to have accuracies between 6 ppm to 10 ppm. The terrestrial gravity data used for PGM1991 were acquired in the early 1960s. A total of 77 gravity base stations (relative gravity) were used for this study nationwide and it was supplemented by 300 gravity observations. It was not mentioned if absolute gravity observations were available. One absolute gravity station was installed in NAMRIA in 2005. A series of gravity profiles were conducted in the early 1990s to validate and supplement these terrestrial gravity data for the geoid model computation (Paringit, Ventura, & Isada, 2009). Satellite altimetry data was calculated from Geos-3 and SeaSat radar altimetry using collocation. The project also produced 111 GNSS/levelling stations used to distort the gravimetric geoid model by comparing the GNSS/levelling geoid height with the gravimetric geoid height to fit the local vertical datum. Although no ellipsoid was mentioned in Kearseley and Ahmad's report (1995), the GNSS data that were used in their computations use the WGS84 (National Imagery and Mapping Agency, 1997) ellipsoid.

Though official, PGM1991 was not useable due to age and development issues. This motivated scientific contributions for alternative geoids in the past decade. Most of these developments, however, were predominantly focused on Manila and its surrounding cities.

In Meneses & Paringit (2009), the long wavelength information of the Earth's gravity field needed for gravimetric geoid determination were derived from satellite-only and combined *global geopotential models* (GGM). The authors used Gravity Recovery and Climate Experiment (GRACE) (Tapley, Bettadpur, Watkins, & Reigber, 2004), Challenging Minisatellite Payload for Geophysical Research and Application (CHAMP) (Reigber, Casper, & Päffgen, 1999), Earth Gravity Model of 1996 (EGM96) (Lemoine et al., 1998), and EIGEN-GL04C (Förste et al., 2005). GRACE and CHAMP datasets were also padded by extending their degrees up to 360 by using EGM96 coefficients. They discovered that in metropolitan Manila, EIGEN-GL04C produced the best fit to local GNSS/levelling-based undulations. The authors found that the average GGM-derived undulation is approximately 45.07 metres with 0.31 metres standard deviation. It is important to note that the majority of the gravity observations from 29 stations used were located near the Manila Bay Area.

Reyes et al., (2014) developed a local geoid model of Manila using the least squares modification of the Stokes' formula with additive corrections method and produced a Root Mean Square (RMS) of 7 to 8 centimetres, accounting GNSS observations and errors in levelled heights. The local geoid model surpassed accuracies of combined-type GGMs, EIGEN-6C2 (Förste et al., 2012) and EGM2008 (Pavlis, Holmes, Kenyon, & Factor, 2012). The RMS of the combined type GGMs after comparing with the GNSS/levelling-derived geoid heights were 12.50 centimetres for EIGEN-6C2 and 13.80 centimetres for EGM2008.

Meneses & Paringit (2009) and Reyes et al., (2014) (and likely, Kearseley & Ahmad (1995)) used the WGS84 ellipsoid in the computations. The author notes that the aforementioned geoid developments did not consider the consistency of permanent tide systems.

A more recent Philippine geoid model (PGM2014) (Forsberg, Olesen, Gatchalian, & Ortiz, 2014) was developed by the team of Dr. Rene Forsberg of the National Space Institute of the Technical University of Denmark (DTU-Space) in collaboration with NAMRIA. The PGM2014 was developed with a shift of +80 centimetres to estimate the mean geoid offset relative to GNSS and levelling in Manila and the surrounding cities. PGM2014 was fitted to the International Terrestrial Reference Frame (ITRF) using least squares collocation and GNSS/levelling data (Forsberg, 2000). Many outliers were observed and need to be corrected for a suitable fit and consistency to the existing vertical datum. Forsberg et al., attributes the outliers to geodynamic effects (2014). PGM2014 was improved to PGM2016.66.

The Philippine setting is complex due to the following reasons (Kearseley & Ahmad, 1995).

1. *Difficult terrain.* A variety of landforms such as mountainous features and agricultural lowlands define the Philippine terrain (Fig. 1.2). This terrain

makes access extremely difficult and limits the options available for geodetic and gravimetric surveys.

2. *Tropical climate.* Some areas are effectively covered by clouds all year round, limiting the options for mapping by satellites and airborne methods. Annual monsoon periods limit the times when effective field campaigns can be undertaken (Fig. 1.5).
3. *Complex tectonics.* The country is located in the Western Pacific domain of the Pacific Ring of Fire where seismic and volcanic activities are very common. In this domain, the movements of three big plates (Pacific, Eurasian and Indo-Australian) make the landmasses very dynamic in a geologic sense. Furthermore, in the Southwestern portion, the Philippine Plate and the Southeastern Edge of the Eurasian Plate causes the diversity of movement directions and velocities in the Philippine tectonic zone (Mines and Geosciences Bureau, 2004). This renders conventional models of the crust used for Bouguer anomaly determination inadequate (Ahmad, Harvey, Kasenda, & Kearseley, 1993). Figure 1.7 shows Philippine geodynamic activity in comparison with the rest of the world.

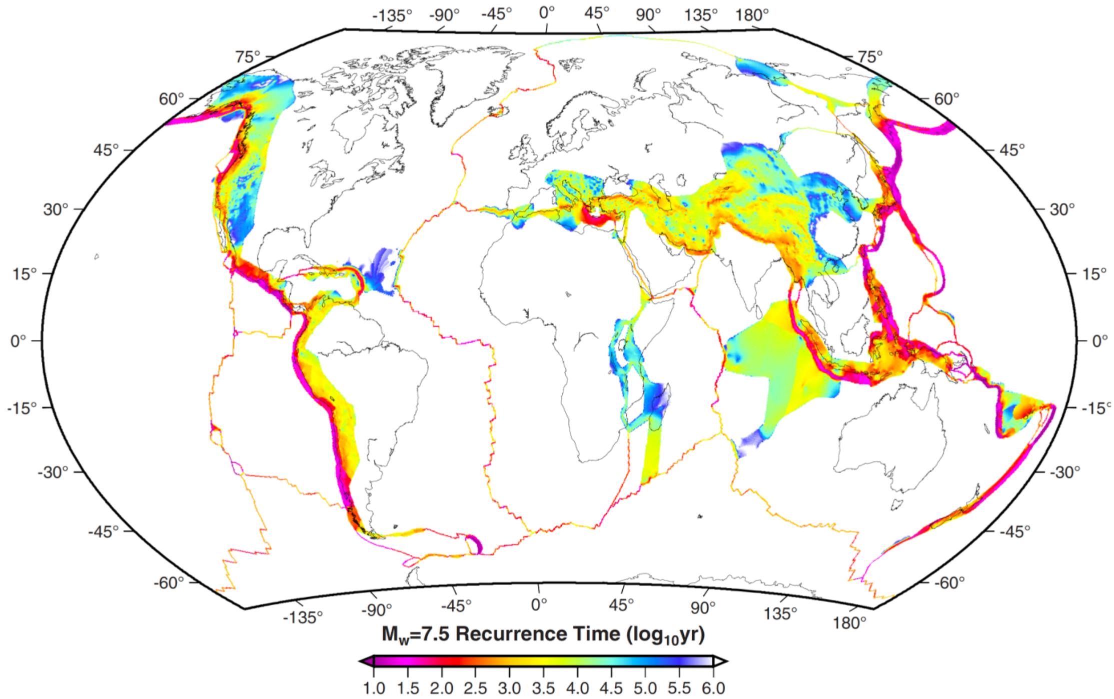

Figure 1.3. Log_{10} of the recurrence time of an $M_w = 7.5$ earthquake, when a geodetic moment is released by a single "characteristic" event but considering an average coupling for the appropriate plate boundary type. For more explanation, the reader is directed to the full study by Kreemer et al., **(Kreemer, Blewitt, & Klein, 2014)** where the above image is sourced.

4. *Archipelago-type Geography.* This makes the connection of local height systems between islands very difficult. As the use of GNSS becomes widespread, the problem of island connection can be solved but the need for a reliable geoid becomes more urgent.

1.2.2. The International Height Reference System/Frame

The initiatives to develop a global, physical, height reference system draw motivation from a similar unification/relationship effort for geometric measurements through the International Terrestrial Reference System/Frame (ITRS/F) development. These initiatives were joined under the umbrella of the IAG through the International Height Reference System/Frame (IHRS/F) development program. The primary objectives for the IHRS/F are (Drewes, Kuglitsch, Adám, & Rózsa, 2016),

1. to provide a reliable frame for consistent analysis and modelling of global phenomena related to the Earth's gravity field (e.g. sea level variations from local to global scales, redistribution of masses in oceans, continents and the Earth’s interior, etc.)
2. to allow the reliable combination of physical and geometric heights in order maximise the advantages of satellite geodesy (e.g. combination of GNSS with gravity field models for worldwide unified precise height determination)

The objectives are achieved through the use of modern geodetic methods and technologies. IHRS/F studies related to this research are presented in Chapter 5.

The IAG resolution for the definition of the IHRS was approved by the International Union of Geodesy and Geophysics (IUGG) in the 26th General Assembly in Prague on July 2015. According to the resolution, the primary objectives of the Global Geodetic Observing System (GGOS) Focus Area 1 from 2015 to 2019 were: (1) the outlining of detailed standards, conventions, and guidelines to make the IAG Resolution applicable, and (2) the realisation of the IHRS (Drewes, Kuglitsch, Adám, & Rózsa, 2016).

The development of national height systems is, in principle, independent from the development of the IHRS/F. It is practical, however, to build a national height system that is compatible and interoperable with other national height systems through the IHRS/F. For an in-depth rationale, the reader is referred to the works of Sanchez et al., (2006) Čunderlík et al., (2012) and Gruber et al., (2012).

A computation of the local geopotential values and height offsets between two or more national height systems will demonstrate interoperability and expose relevant technical issues arising from the process. Challenges surrounding workflows will give insight at how countries with diverse height systems can maximise the benefits of the IHRS/F.

1.3. Research Objectives

The primary objective of this thesis, as mentioned in Section 1.1, is to develop a methodology for the empirical modelling of the temporal variations of a modern, tropical, and archipelagic Philippine Height System from terrestrial and space-borne geodetic data. Part of this objective is to investigate the research challenges associated with creating a modernised Philippine Height System. The development and the definition of the objective is discussed in the next subsections.

1.3.1. Modernisation

Height Systems are challenging to modernise, in general, due to the financial and logistical requirements. Jurisdiction-specific challenges are also realities that need to be considered. Recently, there is an increased interest in moving from levelling-based height systems towards GNSS and gravimetric geoid-based height systems (Véronneau & Huang, 2016; Natural Resources Canada, 2017; Kasenda, 2009). This shift has implications in terms of accessibility and implementation in most countries.

The systematic process of what constitutes the term "modern" in the context of reference systems and frames is the first step in modernisation. A modern height system is characterised by the following (Sánchez, 2013; Rizos, 2015):

1. Ellipsoidal heights *(h)* and (quasi-) geoid heights *(N)* must be given with respect to the same ellipsoid.
2. Physical heights *(H)* and (quasi-) geoid undulations *(N)* must reflect the same reference surface.
3. Physical heights *(H)* and the Ellipsoidal heights *(h)* must represent the same Earth's surface.

A discussion on the different types of heights and reference surfaces and their significance to this study is provided in Chapter 2.

Recent trends demonstrate the increased contribution of space-based positioning technologies and methods (Herceg, Knudsen, & Tscherning, 2012; Lambrou, 2012;

Čunderlík, Minarechová, & Mikula, 2012). Levelling produces observations tied to the Mean Sea Level (MSL) as a vertical reference surface due to its physical accessibility (Balasubramania, 1994) (Chapter 2, Section 2.2.2, 2.2.5, 2.3.1). It has been reliable in most practical applications for decades. On the operational side, traditional levelling uses passive monuments with challenges presented below. New technologies and methods to define the height reference surface have been developed without the issues attributed to the physical complexities of tides (Pan & Sjoeberg, 1998).

The Philippine Height System needs to be modernised because:

1. *The current height system needs improvement.* In most areas, more height observations are required. For areas in between observations, distortions have to be minimized. Setting the MSL as "zero" in a levelling network adjustment over a large region causes discrepancies throughout and beyond the region and the resultant height values have significant differences from those obtained from a free adjustment. (Kasenda, 2009)

   In theory, a move from levelling-based to gravimetric geoid-based height system is a logical modernisation path for a country with a topographic stretch like the Philippines. Levelling-based height systems are practical and precise, but it is also prone to the accumulation of systematic errors over long distances. The mean dynamic topography (MDT) departs the mean sea level (MSL) from the geoid (see Chapter 2, Section 2.3.1 and 2.3.3 and Chapter 3, Section 3.1). Due to the difficulty of terrain, the density and quality of levelling networks are not homogenous throughout the country (Natural Resources Canada, 2017).

2. *The current height system demands expensive maintenance.* The study area's physical, systematic and economic challenges support a modernisation approach with optimal efficiency and minimum financial commitment. Physical height systems have an update rate of only 10-50 years (Ihde & Sanchez, 2005). One of the reasons for this infrequent update rate is cost. Traditional methods of establishing and maintaining height systems require substantial capital outlays (Véronneau & Huang, 2016). Passive monuments are expensive to establish

especially in developing countries. Dynamic Earth processes such as land subsidence and tectonic activity are causing a higher degree of spatial and temporal variability, making these physical monuments unreliable if unmaintained over a period of time. Updating a height system using traditional levelling is economically, logistically and operationally very challenging.

An approachable modernisation strategy also means covering sparsely-surveyed areas and making these areas refinement-ready. Rummel et al., (2014) defines sparsely-surveyed areas as regions that "may be characterized by missing GNSS infrastructure, low accuracy or lack of regional gravity data and lack of surveying and mapping infrastructure". The use of gravimetric geoid models was proven to be instrumental in providing national, regional and global coverage.

3. *Modern geospatial technology has gone mainstream, increasing demand for accurate information and opening opportunities for further research.* The availability of newer and more accurate geospatial technologies presents an opportunity for evaluation and application. The increasing role of GNSS in geodetic procedures demands the provision of a seamless transformation mechanism between physical and geometric heights.

   For archipelagic states, to arrive at a singular MSL that would define the national height system, the respective MSLs of islands were usually averaged (Paringit, Ventura, & Isada, 2009). The recent significant sea-level rise that archipelagic countries are immediately exposed to, may introduce significant errors to the accuracy of the MSL-related heights. As it is, arriving at connectivity is problematic due to the errors it may introduce to offset values.

1.3.2. Globalisation

The idea of a “World Height System” has been studied thoroughly in the past (Balasubramania, 1994; Burša et al., 1998, 1999; Burša et al., 2002). Modern geospatial technology has spurred several initiatives towards modernisation of regional and global height systems in North and South America, Europe and on a global scale through the IHRS/F project of the IAG. This study also contributes to the IHRS/F development and the Asia Pacific Regional Height System Unification efforts of the United Nations Committee of Experts on Global Geospatial Information Management.

In the South American Geocentric Reference System Project (SIRGAS) (Ihde & Sanchez, 2005), relationships between national heights systems were estimated both geometrically and physically by implementing a GNSS campaign to gather information on the SIRGAS 1995 reference frame, principal tide gauges of each participating country, a selection of stations at the borders to connect the first-order levelling networks between neighbouring countries, and additional primary vertical control points. The SIRGAS-referred stations were connected by spirit levelling. Geopotential numbers and normal gravity corrections were also computed. SIRGAS' new coordinates refer to ITRF2000 with an epoch set at 2000.4. For the physical component, the determination of normal heights and the quasigeoid as the corresponding reference surface were required.

Gruber et al., (2012) attempted to establish height system connections based on GOCE and GNSS. The improved accuracies in the new GOCE models encouraged new levels of research in IHRF development. In theory, this development enables the transformation of existing physical heights to ellipsoidal heights of sufficient accuracy and vice versa (Sanchez, 2006). A mean global geoid model from GOCE was used by the authors as a comparison to the mean of the local geoid heights obtained from GNSS/Levelling datasets for regions referring to the same height datum. Then connectivity between a number of regions across the globe was established. GOCE contains omission errors (Hirt, Gruber, & Featherstone, 2011) which were modelled using the Earth Gravitational Model 2008 (EGM2008). EGM2008 were also known to contain omission errors (Hirt, Marti, Bürki, & Featherstone, 2010; Gruber T. , 2009). Intercontinental height system connections were attempted over the North Atlantic and the Pacific using the GOCE geoid (degree and order 0-180) and EGM2008 (degree and order 181-2190). Offsets in the range of -1.12 m to -1.77 m were observed between Europe and North America while offsets between -0.555 m to -0.834 m were observed when connecting Australia/Japan and North America.

There is a need for heights to be approached beyond the local level because of the dynamic environment's impact that goes beyond borders (Ferreira & de Freitas, 2012). Gruber et al., (2012) demonstrated a solution to this need to a level of accuracy that recent advances in gravity field models and ellipsoidal heights can provide. GOCE provides a global geoid with an accuracy of a few centimetres at a resolution of 100 km independent of any terrestrial data. When the authors compared their results with a height connection study done by Rapp (1994), they observed vertical offset differences of up to 10 cm. The perceived improvement is due to the dissimilarity in approach between the two studies provided by the state of existing technologies during their respective times.

In the authors' (Gruber, Gerlach, & Haagmans, 2012) analysis, it was imperative that the GNSS datasets utilised are of high quality. This implies that a dense and high-quality national height system is necessary for intercontinental connection. This reliability factor constrained the authors to the necessary selection of countries with well-maintained and developed geodetic infrastructure. This is a limitation but also an opportunity for me to conduct further research. It will be interesting to see how countries with still-developing geodetic infrastructures participate in the development of an IHRS/F or how countries can use the IHRS/F to develop their local height systems.

1.3.3. Research Focus

To accomplish the primary aim, the study focused on the following.

1. Revisit the persistent limitations of a gravimetric geoid-based height system and provide achievable solutions to manage these limitations (Chapter 3).
2. Model the variations of the geoid and physical benchmarks with respect to time and provide insight on its particularities for tropical archipelagos. Secular and episodic variations related to tropical factors are investigated (Chapter 4).
3. Demonstrate relative connectivity between non-landlocked height systems of different geodetic development states and tectonic realms. The approach will be in the context of the International Height Reference System/Frame development (Chapter 5).

1.4. Thesis Overview

For the convenience of the reader, this thesis is written in six (6) themed chapters and an appendix. It is organised as follows.

Chapter One: Primer. The first chapter of this thesis provides a brief overview and context for the study. The rationale and objectives for the research and the unique challenges of the study area are addressed in this chapter.

Chapter Two: Heights, Height Systems and Vertical Datums. The next chapter begins by laying out the relevant theoretical framework for this study.

Chapter Three: Diagnostic of the Existing Philippine Height System and Philippine Geoid Model. Chapter 3 gives the reader background on the development of the Philippine Height System. The subsequent part focuses on NAMRIA's development of the new Philippine Geoid Model and the author's independent assessment. This chapter addresses item 1 of Section 1.3.3.

Chapter Four: The Philippine Height System Realisation and Tropical Effects. The fourth chapter analyses the tropical effects to the reference frame and the geoid over the study area. It contains discussion on the methodology of capturing these effects. The integration of the geoid rates and the vertical displacement rates into the modernisation process is the main theme of Chapter 4 and provides detail for items 2 and 3 of Section 1.3.3.

Chapter Five: The Philippine Height System and the International Height Reference System. This section proceeds to discuss the IHRS/F and the contribution of the modern Philippine Height System. A demonstration of interoperability and a discussion of technical issues arising from the connection exercise will also be provided in this chapter. Chapter 5 provides content for item 3 of Section 1.3.3.

Chapter Six: Concluding Remarks. The last chapter provides recommendations for implementation and future research. A summary of the document completes this section.

Chapter Two

Heights, Height Systems and Vertical Datums

The previous chapter is an overview of this study's context, motivations, limitations and expectations. Chapter Two presents a condensed theoretical framework that draws on foundational concepts from the texts of Heiskanen and Mortiz (1967), Bomford (1980), Ekman (1989), Jekeli (2000), Featherstone and Kuhn (2006), Drewes (2009), and Filmer et al., (2018). Reference Systems, Reference Frames and Datums are defined in Section 2.1. Heights and height systems are presented in Section 2.2. Information on Vertical Datums are provided in Section 2.3. Section 2.4 gives the summary of the chapter.

2.1. Reference Systems, Reference Frames and Datums

The history of the Philippines is marked with uncertainty and imposition of standards and rules that vary from one colonial administration to another. The constant military and administrative instability in the early days were not an ideal situation for the creation and maintenance of thorough documentation. A contribution of this study is to broaden literature that provides, compiles and clarifies definitions that are related to the Philippine Height System setting. A clear and correct definition is the foundation of scientific reliability and accuracy. The usage of terms, over time, can sometimes deviate from their scientific definitions—causing confusion in communication and development of products. In this section, reference systems, reference frames and datums are defined.

This thesis is adopting the definitions of Drewes (2009) for reference systems, reference frames and datums. A *reference system* is a set of principles, methods, schemes, conventions and parameters according to which, a representation of a geometric and physical attribute is achieved. A *reference frame* is the realisation (producing an actual physical or mathematical form of an abstract concept) of the reference system. *Datum* came from an 18th century Latin word meaning "something given". It is a surface or a point where the relationship (origin, location, orientation and units) between the reference system and reference frame is fixed. The use (and misuse) of the term "datum" has been causing confusion by assigning the term to the coordinates of the points of the network referred to the datum. The misuse can be attributed to the "reference frame" being relatively new in terms of usage.

An order of hierarchy governs the three concepts. In his paper, Drewes (2009) stated, "

1. The definition of a reference system must be completely unaffected by the realisation of the reference frame and the geodetic datum, i.e., the realisation of the system by the frame and the allocation of the datum must not change the definition.
2. The realisation of the datum has to be done by methods independent of the measurements of the reference frame, i.e. measurement errors of physical changes altering the observations of the frame must not affect the datum.
3. The mathematical realisation of the reference frame has to be done by algorithms that keep the datum parameters fixed and follow strictly the principles defined by the reference system. "

As mentioned in the previous chapter, vertical and horizontal systems, frames and datums are usually treated independently. Unified approaches can be done. However, the dependency of one dimension to another introduces systematic compromises that affect accuracy and reliability.

2.2. Heights and Height Systems

Height carries a variety of definitions across different scientific disciplines. In Geodesy, *height* is "the distance, measured along a perpendicular, between a point and a reference surface" (National Geodetic Survey, 1998). A *height system* (often used interchangeably with *height reference system)*, is "a one-dimensional coordinate system used to express the metric distance (height) of a point from some reference surface" (Featherstone & Kuhn, 2006).

2.2.1. Gravity and Gravity Reductions

In a simplified manner, the potential *(V),* is given by,

$$V = G \iiint_{v} \frac{\varrho}{l} dv \tag{2.1}$$

Where *v* is the body's volume and ϱ is the density *dm/dv*. The potential *(V),* through a Laplacian operator *(Δ),* may be shown to satisfy *Poisson's equation*,

$$\Delta V = -4\pi G\varrho = \frac{\partial^2 V}{\partial x^2} + \frac{\partial^2 V}{\partial y^2} + \frac{\partial^2 V}{\partial z^2} \tag{2.2}$$

When $\varrho = 0$, (in empty space, outside the attracting bodies), ΔV is zero and its solutions are called *harmonic functions*.

In Moritz and Mueller's (1987) simplified assumption the Earth is a solid body rotating with constant speed around a fixed axis, *centrifugal force* on a unit mass is given by,

$$\boldsymbol{f} = \omega^2 \boldsymbol{p} \tag{2.3}$$

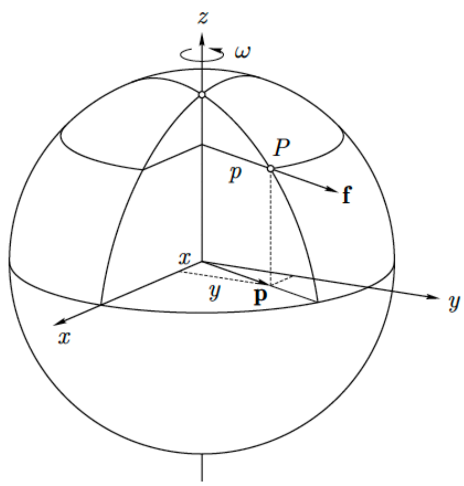

Figure 2.2. Simplified representation of Earth as a solid body. **(Moritz & Mueller, 1987)**

Where ω is the constant rotational angular velocity, and p_{XY} is the distance of the point of interest, projected on the horizontal plane (xy-plane) from the rotation axis (z-axis).

The centrifugal potential, Φ, is given by,

$$\Phi = \frac{1}{2}\omega^2(x^2 + y^2) \tag{2.4}$$

Based on the arguments given above, the *gravity potential, W,* is given by,

$$W = V + \Phi \tag{2.1}$$

The gradient operator to the gravity potential produces the *gravity vector (**g**)* composed of individual components, $\frac{\partial W}{\partial x}, \frac{\partial W}{\partial y}, \frac{\partial W}{\partial z}$.

$$\boldsymbol{g} = \mathrm{grad}W \equiv \left[\frac{\partial W}{\partial x}, \frac{\partial W}{\partial y}, \frac{\partial W}{\partial z}\right]. \tag{2.6}$$

where the z-axis coincides with the mean axis of rotation of the Earth and x- and y-axis represent a right-handed coordinate system. "Gravity" is observed through an object's acceleration due to gravity expressed in *gals*, where 1 gal = 0.01 m·s^{-2}. The (curved) lines that intersect equipotential surfaces orthogonally are called *plumb lines* (Heiskanen & Moritz, 1967). This derivation in this text is simplified for the purpose of illustration. Full relationships between forces and potentials and detailed foundational derivations are discussed in the numerous pages of the physical geodesy textbooks of Heiskanen & Moritz (1967) Vaníček (1976), and Bomford (1980).

To obtain sea-level equivalents, observed gravity undergoes a process called *gravity reduction*. It is an avenue for the determination of the geoid (see Stokes' formula, Section 2.3.3.) and interpolation and extrapolation of gravity and studies of the Earth's crust in the geodetic context. It involves the exclusion or shifting below sea level of topographic masses (introducing topographic effects) outside the geoid, and the lowering of the gravity station from the Earth's surface (P) to the geoid surface (Hoffmann-Wellenhoff & Moritz, 2005).

Gravity anomaly is the difference in the magnitude of the normal gravity vector *(γ)* at a point on the geoid *(P_0)* and the gravity vector *($\mathbf{g}$)* at a corresponding point on the ellipsoid *(Q_0)* (more on ellipsoids in Section 2.3.4) given by,

$$\Delta g = g_{P_0} - \gamma_{Q_0} \tag{2.2}$$

In Kuhn et al., (2009), considering the effects of the gravitational attraction of the topographic masses (δg_{top}) and atmospheric correction (δg_{AC}), the free-air correction (δg_{FC}) and the normal gravity (γ_0) on the surface of the ellipsoid, the *Bouguer gravity anomaly* at the gravity observation is,

$$\Delta g_B = g_P - \delta g_{top} + \delta g_{AC} + \delta g_{FC} - \gamma_0 \tag{2.8}$$

The Bouguer gravity effect is of the order of ten times the geoid undulation because the Earth is isostatically compensated in general. For this reason, the Bouguer anomaly cannot be used for geoid determination (Heiskanen & Moritz, 1967). The *Bouguer gravity reduction* is a process that eliminates the gravity effect of topographic masses above the geoid and applying the *free-air reduction*.

Free-air reduction can be approximated as (Hoffmann-Wellenhoff & Moritz, 2005),

$$\delta g_{FC} = +0.3086 H_P \tag{2.9}$$

where H_P is the height of the gravity observation at P above the geoid. A refined approximation given by (Featherstone, 1995),

$$\delta g_{FC} = \frac{2\gamma_0}{a}(1 + f + m - 2f \sin^2 \emptyset)H_P - \frac{3\gamma_0}{a^2} H_P^2 \tag{2.3}$$

is recommended as it accounts for gravity gradient changes with height and geodetic latitude *(Φ)*. *f* is the geometrical flattening of the reference ellipsoid, *m* is the ratio of gravitational and centrifugal forces at the equator and, *a* is the semi-major axis of the reference ellipsoid.

The *atmospheric correction* for the removal of the gravitational effect of atmospheric masses can be determined by (Featherstone & Dentith, 1997),

$$\delta g_{AC} = 0.0871 - 1.0298 \, X \, 10^{-4} H_P + 5.3105 \, X \, 10^{-9} H_P^2 \tag{2.4}$$

Bouguer gravity anomalies can be determined by introducing different approximations for δg_{top}. Simple planar Bouguer gravity anomalies (Δg_{SPB}) and complete planar Bouguer gravity anomalies (Δg_{CPB}) can be produced by,

$$\Delta g_{SPB} = g_P - \delta g_{B_{plate}} + \delta g_{AC} + \delta g_{FC} - \gamma_0 \tag{2.5}$$

$$\Delta g_{CPB} = \Delta g_{SPB} + \delta g_{PTC} \tag{2.6}$$

where,

$$\delta g_{top} \approx \delta g_{B_{plate}} \tag{2.7}$$

and,

$$\delta g_{B_{plate}} = 2\pi G \varrho H_{plate} \tag{2.8}$$

$\delta g_{B_{plate}}$ is the gravitational effect of the Bouguer plate with constant thickness, H_{plate}. ϱ is the constant mass-density of the Bouguer plate and *G* is the gravitational constant.

δg_{PTC} is the *planar terrain correction* which accounts for the gravitational effect of the topography residual to the Bouguer plate.

The simple spherical Bouguer gravity anomalies (Δg_{SSB}) and complete spherical Bouguer gravity anomalies (Δg_{CSB}) is given by,

$$\Delta g_{SSB} = g_P - \delta g_{B_{shell}} + \delta g_{AC} + \delta g_{FC} - \gamma_0 \tag{2.9}$$

$$\Delta g_{CSB} = \Delta g_{SSB} + \delta g_{STC} \tag{2.10}$$

Δg_{SSB} uses an approximation with the gravitational effect of the Bouguer shell,

$$\delta g_{top} \approx \delta g_{B_{shell}} \tag{2.11}$$

where,

$$\delta g_{B_{shell}} = 2 * (2\pi G \varrho H_{plate}) \tag{2.12}$$

$$\delta g_{top} \approx \delta g_{BS} \tag{2.20}$$

δg_{STC} is the *spherical terrain correction* that accounts for the gravitational effect of the topography residual to the Bouguer spherical shell. More detail on the Bouguer gravity can be found in Heiskanen & Moritz (1967) together with a more recent application by Kuhn et al., (2009).

Taking $W = U_0$ and $U = U_P$, coinciding in P_0, produces the gravity disturbance vector. *Gravity disturbance* is then the difference in the magnitude of the normal gravity vector ($\boldsymbol{\gamma}$) at point P_0 and the gravity vector ($\mathbf{g}$) at the same point given by,

$$\delta g = g_P - \gamma_P \tag{2.13}$$

The difference in direction is called the *deflection of the vertical* (Heiskanen & Moritz, 1967; Vanícék & Krakiwsky, 1986). Figure 2.2 shows different types (Jekeli, 1999).

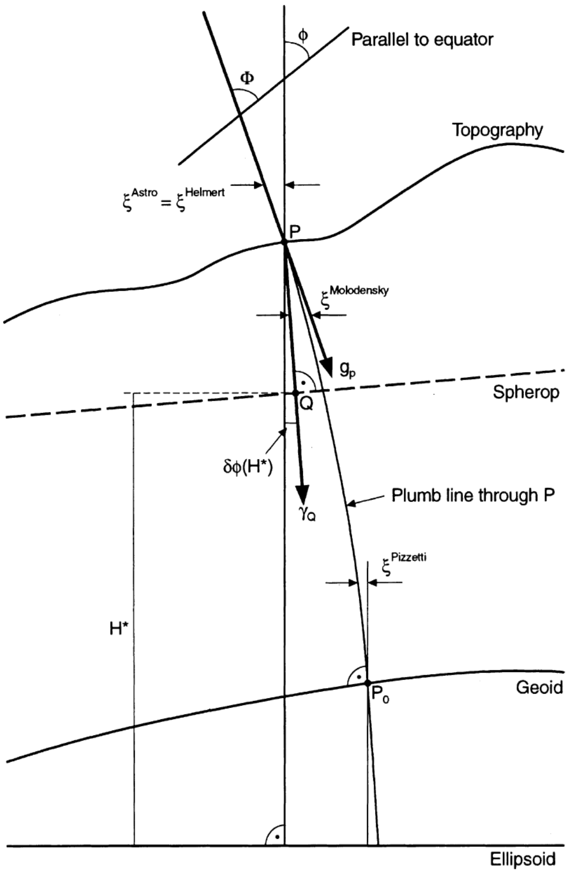

Figure 2.2. Relationships between the different deflections of the vertical (north-south component, ξ. Superscript refers to definitions: ξ^{Astro}, astronomically-determined; $\xi^{Helmert}$, Helmert; $\xi^{Pizetti}$, Pizetti; $\xi^{Molodensky}$, Molodensky) **(Jekeli C. , 1999)**

2.2.2. Observed Heights

Observed heights or *levelled heights* are products of field observations such as spirit levelling. Levelling is the determination of vertical distances of successive points of a line on the Earth's surface above a datum (Bomford, 1980). The levelled difference *(δL)*

between two benchmarks A and B is usually mistaken as similar to a height difference, H_B - H_A. This may be due to the unnoticeable differences of the values for short circuits. Strictly speaking, the levelled difference from observed heights is not the same as the height difference. That is,

$$\int_A^B dL \neq H_B - H_A \tag{2.22}$$

This is due to the non-parallelism of equipotential surfaces (Vaníček P. , 1976). Heights are uniquely defined through values of gravity (assumed, modelled or observed) as presented in the succeeding sections.

2.2.3. Geopotential Numbers and Dynamic Heights

As a measure of height, the *geopotential number (C)* is defined from,

$$\int_O^A g\, dn = W_O - W_A = C \tag{2.23}$$

where g is gravity, O is a point on the reference geopotential surface, A is a point connected to O by a levelling line, dn is the levelling increment, $\int_O^A g\, dn$ is the difference between the gravity potential at the reference geopotential surface *(W_O)* and the potential at point A *(W_A)* (Heiskanen & Moritz, 1967). C is measured in geopotential units (1 geopotential unit = 1000 gal m) To express this measure as a directly measurable dimension of length, it is divided by some value of gravity (Featherstone & Kuhn, 2006).

Prior to the adoption of geopotential numbers by the International Association of Geodesy (IAG) in 1955, the *dynamic height* system was used. The dynamic height *(H^{dyn})* is usually derived using the normal gravity at 45° latitude (g = γ_{45^o} = 980.6294 gals. Another arbitrary standard latitude may also be used.) and related to the geopotential number through,

$$H^{dyn} = \frac{C}{\gamma_{45^o}} \tag{2.144}$$

Dynamic heights are sometimes used in engineering applications covering large geographic areas and near large bodies of water (Holdahl, 1979). An example of this is the International Great Lakes Datum of 1985 (IGLD85).

Let two points A and B be connected by levelling lines (Figure 2.3). The sum of the levelling increments or simply the measured height difference is given by,

$$\Delta n_{AB} = \sum_{A}^{B} \delta n = \int_{A}^{B} dn \tag{2.25}$$

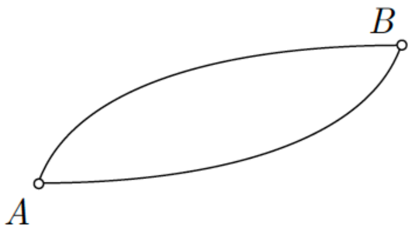

Figure 2.3. Two different levelling lines connecting A and B **(Heiskanen & Moritz, 1967)**.

Introducing a small correction DC_{AB} relates the measured height difference Δn_{AB} and the difference of dynamic heights. DC_{AB} is called the *dynamic correction* and is given by,

$$DC_{AB} = \Delta H_{AB}^{dyn} - \Delta n_{AB} = \sum_{A}^{B} \frac{g - \gamma_0}{\gamma_0} \delta n = \int_{A}^{B} \frac{g - \gamma_0}{\gamma_0} dn \tag{2.26}$$

Since dynamic heights are scaled geopotential numbers, DC_{AB} may also be used to compute the difference in geopotential numbers using,

$$C_B - C_A = \gamma_0 \Delta n_{AB} + \gamma_0 DC_{AB} \tag{2.27}$$

The derivations are presented in the book of Heiskanen & Moritz (1967).

2.2.4. Normal Heights

The actual gravity potential *(W)* can be split as the sum of the *normal potential (U)* and the *disturbing potential (T)*:

$$W = U + T \tag{2.28}$$

Normal heights are independent from a hypothesis of crust density by introducing an approximation to the gravity field that can be computed at any point (Jekeli C. , 2000). Assuming that $W = U$ and $T = 0$, the *normal height (H^{norm}),* or the *Molodensky height*, is the vertical distance from the reference ellipsoid to the telluroid and is expressed mathematically from geopotential numbers as,

$$H^{norm} = \frac{C}{\bar{\gamma}} \tag{2.29}$$

where $\bar{\gamma}$ is the mean normal gravity along the plumb line (Molodensky, Eremeev, & Yurkina, 1962; Heiskanen & Moritz, 1967).

The *telluroid* is defined as the surface "whose height above a geocentric reference ellipsoid is the same as the height of the terrain above a geoid" (Hirvonen, 1960; Vanícék and Krakiwsky, 1986).

Similar to dynamic heights, a *normal correction (NC_{AB})* can be applied to measured height differences (Heiskanen & Moritz, 1967),

$$NC_{AB} = \Delta H_{AB}^{norm} - \Delta n_{AB} = \sum_{A}^{B} \frac{g - \gamma_0}{\gamma_0} \delta n + \frac{\bar{\gamma}_A - \gamma_0}{\gamma_0} H_A^* - \frac{\bar{\gamma}_B - \gamma_0}{\gamma_0} H_B^{norm} \tag{2.30}$$

An experiment showing the difference between orthometric height and the normal height over a small area in the Philippines is given in Chapter 3.

2.2.5. Orthometric Heights

The *orthometric height* is defined as the distance between the geoid and a point measured on the Earth's surface. It is taken positive upward from the geoid. (National Geodetic Survey, 1998). It is mathematically defined as,

$$H^{ort} = \frac{C}{\bar{g}} \tag{2.31}$$

where, $\bar{g}$, refers to the mean gravity along the plumb line between the geoid and the point on the Earth's topographic surface. An absolute determination of $\bar{g}$ requires knowledge of crust density. For computations of orthometric heights, methods based on hypothesis of crust density have been developed in the past.

One of these computation methods uses a mean-gravity value based on an approximation that utilises simplified Poincaré-Prey reduction explained by Helmert (1890). The *Poincaré-Prey gravity reduction* (Fig. 2.4) is a reduction performed from measurable surface gravity to the point within the Earth where gravity is required. The approximation is necessary because of the difficulty in applying the actual curvature of the geopotential surface. More of this issue and a comprehensive derivation of the *Poincaré-Prey* formula can be found in Hoffman-Wellenhoff and Mortiz (2005).

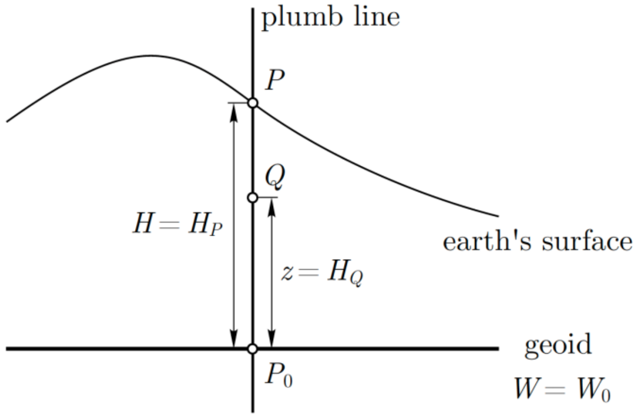

Figure 2.4. Poincaré-Prey reduction. **(Hoffmann-Wellenhoff & Moritz, 2005)**

In this approximation, H^{ort} becomes,

$$H^{ort} = \frac{C}{g + 0.0424H^{ort}} \tag{2.32}$$

where 0.0424 is the factor that holds the normal density $\rho = 2.67$ g/cm^3.

As with the dynamic and the normal heights, an *orthometric correction (OC_{AB})* can be applied to measured height differences (Heiskanen & Moritz, 1967),

$$OC_{AB} = \sum_{A}^{B} \frac{g - \gamma_0}{\gamma_0} \delta n + \frac{\bar{g}_A - \gamma_0}{\gamma_0} H_A^{ort} - \frac{\bar{g}_B - \gamma_0}{\gamma_0} H_B^{ort} \tag{2.33}$$

where $\bar{g}_A$ and $\bar{g}_B$ are mean values of gravity along the plumb lines of A and B and γ_0 is an arbitrary normal gravity constant (Heiskanen & Moritz, 1967).

As the official height system type of the Philippines, orthometric heights (of the Helmert approximation) were used in this thesis (Chapter 3, 4 and 5). More refined methods of approximations were developed and proposed in literature. Niethammer (1932), Mader

(1954), Ledersteger (1955) and more recently, Allister and Featherstone (2001) and Tenzer et al., (2005). Ample information is provided in the listed text.

2.2.6. Normal-orthometric Heights

The *normal-orthometric height* (Fig. 2.5) is the distance along the normal plumbline between a surface called the *quasigeoid* (details in Section 2.3.3) and the point on the surface, *P* (Rapp, 1961). It is computed by using a normal-geopotential number derived from the normal gravity field *(C^N)* in place of the geopotential number *(C)*. Normal gravity *(γ)* is also used in place of actual gravity that yields the formula,

$$H^{norm-ort} = \frac{C^{norm}}{\bar{\gamma}} \tag{2.34}$$

Normal-orthometric heights are simpler to produce because it does not require actual gravity observations. As such, the normal-orthometric height system is used in areas with not enough gravity observations.

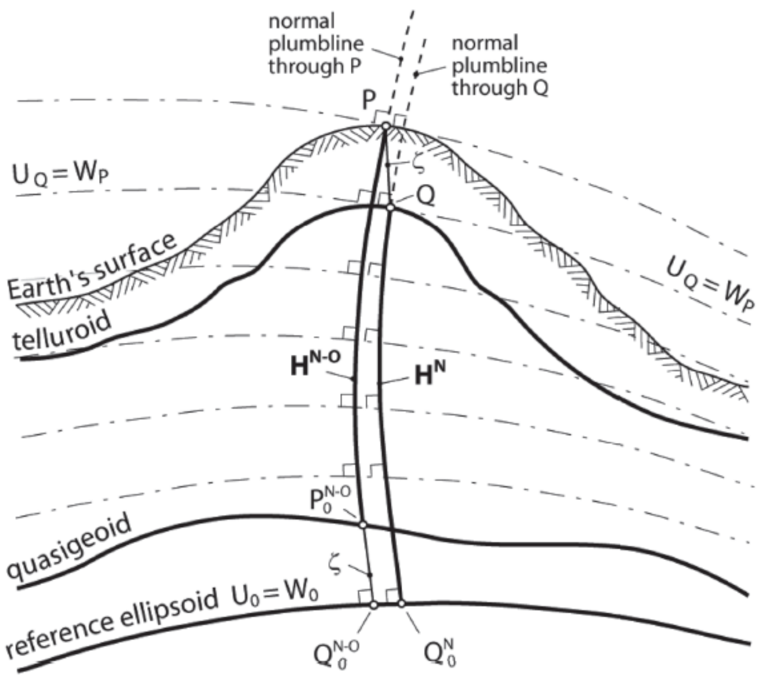

Figure 2.5. The basic geometry for Earth surfaces. The figure shows the comparison between the normal-orthometric height (denoted in source as $H^{N\text{-}O}$) and the normal height (denoted in source as H^N) (Featherstone & Kuhn, 2006)

Applying the *normal-orthometric correction*, NOC_{AB}, yields $H^{norm\text{-}ort}$ from spirit levelling differences (Torge, 2001). Rapp (1961) provided a way to compute for the *NOC* through the relationship,

$$NOC_{AB} = (p_1 \bar{H}_{AB}^{norm-ort} + p_2 B \bar{H}_{AB}^{norm-ort^2} + p_3 C \bar{H}_{AB}^{norm-ort^3}) \emptyset_{AB} \tag{2.35}$$

where

$$p_1 = 2 \sin 2\bar{\phi} \alpha \left[1 + \cos 2\bar{\phi} \left(\alpha - \frac{2\kappa}{\alpha} \right) - 3\kappa \cos^2 2\bar{\phi} \right] Q \tag{2.36}$$

$$p_2 = 2 \sin 2\bar{\phi} \alpha \, t_2 \left[t_3 + \frac{t_4}{2\alpha} + \cos 2\bar{\phi} \left(\frac{3}{2} t_4 + 2\alpha t_3 - \frac{2\kappa}{\alpha} t_3 \right) \right] Q \tag{2.37}$$

$$p_3 = 2\sin 2\bar{\phi}\alpha\, t_2^2\, t_3 \left[t_3 + \frac{t_4}{2\alpha} + \cos 2\bar{\phi}\left(2\alpha t_4 - \frac{2\kappa}{\alpha} t_3\right)\right] Q \tag{2.38}$$

$\bar{H}_{AB}^{norm-ort}$ is the mean normal-orthometric height between benchmarks *A* and *B*; $\emptyset_{AB}$ is the difference between the *A* and *B* latitudes in arc minutes; *Q* is 1 arc minute in radians; $\bar{\phi}$ is the mid-latitude between *A* and *B*; and,

$$\alpha = \frac{\beta}{2 + \beta + 2\epsilon} \tag{2.39}$$

$$\kappa = \frac{-2\epsilon}{2 + \beta + 2\epsilon} \tag{2.40}$$

$$t_2 = \frac{-2\epsilon}{2 + \beta + 2\epsilon} \tag{2.41}$$

$$t_3 = 0.5\left\{1 - \left[1.5f - 1.25\left(\frac{\omega^2 a^3}{GM}\right)\right]\right\} \tag{2.42}$$

$$t_4 = 1 - t_3 \tag{2.43}$$

where *a* is the semi-major axis of the reference ellipsoid (Section 2.3.4); β is the gravity flattening; ϵ is a constant in the normal gravity formula; ω is the angular velocity of the Earth's rotation and *GM* is the geocentric gravitational constant. Normal-orthometric corrections only apply to north-south stretched levelling lines. This is due to the rotational symmetry of the reference ellipsoid (Featherstone & Kuhn, 2006).

Other versions of normal-orthometric corrections exist, such as those found in Bomford (1980), Heck (1995), Amos & Featherstone (2001) as noted by Filmer et al., (2010), and simpler ones such as in Odumosu et al., (2018).

2.2.7. Ellipsoidal Heights

Ellipsoidal heights are referred from the reference ellipsoid. Different definitions of reference ellipsoids may give different ellipsoidal height values over the same point (Featherstone, 1996). Ellipsoidal heights are not directly related to gravity and do not have physical meaning (Featherstone, Dentith, & Kirby, 1998).

The reference ellipsoid representation stems from Isaac Newton's 1687 description of a self-gravitating fluid body in rotation and equilibrium. A "physical" compromise is produced by introducing physical elements to the formation of the reference ellipsoid. This is called *normal ellipsoid*. In other literature, *level ellipsoid* or *equipotential ellipsoid* is used (Vanícék & Krakiwsky, 1986; Torge & Müller, 2012). It is defined by geometric (the semi-major axis, flattening) and independent physical parameters (mass, angular velocity); or other sets of four (4) independent parameters. Though the level ellipsoid contains parameters with physical meaning, it is still a limited reference for physical processes (i.e. determination of the piezometric head.) as the physical parameters are constants that imply homogeneity for a complex Earth.

Ellipsoidal heights *(h)* are commonly derived from Global Navigation Satellite Systems (GNSS) and are related to orthometric heights *(H)* through the geoid *(N)*, using the basic equation,

$$H \approx h - N \tag{2.44}$$

In an ideal set up, Figure 2.6 shows the relationship between two points on the Earth's surface, A and B, related by Equation 2.46,

$$H_B - H_A = h_B - h_A - N_B + N_A \tag{2.45}$$

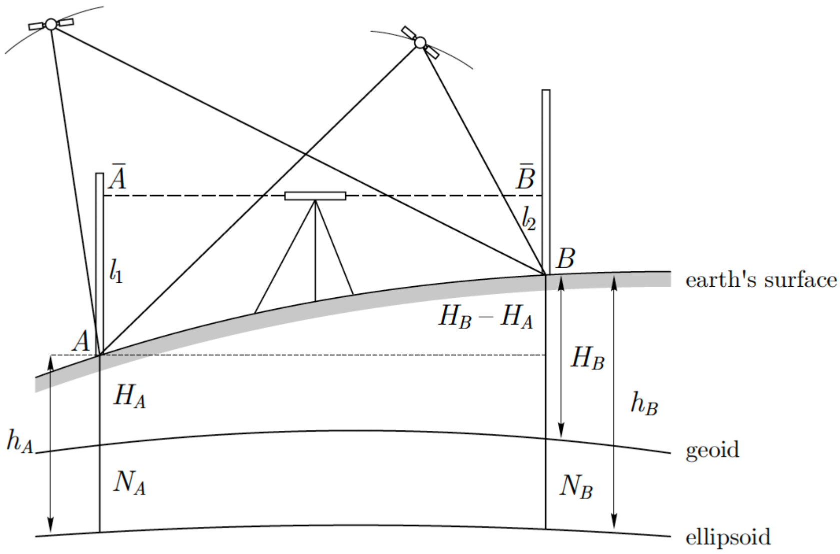

Figure 2.6. GNSS/levelling. **(Hoffmann-Wellenhoff & Moritz, 2005)**

The practical relationship between GNSS-derived ellipsoidal heights and orthometric heights depend on factors such as geometry, the atmosphere and the geoid. The complexities of this relationship is addressed in literature (Featherstone, 2000; Khazrei, Nafisi, Kenyeres, 2016; Amiri-Simkooei & Asgari 2017).

The reader is referred to the published work of Heiskanen and Moritz (1967), Santos et al., (2006), Tenzer et al., (2005), Allister and Featherstone (2001), and Vaníček et al., (1999) for the full mathematical derivations of the different types of gravity-based heights and corresponding approximations.

2.3. Vertical Datums

Height carries a variety of definitions across different scientific disciplines. In Geodesy, height is formally defined as “the distance, measured along a perpendicular, between a point and a reference surface.” (National Geodetic Survey, 1998)

Looking into the history of how man first described the Earth provides an insight into the complexities of height measurement. In the early days, a point on the Earth's surface is referred to as something that can be physically observed. For example, prominent landmarks, easily identifiable land or water features. As our ancestors' understanding of the basic sciences grew, ways to describe the size and the shape of the Earth mathematically through geometry were developed.

One way to categorize the measurement of heights is through the way they are defined. The qualification lies in the reference surfaces: A *gravity-based surface* for the physical heights and a *reference ellipsoid* for the geometric heights. These two heights are of different nature and cannot be substituted for one another.

2.3.1. The Mean Sea Level

Gravity is an observable, however invisible, parameter that gives height measurements physical meaning. A condensed summary on the mathematics of gravity is presented in Section 2.2.1. and in-depth explanations can be found in the foundational textbooks of Heiskanen & Moritz (1967). A demonstration of the use of gravity in height system practice is associated with a surface that has a visible implication in the field. For years, the *mean sea level* (MSL) is the most adopted surface from which physical heights are referred from. The MSL, as a reference, is tied to one (local point MSL) or more (surface MSL) tide gauges at a specified time epoch. It is defined as "the average value of levels observed each hour over a period of at least a year, and preferably over about 19 years, to average over the cycles of 18.61 years in the tidal amplitudes and phases" (Pugh & Woodworth, 2014). 18.61 years is the lunar *nodal period* (Pugh, 1987).

The MSL is mathematically described by,

$$Z_{MSL}(t) = \left(\frac{1}{M}\sum_{1}^{M} Z_{observed}(t)\right) - Z_{tidal}(t) - Z_{residual}(t) \qquad (2.46)$$

where, Z_{MSL} is the MSL as a function of time t and $Z_{observed}$ is the observed sea level in M observations. The time-variable quantity, Z_{tidal}, refers to the *tidal component* described by,

$$Z_{tidal} = A\cos(\omega t - g_t) \tag{2.47}$$

where, A is the oscillation amplitude; ω is the angular speed and; g_t is the phase lag relative to time, t_0.

$Z_{residual}$ refers to the *meteorological residual component* which occurs when a significant episodic tidal event (e.g. storm surge) is described.

The two components satisfy the criteria for statistical independence through the variance relationship,

$$\sum_{n=1}^{M} (Z(n\Delta t) - Z_{MSL})^2 = \sum_{n=1}^{M} Z_{tidal}{}^2(n\Delta t) + \sum_{n=1}^{M} Z_{residual}{}^2(n\Delta t) \tag{2.48}$$

Ideally, the full formula should be applied in the computation of the MSL. It is not clear if the Philippine tidal records considered the tidal component and the meteorological residual component. The author recommends future tide records to reflect the full MSL equations in support of the country's understanding of the sea level situation. The nodal period, in relation to the regression of the moon's nodes, is the conventional period to which height systems are referenced. The averaging period effectively corrects tide fluctuations caused by astronomic forces.

For the Philippines, 8 stations (out of 47) barely fit the ideal 18.61 years as discussed in Chapter 3. Philippine MSL is derived from a long series of hourly observations averaged arithmetically as in the first term of Eq. 2.46. The trend is visualised in Figure 3.2 using a second order polynomial method,

$$f(x) = c_2x^2 + c_1x + b \tag{2.49}$$

In the absence of hourly measurements (as in the case of non-automatic levels), the mean is computed by averaging the *mean high water* (MHW) and *mean low water* (MLW). This method produces the *mean tide level* (MTL). The MTL is often used in the absence of the MSL in practice. The difference between the two becomes distinct for measurements in shallow waters. A study of MSL and its usage in the Philippine context is provided in Chapter 3, Section 3.1.1.

2.3.2. Permanent Tides

Tides play a significant role in defining height systems. Tidal deformation of the Earth is composed of a periodic and a permanent part (Poutanen, Vermeer, & Mäkinen, 1996). The *permanent tide,* discovered by Darwin (1899), is caused by the tide-generating potentials of the Sun and the Moon that is time-independent (Mäkinen, 2009). Permanent tide effects, are found to be low in the polar areas and high in the equatorial areas (Ekman M. , 1989). The permanent tide is treated in three systems: *non-tidal* or *tide-free* system, *mean* system and *zero* system.

In the *non-tidal* or *tide-free* system, the whole tidal effect is treated by tidal corrections that eliminates the permanent tide effect. Instead of using estimates for fluid Love numbers, the effects are treated using the same Love numbers (*h* and *k,* relating radial deformation with disturbing gravity potential) and Shida number (*l,* relating horizontal displacement to potential) as for the time-dependent tide effects. This was the case for old GPS-based coordinates. As a consequence**,** ITRF was in the non-tidal system (Poutanen, Vermeer, & Mäkinen, 1996). In the *mean* system, no Earth tide corrections are applied. The mean geoid is “the potential sum of the gravity field of the Earth with the permanent tidal deformation plus the time independent part of the tide-generating potential of the Sun and the Moon” (Poutanen, Vermeer, & Mäkinen, 1996). In the Philippines, ellipsoidal heights refer to a tide–free system and levelled heights refer to a mean tide system. In 1983, after significant discussions, the IAG recommended the zero tide system (International Association of Geodesy, 1984) to eliminate errors produced by inconsistent tide systems. In the *zero* system, the tide-generating potential is removed but retains the permanent effect.

Ekman (1989) provided a treatment of permanent tides through transformations of gravity, height difference, geoid heights and GNSS heights. Transformations (in μGals) of zero gravity *(g_z)*, mean gravity *(g_m)* and non-tidal gravity *(g_n)* are given by,

$$g_m - g_z = -30.4 + 91.2 \sin^2 \varphi \tag{2.50}$$

$$g_z - g_n = (\delta - 1)(-30.4 + 91.2 \sin^2 \varphi) \tag{2.51}$$

$$g_m - g_n = (\delta)(-30.4 + 91.2 \sin^2 \varphi) \tag{2.52}$$

where φ is the latitude of the station and δ is a permanent tide factor. Transformations of height differences above the zero geoid *(ΔH_z)*, the mean geoid *(ΔH_m)* and non-tidal geoid *(ΔH_n)* between a northern and a southern station are given by (in cm),

$$\Delta H_m - \Delta H_z = 29.6 \left(\sin^2 \varphi_N - \sin^2 \varphi_S\right) \tag{2.53}$$

$$\Delta H_z - \Delta H_n = 29.6\,(\gamma - 1)\left(\sin^2 \varphi_N - \sin^2 \varphi_S\right) \tag{2.54}$$

$$\Delta H_m - \Delta H_n = 29.6\,(\gamma)\left(\sin^2 \varphi_N - \sin^2 \varphi_S\right) \tag{2.55}$$

The corresponding zero geoid heights *(N_z)*, mean geoid heights *(N_m)*, and non-tidal geoid heights *(N_n)* are transformed using the following relationships (in cm),

$$N_m - N_z = 9.9 + 29.6 \sin^2 \varphi \quad (2.56)$$

$$N_z - N_n = k\,(\gamma - 1)(9.9 + 29.6 \sin^2 \varphi) \quad (2.57)$$

$$N_m - N_n = (1 + k)(9.9 + 29.6 \sin^2 \varphi) \quad (2.58)$$

For GNSS heights, subtracting,

$$h' = h\frac{W}{g} \quad (2.59)$$

yields the height of the non-tidal crust above the ellipsoid *(h')*. h in this context is the Love number, usually estimated as 0.62. The height of the mean crust *(h'')* and zero crust above the ellipsoid *(h''')* is identical and is given by,

$$h'' = h''' = h\frac{W}{g} - h\frac{\bar{W}}{g} \quad (2.60)$$

For transformations of GNSS heights, the added relationship is expressed by Ekman as,

$$\Delta h_m - \Delta h_n = \Delta h_z - \Delta h_n = -29.6h\left(\sin^2 \varphi_N - \sin^2 \varphi_S\right) \quad (2.61)$$

Penna et al., (2013) notes the absence of a minus sign in Eq. 2.61 (Eq. 20 in Ekman, 1989).

More details are provided in Chapter 3, Section 3.1.2.

2.3.3. The Geoid and the Quasigeoid

Equipotential surfaces are surfaces on which,

$$W = constant \tag{2.62}$$

The mean sea level of the sea in static equilibrium coincides with an equipotential surface called the *geoid*. Unlike the ellipsoid, the topography of the Earth plays a major factor in the development of the geoid.

The deviation of the mean height of the geometrical ocean surface from the geoid is the *mean dynamic topography* (MDT) (Pail et al., 2014). MDT models can be classified based on the estimation approach, generally determined using oceanographic and geodetic methods (Woodworth et al., 2012).

Filmer et al., (2018) provides a summary of MDT model approaches.

1. Oceanographic approach using numerical ocean models (Menenmelis, Fukumori, & Lee, 2005).
2. Oceanographic approach using sets of *in situ* oceanographic and meteorological measurements for sea surface gradients (Cartwright & Crease, 1963; Amin M. , 1988; Ridgeway, Dunn, & Wilkin, 2002).
3. Geodetic approach using ellipsoidal heights of MSL observations at tide gauges connected to a geodetic reference frame (Woodworth, Gravelle, Marcos, Wöppelman, & Hughes, 2015).
4. Geodetic approach using mean sea surface models from altimetric observations (Jayne, 2006; Andersen & Knudsen, 2009; Bingham, Haines, & Lea, 2014).
5. Combined approach using ocean information as a supplement to altimetric mean sea surface and geoid information (Rio, Mulet, & Picot, 2014).

A demonstration of MDT approaches can be found in Chapter 3, Section 3.1.3.

The *geoid height (N)*, also known as the *geoid undulation*, is the distance from point (*Q)* on the reference ellipsoid to point *(P)* on the geoid, along an ellipsoidal normal. The relationship between the geoidal height and the disturbing potential *(T)* is given by *Bruns formula*,

$$N = \frac{T}{\gamma} \tag{2.63}$$

The geoid can be determined from gravity data through the Stokes formula given by Eq. 2-163b in Heiskanen & Moritz (1967),

$$N = \frac{R}{4\pi\gamma} \iint_{\sigma} \Delta g S(\Psi) d\sigma \tag{2.64}$$

where $S(\Psi)$ is the Stokes kernel

$$S(\Psi) = \sin^{-1}\frac{\Psi}{2} - 6\sin\frac{\Psi}{2} + 1 - 5\cos\Psi - 3\cos\Psi \, ln\left(\sin\frac{\Psi}{2} + \sin^2\frac{\Psi}{2}\right) \tag{2.65}$$

Ψ is the spherical distance, and *dσ* is the surface element of the sphere.

In section 2.2.6., *height anomaly (ζ)* is defined as the difference between the ellipsoidal height *h* and the normal height H^{norm},

$$\zeta = h - H^{norm} \tag{2.66}$$

The surface defined by the height anomaly from the ellipsoid is called the *quasigeoid*. Over the oceans, this surface is analogous to the geoid but the quasigeoid is not a level surface and has no physical meaning. The reader is referred to Jekeli (2000) and Heiskanen & Moritz (1967) for more information.

The fundamental relation for the *geoid-quasigeoid separation* provided by Heiskanen & Mortiz (1967) is,

$$\zeta - N = \frac{\bar{\gamma} - \bar{g}}{\bar{\gamma}} H^{ort} \tag{2.67}$$

where $\bar{\gamma}$ is the mean normal gravity between a point Q_0 on the ellipsoid and the corresponding Q on the telluroid; $\bar{g}$ is the mean gravity along the plumbline between P_0 and P. This equation is essential for geoid-quasigeoid conversions of the GGMs in Chapter 3. Knowledge of this separation is essential not only in the derivation of orthometric and normal heights from GNSS heights but also for consistency in activities involving different height systems (Featherstone & Kirby, 1998).

W_0 defines which of the infinite number of equipotential surfaces is selected as the geoid. The estimation, conventional adoption and realisation of W_0 is a significant component in the development of the International Height Reference System/Frame (IHRS/F) (Sánchez et al., 2016). Some estimations are given in Table 2.1.

Table 2.1 Some estimations of W_0. Different data and treatment produce different estimations of W_0.

Year	**W_0 ($m^2\ s^{-2}$)**	**Reference**
1992	62 636 856.5 ± 3	(Burša, Šíma, & Kostelecky, 1992)
1998	62 636 856.85 ± 1	(Burša et al., 1998)
1995	62 636 856.88 ± 1	(Rapp, 1995)
1999	62 636 856 ± 30	(Burša et al., 1999)
2000	62 636 860.85 ± 30	(Moritz, 2000)
2004	62 636 856.0 ± 0.5	(McCarthy & Petit, 2004)
2007	62 636 854.6 ± 0.5	(Burša et al., 2007)
2007	62 636 853.4	(Sánchez, 2007)
2009	62 636 860 ± 30	(Čunderlík & Mikula, 2009)
2012	62 636 860 ± 30	(Dayoub, Edwards, & Moore, 2012)
2016	62 636 853.4 ± 0.02	(Sánchez et al., 2016)

Burša, Šíma, & Kostelecky (1992) determined the W_0 corresponding to the level surface that minimises the square sum of the dynamic ocean topography approximated over all ocean areas. The geoid is assumed to be equivalent to the displacement of the sea surface relative to a mathematical model of the Earth or the *mean sea surface* (Andersen & Knudsen, 2009). Rapp (1995) equated W_0 with the normal potential *(U)* at the surface of the best-fitting ellipsoid for the TOPEX/Poseidon mean sea surface. Burša et al., (1998) estimated W_0 considering mean sea surface as a difference between a mean sea surface model and a mean dynamic topography model Burša et al., (1999, 2007) also investigated the sensitivity of the estimated W_0 to the tidal reference system of the Earth's gravity field and the secular variations in W_0. Sánchez (2007) considered the global determination of the geoid potential and its sensitivity to global gravity field models (GGM) and concluded the insensitivity of the W_0 estimate to the choice of the GGMs. Dayoub, Edwards, & Moore (2012) estimated W_0 and its change over time by utilizing altimetry-derived mean sea surface models and an independent mean dynamic topography model. The authors concluded that the uncertainty in W_0 is mainly attributed to the selected MDT. Sánchez et al., (2016) determined W_0 based on the scalar-free geodetic boundary value problem (see Section 2.3.5. The Geodetic Boundary Value Problem). The value 62 636 853.4 is adopted by the International Association of Geodesy (IAG) through the IAG resolution number 1 (Drewes, Kuglitsch, Adám, & Rózsa, 2016). As of 6 November 2017, the International Earth Rotation and Reference Systems Service (IERS) updated their accepted value of the W_0 to be consistent to the value adopted by the IAG. The IAG/IERS recommended value was used in Chapter 5. Additional estimations and their corresponding distinctives can be found in Amin, Sjöberg & Bagherbandi (2019).

2.3.4. The Reference Ellipsoid

The ellipsoidal representation stems from Isaac Newton's 1687 description of a self-gravitating fluid body in rotation and equilibrium. Introducing physical elements to the formation of the *reference ellipsoid* (Fig. 2.7), produces the *equipotential ellipsoid* or the *level ellipsoid* (Vanícék & Krakiwsky, 1986; Torge & Müller, Geodesy, 2012). The equipotential ellipsoid was given by Pizetti (1894; 1913) and expounded further by Somigliana (1929; 1930). It is defined by geometric (the semi-major axis, flattening) and independent physical parameters (mass, angular velocity); or other sets of four (4) independent parameters (Torge & Müller, Geodesy, 2012). Though the equipotential ellipsoid contains parameters with physical meaning, it is still a limited reference for physical processes (i.e. Determination of the piezometric head.) as the physical parameters are constants that imply homogeneity for a complex Earth.

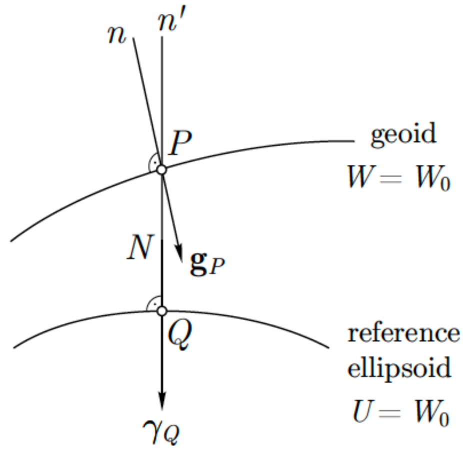

Figure 2.7. The geoid and the reference ellipsoid. **(Hoffmann-Wellenhoff & Moritz, 2005)**

For ellipsoidal heights, the Philippines relies heavily on the World Geodetic System 1984 (WGS84) reference system and generations of its reference frame. Following the WGS84's definition of a right-handed, Earth-fixed orthogonal coordinate system, the origin of the WGS84 reference ellipsoid is the Earth's centre of mass and the rotational axis is the direction of the International Earth Rotation Service Reference Pole. WGS84 and the IERS-recommended GRS80 have subtle differences (Petit & Luzum, 2010).

2.3.5. The Geodetic Boundary Value Problem

The *geodetic boundary value problem* (GBVP) is "mathematically a free-boundary, oblique derivative boundary value problem for the Laplace operator." (Sánso, 2018). The solution of the problem deals with special partial differential equations for the determination of the Earth's shape and gravity field.

Stokes (1849) and Molodensky et al. (1962), proposed foundations that paved way for modern GBVPs (Heiskanen & Moritz, 1967). Observables collected on the Earth's surface and its vicinity have more precise practical considerations due to improved means and methods of observation. To solve the problem, a reference field *(U)* that is generated by the total mass of the Earth and its rotation effects is used. The level ellipsoid is used as a reference field (Heiskanen & Moritz, 1967), as well as other reference surfaces (Grafarend & Ardalan, 1999; Heck, 1989).

Expressing Equation 2.28 as a function of $x = (x_1, x_2, x_3)$ or the coordinates of the point of interest in the three-dimensional space R^3,

$$T(x) = W(x) - U(x) \tag{2.68}$$

The GBVP can be formally expressed as (Wang, 2016),

$$\begin{cases} \Delta T(x) = 0 & x \in R^3 \\ f = g(x) - \gamma(x') & x \in S, x' \in S' \\ T(x) = 0 & |x| \to \infty \end{cases} \tag{2.69}$$

where Δ is the Laplace operator; g is gravity (norm of gravity); γ is normal gravity; f is the difference between the two gravities; S is the surface on which the gravity is given; and S' is the reference surface to be selected.

A *free geodetic boundary value problem* arises if S is unknown. In relation, a *fixed geodetic boundary value problem* is when S is assumed to be known. Forms of the GBVP vary depending on selections of the S and S'. Common GBVP types are described in the Appendix and the most common are described in Wang (2016). GBVPs were used in the vertical connectivity study described in Chapter 3, Section 3.2. and recommendations on the treatment of temporal effects in Chapter 4, Section 4.4.

2.4. Chapter Summary

This chapter has presented definitions of heights, height systems and vertical datums from literature.

The observables (e.g. orthometric heights, GNSS heights, gravity) for the Philippine Height System used in Chapters 3, 4 and 5 is governed by Equations 2.1, 2.7, 2.8, 2.9, 2.10, 2.21, 2.22 and 2.44. Computations in Chapters 3, 4, and 5 follow the IERS Conventions on the permanent tides. Equations 2.50 to 2.61 provides foundations for their treatment, described in Chapter 3, Section 3.1.2. The geodetic boundary value problems (GBVP) used in the vertical connectivity study described in Chapter 3, Section 3.2., the recommendations on the treatment of temporal effects in Chapter 4, Section 4.4. and Sansò's GBVPs in the Appendix were described from Equations 2.28, 2.68 and 2.69. Equations 2.29 and 2.30 for normal heighting is important in the generation of the Helmert orthometric vs normal height experiment found in Chapter 3, Section 3.4. The full formula for the MSL was provided in Equation 2.46. Commentary about Philippine MSL is found in Chapter 3, Section 3.1.1. Geoid-related computations in Chapters 3, 4 and 5 consider equations 2.63, 2.66 and 2.67. The rest of the equations in this chapter provided the mathematical background of the concepts introduced and utilised routinely in the next chapters.

PHS-related evaluations are presented in **Chapter Three: Diagnostic of the Existing Philippine Height System and Philippine Geoid Model**.

Chapter Three

Diagnostic of the Existing Philippine Height System and Philippine Geoid Model

3.1 Local Height Systems

The Philippine Height System (PHS) is a geodetic levelling-based height system. It uses a reference surface that defined by averaging sea level observations at one or more fundamental tide gauges. In its current usage, the term Philippine Height System pertains to the reference system, the reference frame and the datum. This is recommended to be addressed in future professional education campaigns of NAMRIA. The PHS is using orthometric heights. The orthometric height is realised by means of geodetic levelling in combination with gravity reductions. Upon closer investigation of available records, most of the orthometric heights are of the Helmert approximation. There were some instances (usually subcontracted in less developed areas) that recordings of observed/levelled heights were assumed to be orthometric heights. Officially, the PHS is using the MSL fixed in Manila. Practically, the establishment refers to local tide gauge reference benchmarks which produced multiple local height systems.

Until recently, the demand of height systems in the Philippines has been limited to local, practical engineering applications resulting in a localised development of the "national" height system. The unfiltered layout of the level lines of the Philippine is shown in Figure 3.1.

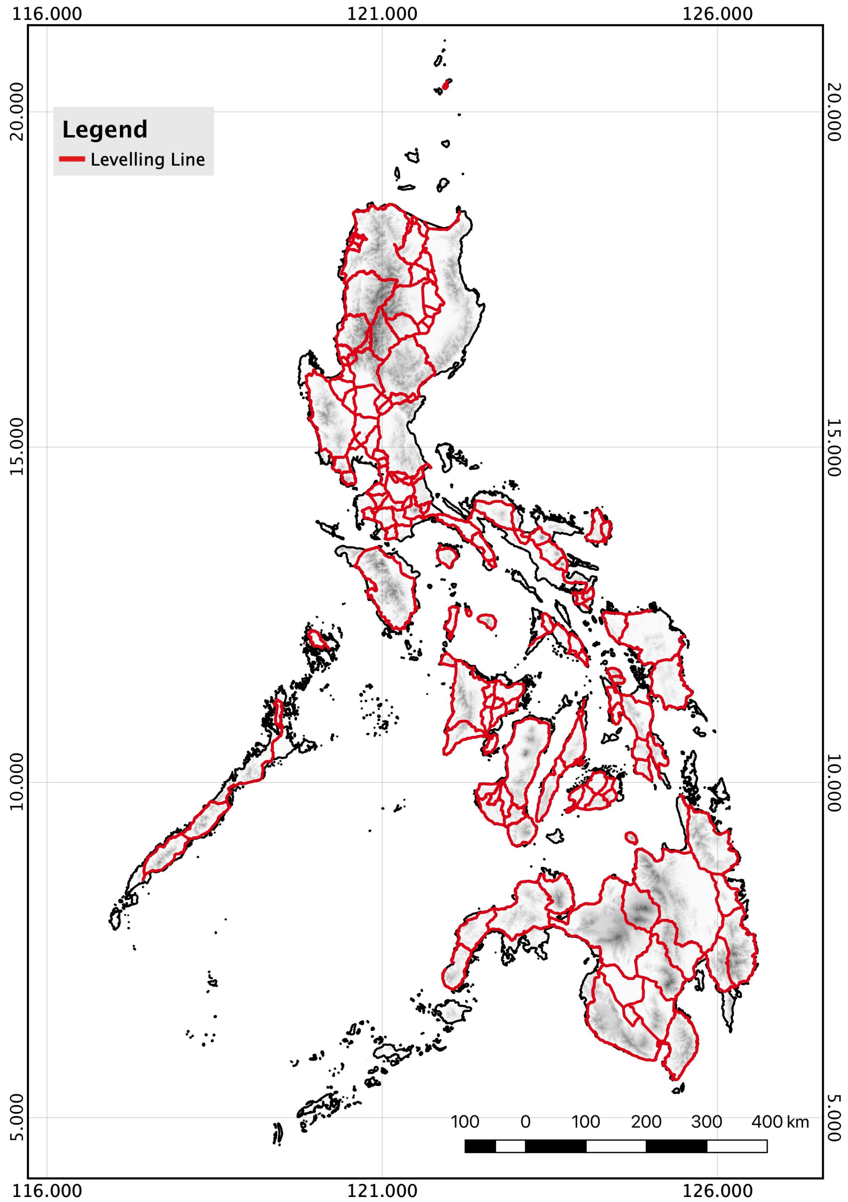

Figure 3.1. A layout of the levelling lines of the Philippines.

3.1.1. Mean Sea Level in the Philippines

The National Mapping and Resource Information Authority (NAMRIA) operates 47 tide stations (National Mapping and Resource Information Authority, 2018). A *primary control tide station* is a tide station at which continuous observations have been made over a minimum period of 18.61 years. The purpose of a primary control tide station is to provide data for computing accepted values of the harmonic and non-harmonic constants essential to tide predictions and to the determination of tidal datums for charting and for coastal and marine boundaries (National Oceanic and Atmospheric Administration, 2000) (Fig. 3.1). A *secondary tide control station* is a tide station that has been observed continuously for more than a year and has its series reduced by comparison with simultaneous tide observations from a primary control tide station (National Oceanic and Atmospheric Administration, 2000). The MSL from the tide stations are instrumental in the formation of local height systems, realised by their corresponding local vertical frames and datums. In the absence of hourly measurements (as in the case of non-automatic levels), the mean is computed by averaging the mean high water (MHW) and mean low water (MLW). This method produces the mean tide level (MTL). In the Philippines, the MTL is used (and often labelled as MSL) in the absence of the MSL in practice.

Figure 3.2. The renovated San Fernando Primary Tide Station. (Latitude: 16.616667, Longitude: 120.3)

Table 3.1 is a list of Philippine tide stations from the NAMRIA Coast and Geodetic Survey Department (CGSD). The mean sea level values in the table are referred to the local tide gauge benchmarks (NAMRIA Coast and Geodetic Survey Department, 2016). The list is provided through the 2016-1011 NAMRIA free-issue licence.

Table 3.1. Local mean sea level of Philippine tide stations (as of October 2016).

Station	**Observation Period for the Tidal Datum Epoch**	**Mean Sea Level** (m)
Manila	1989-2008	2.789
Legaspi	1989-2007	1.810
Davao	1970-1988	2.020
Cebu	1989-2007	1.751
Surigao	1987-2005	2.387
San Jose	1987-2005	1.722
Puerto Princesa	1990-2008	1.785
Real	2008-2014	1.956
Mariveles	2002-2014	2.080
Zamboanga	2008-2014	1.414
Batangas	2007-2012	2.800
Subic	2007-2014	1.432
Cagayan De Oro	2007-2014	2.498
General Santos	2007-2014	1.512
Balanacan	2007-2014	1.701
Guiuan	2007-2014	1.895
Caticlan	2008-2010	1.451
Tandag	2008-2014	1.956
Coron	2008-2015	1.426
Bulan	2012-2015	1.526
Pulupandan	2009-2012	1.417
Balintang	2009-2012	1.555
Calapan	2009-2012	2.068
Mamburao	2009-2010	1.289
Sta. Ana (P. Irene)	2009-2010	1.580
Currimao	2007-2014	1.415
Tagbilaran	2009-2014	2.087
Baler	2009-2014	1.235
Jolo	2009-2014	1.100
Mati	2010-2014	2.640
El Nido	2009-2014	1.611
Virac	2010-2014	1.631
San Jose, Samar	2011-2014	2.142
Iloilo	2011-2013	2.644
Jose Panganiban	2011-2014	1.962
Catbalogan	2010-2015	2.076
Lubang	2011-2014	0.890
Batanes	2011-2012	1.155
Bongao	2011-2015	2.620

Brookes Point	2011-2012	1.684
Dumaguete	2009-2012	1.779
Leyte-Samar	1951-1969	1.548
Masbate	2011-2014	1.822
Odiongan	2012-2015	1.126
Pagadian	2011-2014	1.196
San Carlos	2011-2015	1.548
San Fernando	1984-1989	1.540

For the Philippines, 8 stations (out of 47) barely have records over the 18.61-year nodal period, or the nodal cycle. The nodal cycle is a cycle that captures the seasonal, annual and decadal variations in tide amplitudes (Pugh & Woodworth, 2014). Observing tides through the nodal cycle removes the bias of the tidal amplitude variations from the tide datum computation. An important question is whether the bias brought about by incomplete-cycle tide gauge data would be significant relative to the rapidly accelerating MSL rise or not. Coleman et al., (1979) tested the sensitivity of tide gauge geodetic MDT to shorter time periods. The Philippines, in general, have sea levels that are rising approximately five times more than the global average (Saxena, 2016). Examination of the Manila station's long-term tide gauge data (Fig. 3.2, 145-Manila) shows a positive trend in MSL readings that goes beyond the nodal cycles. From the 1960's up to the present, a rate of approximately 15 mm/yr rise in MSL readings is observed for the Manila station (Perez, Feir, Carandang, & Gonzalez, 1996). Other natural and human-caused contributors were not separated from the readings, therefore, true sea level rise is not isolated in the trend. The use of the readings for reference purposes contains the positive trend regardless of whether the trend contributors are separated or not. 394-Cebu, 522-Legaspi and 537-Davao MSL readings also exhibit a positive trend, but without the aforementioned issues. This means that based on the limited long-term tide gauge data, the bias brought about by incomplete-cycle data would be relatively small compared to the secular changes in MSL for the Philippines.

To give the reader an overview of Philippine tide gauge data, selected tide stations are shown in Figure 3.2.

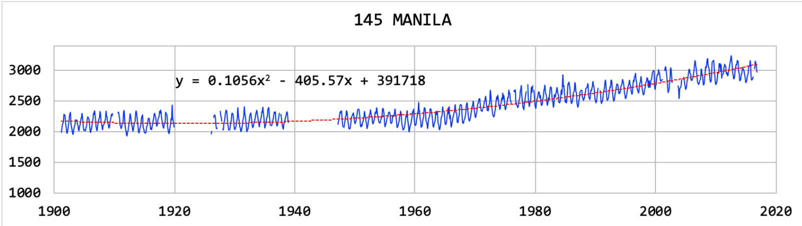
145 MANILA
y = 0.1056x² - 405.57x + 391718
3000
2500
2000
1500
1000
1900
1920
1940
1960
1980
2000
2020

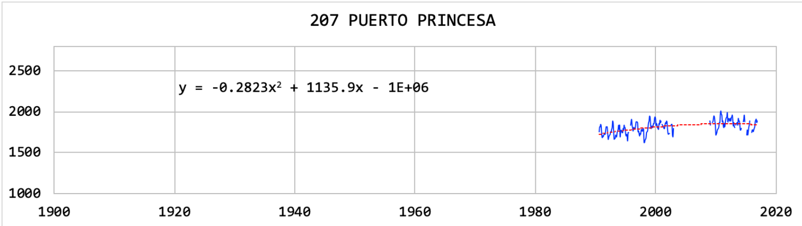
207 PUERTO PRINCESA
y = -0.2823x² + 1135.9x - 1E+06
2500
2000
1500
1000
1900
1920
1940
1960
1980
2000
2020

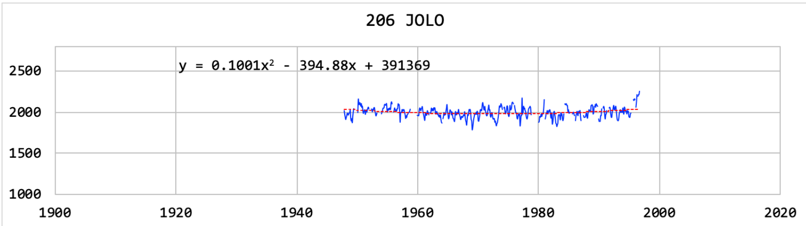
206 JOLO
y = 0.1001x² - 394.88x + 391369
2500
2000
1500
1000
1900
1920
1940
1960
1980
2000
2020

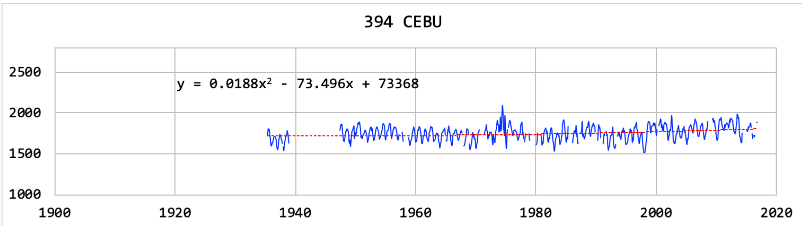
394 CEBU
y = 0.0188x² - 73.496x + 73368
2500
2000
1500
1000
1900
1920
1940
1960
1980
2000
2020

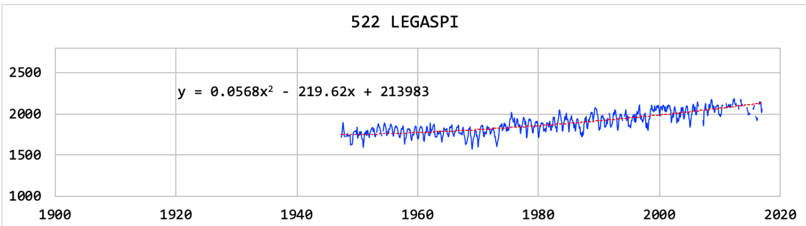
522 LEGASPI
y = 0.0568x² - 219.62x + 213983
2500
2000
1500
1000
1900
1920
1940
1960
1980
2000
2020

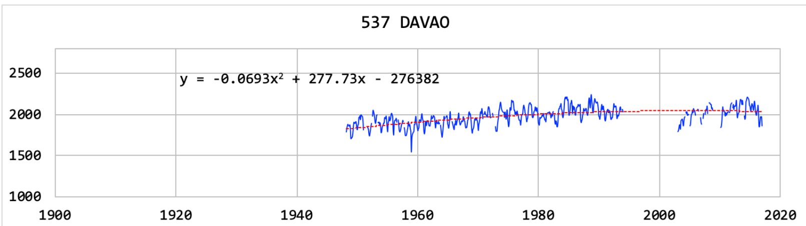
537 DAVAO
y = -0.0693x² + 277.73x - 276382
2500
2000
1500
1000
1900
1920
1940
1960
1980
2000
2020

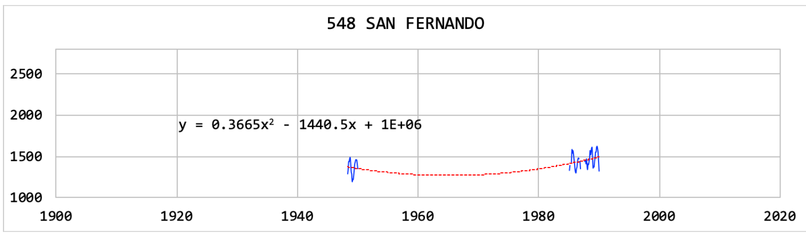
548 SAN FERNANDO
y = 0.3665x² - 1440.5x + 1E+06
2500
2000
1500
1000
1900
1920
1940
1960
1980
2000
2020

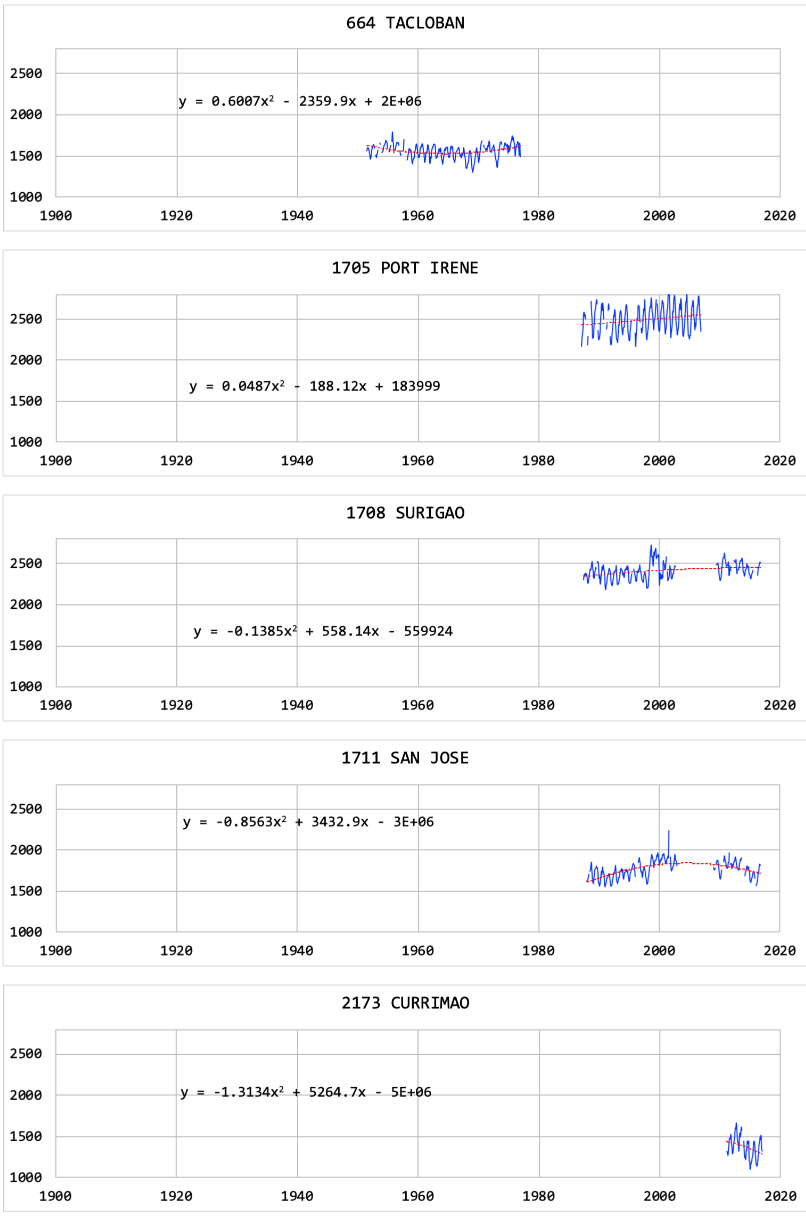

Figure 3.3. Time series of sea level variations registered at selected Philippine tide gauge data (in mm). The red dotted line shows a polynomial-modelled trend.

There is no central repository of tide gauge data in the Philippines. Tide gauge data is released with official permission by the Hydrography Department of NAMRIA, and existing records need to be acquired locally. CGSD provides information pertaining to datums established from tide stations. Multiple official versions of the MSL surface used exist (see Chapter 3, Section 3.1 and Chapter 5, Section 5.1).

Philippine MSL is derived from a long series of hourly observations averaged arithmetically as in the first term of Eq. 2.47. To clarify, observation period is not equal to operation period. An observation period is used to define a tide datum epoch (ideally covering a nodal cycle). An operation period may contain more than one tide datum epoch. For the purpose of time series analysis, the monthly tide gauge data (as in Fig. 3.2) is also referred by the Permanent Service for Mean Sea Level (PSMSL) to a common datum derived using the tide gauge history. The datum, called Revised Local Reference (RLR) is defined arbitrarily to be approximately 7000 mm below MSL (National Oceanography Centre, 2016). Figure 3.2 is a collection of graphs scaled for comparison. The trendlines are visualised in Figure 3.3 using second order polynomials given by Eq. 2.50. The observed local mean sea level rise in Manila (at least, prior to relocation), is overestimated because of deposition from river discharges and other factors such as excessive reclamation (NAMRIA Coast and Geodetic Survey Department, 1987).

The Manila tide station has records beginning from 1901. To facilitate connection to the Manila station, the computed values in Table 3.1 are reckoned traditionally from the TS1901 Datum (NAMRIA Coast and Geodetic Survey Department, 2016; National Oceanography Centre, 2016). As is the case with most of the old tide stations (e.g. Fig. 3.2, 145-Manila, 394-Cebu, 537-Davao), the data is not continuous, homogenous nor physically complete. In February 1981, the Manila station, then named BM4A was destroyed (NAMRIA Coast and Geodetic Survey Department, 1988). It was replaced by BM4B. A section of the physical records lists a different benchmark named GM-1A. Its association with BM4B is unknown to the author. CGSD maintains, however, that BM4B remained as the reference station during that time. In 2002, because of the accuracy issues that were identified previously (i.e. river discharges, reclamation), the tide gauge was moved about a kilometre northwest from the original location (NAMRIA Coast and Geodetic Survey Department, 2003). Post-relocation data is shown in Figure 3.4. The trendline used is linear to approximate the MSL rate of change after the relocation.

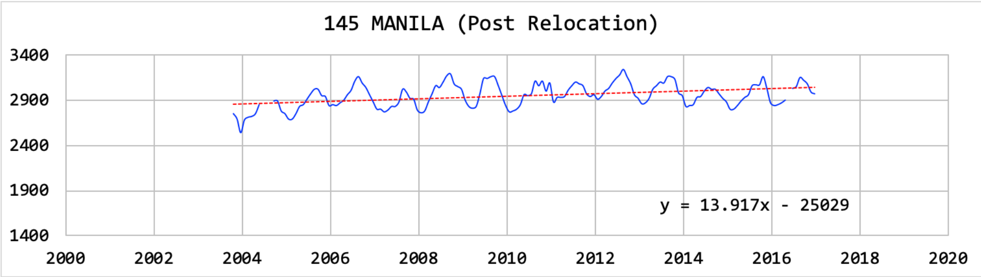

Figure 3.4. Post-relocation data for the Manila tide gauge (in mm).

3.1.2. Treatment of Permanent Tides

For the geopotential models, permanent tide effects are addressed through the geopotential coefficient $\bar{C}_{20}$ (Petit & Luzum, 2010).

$$\Delta\bar{C}_{20}^{zt} = \Delta\bar{C}_{20} - \Delta\bar{C}_{20}^{perm} \tag{3.1}$$

where $\Delta\bar{C}_{20}^{zt}$ is the zero tide geopotential and $\Delta\bar{C}_{20}^{perm}$ is the time-independent part (see Equations 6.6, 6.13 and 6.14 of the IERS Conventions 2010).

The components of the permanent displacement are given by (Eq. 7.14a and 7.14b of the IERS Conventions 2010),

$$Radial: [-0.1206 + 0.0001P_2\,(\sin\phi)]P_2(\sin\phi) \tag{3.2}$$

$$Transverse: [-0.0252 - 0.0001P_2\,(\sin\phi)]\sin 2\phi \tag{3.3}$$

where P_2 is (3sin^2 ϕ - 1)/2 and ϕ is the latitude.

Astronomic correction to precise levelling invariably sets orthometric heights to the zero tide system. The corrections, however, were applied later to local levelling data as the correction was presumed to be only applied for a very large region. The process of astronomic correction is detailed in the text of Jensen (1950).

The author illustrates that inconsistencies in the treatment of permanent tide systems (Chapter 2, Section 2.3.2) can yield discrepancies in corresponding heights (Tenzer, Vatrt, Abdalla, & Dayoub, 2011). Over the Philippines, Figure 3.5 shows that the discrepancies for physical heights can yield up to ~10 cm in the lower latitudes.

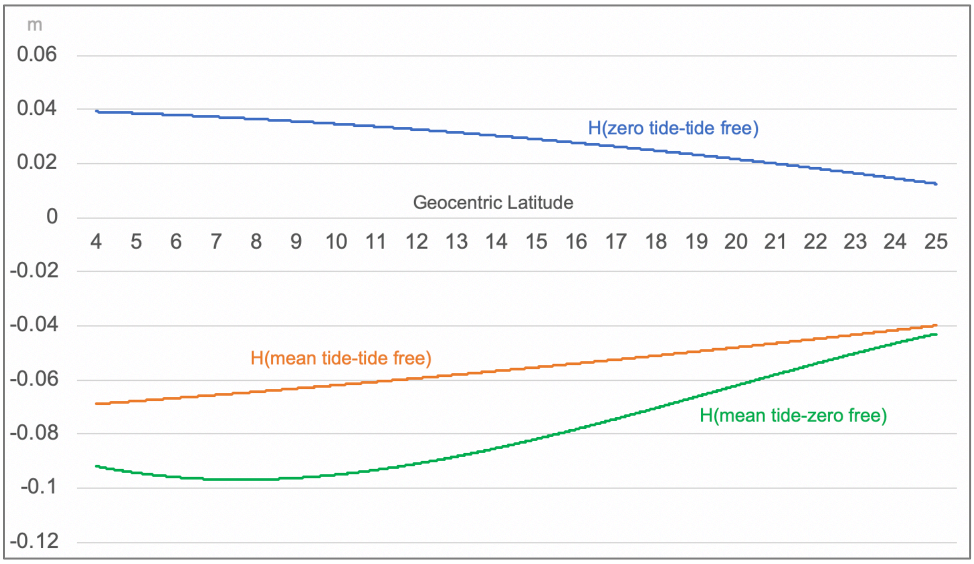

Figure 3.5. Tide system differences over the Philippines. $k = 0.3$ and $h = 0.6$ tidal Love numbers were assumed for this graph (in m).

3.1.3. Mean Dynamic Topography of the Philippines

The definition and the modelling of the *mean dynamic topography* (MDT) is provided in Chapter 2, Section 2.3.3. Modern MDT models make use of satellite altimetry *mean sea surface* (MSS) and gravimetric geoid model differences (Andersen & Knudsen, 2000). A preferred method of producing this information is through the use of tide gauges with GNSS observations through attached receivers or field campaigns. In terms of spatial coverage, however, tide gauge stations do not provide complete coverage. The models used and computed in this study provide more insight on the spatial behaviour of mean dynamic topography.

The DTU10 MDT (Andersen & Knudsen, 2010), VM500-ph MDT (Vianna, Menezes, & Chambers, 2007) and a RADS-derived MDT (RADS-ph) were compared with GNSS-geoid MDTs.

The DTU10 MDT (Fig. 3.6) is an update of the DNSC2008 MDT (Andersen & Knudsen, 2009) which uses the DTU10 mean sea surface and the EGM2008 global geoid model (Pavlis, Holmes, Kenyon, & Factor, The development and evaluation of the Earth Gravitational Model 2008 (EGM2008), 2012). Observation epoch is 1993-2009. Original model is in the mean tide system. The MDT was smoothed with a 75-km half-width Gaussian filter (Featherstone & Filmer, 2012).

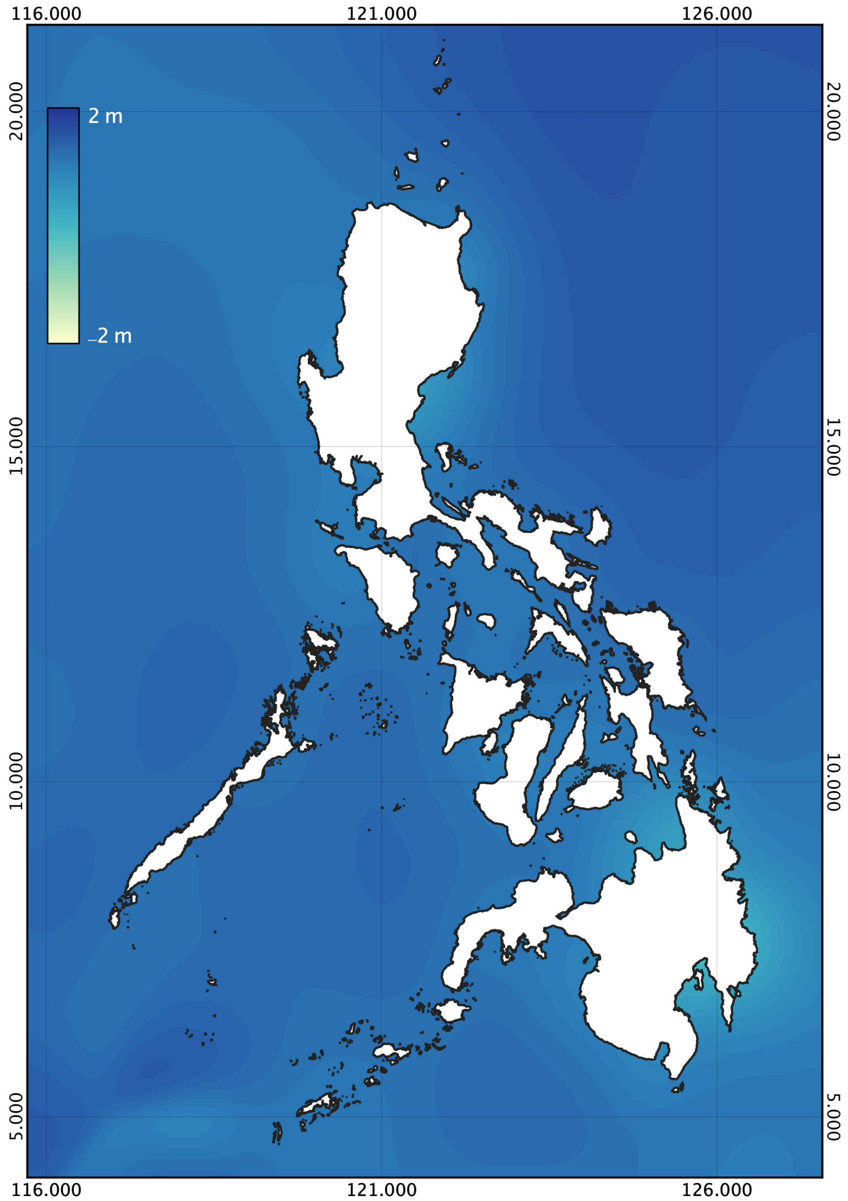

Figure 3.6. DTU10 Mean Dynamic Topography **(Andersen & Knudsen, 2009)**.

VM500 is a high-resolution satellite-only MDT constructed originally for the South Atlantic Ocean (Vianna, Menezes, & Chambers, 2007) and replicated over the Philippines (VM500-ph. Fig. 3.7). It is developed by the differencing of the GRACE Gravity Model 02 (Tapley et al., 2005) based on data from April 2002 to December 2003 from the multi-mission MSS field GSFCMSS00 (1993–1998) (Wang, 2001). An adaptive filter based on singular spectrum analysis (SSA) expansions was also applied to the model (Vianna, Menezes, & Chambers, 2007).

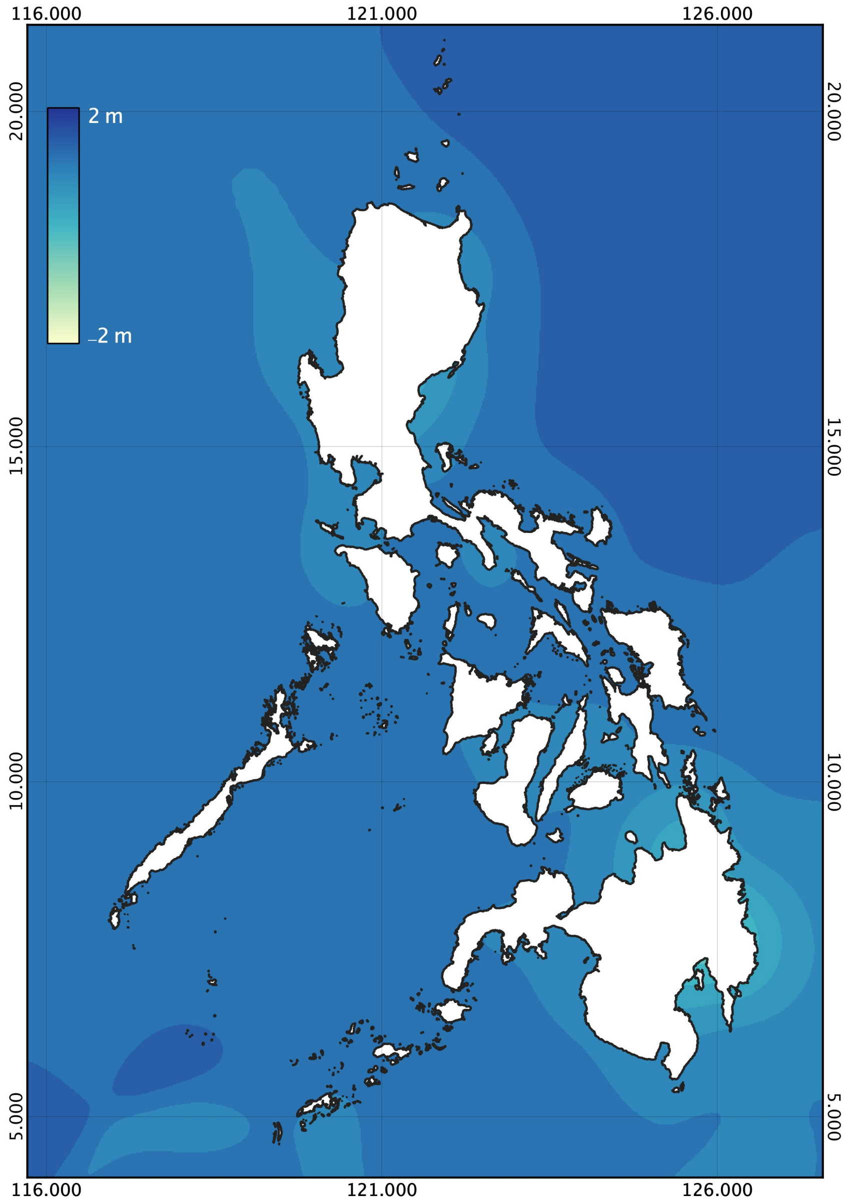

Figure 3.7. VM500-ph Mean Dynamic Topography.

In this study, an MDT (RADS-ph. Fig. 3.8) was constructed based on the datasets from TUDelft's radar altimeter database system (RADS) (Scharroo et al., 2012) for comparison. Saral, JASON-1, JASON-2, CryoSat-2 and Envisat-1 was utilised and processed in a similar manner to the method of Abazu et al., (2017). Error reduction is introduced through a crossover minimization process in the combination of various altimeter data (van Gysen & Coleman, 1997). The sea level anomalies and sea surface heights were acquired from RADS for local mean sea surface computations.

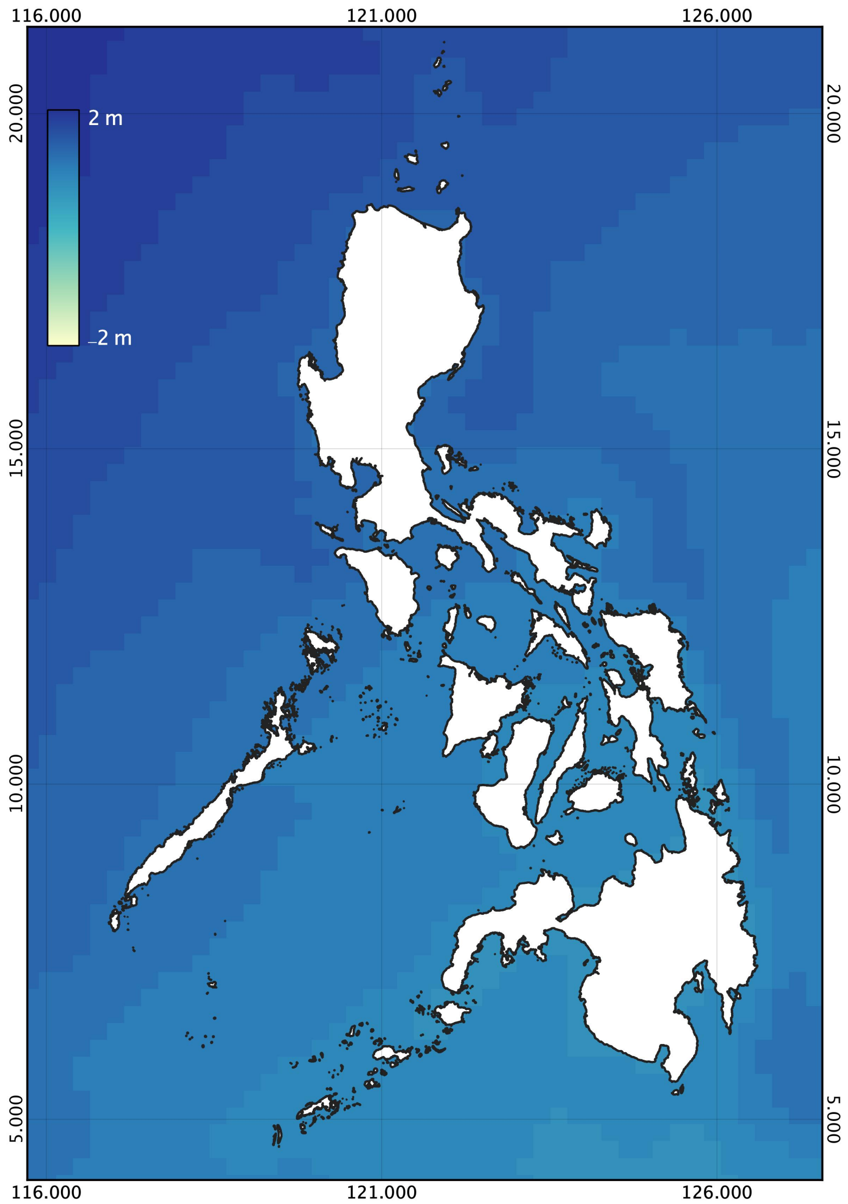

Figure 3.8. RADS-ph Mean Dynamic Topography.

The computed DTU10, VM500-ph and RADS-ph modelled MDT for each tide gauge station is presented in Figure 3.9. The MDTs for the tide gauge stations are computed relative from zero at the Manila station.

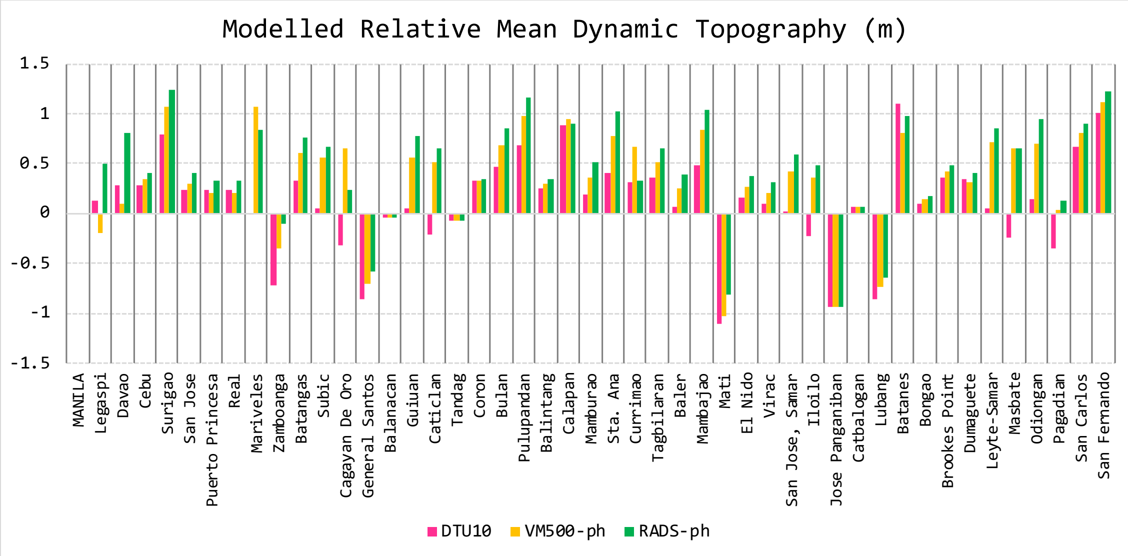

Figure 3.9. Modelled MDT relative to MANILA (in m).

The GNSS-geoid MDTs were computed by subtracting two recently computed Philippine geoids (PGM2016.66 and the previously recommended EIGENGL05C) from the ellipsoidal height of the local tide gauge bench mark, then subtracting the height of the tide gauge benchmark above local MSL at the tide gauge as in Featherstone & Filmer (2012) (Fig. 3.10). The variety of epochs for all observed values were not considered in the computations.

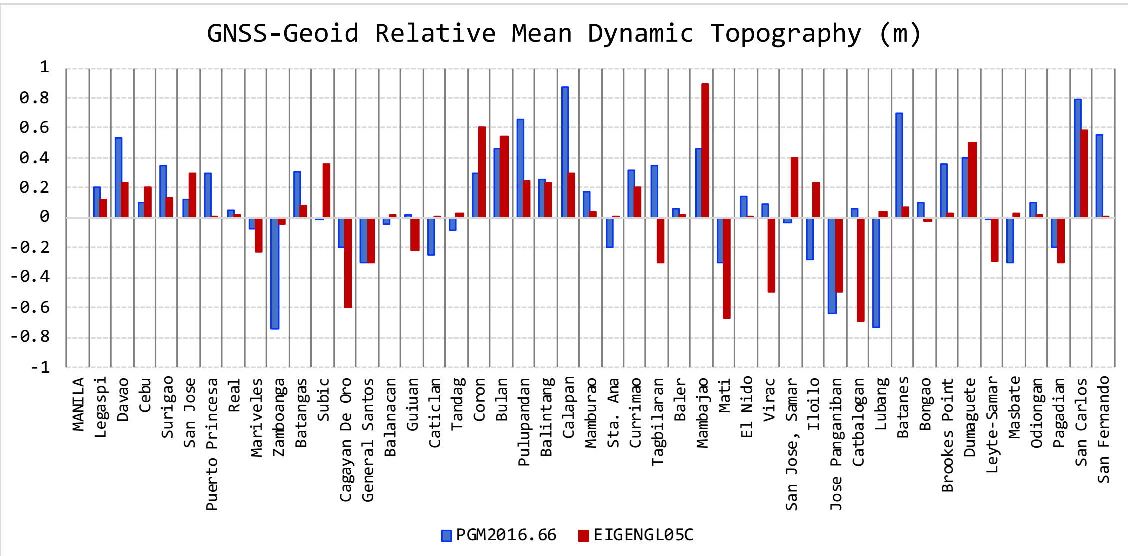

Figure 3.10. GNSS-Geoid MDT Relative to MANILA (in m).

Figures 3.11 to 3.13 show vertical trends inferred from GNSS positioning, tide gauge registrations and satellite altimetry at provided tide gauges. For Figure 3.13, sea surface heights were provided by DTU Space (Andersen & Knudsen, 2009).

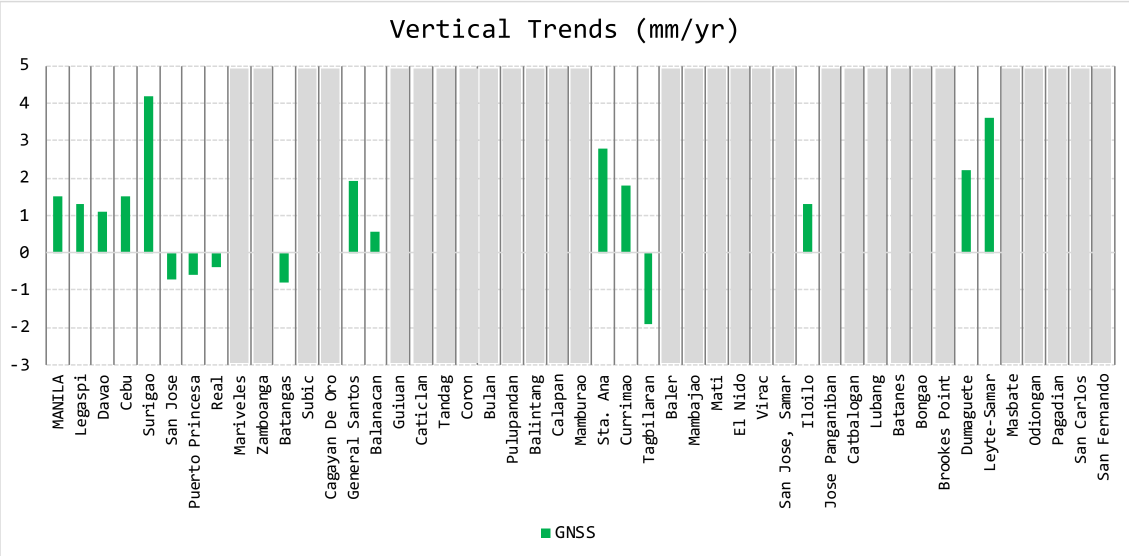

Figure 3.11. Vertical trends inferred from GNSS positioning (in mm/yr). Grayed columns are stations that does not have sufficient information for the computation of the trend.

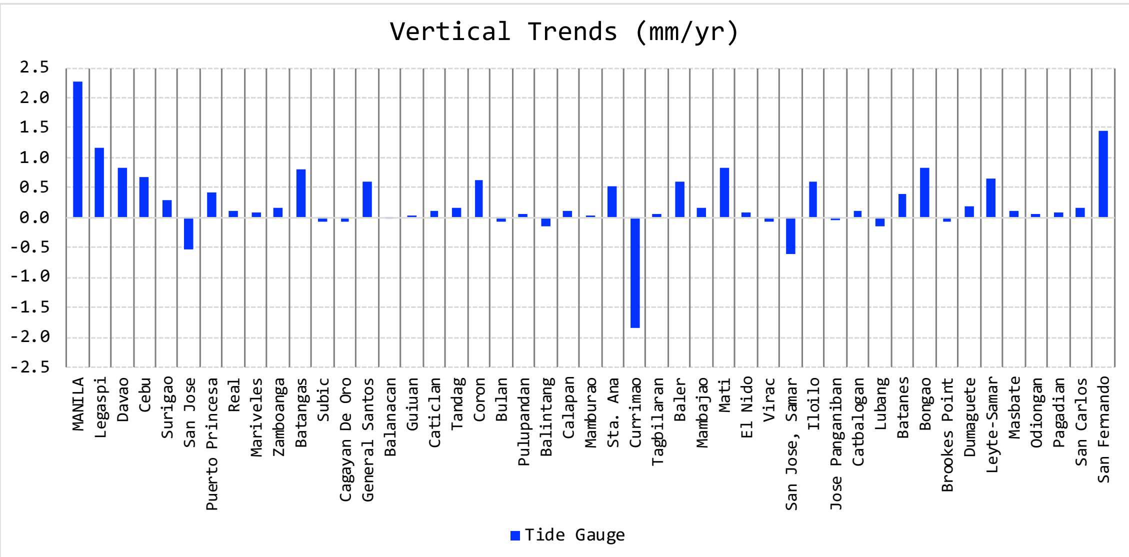

Figure 3.12. Vertical trends inferred from tide gauge registrations (in mm/yr).

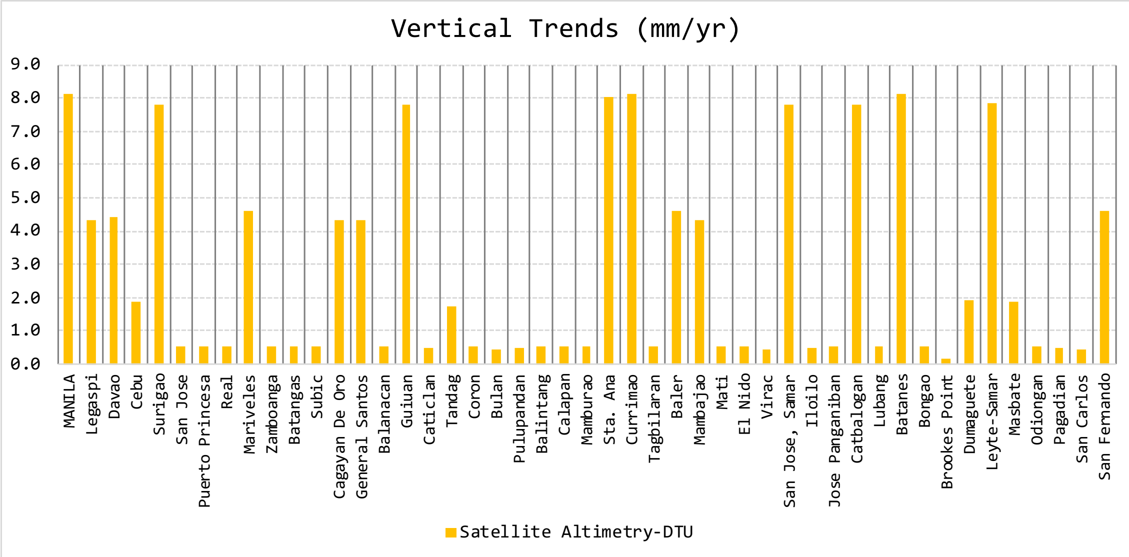

Figure 3.13. Vertical trends inferred from satellite altimetry (in mm/yr).

The computations of GNSS-PGM2016.66 generally agrees (difference < 0.5m) with EIGENGL05C. The largest discrepancies are computed in the Mindanao area (Davao, Cagayan de Oro, General Santos, Calapan, Mambajao, Mati, Pagadian). DTU10 and RADS-ph are multi-mission MDTs that uses satellite and terrestrial data. VM500-ph is based on satellite-only data. The differences highlight the improvement that recent, "in situ" data provides in the MDT development. All the tide gauges of NAMRIA are located in the coastal areas where the MDT is influenced by local effects. Satellite altimetry can be used to infer the MDT in areas that do not currently have tide gauge stations (such as isolated islands), but sufficiently precise measurements at present is not possible (Ihde et al., 2017). The establishment of offshore tide gauge stations is recommended for future development.

3.2. Vertical Connectivity

The Philippines, being an archipelagic country (Fig. 3.14. More detail was provided in Chapter 1, Section 1.2.1.1), has a complex multiple local height system problem. Because it is not possible to run levelling networks directly over large bodies of water, heights are referred locally for engineering applications. This produced multiple local height systems. In the Philippines, the local height systems are referred to reference points and surfaces that are not consistent in definition and characteristics. Though Philippine MSL is rising in general, this was not observed for all tide stations. 1711-San Jose and 2173-Currimao, for example, have MSL readings that shows a negative trend. The development rate and integrity of the local height systems also vary depending on the area covered because of the difference in terrain, environment, socio-economic factors etc. The development history of the PHS was summarised in this section, giving the reader an indication of the way historical, natural and operational challenges affects the PHS. Additional details are provided in Chapter 5.

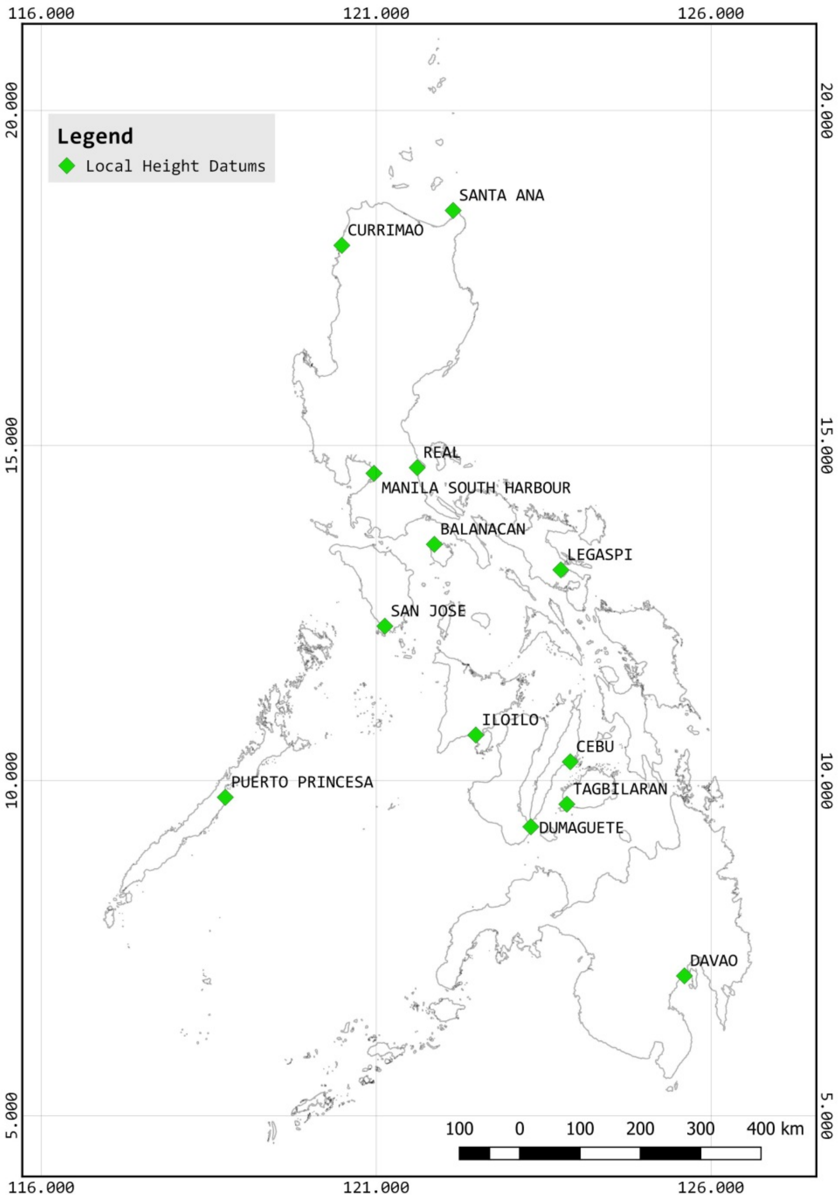

Figure 3.14. Location of tide gauge stations used to define the proposed Philippine local height datums.

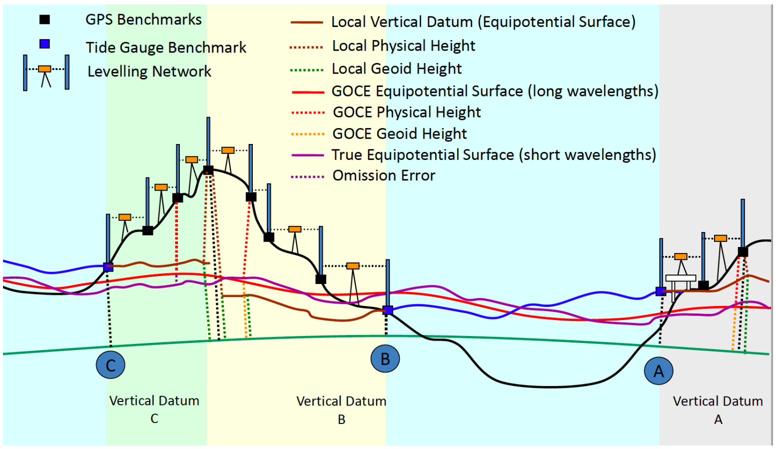

Figure 3.15. An illustration of a multiple height datums scenario defined by respective vertical datums and methods to connect them. **(Gruber T. , 2013)**

The multiple height datums problem can be approached in two ways (UP Training Center for Applied Geodesy and Photogrammetry, 2009):

1. Through the selection of a global reference surface. The approach was described in literature by Sánchez (2017), Ihde & Sánchez (2005), Gruber, and Gerlach & Haagmans (2012) (Fig. 3.15, as an example, illustrates the use of a global surface represented by GOCE).
2. Through the unification of the local height systems.
   a. *Direct Method Unification.* Using levelling and gravimetric data of each tidal benchmarks defining the local height systems. This is challenging for archipelagos and is not possible for areas that are separated by large bodies of water (Lopez, 2014; Ihde & Sanchez, 2005).
   b. *Indirect Method Unification.* Providing a solution to the geodetic boundary value problem (GBVP). This requires a combination of precise geometric heights (from GNSS), orthometric heights and geoid determination (Paringit & Paringit, 2015; Amos & Featherstone, 2008)

In 2009, a local height datums connection study was carried out by the University of the Philippines (UP) in collaboration with the NAMRIA through the NAMRIA-UP Research and Development in Support of the Implementation of the Philippine Reference System of 1992 (PRS92) Project. The NAMRIA-UP Collaboration is made within the umbrella program of improving the PRS92 (2007-2010) that includes the establishment of new geodetic infrastructure such as GNSS benchmarks and an assessment of the status of the PRS92 over 15 years after its formation (UP Training Center for Applied Geodesy and Photogrammetry, 2009; Paringit, Ventura, & Isada, 2009). For the NAMRIA-UP PHS assessment, two geoid height datasets were used: N_{Grav} datasets from the Natural Resources Management Development Project (NRMDP) and $N_{GNSS/levelling}$ datasets from NAMRIA. Ideally N_{Grav} should have been taken from the gravimetric geoid model. However, since the original datasets cannot be recovered, N_{Grav} values were geometrically interpolated from the geoid map published in the NRMDP report. $N_{GNSS/levelling}$ data was derived from the NRMDP-established GNSS stations and pre-1990s NAMRIA levelling data. The author notes that both of the datasets are not up to date and contain errors due to the age and differences in observation epochs. These errors were included in the differences of the values of GNSS/levelling datasets from the NRMDP and the more recent GNSS/levelling data from NAMRIA. Differences in ellipsoidal heights between the two datasets range from 0.041 metres to 4.395 metres and differences in orthometric heights range from 0.001 metres to 30.583 metres (Paringit, Ventura, & Isada, 2009).

The following is a summary of the methods and circumstances of the PRS92 height datum connectivity study (UP Training Center for Applied Geodesy and Photogrammetry, 2009; Paringit, Ventura, & Isada, 2009):

1. Substitutions were made in cases where the fundamental tide station cannot be occupied directly by GNSS methods. The nearest existing GNSS benchmark was adopted as the fundamental station for that zone.
2. Some local height systems have stations that were established with a large distance from the fundamental stations or other tide gauges.
3. The project established additional stations. Ellipsoidal heights were derived from GNSS, and orthometric heights were approximated through levelling observations and gravity corrections. It is assumed that the orthometric heights refer to the same datum as that of the provided datasets.
4. A network scheme for long baselines observation was designed, consisting of 4 points.
5. The US Federal Geodetic Control Committee standards and procedure were adopted for the GNSS and levelling observations.

6. GNSS measurements were processed using the GAMIT baseline processing software and GLOBK used to filter results.
7. Permanent tides were not considered.

Least squares adjustment of $h - H - N$ was carried out on both the NAMRIA and NRMDP datasets. Ideally, the NAMRIA dataset should complement the NRMDP dataset in the computation of the vertical datum separation matrix.

The potential difference between the two fundamental stations is given by (Heiskanen and Moritz, 1967)

$$C_{AB} = W(A) - W(B) = \int_{A}^{B} g dH \approx \sum_{i} g_i \Delta n_i \tag{3.4}$$

where A and B are fundamental stations; Δn_i is the leveled height increments; g_i is the gravity value; i is the benchmark.

This method cannot be utilised if the datum zones are separated by a large body of water. Amos and Featherstone (2008) proposed several methods to solve this but the indirect method of datum unification by Rummel and Teunissen (1988) was utilised by NAMRIA-UP for Tables 3.2 and 3.3, primarily because of the quality of the data required by the said method. The matrix is a tabulation of vertical datum differences between two local height systems represented as the difference between their respective benchmarks (Rummel & Teunissen, 1988),

$$y = \frac{C_{i+1}}{g_{i+1}} - \frac{C_i}{g_i} \tag{3.5}$$

However, because of the undocumented errors for both datasets and the adoption of both as official records, separate matrices were produced for both datasets (UP Training Center for Applied Geodesy and Photogrammetry, 2009).

The computation results of the 2009 NAMRIA-UP Project are shown in Tables 3.2 and 3.3,

Table 3.2. Vertical datum separation matrix (in metres) using NRMDP data (as of 1991). **(Paringit & Paringit, 2015)**

NRMDP 1991	*Manila*	*Legaspi*	*Cebu*	*Davao*	*San Jose*	*P.Prinmcesa*	*Real*	*Dumaguete*	*Tagnilaran*	*Sta. Ana*	*Currimao*	*Iloilo*	*Balanacan*
Manila	0												
Legaspi	+ 0.748	0											
Cebu	+ 2.539	+ 1.791	0										
Davao	+ 1.755	+ 1.007	- 0.784	0									
San Jose	+ 1.574	+ 0.826	- 0.966	- 0.181	0								
P.Princesa	+ 5.498	+ 4.750	+ 2.959	+ 3.743	+ 3.924	0							
Real	+ 0.775	+ 0.026	- 1.765	- 0.980	- 0.799	- 4.723	0						
Dumaguete	+ 1.437	+ 0.689	- 1.102	- 0.318	- 0.137	- 4.061	+ 0.662	0					
Tagbilaran	+ 3.374	+ 2.625	+ 0.834	+ 1.619	+ 1.800	- 2.124	+ 2.599	+ 1.937	0				
Sta. Ana	- 2.502	- 3.250	- 5.041	- 4.257	- 4.076	- 8.000	- 3.277	- 3.939	- 5.876	0			
Currimao	- 0.105	- 0.853	- 2.644	- 1.860	- 1.679	- 5.603	- 0.880	- 1.542	- 3.479	+ 2.397	0		
Iloilo	+ 2.905	+ 2.157	+ 0.366	+ 1.150	+ 1.332	- 2.593	+ 2.131	+ 1.468	- 0.468	+ 5.407	+ 3.010	0	
Balanacan	+ 1.320	+ 0.572	- 1.220	- 0.435	- 0.254	- 4.178	+ 0.545	- 0.117	- 2.054	+ 3.822	+ 1.425	- 1.585	0

Table 3.3. Vertical datum separation matrix (in metres) using NAMRIA data (as of 2009).
(Paringit & Paringit, 2015)

NAMRIA 2009	*Manila*	*Legaspi*	*Cebu*	*Davao*	*San Jose*	*P.Prinmcesa*	*Real*	*Dumaguete*	*Tagnilaran*	*Sta. Ana*	*Currimao*	*Iloilo*	*Balanacan*
Manila	0												
Legaspi	+ 3.09	0											
Cebu	+ 5.72	+ 2.629	0										
Davao	+ 7.51	+ 4.419	+ 1.790	0									
San Jose	+ 0.95	- 2.141	- 4.769	- 6.559	0								
P.Prin.	+ 3.90	+ 0.812	- 1.816	- 3.606	+ 2.953	0							
Real	+ 2.33	- 0.760	- 3.388	- 5.179	+ 1.381	- 1.572	0						
Dum.	+ 4.34	+ 1.249	- 1.380	- 3.170	+ 3.390	+ 0.437	+ 2.009	0					
Tagb.	+ 7.95	+ 4.862	+ 2.234	+ 0.444	+ 7.003	+ 4.050	+ 5.622	+ 3.613	0				
Sta. Ana	- 2.75	- 5.847	- 8.475	- 10.27	- 3.706	- 6.659	- 5.087	- 7.096	- 10.71	0			
Currimao	- 1.69	- 4.788	- 7.416	- 9.206	- 2.647	- 5.600	- 4.028	- 6.037	- 9.650	+ 1.059	0		
Iloilo	+ 5.19	+ 2.107	- 0.521	- 2.311	+ 4.248	+ 1.295	+ 2.867	+ 0.858	- 2.755	+ 7.954	+ 6.895	0	
Balan.	+ 2.28	- 0.809	- 0.348	- 5.228	+ 1.331	- 1.622	- 0.050	- 2.058	- 5.672	+ 5.037	+ 3.978	- 2.917	0

The following are the study's significant findings and recommendations (Paringit, Ventura, & Isada, 2009):

1. Further research is required to reconcile the differences between the NRMDP published data and the NAMRIA data. The resolution of the differences in ellipsoidal heights will achieve this goal.

2. Since the assessment study was done almost 20 years after the NRMDP-produced Philippine Geoid Model (referred to as PGM1991 in this thesis to distinguish from later versions of the PGM) was produced, the authors suggested that the geoid be updated using more recent measurements.
3. The number and distribution of datum zone stations relative to the fundamental stations influence the accuracy of the estimations. The NAMRIA-UP study supports the adoption of the 50-kilometre cap size computed by the team of Kearsley & Ahmad (1995).
4. The availability of levelling and gravity profile connecting two datums zones will improve the validation of the height differences in a single landmass.

3.3. Development History of the Philippine Geoid Model

In Chapter 1 (Section 1.2.1.4), it was mentioned that the first geoid (Fig. 3.17) for the Philippines was computed through the NRMDP. Geoid heights computed from this geoid was projected to have relative accuracies between 6 parts per million (ppm) to 10 ppm. The terrestrial gravity data used were acquired in the early 1960's. As mentioned in Chapter 1, 77 gravity base stations supplemented by 300 gravity stations were used. Through the NRMDP, a series of gravity profiles were measured to validate and supplement the data for the geoid model computation (Paringit, Ventura, & Isada, 2009). Satellite altimetry data was calculated from Geos-3 and SeaSat radar altimetry using least squares collocation (Kearseley & Ahmad, 1995). 111 GNSS/levelling stations from NAMRIA were used to compare the GNSS/levelling geoid height values with the gravimetric geoid height values.

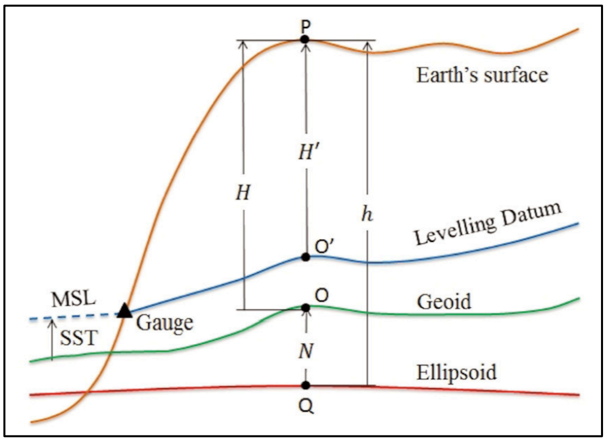

Figure 3.16. Illustration showing the relationship of physical, ellipsoidal and geoid heights **(Véronneau & Huang, 2016)**.

Issues caused by insufficient information on the errors of measured heights (detailed in Kearseley & Ahmad (1995), Ahmad et al., (1993) and Paringit et al (2009)) made the development of the PGM1991 challenging. As part of the 2009 NAMRIA-UP study, Lopez (2014) evaluated the PGM1991 (Fig. 3.17) and concluded that it is not accurate enough to enable conversion between GNSS heights and orthometric heights with sufficient accuracy due to the limited number of gravity measurements in the NRMDP. The recommendation then was a study on the geoid model that will include densified gravity measurements as well as an analysis of the suitability of local geoid models (i.e. one geoid model for each island or island group. Fig. 3.18 is an example).

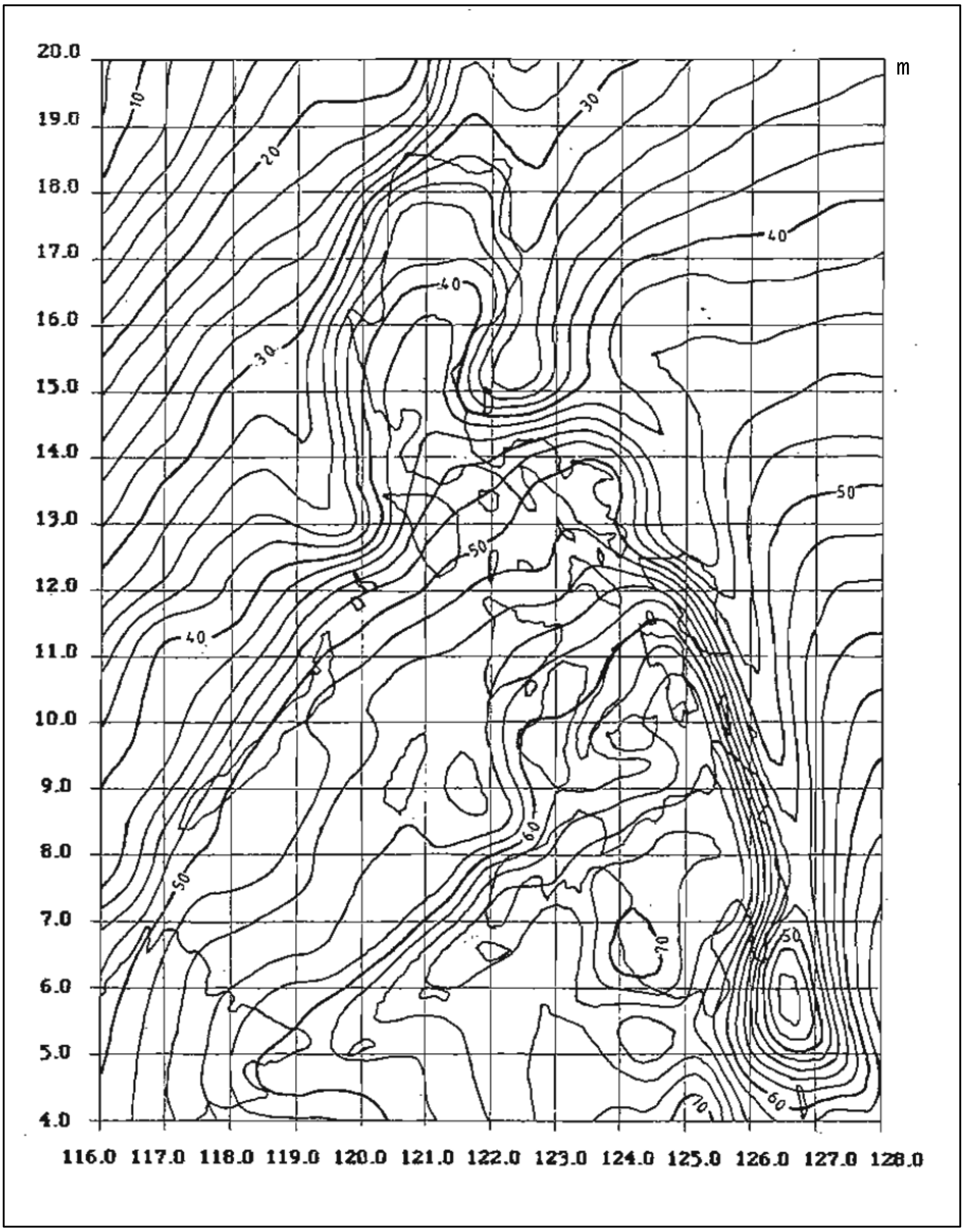

Figure 3.17. The OSU89A-based Philippine Geoid of 1991 (PGM1991) in m. **(Australian International Development Assistance Bureau , 1987)**

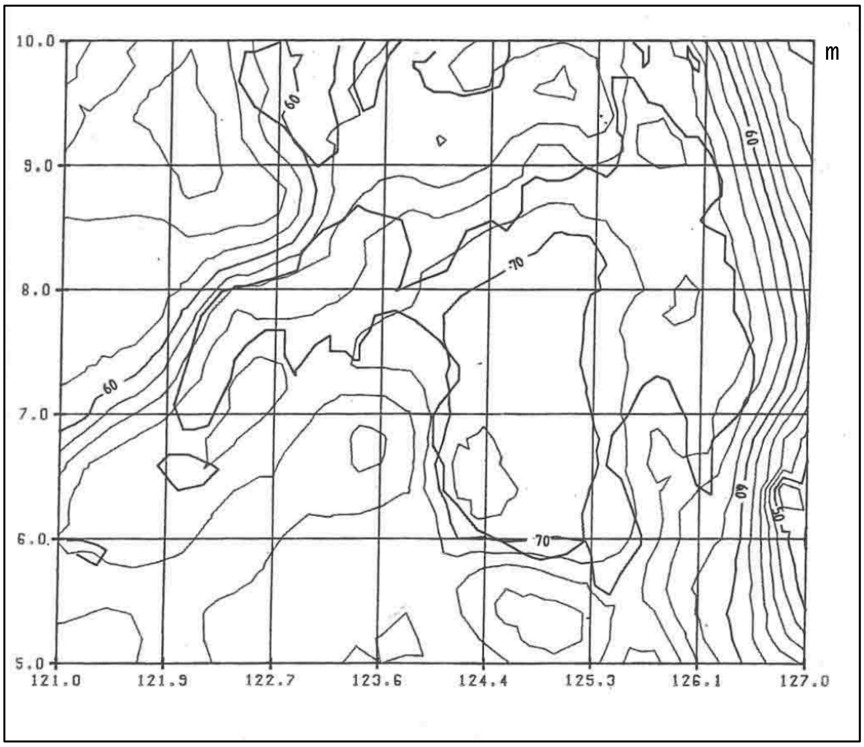

Figure 3.18. Detailed Geoid Map of the Mindanao Island (PGM1991) in m. **(Australian International Development Assistance Bureau , 1987)**

In line with the above recommendations, Lopez (2014) made a comparative statistical analysis of the fit of the computed geoidal heights derived from global geopotential models (GGM). The following GGMs were assessed:

1. *Earth Gravitational Model 1996 (EGM96)* (Lemoine et al, 1998). A geopotential model created by the (then) National Imagery and Mapping Agency (NIMA), the NASA Goddard Space Flight Center (GSFC), and the Ohio State University (OSU). This model has a composite solution complete up to degree and order 360.
2. *Geopotential Model Improvement using POCM4B Dynamic Topography Information (PGM2000A)* (Pavlis, Chinn, Cox, Lemoine, & Smith, 2000). Not to be confused with the Philippine Geoid Model that has a similar acronym, PGM2000A is a derivative of EGM96. It maintains the orbit and land geoid modelling performance of EGM96, while improving its marine geoid modelling capability.
3. *Earth Gravitational Model 2008 (EGM2008)* (Pavlis, Holmes, Kenyon, & Factor, The development and evaluation of the Earth Gravitational Model 2008 (EGM2008), 2012). An updated model in the EGM series, the EGM2008 contains

spherical harmonic information complete up to a degree and order 2159 (which equates to a resolution of 10').

4. *GRACE Gravity Model (GGM02C)* (Tapley et al., 2005). GGM02 is based on a collection of Gravity Recovery and Climate Experiment (GRACE) and is available in two forms: GGM02S (n = 160, GRACE only) and GGM02C (n = 200, constrained with terrestrial gravity data).
5. *European Improved Gravity Model of the Earth CG03C (EIGEN-CG03C)* (Förste et al., 2005). This model uses 376 days of Challenging Minisatellite Payload for Geophysical Research and Application (CHAMP)/GRACE data (up from the 200 days used for the previous EIGEN-CG01C model).
6. *European Improved Gravity Model of the Earth GL05 (EIGEN-GL05)* (Förste et al., 2008). This model (n = 260) was released by GFZ Potsdam and GRGS Toulouse and is derived from a combination of GRACE and LAGEOS satellite tracking data with surface gravity data.

The author notes that there is no mention of permanent tide effects in the Lopez assessment. The study area for the Lopez assessment is Manila and adjacent cities. The following is a summary of the methods and circumstances of the assessment (Lopez, 2014):

1. The number of co-located GNSS/levelling stations on the study area and the entirety of the country was limited (Fig. 3.19).
2. Project duration and financial constraints limited the evaluation method to the occupation of level benchmarks (3rd order or higher) with carrier phase differential GNSS receivers, instead of ideally connecting GNSS stations by differential levelling.
3. Statistical measures were computed for each GGM from the geoid height values (GNSS/levelling and GGM).
4. EGM2008 was applied up to degree and order 360 only due to hardware restrictions at that time.

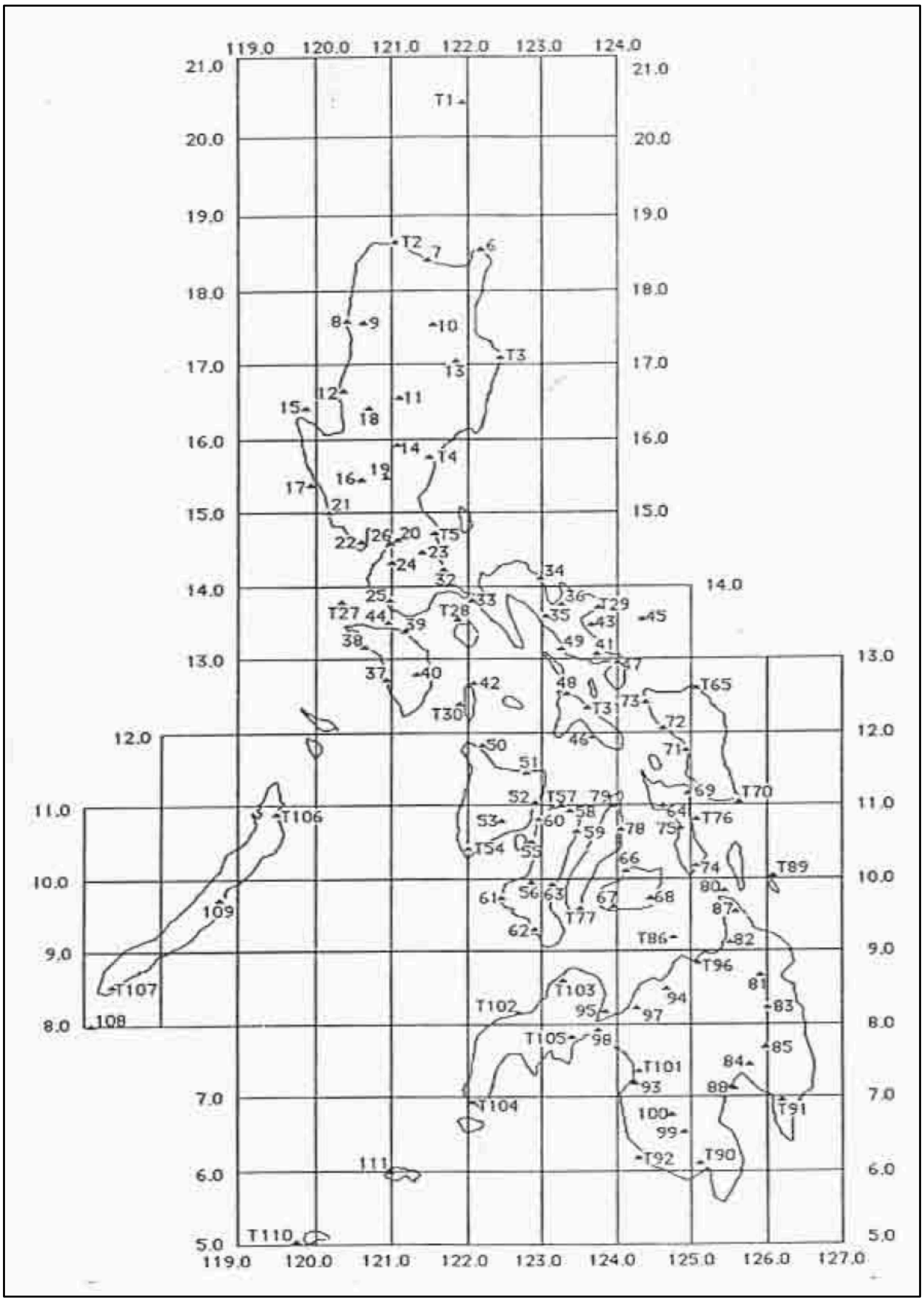

Figure 3.19. GNSS control points available for the NRMDP. **(Australian International Development Assistance Bureau , 1987)**

24 baselines in the NCR were used for relative verification (Featherstone W. , 2001). Table 3.4 shows that EIGEN-GL05C produced the best fit among the assessed GGMs. However, in terms of standard deviations, EGM2008 produced the lowest measure (~17 ppm).

Table 3.4. Difference between $N_{GNSS/levelling}$ and N_{GGM}. **(Lopez, 2014)**

Location	EGM96	EIGEN CG03C	EIGEN GL05C	GGM02C	OSU89A	PGM2000 A	EGM2008
Marilao	2.33	0.173	-0.143	-0.141	1.385	2.204	1.953
Navotas	1.665	-0.492	-0.871	-0.701	0.796	1.538	1.41
Cavite	2.39	0.864	0.243	0.633	1.702	2.259	2.249
Roxas Blvd	2.242	0.422	-0.074	0.237	1.545	2.112	2.063
Lawton	2.087	0.11	-0.334	-0.05	1.338	1.958	1.87
Ayala	2.442	0.664	0.196	0.501	1.81	2.312	2.216
Paranaque	2.294	0.644	0.098	0.403	1.632	2.163	2.137
Pasig	2.865	1.225	0.84	1.199	2.449	2.735	2.528
Fairview	2.788	0.904	0.6	0.892	2.214	2.66	2.321
UPD	2.631	0.749	0.391	0.693	2.036	2.502	2.253
Bicutan	2.527	0.942	0.453	0.746	1.991	2.396	2.283
Mean	2.388	0.564	0.127	0.401	1.718	2.258	2.092
Stdev	0.334	0.483	0.474	0.537	0.459	0.334	0.296

Table 3.5. Relative verification of GGMs. (in ppm) **(Lopez, 2014)**

Relative verification of GGMs (in ppm)							
	egm96	**eigen-cg03c**	**eigen-gl05c**	**ggm02c**	**osu89a**	**pgm2000a**	**egm2008**
Max	74.884	94.737	98.058	106.350	94.650	74.819	63.552
Min	5.703	2.226	11.073	11.022	13.395	5.567	2.221
Mean	37.548	50.901	53.689	56.518	50.854	37.498	30.642
Stdev	20.096	25.252	24.742	26.723	23.641	20.098	17.698

In 2014, NAMRIA and DTU-Space developed the preliminary Philippine Geoid Model (PGM2014. Fig. 3.20) using data from an airborne gravity survey, marine satellite altimetry gravity data, NAMRIA's 1st and 2nd order terrestrial gravity data GOCE and the 15” Shuttle Radar Topography Mission (SRTM) digital terrain models (DTM). In its development, it was shifted by a constant amount of +80 cm to estimate the average geoid offset relative to an updated GNSS/levelling dataset in Metro Manila (Forsberg, Olesen, Gatchalian, & Ortiz, 2014).

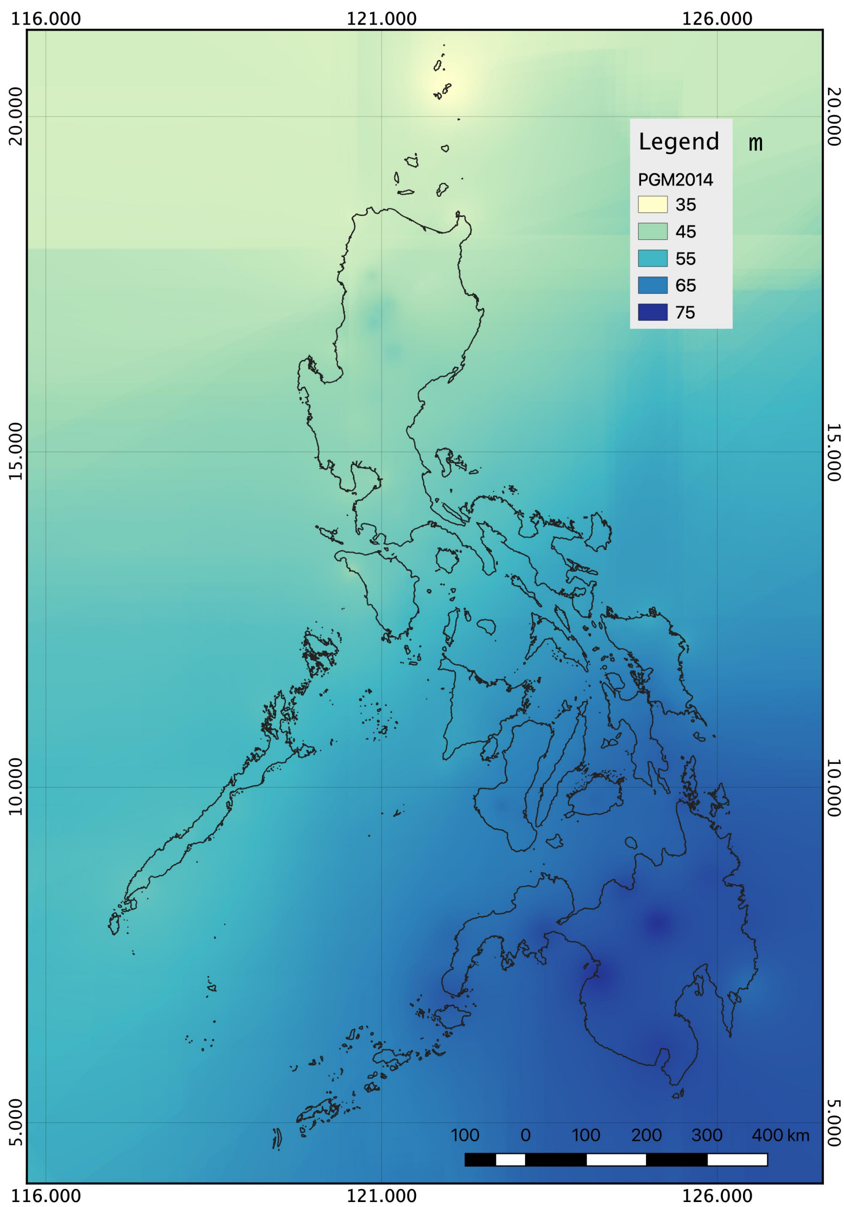

Figure 3.20. The Philippine Geoid Model 2014 (in m).

3.4. Assessment of the Philippine Geoid Model (PGM2016.66) and Global Geopotential Models over the Philippines

The release of PGM2014 motivated the need for an independent assessment that is performed in this study. Ground-observed geodetic data (GNSS/levelling) was used to assess GGM-based geoids and the PGM2014. Using geoid heights from GNSS/levelling to assess external geoid models is a proven method applied to a number of geodetic studies (Gruber T. , 2009; Hirth, 2011; Hirt, Gruber, & Featherstone, Evaluation of the first GOCE static gravity field models using terrestrial gravity, vertical deflections and EGM2008 quasigeoid heights, 2011; Gruber, Visser, Ackermann, & Hosse, 2011). The practical goal of the assessment is to help NAMRIA to prioritise areas that are in need of improvement in terms of reobservations and/or densification. This assessment is also useful as a preliminary process for the estimation of vertical datum parameters discussed in Chapter 5.

367 GNSS/levelling benchmarks (GNSS and levelling data were taken between 2015 and 2016) and 1261 gravity points (multiple campaigns from 2009 to 2015) were provided for use through the Mapping and Geodesy Branch of NAMRIA. Supplementary assessment points were sourced from the CGSD and UP. These datasets are independent from the computation of the GGM or the PGM2016.66. The 2016.66 version of the PGM was evaluated to minimise errors due to epoch differences with the available ground observations. PGM2016.66 improved PGM2014 by incorporating additional GNSS and gravity measurements (Gatchalian, 2016). Figure 3.21 shows the difference between PGM2016.66 and PGM2014.

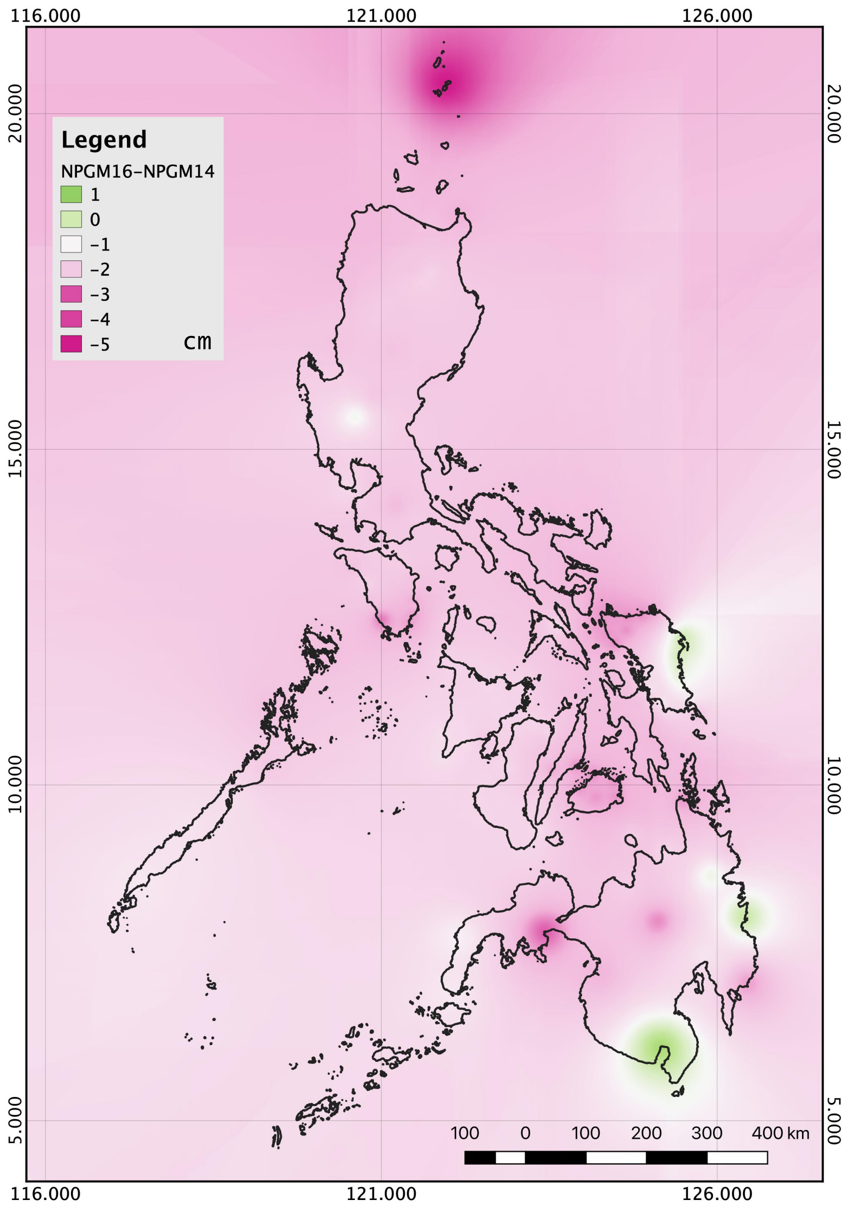

Figure 3.21. Differences in geoid heights between PGM2016.66 and PGM2014 (in cm).

GGMs over the past 15 years (until June 2017. Table 3.6) were examined to identify the GGMs that can yield the most meaningful results and interpretation from the evaluation. GGMs up to max degree were computed and geoid heights were evaluated at the German Research Centre for Geosciences (GFZ) Potsdam facility and downloaded through the IAG's International Centre for Global Earth Models (ICGEM) Service (Barthelmes & Köhler, 2016; Ince et al., 2019). The assessment was made in the zero tide system, using the GRS80 ellipsoid according to IERS conventions (Petit & Luzum, 2010). A full mathematical explanation of spherical harmonic coefficients for the geoid is available through the "*Definition of Functionals of the Geopotential and Their Calculation from Spherical Harmonic Models*" of Franz Barthelmes (2013). Geoid height differences and root-mean-square (RMS) variations of the gravity anomalies are then computed. Omission errors (Gruber T. , 2009) were not treated in the assessment. It is assumed that the order of magnitude of the omission error is lower than the actual gravity signal (Vergos, Grigoriadis, Tziavos, & Kotsakis, 2014; Papanikolaou & Papadopoulos, 2015)

Table 3.6. Assessed global geopotential models. *S* is for satellite (e.g., GRACE, GOCE, LAGEOS), *A* is for altimetry, and *G* for ground data (e.g., terrestrial, shipborne and airborne measurements) (Barthelmes & Köhler, 2016) Entries in yellow are GGMs shortlisted for further examination.

Model	Year	Max Degree	Data	Reference
HUST-GRACE2016s	2016	160	S(GRACE)	(Zhou et al., 2016)
ITU_GRACE16	2016	180	S(GRACE)	(Akyilmaz et al., 2016)
ITU_GGC16	2016	280	S(GOCE), S(GRACE)	(Akyilmaz et al., 2016)
EIGEN-6S4 (v2)	2016	300	S(GOCE), S(GRACE), S(LAGEOS)	(Förste & Bruinsma, 2016)
GOCO05C	2016	720	A, G, S	(Fecher, Pail, & Gruber, 2015)
GGM05C	2015	360	A, G, S(GOCE), S(GRACE)	(Ries et al., 2015)
GECO	2015	2190	EGM2008, S(GOCE)	(Gilardoni, Reguzzoni, & Sampietro, 2016)
GGM05G	2015	240	S(GOCE), S(GRACE)	(Bettadpur et al., 2015)
GOCO05s	2015	280	S	(Mayer-Gürr et al., 2015)
GO_CONS_GCF_2_SPW_R4	2014	280	S(GOCE)	(Gatti, Reguzzoni, Migliaccio, & Sanso, 2014)
EIGEN-6C4	2014	2190	A, G, S(GOCE), S(GRACE), S(LAGEOS)	(Förste et al., 2014)
ITSG-GRACE2014s	2014	200	S(GRACE)	(Mayer-Gürr, Zehentner, Klinger, & Kvas, 2014)
ITSG-GRACE2014k	2014	200	S(GRACE)	(Mayer-Gürr, Zehentner, Klinger, & Kvas, 2014)
GO_CONS_GCF_2_TIM_R5	2014	280	S(GOCE)	(Brockmann et al., 2014)

GO_CONS_GCF_2_DIR_R5	2014	300	S(GOCE), S(GRACE), S(LAGEOS)	(Bruinsma et al., 2014)
JYY_GOCE04S	2014	230	S(GOCE)	(Yi, Rummel, & Gruber, 2013)
GOGRA04S	2014	230	S(GOCE), S(GRACE)	(Yi, Rummel, & Gruber, 2013)
EIGEN-6S2	2014	260	S(GOCE), S(GRACE), S(LAGEOS)	(Rudenko et al., 2014)
GGM05S	2014	180	S(GRACE)	(Tapley, Flechtner, Bettadpur, & Watkins, 2013)
EIGEN-6C3stat	2014	1949	A, G, S(GOCE), S(GRACE), S(LAGEOS)	(Förste et al. , 2012)
Tongji-GRACE01	2013	160	S(GRACE)	(Chen, Shen, Zhang, Chen, & Hsu, 2015)
JYY_GOCE02S	2013	230	S(GOCE)	(Yi, Rummel, & Gruber, 2013)
GOGRA02S	2013	230	S(GOCE), S(GRACE)	(Yi, Rummel, & Gruber, 2013)
ULux_CHAMP2013s	2013	120	S(CHAMP)	(Weigelt et al., 2013)
ITG-GOCE02	2013	240	S(GOCE)	(Schall, Eicker, & Kusche, 2014)
GAO2012	2012	360	A, G, S(GOCE), S(GRACE)	(Demianov, Sermyagin, & Tsybankov, 2012)
EIGEN-6C2	2012	1949	A, G, S(GOCE), S(GRACE), S(LAGEOS)	(Förste et al., 2012)
DGM-1S	2012	250	S(GOCE), S(GRACE)	(Farahani et al., 2013)
GOCO03s	2012	250	S(GOCE), S(GRACE)	(Mayer-Gürr et al., 2012)
GIF48	2011	360	A, G, S(GRACE)	(Ries, Bettadpur, Poole, & Richter, 2011)
EIGEN-6C	2011	1420	A, G, S(GOCE), S(GRACE), S(LAGEOS)	(Förste et al., 2011)
EIGEN-6S	2011	240	S(GOCE), S(GRACE), S(LAGEOS)	(Förste et al., 2011)
GOCO02s	2011	250	S(GOCE), S(GRACE)	(Goiginger et al., 2011)
AIUB-GRACE03S	2011	160	S(GRACE)	(Jäggi et al., 2011)
GOCO01S	2010	224	S(CHAMP), S(GRACE)	(Pail et al., 2010)

EIGEN-51C	2010	359	A, G, S(CHAMP), S(GRACE)	(Bruinsma et al., 2010)
AIUB-CHAMP03S	2010	100	S(CHAMP)	(Prange, 2010)
EIGEN-CHAMP05S	2010	150	S(CHAMP)	(Flechtner et al., 2010)
ITG-GRACE2010s	2010	180	S(GRACE)	(Mayer-Gürr, Kurtenbach, & Eicker, 2010)
AIUB-GRACE02S	2009	150	S(GRACE)	(Jäggi et al., 2012)
EGM2008	2008	2190	A, G, S(GRACE)	(Pavlis, Holmes, Kenyon, & Factor, 2012)
ITG-GRACE03	2007	180	S(GRACE)	(Mayer-Gürr, Eicker, & Ilk, 2007)
ITG-GRACE02s	2006	170	S(GRACE)	(Mayer-Gürr, Eicker, & Ilk, 2006)
EIGEN-GL04S1	2006	150	S(GRACE), S(LAGEOS)	(Förste et al., 2006)
EIGEN-GL04C	2006	360	A, G, S(GRACE), S(LAGEOS)	(Förste et al., 2006)
EIGEN-CG03C	2005	360	A, G, S(CHAMP), S(GRACE)	(Förste et al., 2005)
EIGEN-CHAMP03S	2004	140	S(CHAMP)	(Reigber et al., 2004)
EIGEN-GRACE02S	2004	150	S(GRACE)	(Reigber et al., 2005)
GGM01C	2003	200	S(GRACE), TEG4	(Tapley, Bettadpur, Watkins, & Reigber, 2004)
GGM01S	2003	120	S(GRACE)	(Tapley, Chambers, Bettadpur, & Ries, 2003)
EIGEN-CHAMP03Sp	2003	140	S(CHAMP)	(Reigber et al., 2004)

Figure 3.21 shows the RMS variations in gravity anomaly for the range of spherical harmonic degree coefficients 120 to 360. RMS decreases from degree 160. HUST-GRACE16S is a GGM defined only up to degree 160. From degree 220, significant discrepancies begin to occur. Specifically, the direct, timewise and spacewise GOCE models (GO_CONS_GCF_2_DIR_R5, GO_CONS_GCF_2_TIM_R5 and GO_CONS_GCF_2_SPW_R4) exhibit a deterioration of residuals from degree 220. PGM2016.66 uses a linear blending of EGM2008 and GOCE DIR in band 180 to 200 and EGM2008 up to 720. EIGEN-GL04C, which was recommended in 2009 (UP Training Center for Applied Geodesy and Photogrammetry, 2009) as a possible replacement for

PGM1991 (Fig. 3.17) has RMS that is ~10% larger than EGM2008 from degree 120 up to ~100% from degree 360. EGM2008 produced the lowest RMS across the profile which implies good fit to the Philippine terrestrial gravity data.

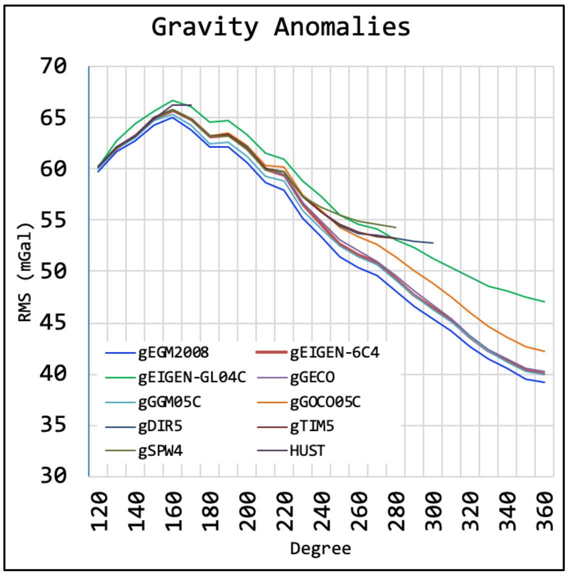

Figure 3.22. RMS variations in gravity anomalies from comparison of terrestrial data and GGM-derived computed values.

Figure 3.23 shows the longitudinal and latitudinal profile of the differences between the geoid heights derived from the GGMs and geoid heights from GNSS/levelling. The datasets used are in the zero tide system. The zero degree term was computed for the GGMs. GRS80 was used as the reference ellipsoid. For areas near the equator, GGMs overestimate geoid heights. Some studies, (e.g. Ziebart et al., (2004), Deng et al., (2013), and Lin et al., (2013)), recommends the use of corrector surface models to compensate for these values. A *corrector surface model* is a model that corrects datum inconsistencies and systematic distortions in the height datasets (Fotopoulos, Kotsakis, Sideris, & M, 2003). From Figure 3.23, it can be seen that points in the eastern and southern part of the country have relatively large differences. One explanation is that the frequent geodynamic activity in the area is not accounted for in the relatively long gap between the observations of the orthometric heights and the ellipsoidal heights (Forsberg, Olesen, Gatchalian, & Ortiz, 2014). As an example, in the most recent Surigao Earthquake of 10 February 2017, NAMRIA's active geodetic station (AGS-PSUR) recorded a displacement of 10.1 cm to the north, 8.0 cm to the west, and 2.8 cm downward (Cayapan, 2017). Another potential unaccounted contributing factor is extreme weather. The accumulation of levelling systematic effects over distance also contributes to the discrepancies. Its potential effects on the geoid and the benchmarks are investigated in the next chapter.

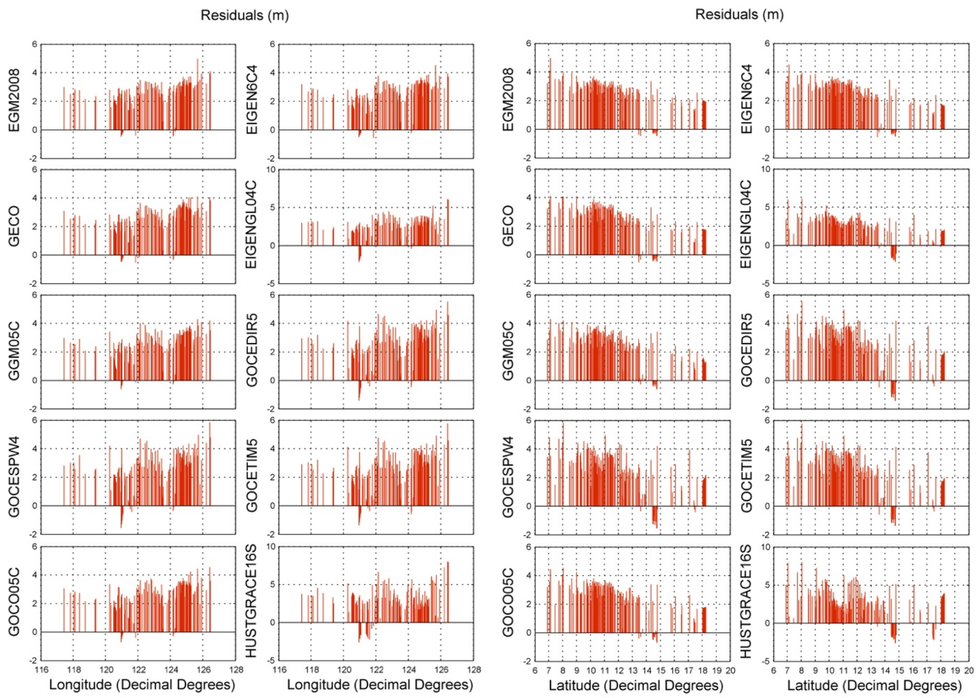

Figure 3.23. Difference in GNSS/levelling geoid heights and PGM2016.66-derived geoid heights without a corrector surface model.

Systematic errors can be absorbed through a least-squares estimation of bias based on (Papanikolaou & Papadopoulos, 2015),

$$N^{GNSS/Levelling} = N^{GGM} + bias + random\ errors \quad (3.6)$$

435 of 1261 gravity anomalies were used. The general accuracy of the gravity values for the points is ≈ 0.08 mGal. Combined models (e.g. GECO, EIGEN-6C4 etc. See Table 3.5) show better fits to Philippine ground data as shown by the RMS computations in Table 3.7. The computed biases range from approximately 80 to 95 centimetres. Systematic differences between the level surfaces and the geoids from the GGMs are potential sources of the computed biases (Papanikolaou & Papadopoulos, 2015).

Table 3.7. Statistics of the comparison between GNSS/levelling data and geoid heights based on GGMs and PGM2016.66 after the estimation of a constant bias (in metres). Maximum degrees of the models were used.

Gravity Field Model	**RMS**	**Bias**	**Min**	**Max**
HUST-Grace2016S	0.618	0.814	-3.299	4.998
GOCO05C	0.434	0.862	-0.309	1.641
GGM05C	0.454	0.883	-0.218	2.068
GECO	0.389	0.851	0.0348	2.037
EIGEN-6C4	0.326	0.840	0.245	2.047
GO_CONS_GCF_2_SPW_R4	0.933	0.940	-1.416	3.454
GO_CONS_GCF_2_TIM_R5	0.899	0.941	-1.348	3.167
GO_CONS_GCF_2_DIR_R5	0.902	0.923	-1.399	3.209
EGM2008	0.324	0.842	0.0140	2.607
EIGEN-GL04C	0.787	0.870	-1.505	4.675
PGM2016.66	0.263	0.802	0.004	1.982

Zoning was implemented to cluster levelling points of similar characteristics (Fig. 3.24). These were formed to contain the analyses to small regions and relatively short baselines since the PHS is of non-uniform quality.

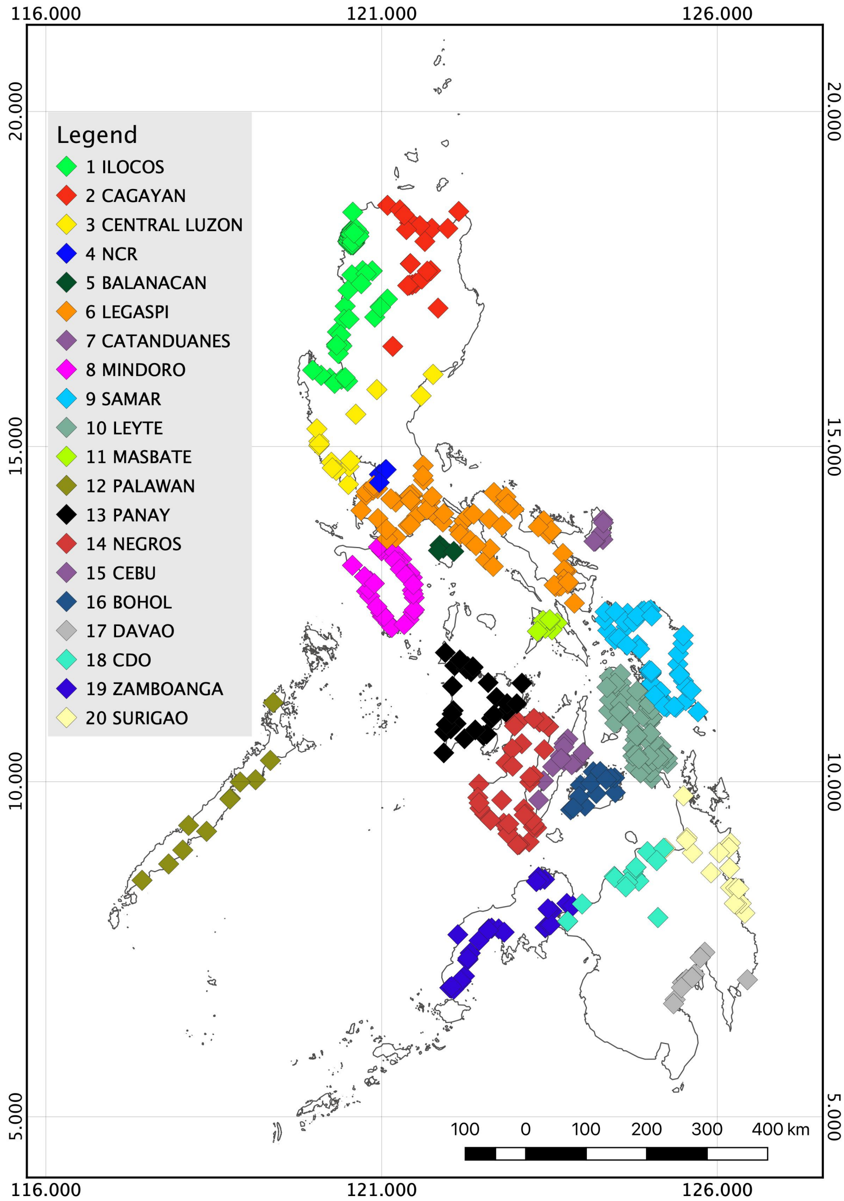

Figure 3.24. Distribution of evaluation points per zone.

Of the twenty (20) zones, three (3) used supplementary coordinates from CGSD and UP (5-Balanacan, 7-Catanduanes, 11-Masbate). Supplementary coordinates were necessary due to the absence of adequate NAMRIA coordinates in the area. Control points in zones 17, 18, 19, and 20 are sparse and non-homogenous in distribution. The challenging terrain, land cover and security instability are contributing factors. There is an ongoing effort by the NAMRIA to update and densify the levelling and GNSS networks in these four zones.

As anticipated, combined models show small differences (about 0.5 to 2 metres) in GNSS/levelling geoid heights and GGM-derived geoid heights in about 70% of the assessment points (Fig. 3.25) compared to satellite-only models. Though majority of the points exhibit these relatively small differences, care should be taken in interpreting these as sufficient measure of GGM performance because of the non-uniform spatial distribution of the assessment points (Fig. 3.24).

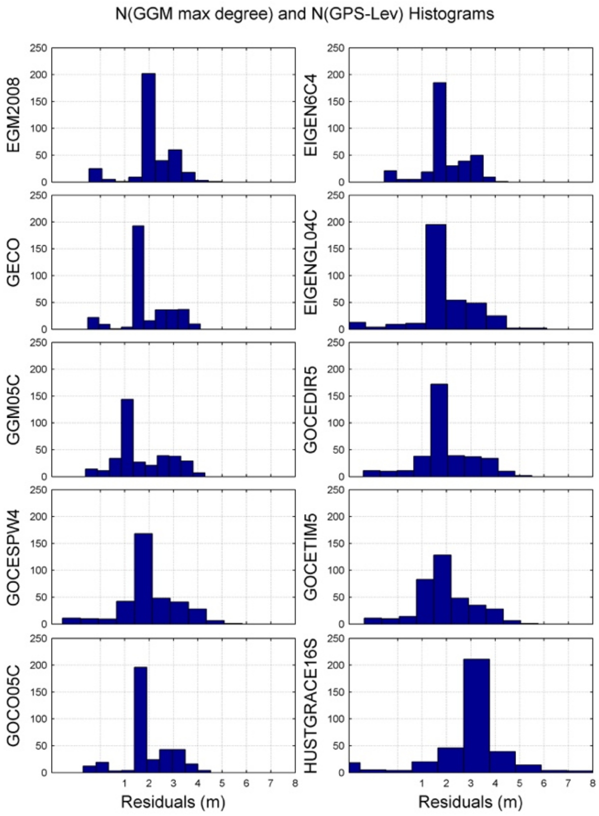

Figure 3.25. Histograms of the differences in GNSS/levelling geoid heights and GGM-derived geoid heights without a corrector surface model.

Compared to the GGMs, PGM2016.66 shows better agreement (between -0.5 m to 0.5 m) for a larger percentage of points (Fig. 3.25). Prudence, however, is advised on using this agreement to indicate PGM2016.66 performance on a national scale due to the non-uniform distribution and density of the assessment points, in addition to the poorly known integrity of these points due to the differences in their locations' physical characteristics. Campaigns to produce dense gravity information using calibrated instruments is recommended in addition to the re-observation and densification of the levelling and GNSS networks.

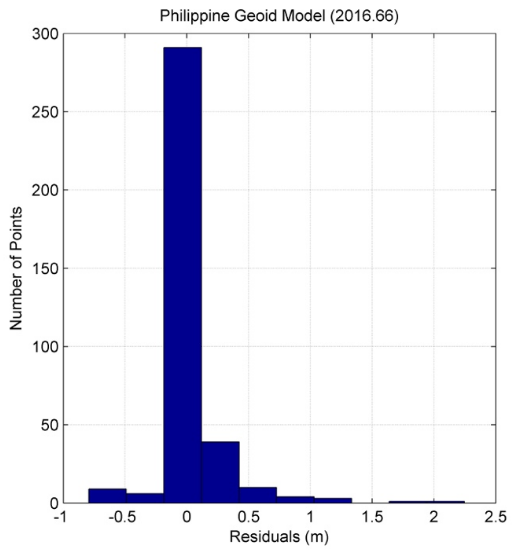

Figure 3.26. Histogram of the differences in GNSS/levelling geoid heights and PGM2016.66-derived geoid heights without a corrector surface model.

Using the zones presented in Figure 3.24, areas with large geoid height differences are isolated. Zones 17 to 20 are all located in the Mindanao island. The difficulty to conduct fieldwork campaigns in the area because of reasons mentioned previously means that this result is expected. This is not the case for Zones 12, 13 and 14. Producing this information is useful for the planning and prioritisation of areas for future geodetic campaigns.

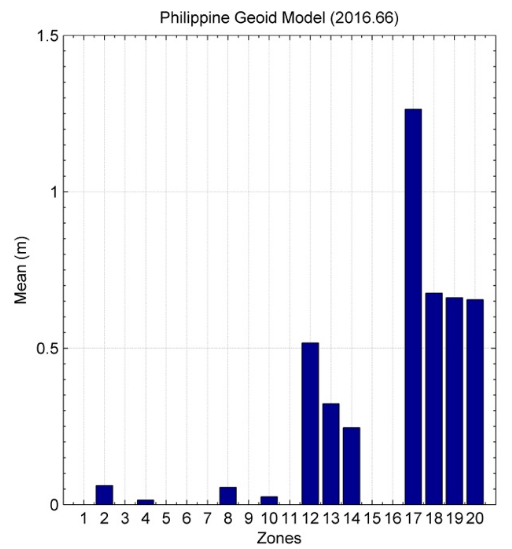

Figure 3.27. Mean-per-zone differences in GNSS/levelling geoid heights and PGM2016.66-derived geoid heights without a corrector surface model.

NAMRIA commissions contractors to conduct fieldwork campaigns for operational efficiency. Due to the number of campaigns being commissioned and minimal personnel available for quality control, errors due to improper execution of fieldwork and undocumented accuracy assumptions may exist in the datasets produced. To gain an insight on PGM2016.66 performance without these errors, a controlled procedure in establishing an assessment network over a demonstration area was carried out.

A research collaboration (DGE-22012016) with the Guiguinto Project produced fieldwork campaigns from 11 April 2016 to 16 May 2016. The campaigns were conducted approximately 15 kilometres north of Manila and took a total duration of 19 fieldwork days (including reconnaissance). The field campaigns were executed by Yvan Pagdonsolan, Marvic Anasarias and Louie Balicanta. A 3-station setup was used per 2-hour observation for GNSS occupations. For the same points, first-order differential levelling was observed at the same time. The layout of the network is shown in Figure 3.28. Each level line (less than 5-kilometre length) was run forward and backward with two setups at every turning point. Care was taken to achieve sub-millimetre errors for every setup pair. Validation points, different from the first set, were then established within the same area through GNSS observations and levelling.

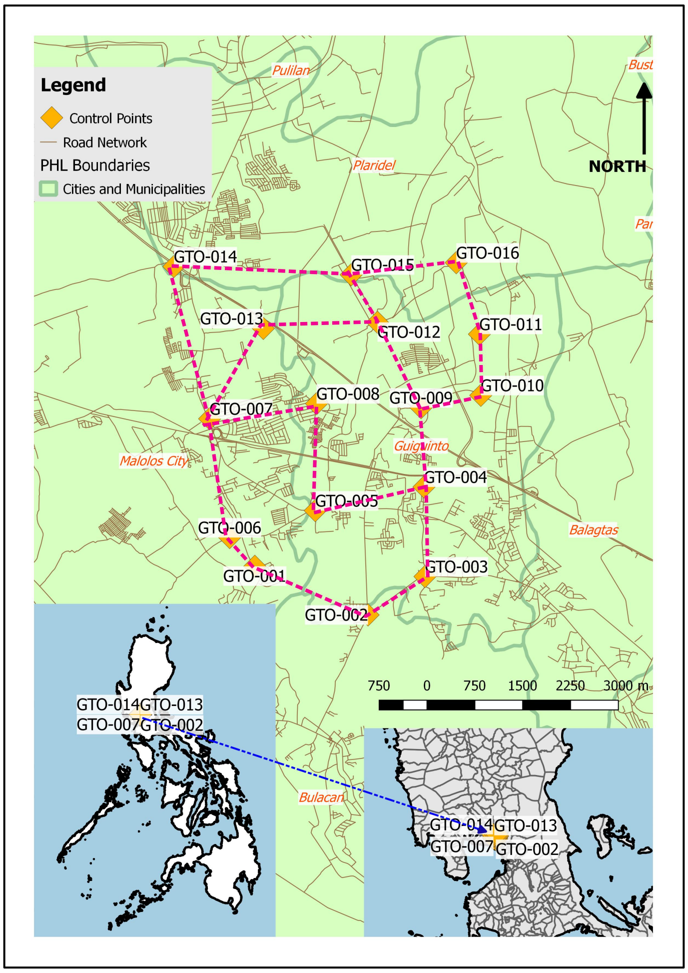

Figure 3.28. Guiguinto calibration network.

The campaigns produced two sets of values $N_{GNSS/levelling}$ and $N_{PGM2016.66}$ which are then compared with each other. For this demonstration area, the mean absolute difference of geoid heights between the two sets of values is 1.352 metres with a standard deviation of 0.018 metres. The difference in geoid heights for the stations are visualised in Figure 3.29.

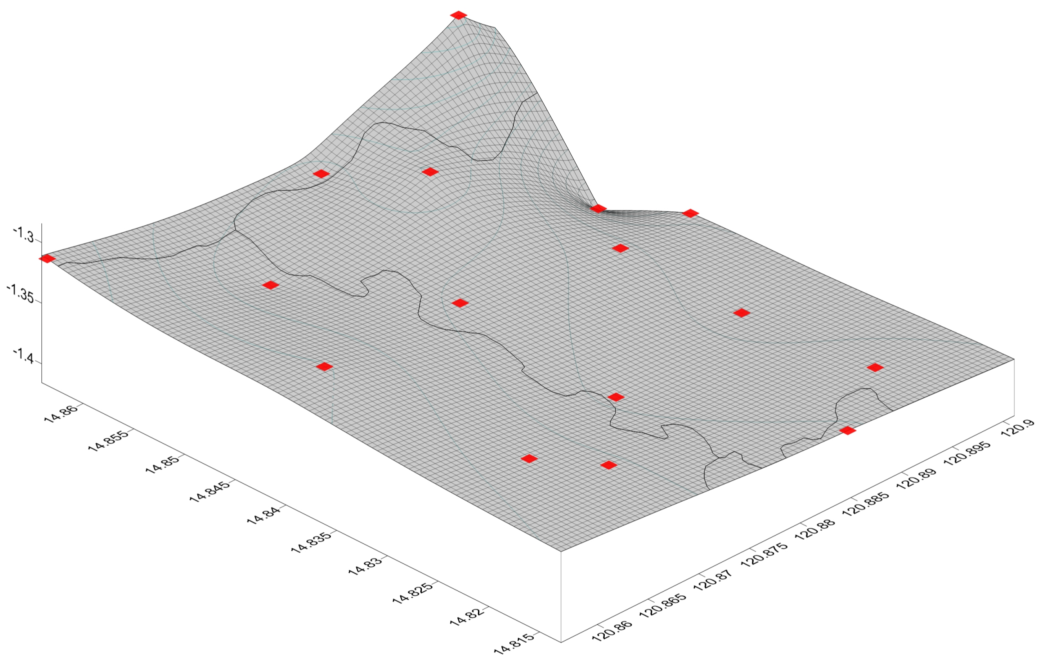

Figure 3.29. A visualisation of $N_{PGM2016.66}$-$N_{GNSS/levelling}$ for the Guiguinto calibration network.

Because the mean absolute difference and standard deviation is relatively high, a commonly-called *corrector surface model* (Fotopoulos, Kotsakis, Sideris, & M, 2003) is necessary to absorb systematic distortions. It is important to note that the term "corrector surface", should not be misunderstood to imply that errors are exclusive on the geoid as errors also exist in the GNSS and levelling data (Featherstone & Sproule, 2006).

To determine which surface model best suits the study area, parametric combinations of spatial interpolation methods (Inverse Distance Weighting and Empirical Bayesian Kriging) from the algorithmic degree, neighbourhood characteristics and radius of interpolation were compared over the study area. This method was implemented over Turkey by Erol and Çelik (Erol & Çelik, 2006).

Inverse Distance Weighting (IDW) is a deterministic geospatial interpolation method that assumes that a point has mathematical influence over another point and the weight of influence is related to the distance between the two points (De Mulder, Molenberghs, & Verbeke, 2018). This is described by the equation

$$\Delta N' = \frac{\sum_{i=0}^{n} \Delta Ni\ Pi}{\sum_{i=0}^{n} Pi} \tag{3.7}$$

where i is a reference point, ΔN_i is the difference between $N_{GNSS/levelling}$ and $N_{PGM2016.66}$ of the i^{th} reference point, $\Delta N'$ is the estimated value, and P_i is the weight of the i^{th} reference point.

Empirical Bayesian Kriging (EBK), on the other hand, uses weights that depend on both distance and direction. It is computed using the relationship

$$Semivariogram\ (distance_h) = 0.5 * average\ [(value_i - value_{i+1})^2] \tag{3.8}$$

EBK accounts for the uncertainty of the semivariogram by the iteration of models. The semivariogram formula, derived from the work of Mather (1963) assumes intrinsic stationarity wherein the difference variance is equal between any two points that are at the same distance and direction apart regardless of the point selection. A comprehensive explanation of the EBK algorithm is provided by Krivoruchko (2012).

For IDW, the mean absolute difference is 0.081 metres while EBK produced 0.078 metres. Results were validated using the classical empirical approach with RMS error of around 0.035 metres for both surfaces (Table 3.8 and 3.9). The average expected RMS error for corrector surfaces in 0.012 m. After post-processing, two stations were eliminated from the computations resulting in a reduced average RMS error of 0.0125 m.

Table 3.8. RMS of IDW parametric combinations.

Degree	Neighbourhood	Radius	RMS
1st	Smooth	3km	0.035
2nd	Smooth	3km	0.035
Optimal	Smooth	3km	0.035

Table 3.9. RMS of EBK parametric combinations.

Model	Neighbourhood	Radius	RMS
Linear	Smooth	Default	0.035
Power	Smooth	Default	0.035

Linear	Standard	Default	0.035

The *Akaike Information Criterion* (AIC) is an additional test that estimates the relative quality of the model for a given dataset (Akaike, 1974). It is an estimate expressed as

$$AIC = n\ln\hat{\sigma}^2 + 2K \tag{3.8}$$

where, $\hat{\sigma}$ is the average of the residual sum of squares, n is the sample size, and K is the number of parameters. The criterion is ideal for the type of datasets and models being compared as it relates the quality and complexity of the model to the dataset (Moffatt, 2017). The preferred model is the one that produces a lower AIC value. From the test, IDW produced an AIC value of 54.22 while EBK produced 54.18.

It is acknowledged that in this exercise, least squares collocation (LSC) is a common approach (Birardi et al., 1995; Lyszkowicz, 2000; Featherstone, 2000; Featherstone & Sproule, 2006). An updated computation using LSC for the whole country, to be published by NAMRIA, is ongoing. The records of the fieldwork in this study were transmitted for inclusion in the computations. Once released officially, the results of the NAMRIA LSC computations will be compared to the results of this study, and the recommendations will be properly reconsidered.

In conclusion, 3rd order orthometric heights derived from GNSS/levelling may be obtained, with EBK as the recommended corrector surface model for the surveyed area.

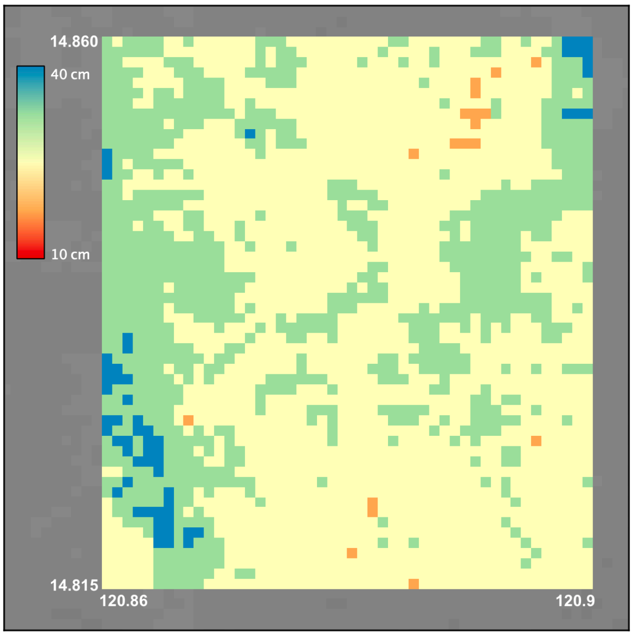

Figure 3.30. Magnitude of the difference in orthometric (Helmert) gravity reductions and the normal (Molodensky) reduction for Guiguinto (in cm).

Figure 3.30 shows a gridded estimation of the magnitude of the difference in orthometric (Helmert) gravity reductions and the normal (Molodensky) reduction for Guiguinto. The gravity information used were dated November 2019. It is assumed that changes in gravity from the original levelling campaign (2016) are negligible. The differences range from 5 cm to ~40 cm and were observed to be larger in higher elevations.

3.5. Chapter Summary

This chapter compiled available literature and local knowledge of the existing Philippine Height System (PHS) and the latest Philippine Geoid Model (PGM). PGM2016.66 was assessed by comparing it to selected global geopotential models (GGM), and using GNSS/levelling datasets in nationwide, zonal and localised methods. From the evaluations, it was clear that assessment benchmarks in the eastern and southern part of the country have relatively higher residuals.

Inconsistencies in the treatment of permanent tide systems can yield discrepancies to up to ~10 cm in corresponding heights, if not treated, especially in the southern part of the

Philippines. This reiterates the international community's recommendations of permanent tide treatment for height computations.

The mean dynamic topography (MDT) was also investigated. DTU10 (Andersen & Knudsen, 2010), VM500-ph (Vianna, Menezes, & Chambers, 2007) and RADS-ph were compared with GNSS-geoid MDTs (GNSS-PGM2016.66, GNSS-EIGENGL05C). The largest discrepancies were computed in the Mindanao area (Davao, Cagayan de Oro, General Santos, Calapan, Mambajao, Mati, Pagadian). Satellite altimetry can be used to infer the MDT in areas that do not currently have tide gauge stations (such as isolated islands), but sufficiently precise measurements at present is not possible (Ihde et al., 2017). Among the models, GNSS-PGM2016.66 MDT is best used for such areas.

The shift of emphasis from a levelling-based height system to a GNSS and high-resolution gravimetric geoid-based height system as the most practical next generation heighting solution for the Philippines was explored in this chapter. For the long term, a geoid-based system is desirable, orthometric heights will still be used and the same orthometric hypotheses is to be conventionally applied in the geoid for consistency. A geoid-based height system would theoretically guarantee that the archipelago is using a consistent reference surface. This provides a reliable solution to the issues caused by isolated reference to local tide gauges.

Vertical coordinates can be assigned with normal heights to avoid dealing with the complexities of the orthometric hypothesis. In doing so, the reference surface would be the quasigeoid and not the geoid. A gridded estimation of the magnitude of the difference in orthometric (Helmert) gravity reductions and the normal (Molodensky) reduction for a pilot area was shown. The differences were observed to be larger in higher elevations, as expected. Conversion to the use of normal heights from the long-preferred orthometric heights would be ideal in the context of the IHRS/F but would create undesired misinterpretation issues in the Philippine geodetic industry.

The modern PHS should be realised with a reference network with precise ITRS/F-based GNSS coordinates, geoid undulations and orthometric heights. It is necessary, however, to emphasize that for high-accuracy, high-precision, localised engineering applications, provisions for geodetic levelling is still desirable. Based on the diagnostic, the reliability of long-term registrations at the tide gauges are not sufficient. However, given NAMRIA's recent densification of the tide gauge network and operational improvement, the ongoing tidal registrations should be protected for future integrity and consistency. The establishment of offshore tide gauge stations is recommended in the future. This will make future geoid/inferred MSL relationships reliable.

In line with the recommendation to continue utilising orthometric heights, campaigns that densify gravity observations must be pursued. The PGM2016.66, though shown to be useable for third-order engineering applications is not yet sufficient as a basis for the new PHS in its current form. For the PGM to be a viable alternative, more gravity data from calibrated instruments (starting from the developed zones for practicality of security and access—Manila, Ilocos, Cebu, Palawan, CDO, Davao, Leyte), is recommended.

Tropical effects on the geoid and the benchmarks are further investigated in **Chapter 4: The Philippine Height System Realisation and Tropical Effects.**

Chapter Four

The Philippine Height System Realisation and Tropical Effects

4.1. The Philippine Hydrological Setting

Chapter 1, Sections 1.2.1.1 to 1.2.1.3 presented the geography, geology, weather and climate of the Philippines. In summary, the Philippines is an archipelagic nation with ~ 7,641 islands clustered into three major island groups: Luzon, Visayas and Mindanao. High-silica igneous rocks (granite and rhyolite) and low-silica rocks (basalt) as well as scattered sedimentary rocks define most of the islands (Gervasio, 1967). Different forms of predominantly clay loam and sandy loam soils cover the archipelago. The soil make-up of the Philippines is a combination of low land soils for tilling and upland soils prone to erosion.

Hydrology is broadly defined in literature as the study of water (Brutsaert, 2005) (Deodhar, 2008; Reddy, 2005). In this study, hydrology (and consequently *hydrologic/hydrological*) is limited to the study of occurrence, transfer and effects of water from the atmosphere to the Earth's surface and immediate subsurface. *Tropical hydrology* is distinctly characterised by "greater energy inputs and faster rates of change" (Wohl et al., 2012). Rainfall distribution varies across the Philippine archipelago and is influenced by the direction of the winds and the terrain. An average of 20 typhoons a year (Calang, 2017), in addition to tropical monsoons, bring destruction to lives and livelihood, as well as disruption to critical infrastructure and processes. Figure 4.1 illustrates the Philippine typhoon experience for the past 50 years. Figure 4.2 shows an example of a typhoon that entered the Philippine Area of Responsibility. To mitigate, the government is investing in new technology such as Light Detection and Ranging (Sarmiento, Paringit, Balicanta, & Cruz, 2014; Paringit, Balicanta, & Sarmiento, 2015) equipment, high-resolution satellite imagery (Sarmiento, Castro, & Gonzalez, 2012) and web-based geographic information systems (Sarmiento, Macapinlac, Sempio, & Simbulan, 2013; UP Resilience Institute, 2019) to model flood and identify flood prone areas. This includes the establishment of a dense automated rain and stream sensors network of the Philippine Atmospheric, Geophysical and Astronomical Services

Administration (PAGASA) through the National Operational Assessment of Hazards (NOAH) Program (Fig. 4.3). Precipitation information is provided by these sensors and supplemented by Tropical Rainfall Measuring Mission (TRMM) data for the period of the study (2015-2018) (Sarmiento, Rizos, & Roberts, 2018).

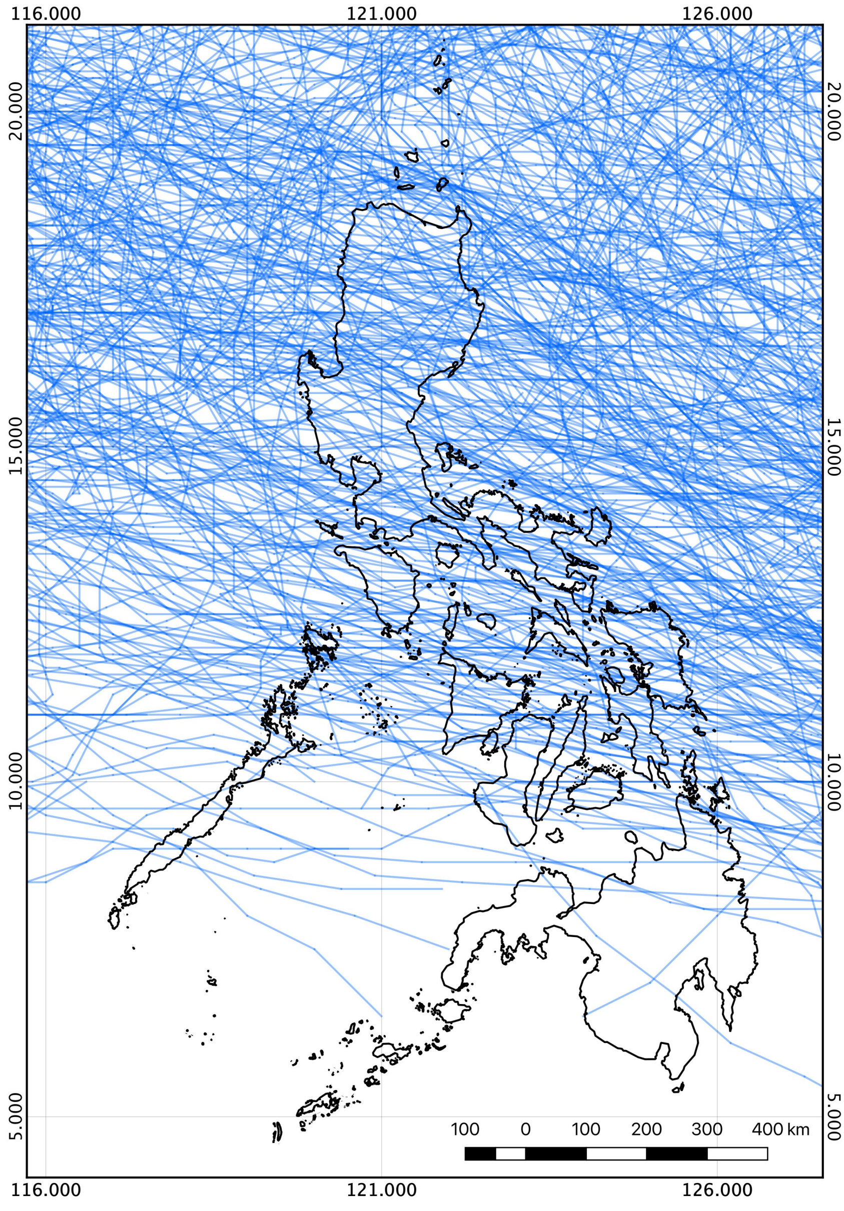

Figure 4.1. Typhoon tracks over the Philippines for the past 50 years **(IBTrACS, 2018)**. Official typhoon tracks can be viewed at http://bagong.pagasa.dost.gov.ph/information/annual-cyclone-track.

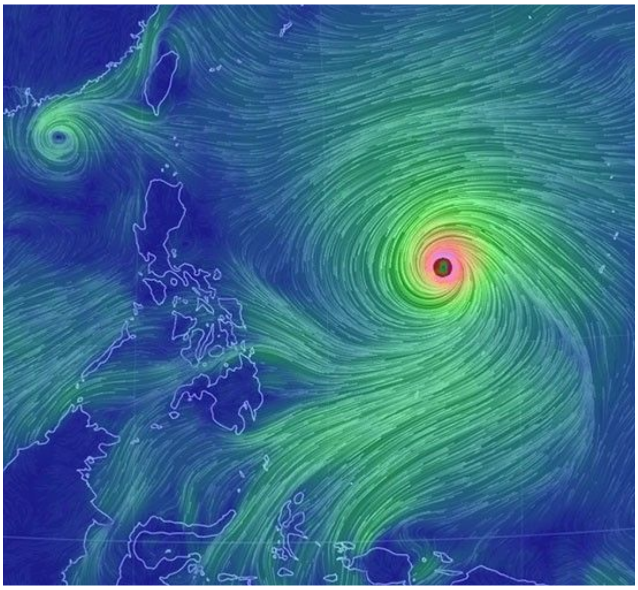

Figure 4.2. Super Typhoon Mangkhut (local name: Ompong) 0300PST 12092018 **(Beccario, 2018)**.

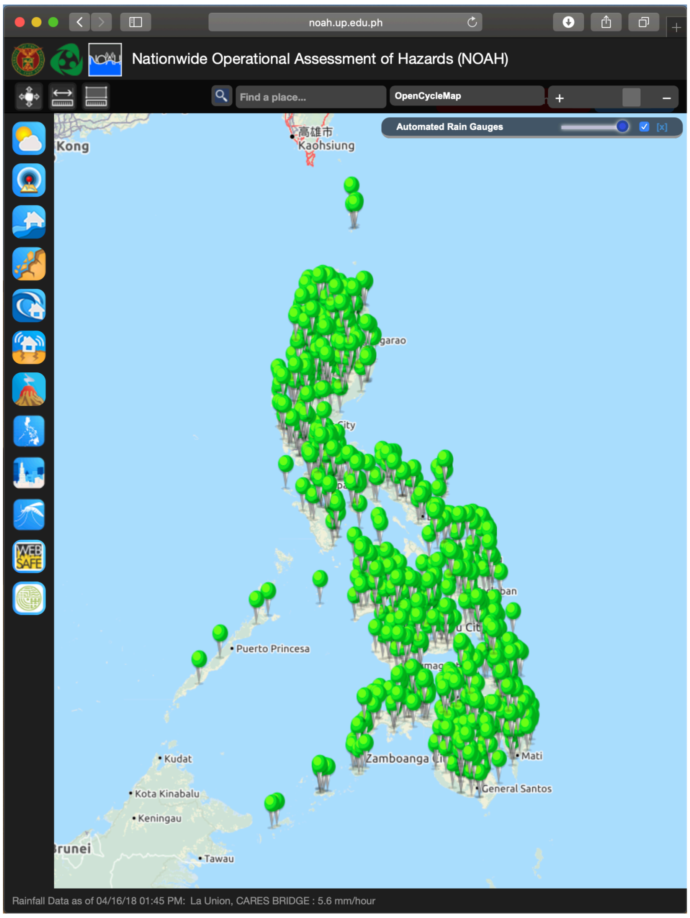

Figure 4.3. PAGASA/NOAH Rain Sensor Layout. **(UP Resilience Institute, 2019)**

Land cover information is an important component in modelling surface exposure to water. For updated land cover information at selected areas, GeoTIFF format covering the Philippines from the Landsat 4, 5, 7 and 8 missions were acquired and classified. The 30-metre spatial resolution gives sufficient information for the purposes of this study.

Land cover information can be derived from image classification. An illustration of the classification process is presented in Figure 4.4.

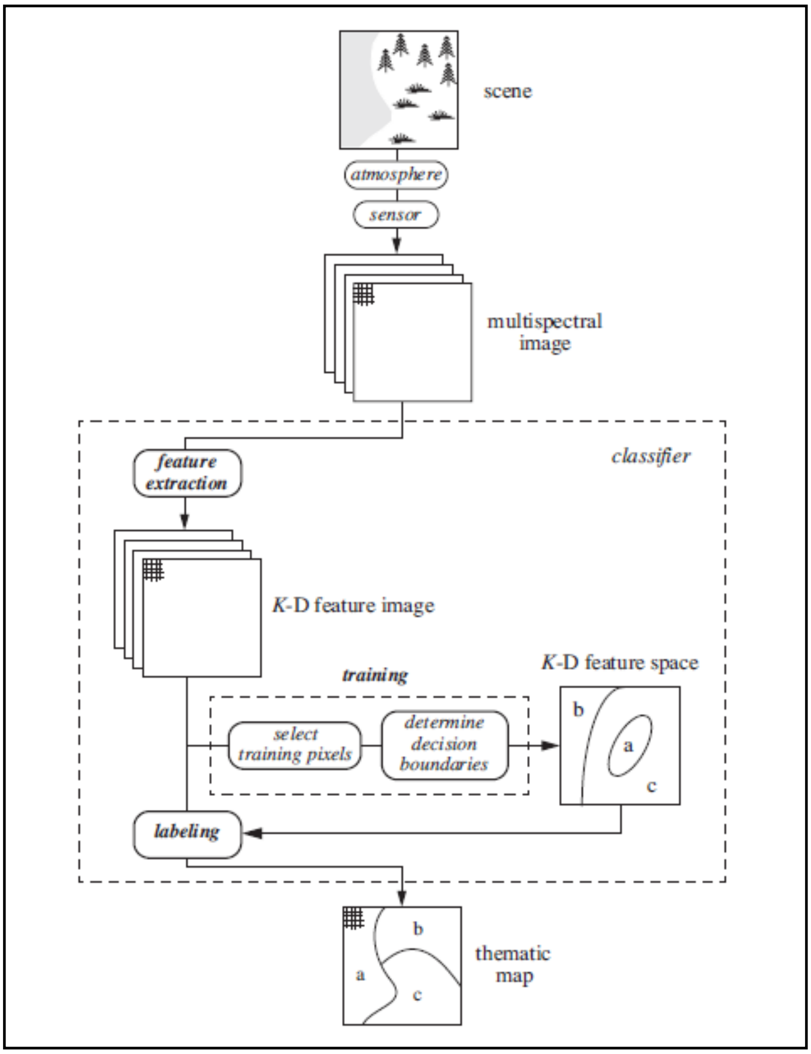

Figure 4.4. Image Classification Process. **(Schowengerdt, 2007)**

Supervised classification (Parallelepiped, Minimum Distance, Mahalanobis Distance and Maximum Likelihood) and unsupervised classification techniques (Isodata and K-means) were implemented (accuracy table in the Appendix, Table A2.) from 2012 to 2016 through official collaboration with research projects listed in Table 4.1.

Table 4.1. Supporting projects for hydrological characterisation.

Project	Involvement	Period	Supporting Agency	Area Coverage	Documentation
DREAM	Project Leader-Data Acquisition	2012-2014	DOST	Nationwide	(Sarmiento, Paringit, Balicanta, & Cruz, 2014; UP Training Center for Applied Geodesy and Photogrammetry, 2013)
PhilLIDAR 1	Project Leader-Data Acquisition	2014-2016	DOST	Nationwide	(Sarmiento, Paringit, Balicanta, & Cruz, 2014; UP Training Center for Applied Geodesy and Photogrammetry, 2013)
Project Climate Twin Phoenix	Component Leader-Watershed Simulation	2012-2013	UNDP; CCC; AusAID	Northern Mindanao (Cagayan de Oro, Iligan)	(Sarmiento, Sempio, & Paringit, 2013; Climate Change Commission, 2013)
Project ReBUILD	Component Leader-Watershed Simulation	2012-2013	UNDP; CCC; NZAID	Central Luzon (Tuguegarao, Enrile, Iguig); Central Visayas (Passi, Zarraga, Dumangas)	(Sarmiento & Paringit, 2013; United Nations Development Programme, 2015)
Magat Geosimulation Project	Project Leader	2012	DOST; UP Geosimulation Laboratory	Magat	(Sarmiento, Castro, & Gonzalez, 2012)

Ground truth campaigns for the classification iterations and validations were conducted. Several local setting issues that have hydrologic implications were encountered. Thick plantations and forest cover have different *hydrologic properties* (e.g. permeability, evapotranspiration indices, retention etc. (Taniguchi, 2012; Sarmiento, Gonzalez, Castro, & Ayson, 2010) but look spectrally (Adams & Gillespie, 2006) similar. Another similar situation is the “nipa” plantation classification. It is a plantation in terms of utilisation, but hydrologically it is similar to fallow land (Sarmiento, Sempio, & Paringit, 2013; Steven & Clark, 2013). In these cases, the hydrologic property of the land cover as defined through land use and fieldwork validation overrides the hydrologic property as defined spectrally through satellite imagery. Secondary information from archived National Mapping and Resource Information Authority (NAMRIA) and local forestry data were used to fill cloud cover gaps. The Maximum Likelihood Classifier (Richards, 2013) produced the highest overall classification accuracy that goes as high as 87% for areas that are well-surveyed.

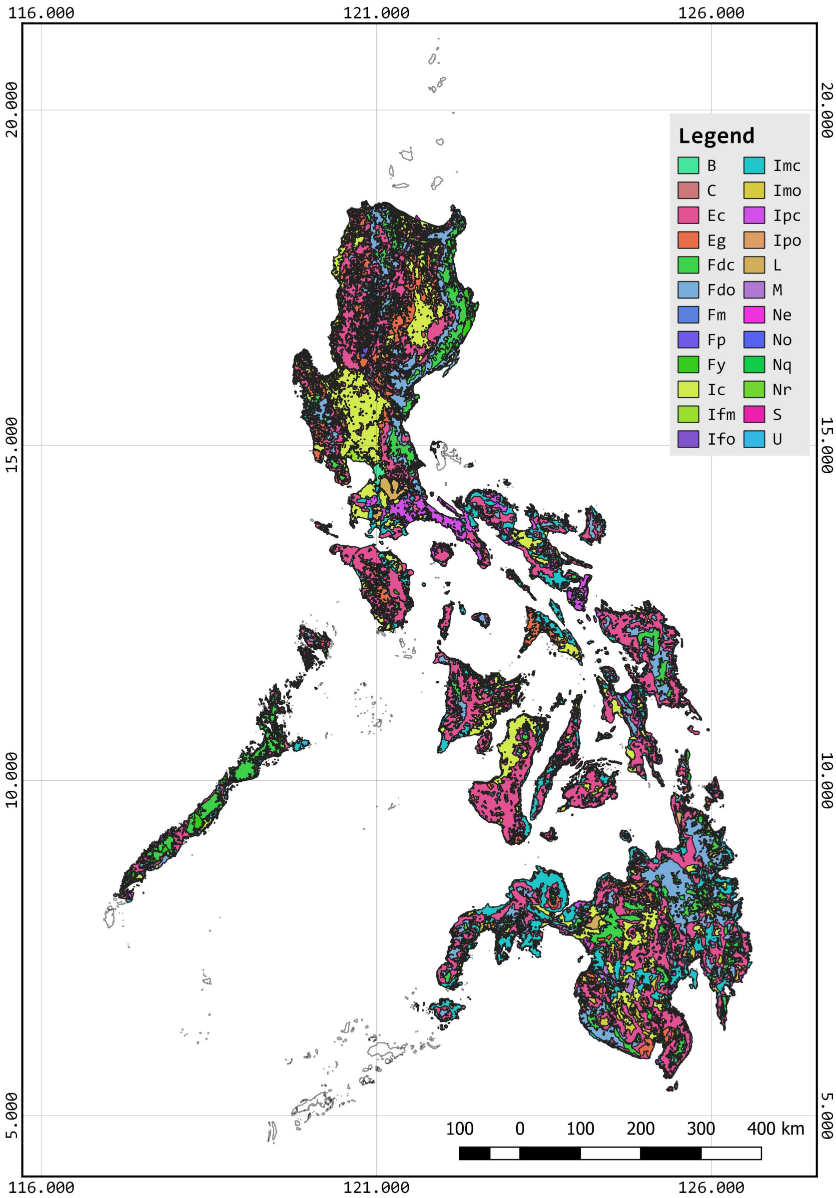

Figure 4.7. Philippine Generalised Land Cover Information. The different colours represent the different land cover classes standardised by NAMRIA. Full descriptions of the legend is provided by NAMRIA through http://www.geoportal.gov.ph/viewer/. **(National Mapping and Resource Information Authority, 2017)**

The information discussed in this section are important in understanding how hydrologic processes affect the height of the benchmarks that realise the Philippine Height System. Infiltration and saturation, evapotranspiration that becomes part of atmospheric loading, are processes that affect heights on the surface.

4.2. Effect on Physical Benchmarks

Positions of physical benchmarks are affected by a combination of time-variable loading factors that deforms the Earth's surface. Expressing $\boldsymbol{X}(t)$ as the instantaneous position of a point on the Earth's surface at epoch t, the following relationship accounts for various time-varying effects (Sośnica, 2014),

$$\boldsymbol{X}(t) = \boldsymbol{X}_R(t) + \sum_i \Delta\boldsymbol{X}_i\,(t) \tag{4.1}$$

where $\Delta\boldsymbol{X}_i(t)$ are position corrections and $\boldsymbol{X}_R(t)$ is the site position modelled as,

$$\boldsymbol{X}_R(t) = \boldsymbol{X}_0(t) + \sum_i \Delta\dot{\boldsymbol{X}}\,(t - t_0) \tag{4.2}$$

which is a function of a reference position $\boldsymbol{X}_0(t)$, epoch t_0 and site velocity $\Delta\dot{\boldsymbol{X}}$.

4.2.1. Tidal and Non-tidal Loading

Loading effects are categorised into *tidal loading* and *non-tidal loading*. Tidal loading effects are induced due to the gravitational attractions of the Sun, Moon and the planets (Bos & Scherneck, 2013; Lyard, Lefevre, Letellier, & Francis, 2006). Non-tidal loading effects are caused by mass redistributions in the atmosphere, the hydrosphere and in the oceans (König, Fagiolini, Raimondo, & Vei, 2016; Williams & Penna, 2011). These effects are estimated through tidal and non-tidal models of *atmospheric loading*, *oceanic loading* and *hydrospheric (or continental hydrology) loading*.

Atmospheric tidal loading is due to global-scale wave motions in the atmosphere with periods that are an integer fraction of a solar or lunar day. The *solar diurnal tides (S1)* have periods of 24 hours. Consequently, *solar semidiurnal tides (S2)* have periods of 12 hours. The *lunar diurnal tide (M1)* period is approximately 24.8 hours. The *lunar semidiurnal tide (M2)* period is 12.4 hours. Planetary contributions are very minimal and may only be detectable by specialized instruments. (Oberheide, Hagan, Richmond, & Forbes, 2015; van Dam & Wahr, 1987)

Atmospheric non-tidal loading is due to "spatial variations in atmospheric pressure acting on the surface of the Earth" (Teunissen & Mentenbruck, 2017). Models based on the European Centre for Medium-Range Weather Forecasts (ECMWF) operational model were used to derive effects from atmospheric loading. The ATMIB (ECMWF + static ocean response) and the ERAin (ECMWF re-analysis model) assumes a partial compensation of the change in air pressure (inverted barometer) by the sea. The ATMMO model (ECMWF + dynamic ocean response) computes loading with the Toulouse Unstructured Grid Ocean Model (TUGO-m). Carrère and Lyard (2003) and Boy and Chao (2005) provide more information on the ECMWF models.

Oceanic tidal loading is the deformation of the Earth due to the periodic loading of mass redistributions caused by ocean tides. Oceanic tidal loading is composed of many tides with different periods. The oceanic tidal loading is usually computed for the harmonics *M2, S2, N2, K2, K1, O1, P1, Q1, Mf, Mm* and *Ssa*—the 11 largest-in-amplitude harmonics that represent most of the total tidal signal. (Bos & Scherneck, 2013; Watkins & Eanes, 1997). For the complete designations and definitions of tidal harmonics, the reader is referred to the work of Hendershott (Hendershott, n.d.).

Oceanic non-tidal loading refers to loading caused by "non-tidal oceanic mass redistribution such as seasonal changes in freshwater runoff, sea surface height, salinity or variations in oceanic dynamic topography due to changes in currents, winds and so on" (Teunissen & Mentenbruck, 2017). Effects from oceanic non-tidal loading are determined from the Estimating the Circulation and Climate of the Ocean model (ECCO. Wunch et al., (1997)) and the Global Ocean Reanalysis and Simulation model (GLORYS2 version 3. Ferry et al., (2007)). ECCO has a 12-hour, 1-degree resolution, whereas ECCO2 (Menemenlis, Fukumori, & Lee, 2005) and GLORYS have 24-hour, 0.25-degree resolution. The resulting graphs are presented in the next section.

Hydrospheric tidal loading pertains to the deformation caused by the transfer of water between the continents and the oceans due to gravitational attractions of the Sun, Moon and the planets. This effect is detectable but very minimal and often neglected or lumped with the non-tidal effects in geodetic measurements. Estimation of these tidal effects are not possible to verify practically because "in-situ measurements of all aspects of the hydrological cycle are discrete and extrapolation to large-scale is not always informative." (Tregoning, Watson, Ramillien, McQueen, & Zhang, 2009).

Hydrospheric non-tidal loading refers to loading caused by "water mass variations within the continental hydrological cycle" (Werth, Güntner, Schmidt, & Kusche, 2009). These effects are computed using the ERAin model (ECMWF reanalysis), Global Land Data Assimilation System model (GLDAS + canopy. Rodell et al., (2004)) and the Modern Era Retrospective Analysis for Research and Applications (MERRA), (Rienecker et al., (2011)) model. The models are summarised in Table 4.2.

Table 4.2. Summary of the loading models used.

Name of Model	Type	Spatial Resolution	Temporal Resolution	Reference
Ray & Ponte	Atmospheric Tidal	1°	-	(Ray & Ponte, 2003)
DTU10	Oceanic Tidal	0.5°	-	(Cheng & Andersen, 2010)
TPXO09_Atlas	Oceanic Tidal	0.25°	-	(Egbert & Erofeeva, 2010; Letellier, 2004)
ATMIB (ECMWF + static ocean response)	Atmospheric Non-tidal	0.15°	3-hourly	(Carrère & Lyard, 2003; Boy & Chao, 2005)
ATMMO (ECMWF + dynamic ocean response)	Atmospheric Non-tidal	0.15°	3-hourly	(Carrère & Lyard, 2003; Boy & Chao, 2005)
ERAin	Atmospheric Non-tidal	0.7°	6-hourly	(Boy & Chao, 2005)
TUGO-m	Oceanic Non-tidal	1°	3-hourly	(Carrère & Lyard, 2003)
ECCO	Oceanic Non-tidal	1°	12-hourly	(Wunsch, Iskandarani, Haidvogel, & Hughes, 1997)

ECCO2	Oceanic Non-tidal	0.25°	24-hourly	(Menemenlis, Fukumori, & Lee, 2005)
GLORYS2 v.3	Oceanic Non-tidal	0.25°	24-hourly	(Ferry, Remy, Brasseur, & Maes, 2007)
ERAin model	Hydrospheric Non-tidal	0.7°	6-hourly	(Boy & Chao, 2005)
GLDAS + canopy	Hydrospheric Non-tidal	0.25°	3-hourly	(Rodell et al., 2004)
MERRA	Hydrospheric Non-tidal	0.5°	hourly	(Rienecker et al., 2011)

The École et Observatoire des Sciences de la Terre (EOST) loading service is a service that provides displacement computations at high samplings rates and in three dimensions for International Terrestrial Reference Frame (ITRF) stations and additional sites. The service is supported by the Centre National D'études Spatiales (EOST, 2015). To capture displacement, weekly solutions (Fig. 4.6) from the Philippine Active Geodetic Network (PAGeNet) and EOST sites (KAYT, TVST, see Fig. 4.1) over the Philippines were processed, and their height displacements were computed using the EOST loading service from 2008 to 2015. Some of the stations were also provided in the SONEL (https://www.sonel.org/) GNSS service. GNSS estimates were processed through the GAMIT/GLOBK processing software (King & Bock, 2008) with use permission through the University of the Philippines. Loading effects were computed in the Centre-of-Mass (CM) frame.

The Centre-of-Mass (CM) frame is one of the three most commonly adopted terrestrial reference frame origins. The other two being the Centre-of-Figure (CF) and the Centre-of-Earth (CE) (Dong, Dickey, Chao, & Cheng, 1997). The positions in the attached frame origin (AT) is given by the following relationships (Dong, Yunck, & Heflin, 2003),

$$\boldsymbol{X}_{CM}^{AT}(t) = \frac{\sum \boldsymbol{X}_i^{AT}(t) m_i}{\sum m_i} \tag{4.3}$$

$$\boldsymbol{X}_{CF}^{AT}(t) = \frac{\sum \boldsymbol{X}_i^{AT}(t) m_i}{n} \tag{4.4}$$

$$\boldsymbol{X}_{CE}^{AT}(t) = \frac{\sum \boldsymbol{X}_i^{AT}(t) m_i}{\sum m_i} \tag{4.5}$$

where $\boldsymbol{X}_{CM}^{AT}(t)$ represent the centre of mass of the whole Earth including the atmosphere, oceans and groundwater. This is used in applications where satellite dynamics are considered; $\boldsymbol{X}_{CF}^{AT}(t)$ represent the centre of figure of the outer surface of the solid Earth. This is commonly used in applications where the only measurable quantity is the geometry between ground sites; and $\boldsymbol{X}_{CE}^{AT}(t)$ represent the centre of mass of the solid Earth exclusive of mass load. This is usually used in geophysical studies. n is the number of summation points and m_i is the mass at any point in the frame (subscript i). The Earth's Centre-of-Mass and Centre-of-Figure are no longer indistinguishable with recent space geodesy developments (Dong, Yunck, & Heflin, 2003)

Figure 4.6 presents the selected stations for the loading computations. The stations were selected based on granted official permissions and access. No isolated hydrospheric tidal model was computed for this study.

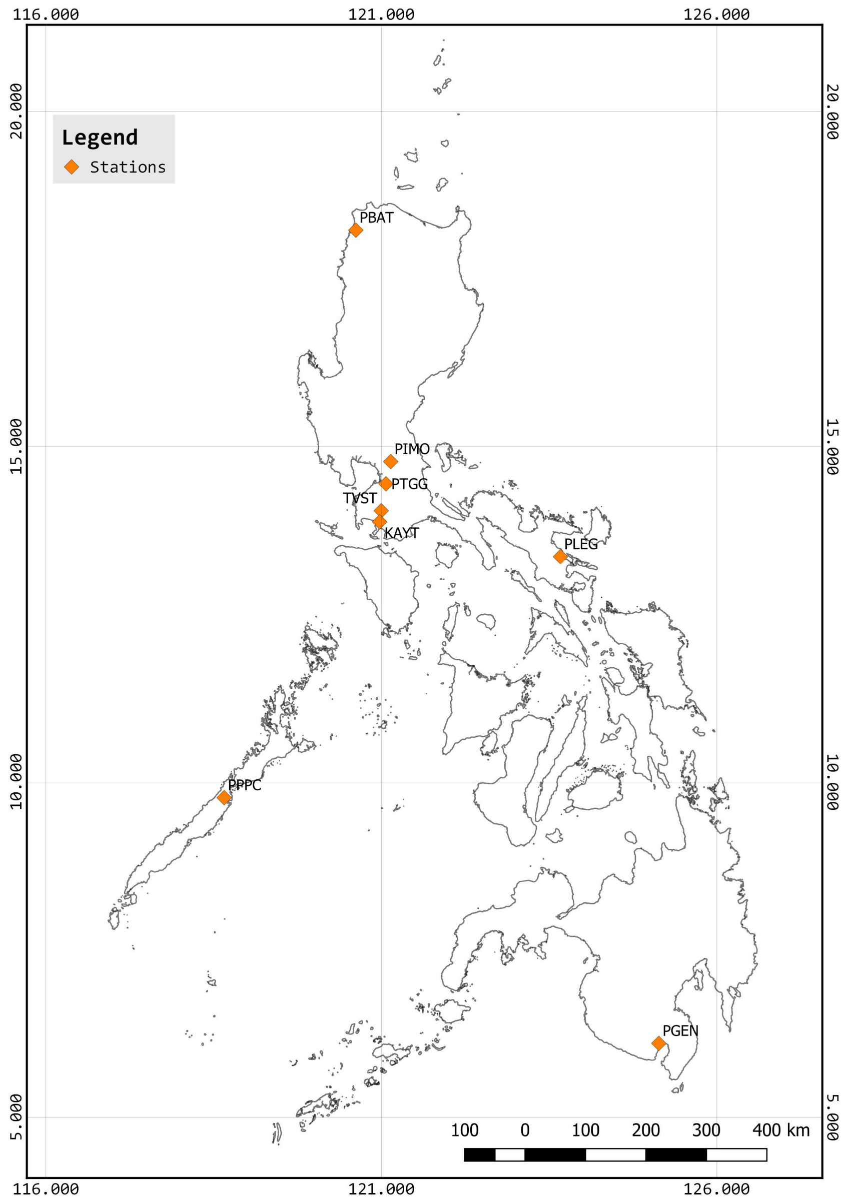

Figure 4.6. The orange dots represent the active geodetic stations used to estimate the vertical displacements inferred from geophysical non-tidal models (see Table 4.2).

The atmospheric tidal loading displacement is approximated using *atmtide_ld.f* program of van Dam & Wahr (2010) through the atmospheric tidal model of Ray & Ponte (2003) Green's functions (a set of functions that describe tides as computed by Farrell (1972)) for a Gutenberg-Bullen Earth (Dziewonski & Anderson, 1981) with a continental crust were used. Displacement is defined positive up and were computed in the CM frame.

Table 4.3. Approximations of the atmospheric tidal loading displacements (in mm).

	S1	*S2*
PBAT	0.940	1.098
PIMO	0.985	1.150
PTGG	0.986	1.151
TVST	0.989	1.157
KAYT	0.991	1.162
PLEG	0.980	1.170
PPPC	1.035	1.207
PGEN	1.068	1.238

Oceanic tide loading were computed using the DTU10 model (Cheng & Andersen, 2010) and TPXO09_Atlas (Egbert & Erofeeva, 2010). The TPXO09_Atlas is an adjustment of FES2004. FES2004 was developed by Letellier (2004). It utilizes TOPEX/Poseidon altimetry into a hydrodynamic tide model.

TPXO09_Atlas model. The TPXO09_Atlas models is essentially TPXO.7.2 improved with local tide models. It uses an inverse theory using tide gauge, TOPEX/Poseidon data and GRACE data which gives an optimum balance between observations and hydrodynamics.

Computing for the oceanic tidal loading for *M2, S2, N2, K2, K1, O1, P1, Q1, Mf, Mm* and *Ssa* was done using the routine implemented in the *olfg* program (Bos & Scherneck, 2013). The Farrell (1972) Green's functions were used. A water layer with a certain phase lag is also removed from the models globally to force conservation of tidal water mass. Displacement is defined positive up and were computed in the CM frame. The DTU10 ocean model has been post-processed with interpolation near the station (Fig. 4.6) using the *olmpp* routine of Scherneck (1991).

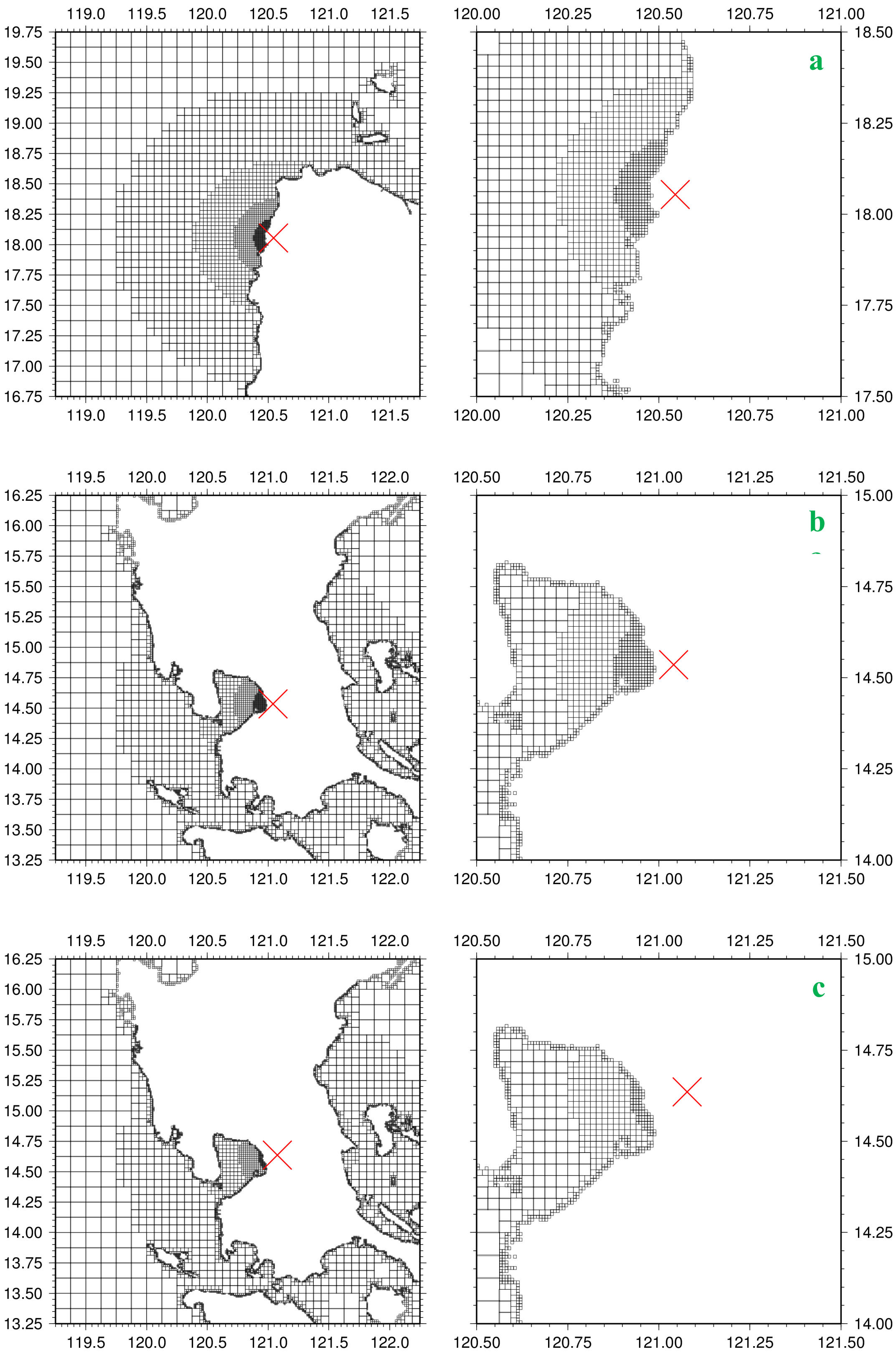
a
b
c
119.0 119.5 120.0 120.5 121.0 121.5
19.75 19.50 19.25 19.00 18.75 18.50 18.25 18.00 17.75 17.50 17.25 17.00 16.75
120.00 120.25 120.50 120.75 121.00
18.50 18.25 18.00 17.75 17.50
119.5 120.0 120.5 121.0 121.5 122.0
16.25 16.00 15.75 15.50 15.25 15.00 14.75 14.50 14.25 14.00 13.75 13.50 13.25
120.50 120.75 121.00 121.25 121.50
15.00 14.75 14.50 14.25 14.00

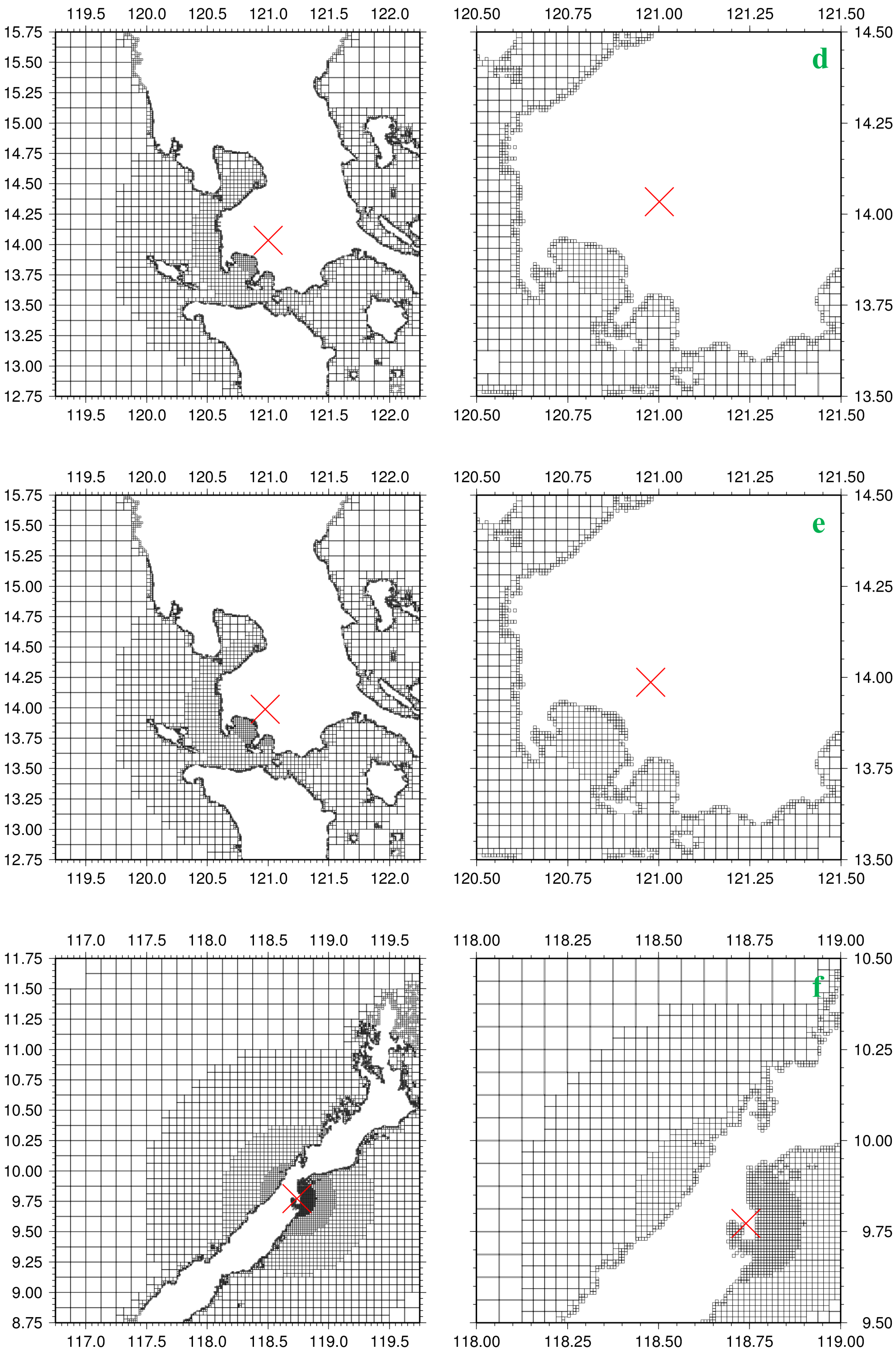
d
e
f
119.5 120.0 120.5 121.0 121.5 122.0
15.75 15.50 15.25 15.00 14.75 14.50 14.25 14.00 13.75 13.50 13.25 13.00 12.75
120.50 120.75 121.00 121.25 121.50
14.50 14.25 14.00 13.75 13.50
117.0 117.5 118.0 118.5 119.0 119.5
11.75 11.50 11.25 11.00 10.75 10.50 10.25 10.00 9.75 9.50 9.25 9.00 8.75
118.00 118.25 118.50 118.75 119.00
10.50 10.25 10.00 9.75 9.50

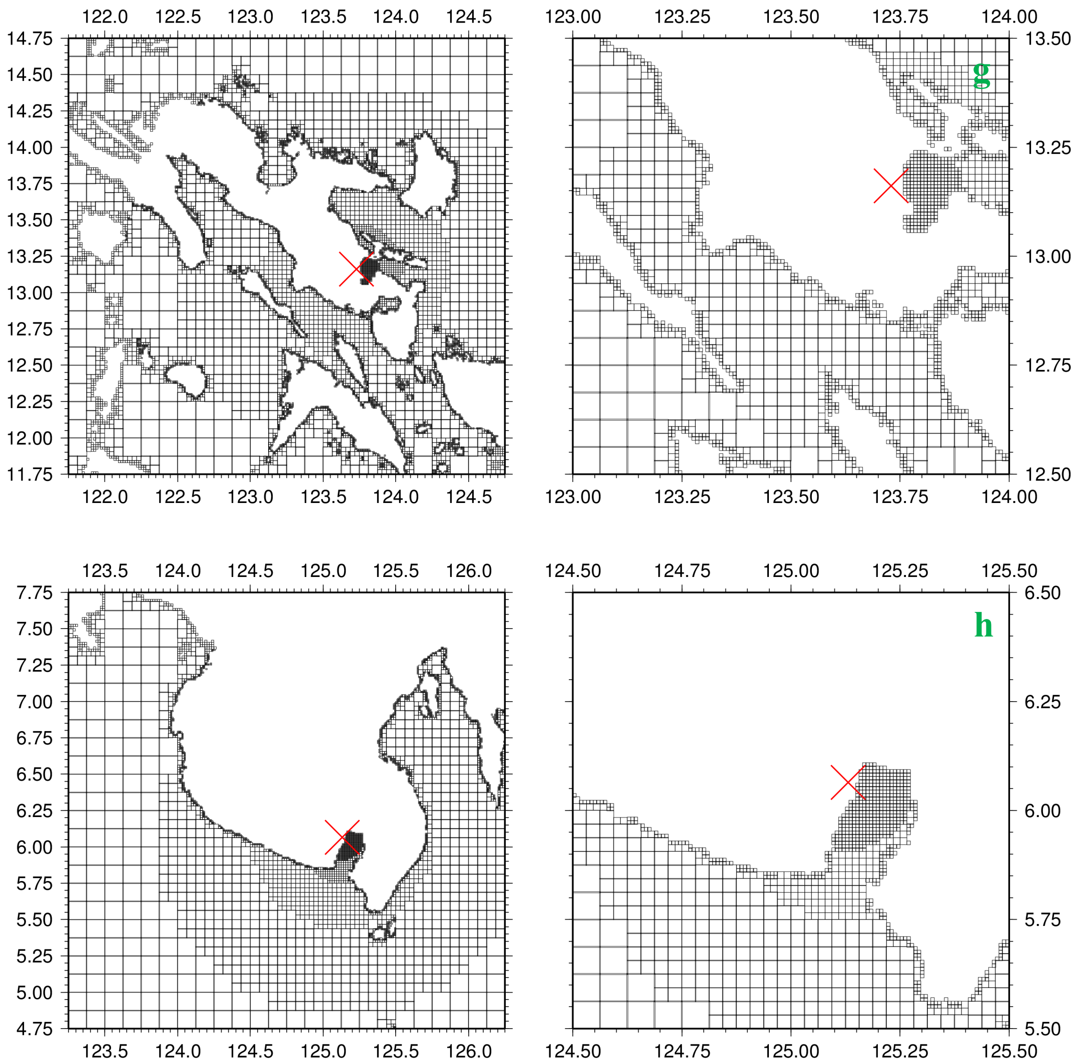

Figure 4.7. Near field coastline resolution generated for sites that involves loading post-processor OLMPP. *(a)* PBAT. *(b)* PIMO. *(c)* PTGG. *(d)* TVST. *(e)* KAYT. *(f)* PLEG. *(g)* PPPC. *(h)* PGEN.

Table 4.4. Approximations of oceanic tidal loading displacement (in mm).

DTU10											
	M2	*S2*	*N2*	*K2*	*K1*	*O1*	*P1*	*Q1*	*MF*	*MM*	*SSA*
PBAT	9.370	3.860	2.010	1.050	7.470	7.730	2.470	1.570	0.820	0.550	0.510
PIMO	8.100	3.040	1.740	0.860	7.750	7.890	2.620	1.620	0.890	0.580	0.550
PTGG	7.790	2.900	1.680	0.820	7.870	8.050	2.660	1.640	0.900	0.580	0.550
TVST	6.970	2.420	1.500	0.680	8.370	8.490	2.860	1.720	0.910	0.590	0.560
KAYT	6.830	2.340	1.470	0.660	8.490	8.600	2.900	1.740	0.910	0.590	0.570
PLEG	12.23	4.310	2.610	1.290	7.950	7.610	2.700	1.650	0.950	0.620	0.590
PPPC	5.110	1.680	1.080	0.440	13.13	12.39	4.650	2.480	1.070	0.680	0.630

PGEN	18.39	8.460	3.420	2.310	9.770	7.690	3.260	1.670	1.050	0.670	0.630
TPXO09_Atlas											
PBAT	9.400	3.940	1.980	1.070	7.560	7.740	2.500	1.630	0.730	0.570	0.550
PIMO	8.310	3.120	1.750	0.830	8.090	8.000	2.680	1.660	0.790	0.600	0.570
PTGG	8.020	2.970	1.700	0.790	8.260	8.170	2.730	1.690	0.790	0.610	0.580
TVST	7.120	2.450	1.530	0.650	8.690	8.570	2.870	1.770	0.810	0.620	0.580
KAYT	6.770	2.300	1.460	0.650	8.560	8.670	2.930	1.750	0.900	0.590	0.560
PLEG	11.80	4.490	2.430	1.160	7.830	7.650	2.640	1.610	0.830	0.640	0.610
PPPC	6.990	2.380	1.510	0.630	8.790	8.670	2.900	1.790	0.810	0.620	0.590
PGEN	18.31	8.550	3.410	2.420	9.670	7.720	3.170	1.600	0.960	0.690	0.660

The tidal effects are already routinely corrected for in standard GNSS data analysis.

Comparison of GNSS time series and computed height displacements inferred from atmospheric non-tidal loading models are shown in Figure 4.8.

GNSS data were processed using recommended GAMIT procedure (King & Bock, 2008; Gegout, Boy, Hinderer, & Ferhat, 2008) without loading, as comparison. The study was permitted to use January 2008 to December 2015 GNSS data of selected stations from NAMRIA.

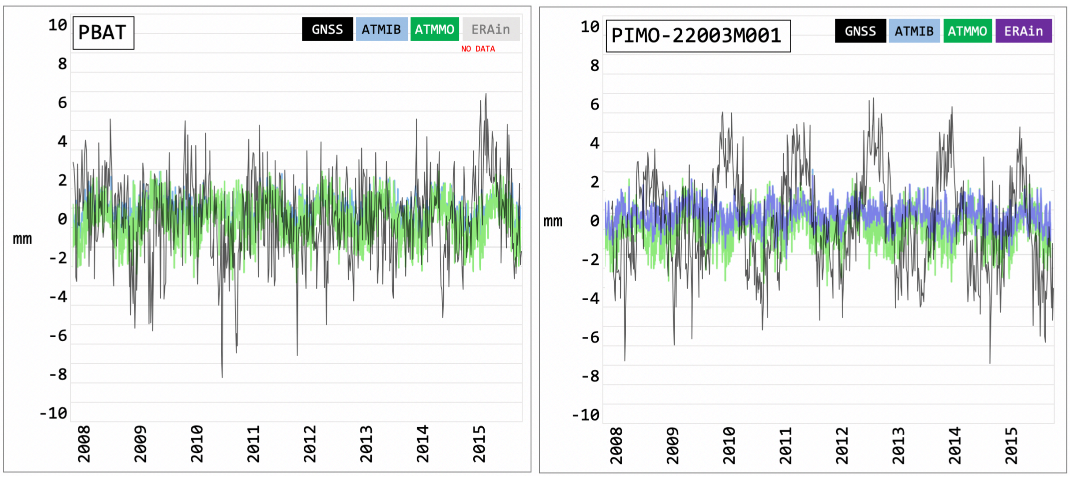

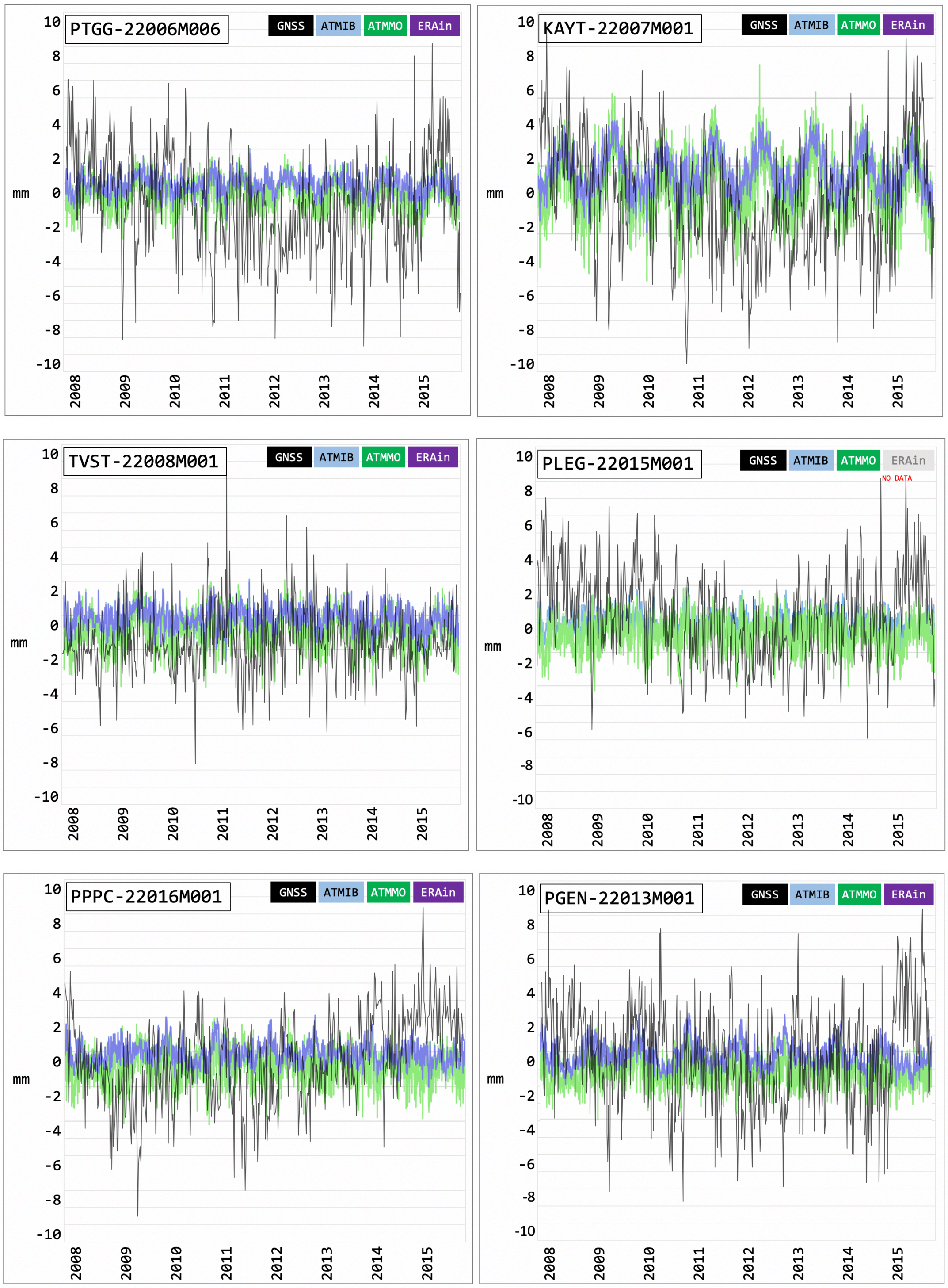

Figure 4.8. Vertical displacements inferred from atmospheric non-tidal loading models for selected Philippine stations. ATMIB in light blue, ATMMO in green and ERAin in purple and GNSS time series in black.

The seasonality in precipitation is shown to produce an average non-tidal loading effect between -2 mm to 2 mm for PLEG, PPPC and PGEN; -2.5 mm to 2.5 mm between PIMO, PTGG and PBAT (Fig. 4.7). TVST exhibits an asymmetrical displacement pattern (more compressive than expansive) and KAYT produced the largest height displacements of approximately -5 mm to 5 mm.

Compared to the behaviour of other non-tidal loading effects, to be presented shortly, the response of TVST and KAYT to atmospheric non-tidal loading is notable. The mechanism for the “irregularity” may be caused by their location. Both of these stations are located inside the Taal Volcano national park. The Taal Volcano is the second most active volcano in the Philippines, and the only volcano that is located on an island within a lake within an island. The land cover seasonality of the location of the stations may introduce multipath errors in GNSS computations.

The characteristic movement of tropical typhoons produce short duration (typically less than 48 hours) changes in air pressure over an area. This makes the static ocean response model unsuitable. The dynamic ocean response from the TUGO-m model (Carrère & Lyard, 2003) suggests that the ATMMO is an optimal model for tropical regions. The TUGO-m model is used by the Groupe de Recherche de Géodésie Spatiale for the computation of the space and time gravity field variations from the GRACE mission. It has been used to decrease the variance of gravity and tilt observations (Carrère & Lyard, 2003).

Seasonal trends for oceanic non-tidal loading is not as pronounced as those for atmospheric non-tidal and hydrospheric non-tidal loading (Fig. 4.9). GLORYS data is incomplete for the period of the study. The GLORYS data for the station on the island adjacent to the West Philippine Sea (PPPC) began a steep drop of approximately 5 mm from 2009, which is not the case for ECCO-based models. PPPC is located near the coast and non-tidal loadings are known to produce significant deformation. However, both ECCO and ECCO2 models do not reflect the same behaviour. The reason for the drop is unclear.

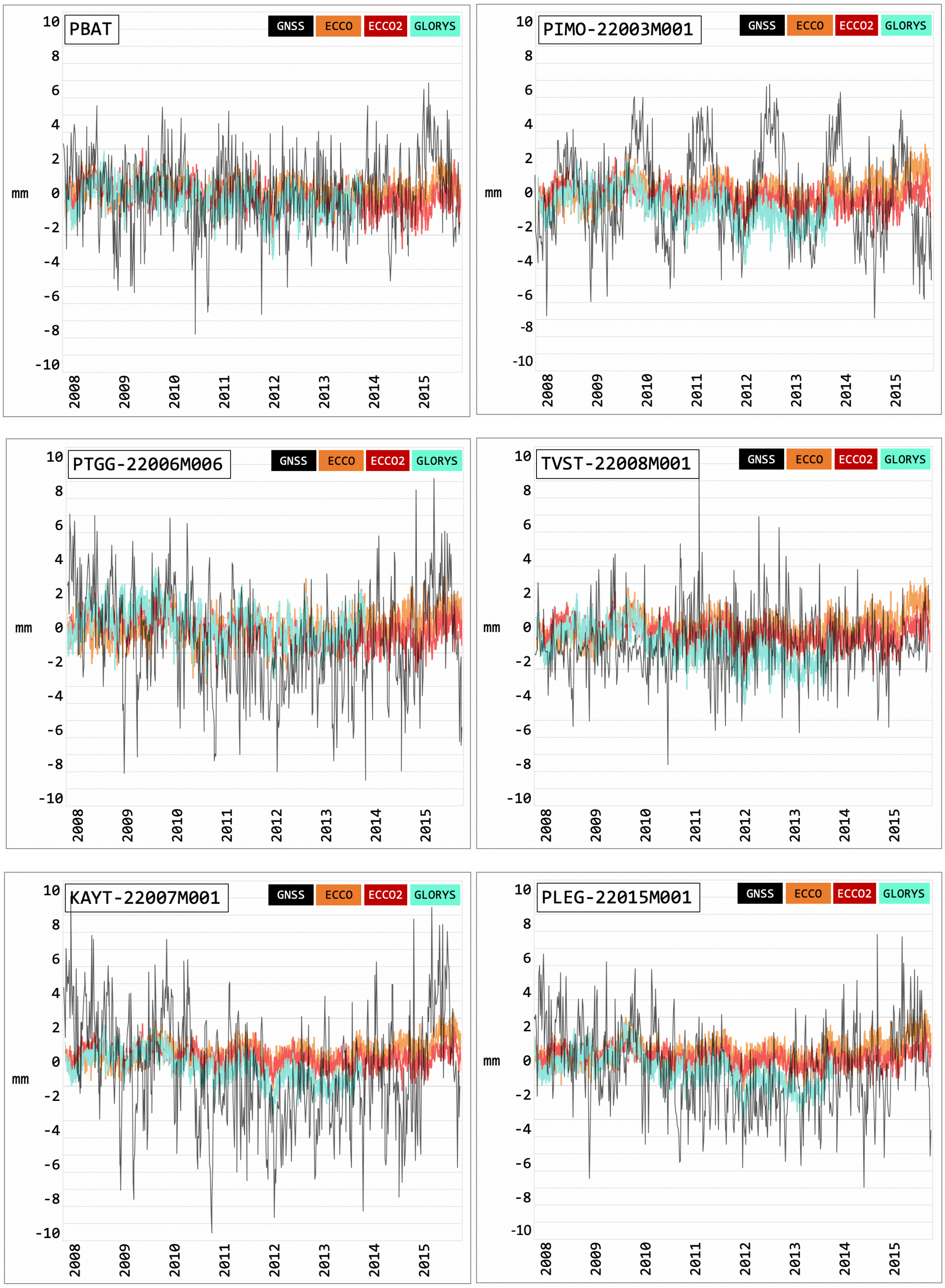
PBAT
PIMO-22003M001
PTGG-22006M006
TVST-22008M001
KAYT-22007M001
PLEG-22015M001
GNSS
ECCO
ECCO2
GLORYS
mm
10
8
6
4
2
0
-2
-4
-6
-8
-10
2008
2009
2010
2011
2012
2013
2014
2015

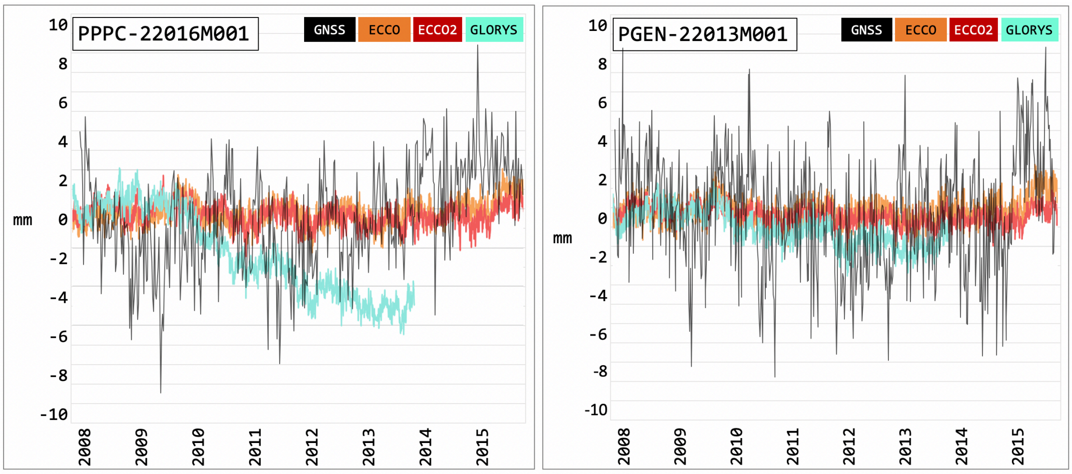

Figure 4.9. Vertical displacements inferred from oceanic non-tidal loading for selected Philippine stations. ECCO is in orange, ECCO2 is in red and GLORYS is in light blue and GNSS time series in black.

ECCO is similar to ECCO2 but produced higher values (an average of 1 mm) of displacement. This may be due to ECCO2's higher temporal resolution (Table 4.2). The difference is on the upward trend since 2010. As will be discussed later, 2010 is a milestone year in terms of rainfall and Philippine weather patterns.

The dynamic ocean response from TUGO-m includes surface winds, which makes it incompatible with classical ocean circulation models. ECCO models are classical ocean circulation models. It should not be combined with atmospheric loading with TUGO-m (EOST, 2015).

The height displacement effects of hydrospheric non-tidal loading are compared for the selected stations (Fig. 4.10. See Fig. 4.6 and 4.7 for the location of the stations).

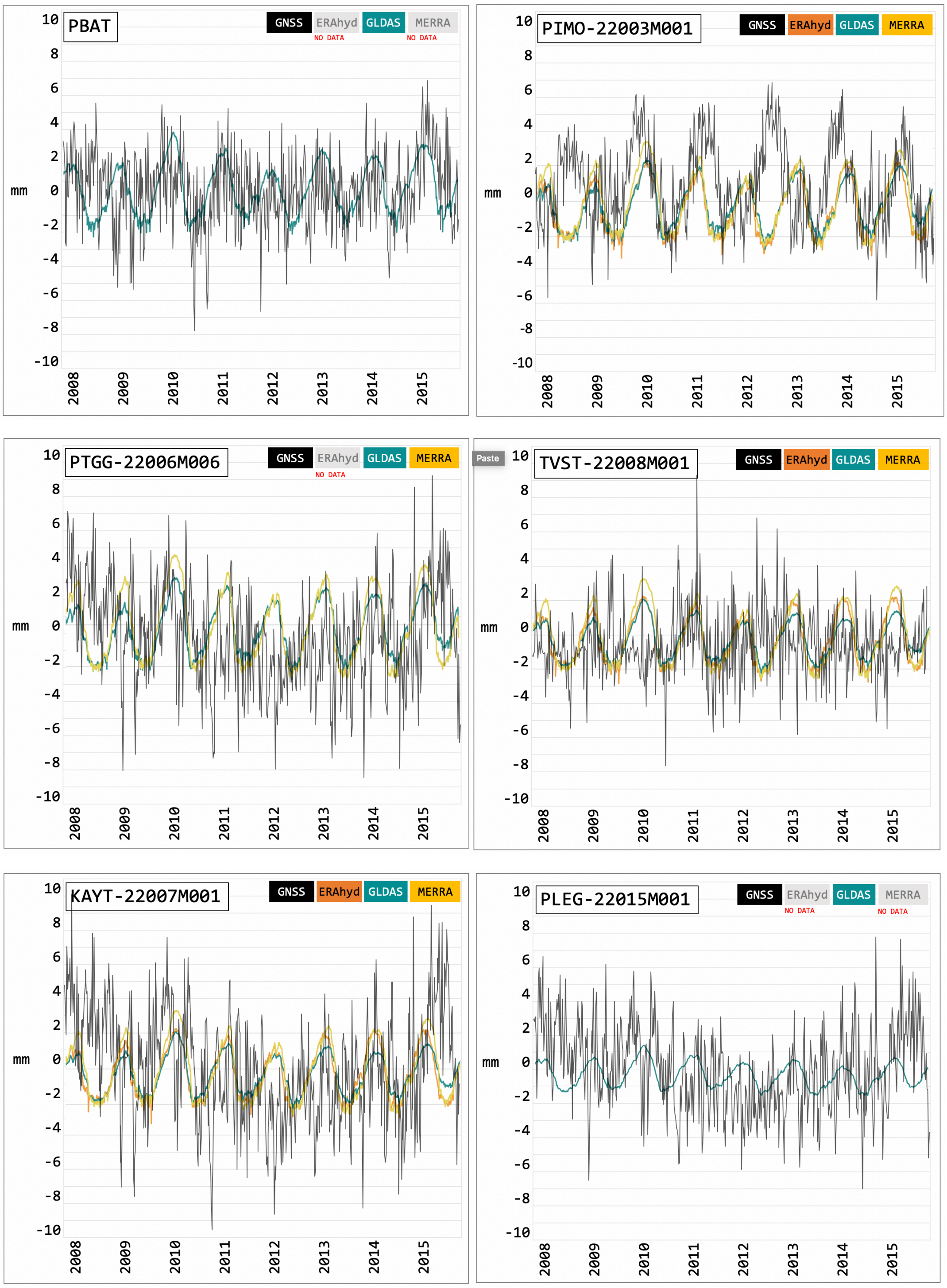
PBAT
GNSS ERAhyd GLDAS MERRA
NO DATA NO DATA
PIMO-22003M001
GNSS ERAhyd GLDAS MERRA
PTGG-22006M006
GNSS ERAhyd GLDAS MERRA
NO DATA
TVST-22008M001
GNSS ERAhyd GLDAS MERRA
Paste
KAYT-22007M001
GNSS ERAhyd GLDAS MERRA
PLEG-22015M001
GNSS ERAhyd GLDAS MERRA
NO DATA NO DATA
mm
10 8 6 4 2 0 -2 -4 -6 -8 -10
2008 2009 2010 2011 2012 2013 2014 2015

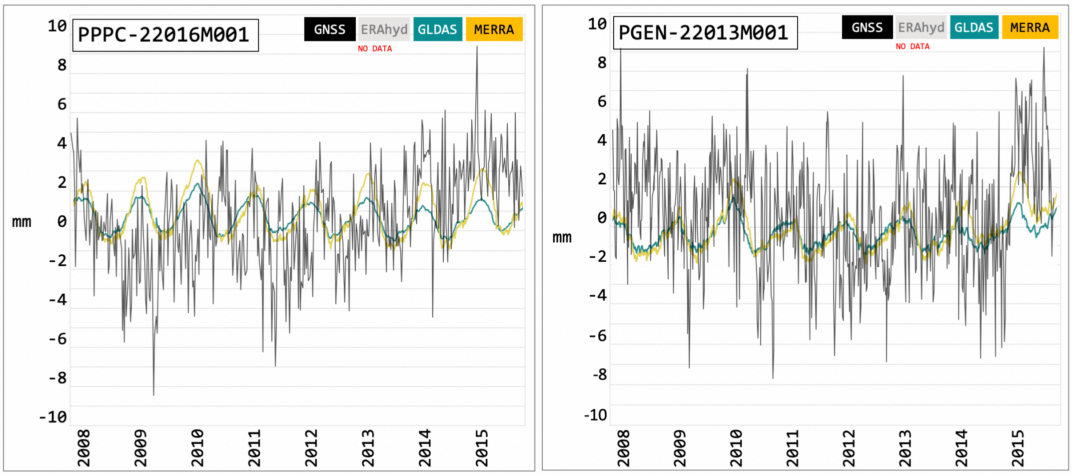

Figure 4.8. Vertical displacements inferred from hydrospheric non-tidal loading for the selected Philippine stations. ERAhyd is in orange, GLDAS is in teal and MERRA is in yellow and GNSS time series in black.

Notable peaks were observed in the years 2010, 2013 and 2015. These are record-breaking years in terms of typhoons and monsoon occurrences for the Philippines over the last decade. In general, the linear trend from 2008 to 2015 implies subsidence of around -0.019 mm per year. However, if the 2014 and 2015 oceanic non-tidal and hydrospheric non-tidal loading are indicators, an upward trend may be emerging.

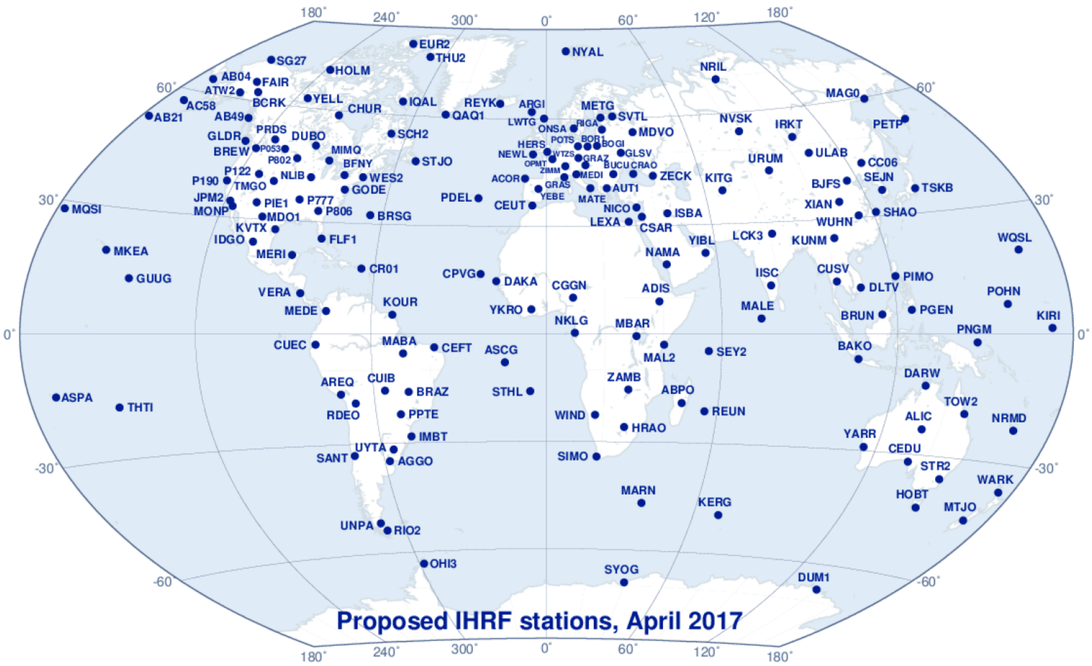

Figure 4.11. Proposed IHRF Stations (as of April 2017) **(Sánchez et al., 2017)**.

The total magnitude of effect for combined non-tidal loading models (atmospheric + oceanic + hydrospheric) range from 6 mm to 8 mm. The hydrospheric loading is larger, in general, than atmospheric non-tidal and oceanic non-tidal loading.

Figures 4.12 and 4.13 provide a closer look at the two stations PIMO and PGEN which were selected for inclusion in the first iteration of the International Height Reference Frame (IHRF) (Fig. 4.11). As mentioned previously, 2013 is a year of high annual rainfall and the occurrence of Typhoon Haiyan in November 2013.

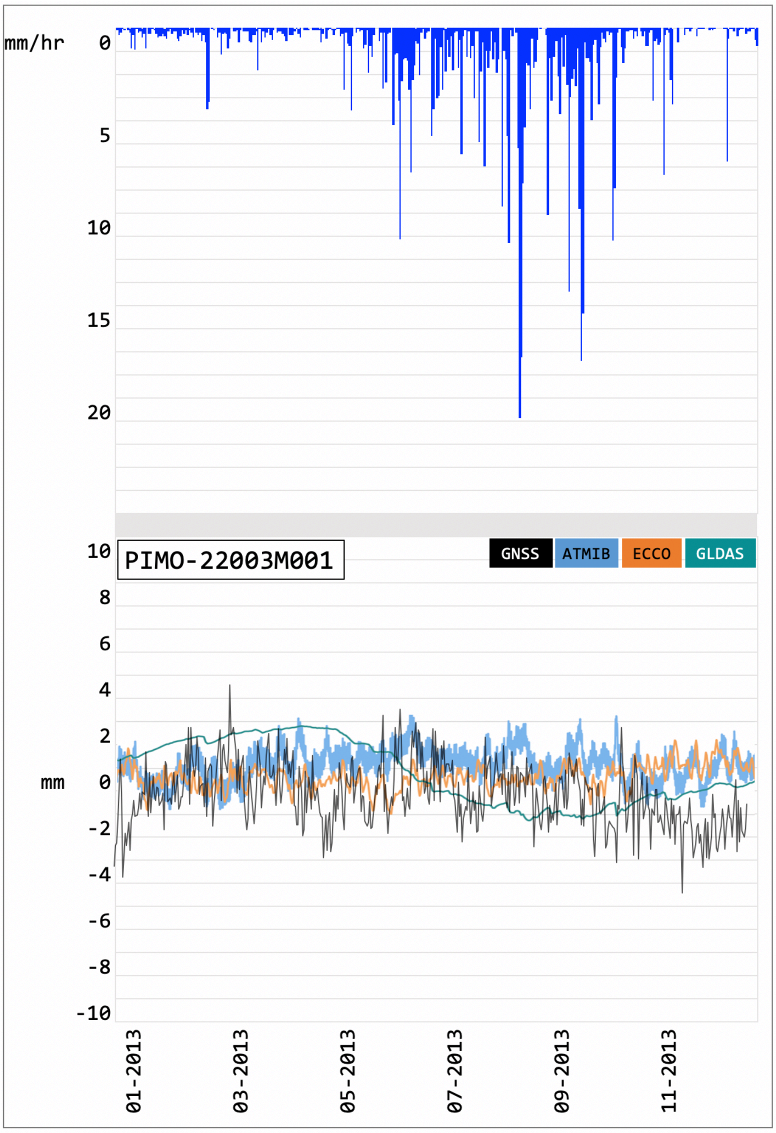

Figure 4.12. (a) 2013 Rainfall Rate over Metro Manila (in mm/hr). (b) Vertical displacements inferred from sample loading models over Metro Manila. ATMIB is in light blue, ECCO is in orange and GLDAS is in teal. GLDAS showed correlation between heavy rainfall rate and subsidence for PIMO.

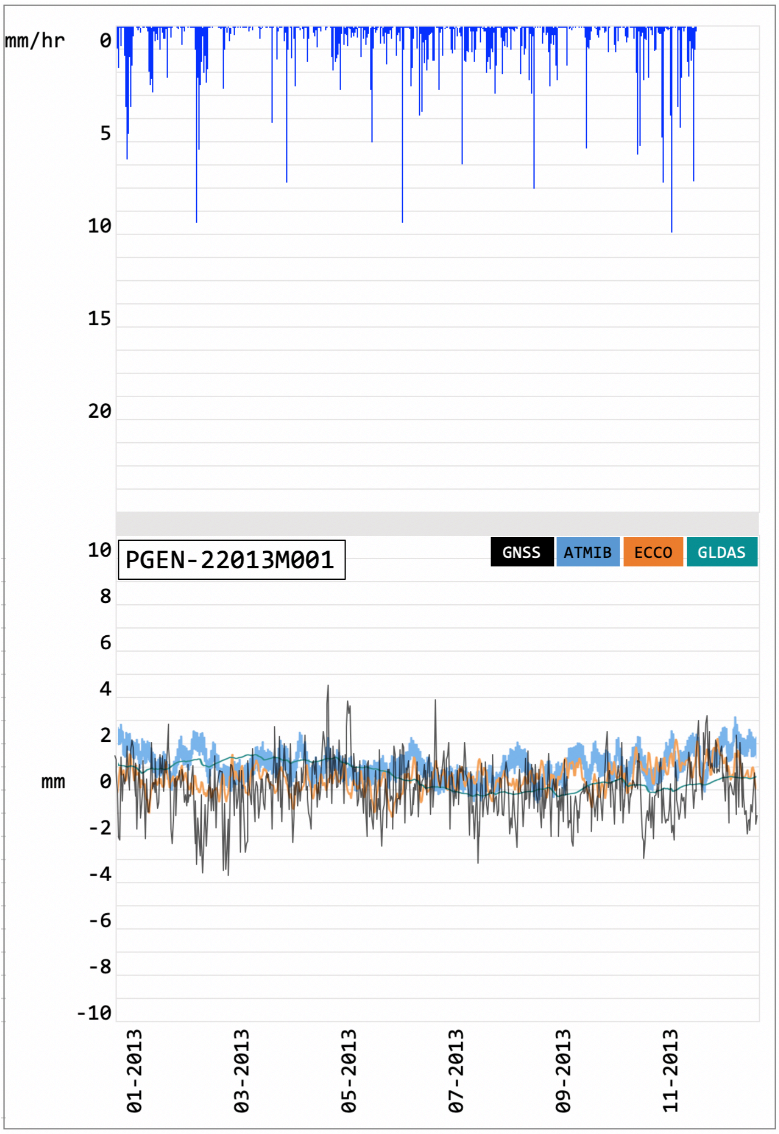

Figure 4.13. (a) 2013 Rainfall Rate over General Santos City (in mm/hr). (b) Vertical displacements inferred from sample loading models over General Santos City. ATMIB is in light blue, ECCO is in orange and GLDAS is in teal.

Tropical typhoons typically carry heavy rainfall. In the Philippines, rainfall does not only come from typhoons but also from tropical monsoons which also affect the trajectory of tropical typhoons should they occur simultaneously. Ideally, borehole strain-meters can be used to determine volumetric deformation by measuring borehole dimension changes at depths of about 100 m to 250 m (UNAVCO, 2014). The signature of heavy rainfall situations typically consists of ground dilation or uplift from atmospheric pressure followed by ground compression or subsidence from water. This signature is shown clearly in Figure 4.12 (from May 2013 to November 2013) because the rainfall occurrence is concentrated over a distinct period as compared to PGEN, whose rainfall intensity distribution is spread out. Consecutive multi-day rainfall situations and water retention properties based on surrounding land cover and soil composition can affect the permanence of displacement (Bressan, 2017).

4.2.2. Land Motion Detection through Satellite Interferometry.

Land subsidence and uplift studies in the Philippines are sparse and limited to highly urbanised areas. Studies are mostly confined in Manila and surrounding cities, Bulacan and Pampanga (Eco et al., 2018), and Davao (Cruz, 2019) in the south. To augment the understanding on benchmark effects, a nationwide scale, low-resolution vertical ground motion map was generated for the Philippines for the first time using a large volume of Sentinel-1A (European Space Agency, 2018) scenes from January 2015 to December 2019. Sentinel-1A was launched April 2014. Processing, co-registration, interferometric processing, phase unwrapping and geocoding were done piecewise in the Sentinel Application Platform (SNAP) software over a three-month period. SNAP is an open source software platform that has a collection of executable tools and Application Programming Interface (API) which is developed by the European Space Agency (ESA) to facilitate the utilization and processing of Sentinel 1, Sentinel 2, and Sentinel 3 datasets (European Space Agency, 2018).

112 Sentinel 1-A Single Look Complex (SLC) products in Interferometric Wide (IW) swath mode were used (Fig. 4.14). These are images in the slant range by azimuth imaging plane, in the image plane of satellite data acquisition (Delgado Blasco, Foumelis, Stewart, & Hooper, 2019). IW captures 3 burst sub-swaths using Terrain Observation with 3 Progressive Scans. Phase filtering of the interferogram for phase noise reduction was applied. The filtering method applied was the method by Goldstein & Werner (1998). Distance distortions, due to the scene’s topographical variations and satellite sensor tilt were corrected by applying the Range Doppler Terrain Correction (RDTC) operator that implements the Range Doppler orthorectification method (Huber, Hummelbrunner,

Raggam, Small, & Kosmann, 2004). The processing was made possible using access and high-power computing facilities of the Advanced Science and Technology Institute (ASTI) of the Philippines. A map of the results is presented in Figure 4.15.

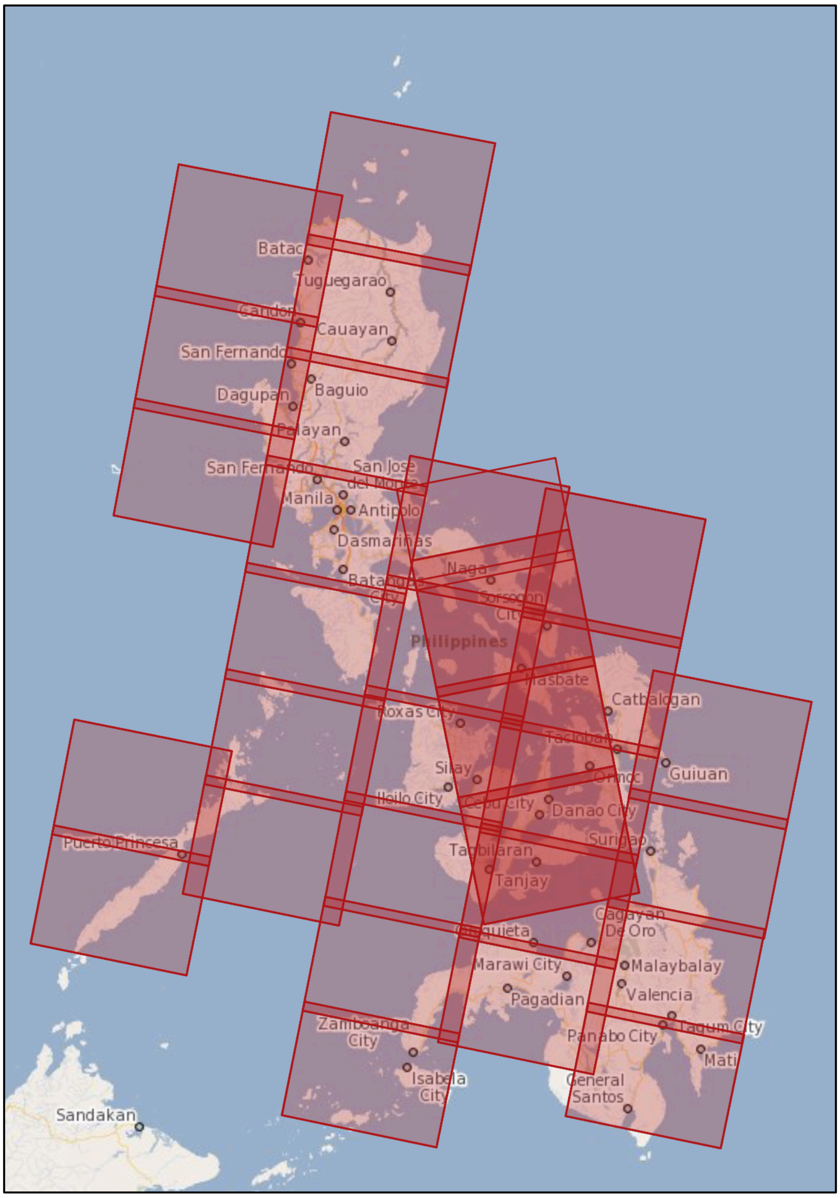

Figure 4.14. Footprint of the Sentinel-1A scenes used for the Philippine vertical ground motion map.

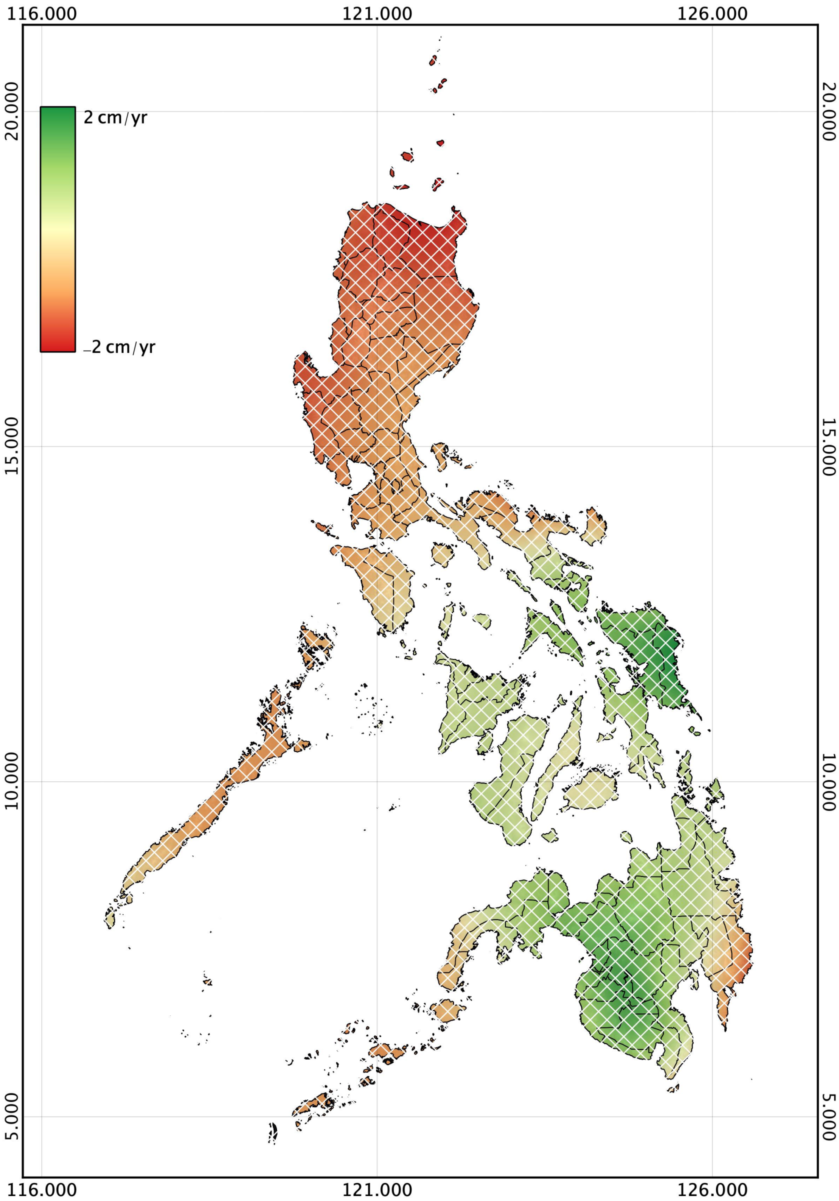

Figure 4.15. A nationwide scale, low-resolution Philippine vertical ground motion map inferred from Sentinel-1A scenes from January 2015 to December 2019 (in cm/yr).

Estimations confirm the intensity of land motion in the eastern and southern part of the country. Ideally, field validation can be done through overlapping observations between geodetic stations and satellite missions over a period of more than five years to account for "trend swings" in the direction of the vertical land motion as seen in PTGG, PGEN KAYT, and PLEG. This is recommended for future studies. A higher-resolution computation is also possible in the future upon the availability of necessary resources. Resolution may explain the apparent inconsistency between the predicted uplift in PPPC and the inferred subsidence from Sentinel-1A, and a "cushioning" of magnitudes. Comparing the Sentinel-1A results with previous studies (Raucoules et al., 2013; Rodolfo, 2014; Eco et al., 2018) in a smaller, localised area yield discrepancies of ~2 cm/yr. Some very small areas in Manila, for example were shown to subside ~5 cm/yr. Some areas in Manila, such as areas where PIMO is located, is not subsiding based on long term GNSS information (uplift of ~2 mm/yr observed over 20 years) Despite the computational limitations, the nationwide results visualised in Figure 4.15 contributes to the very limited large-scale studies of surface behaviour in the Philippines.

4.3. Effect on the Gravimetric Geoid

An assessment of the new Philippine Geoid Model (PGM2016.66, Chapter 3) (Sarmiento, Rizos, & Roberts, 2018) and analysis of the country's hydrological setting identified areas with realisations of geodetic systems that are likely to be affected by extreme hydrological conditions. In the case of the geoid, temporal gravity solutions are necessary to capture variations of the geoid height with respect to time. Monthly Gravity Recovery and Climate Experiment (GRACE) temporal solutions (Kusche, Schmidt, Petrovic, & Rietbroek, 2009) from 2002 to 2015 were used in the investigations. Level 2 solutions from three independent solution providers: Centre for Space Research (CSR) (Save, Bettadpur, & Tapley, 2016), the Jet Propulsion Laboratory (JPL) (Watkins et al., 2005) and German Research Centre for Geosciences (GFZ) (Dahle, et al., 2019) were used through the International Centre for Global Earth Models (ICGEM) computing service (Barthelmes, 2013; Ince et al., 2019).

The rate of change of a gravity functional is given by (Rangelova, 2007),

$$L\dot{T}(\theta,\lambda,t) = \sum_{l=2}^{\infty}\sum_{m=0}^{l}\beta_l\bar{P}_{lm}(\cos\theta)\left(\dot{\bar{C}}_{lm}(t)\cos(m\lambda) + \dot{\bar{S}}_{lm}(t)\sin(m\lambda)\right) \qquad (4.6)$$

Where β_l are the gravity functionals transfer coefficients; $\bar{P}_{lm}$ are fully normalised Legendre functions of degree and order l and m; and $\dot{\bar{C}}_{lm}$(t) and $\dot{\bar{S}}_{lm}$(t) are time (t) derivatives of the geopotential coefficients; λ is geodetic longitude.

The rate can be estimated using least squares by,

$$K_{lm}(t_j) = k_1 t_j + k_2 \cos(\omega t_j) + k_3 \sin(\omega t_j) + k_4 \cos\left(\frac{\omega t_j}{2}\right) + k_5 \sin\left(\frac{\omega t_j}{2}\right) + v(t_j) \tag{4.7}$$

where $K_{lm} = \{\dot{\bar{C}}_{lm}, \dot{\bar{S}}_{lm}\}$ at epoch t_j. k_1 is the trend, k_2 is the annual cosine amplitude and k_3 is the annual sine amplitude, k_4 and k_5 are semi-annual component amplitudes, ω is the frequency of one cycle per year and $v(t_j)$ is the random error.

GRACE spherical harmonics contain noise that appear in the dataset as a striping pattern with a north-south orientation (Fig. 4.16). The following are possible causes (Schrama, Wouters, & Lavallée, 2007):

1. The ground track produces an error structure that, when combined with the range-rate observable affects observations.
2. A misidentification of signal frequency because of the under sampling of the time variable signal in its temporal and spatial components.
3. Limited signal correction products.

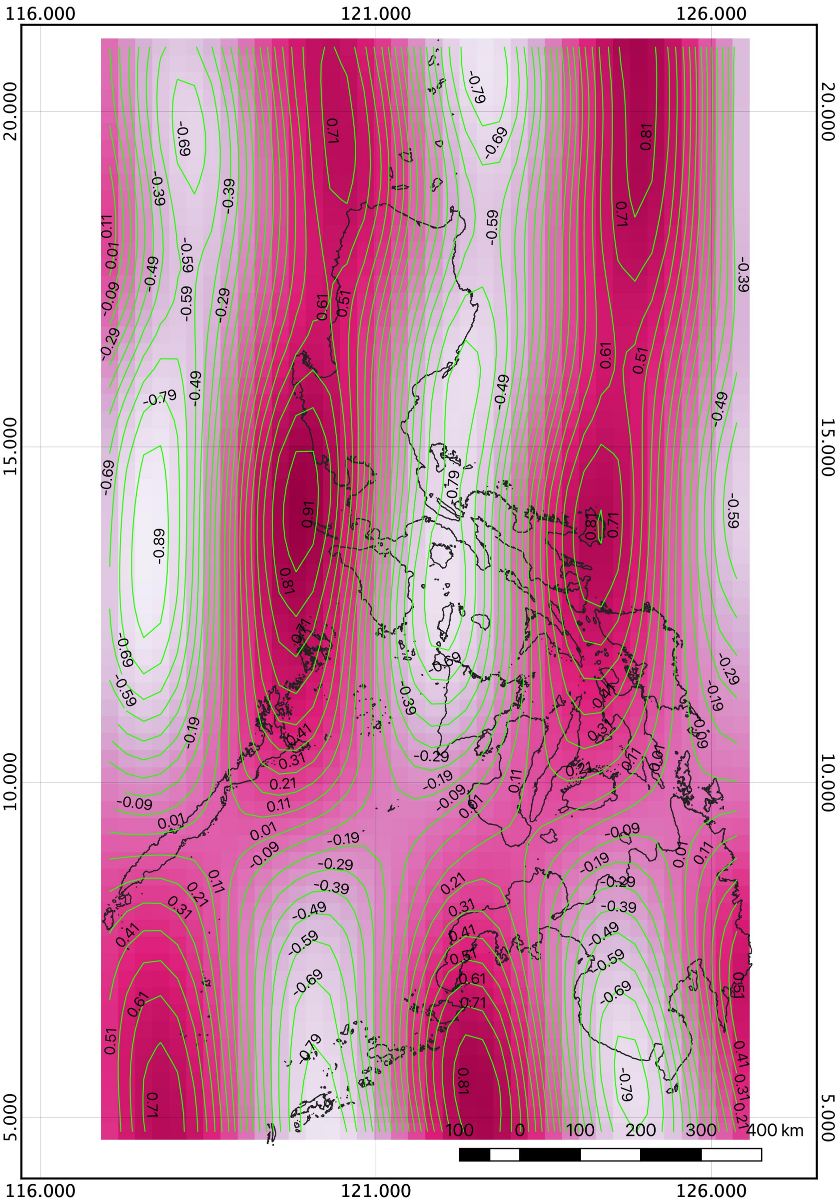

Figure 4.16. Unfiltered formal errors of Philippine geoid rates (in mm).

Non-tidal loading effects were treated (van Dam, Collilieux, & Wuite, 2012; Knudsen, Andersen, Khan, & Høyer, 2001) and tidal effects were removed in the Level 2 processing. Provided that these effects are still present in the GNSS data, the effects were restored to the spherical harmonic solutions for consistency. The models were computed in the CM frame. Satellite geometry (orbits, satellite separation) affects the accuracy of the determination of low-degree spherical harmonic coefficients (Chen, Wilson, & Seo, 2006). The C_{20} coefficient in GRACE gravity field models, which describes changes of the Earth's dynamic oblateness (Chen, Rodell, Wilson, & Famiglietti, 2005), was replaced with satellite laser ranging-derived estimates from Cheng, Tapley & Ries (2013). An approach that can be explored for the Philippines in future determination of variations of low-degree coefficients is through the use of surface mass loading inferred from the GNSS-sensed solid Earth deformation studies (Blewitt, Lavalleé, Clarke, & Nurutdinov, 2001; Wu, Ray, & van Dam, 2012).

The unfiltered formal errors (Fig. 4.16) can be minimised by omitting the higher degree and order spherical harmonics. Another way to deal with these errors is through suppression, and in some cases "masking", using filters (Wahr, Molenaar, & Bryan, 1998; Sasgen, Martinez, & Fleming, 2007; Seo, Wilson, Famiglietti, Chen, & Rodell, 2006). Filters can be isotropic or non-isotropic. An example of an isotropic filter is the Gaussian filter. It is often used to deal with higher degree noise for large areas. It is expressed using an averaging function (Jekeli, 1981)

$$W\,(\Psi) = \frac{b}{2\pi}\left(\frac{exp[-b(1-cos\psi)]}{1-e^{-2b}}\right) \tag{4.8}$$

where $b = \frac{\ln(2)}{1-\cos(\frac{r}{R})}$, and the averaging radius $r = R\psi$ is the half-width of the filter with ψ as the spherical distance. Figure 4.17 shows an implementation of the Gaussian filter at multiple half-widths. Comparison with Figure 4.18 shows the increasing discrepancies of estimates near the boundaries of the computational area with increasing halfwidths.

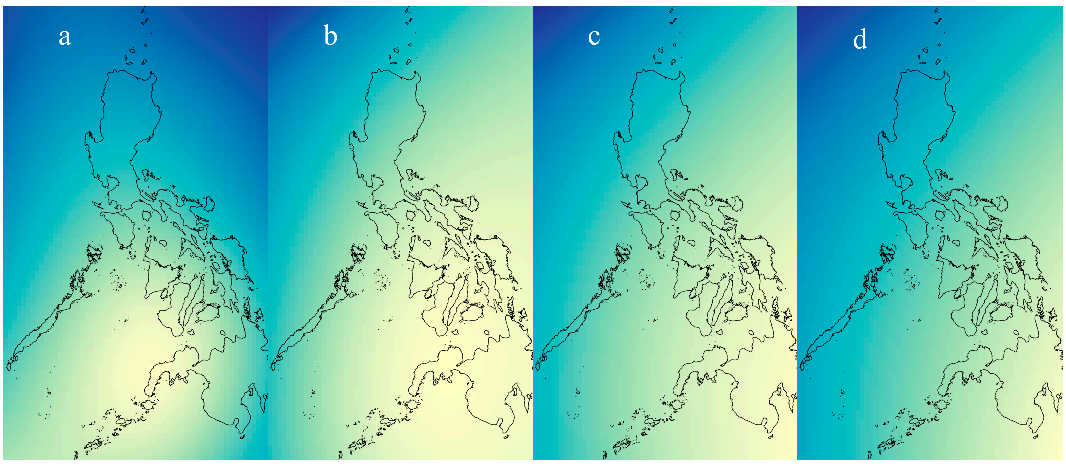

Figure 4.17. Effect of the Gaussian filter of half-widths, a. 400 km b. 600 km c. 750 km d. 1000 km, on geoid rates.

In the literature, the optimal filter half-width can range from 400 to 1000 km (Rangelova E. V., 2007). Higher half-widths increase the occurrence of errors coming from outside the study area upon the application of the filter near the study area boundaries. The spatial distribution of GRACE noise, as shown in Figure 4.13, is non-isotropic. This means that an isotropic filter does not remove the error, though some filters have demonstrated an ability to agree with estimates made using alternative methods, as in the case of Gaussian filters.

A non-isotropic filter is defined as (Chen, Wilson, & Seo, 2006),

$$W_{lm} = \frac{var(K_{lm}, K_{lm})}{var(K_{lm}, K_{lm}) + \sigma^2_{K_{lm}}} \tag{4.9}$$

where $K_{lm} = \{C_{lm}, S_{lm}\}$; $\sigma^2_{K_{lm}}$ is the error variance for the coefficient K_{lm}

This filter has been shown to be more appropriate and effective at suppressing the GRACE coefficients with dominant errors (Chen, Wilson, & Seo, 2006). Figure 4.15 shows the GRACE geoid rate after application of the non-isotropic filter. Higher rates of change were computed towards the equator. The computed rates of change are small (max ~0.16 mm/yr) compared to areas with effects from post-glacial rebound (max ~1.5 mm/yr. (Rangelova, van der Wal, & Sideris, 2007)). GRACE geoid errors listed in Rangelova (2007) is approximately 11 mm which exceeds the geoid rate estimates produce in this study.

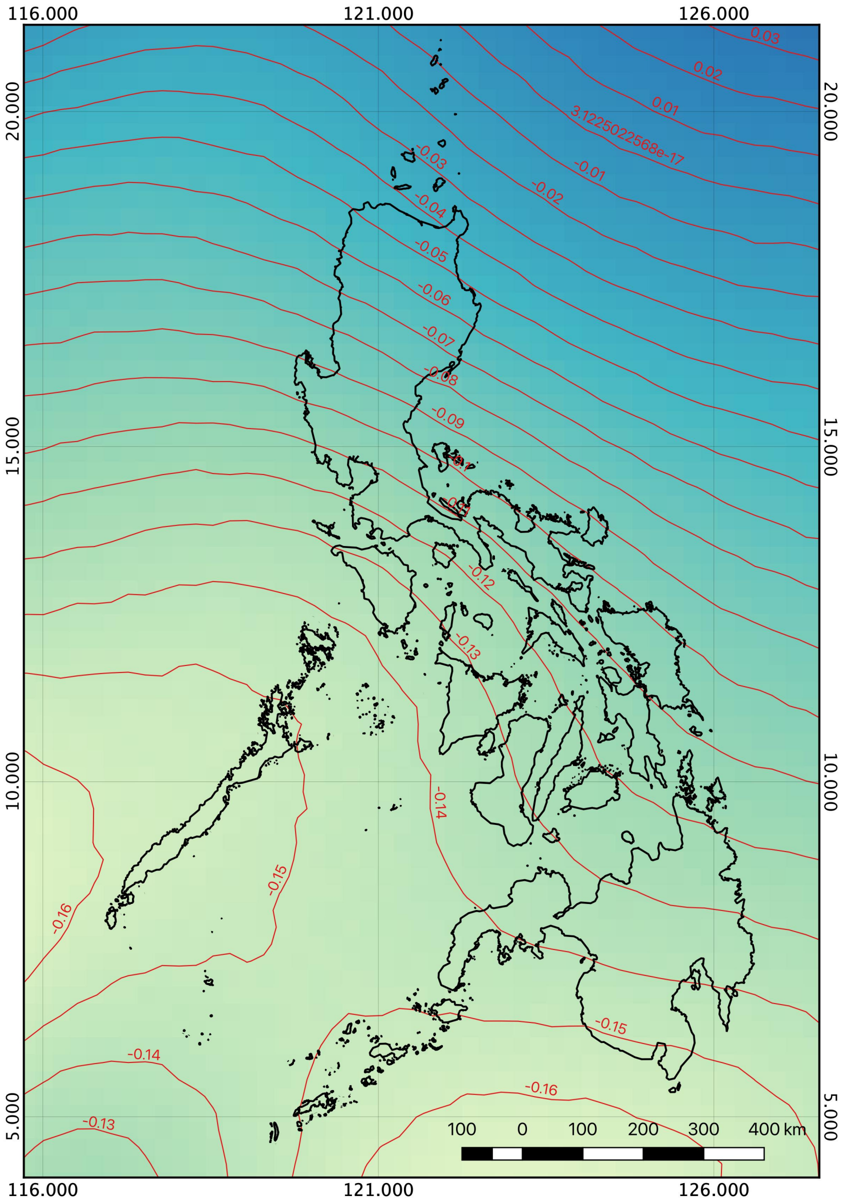

Figure 4.18. Rates of change of the geoid height with the non-isotropic filter (in mm/yr).

Figure 4.19 shows interesting changes in geoid heights. The figure shows two stations, PIMO and PGEN that were proposed to be the contribution of the Philippines to the development of the International Height Reference Frame (Fig. 4.16) (Sánchez et al., 2017).

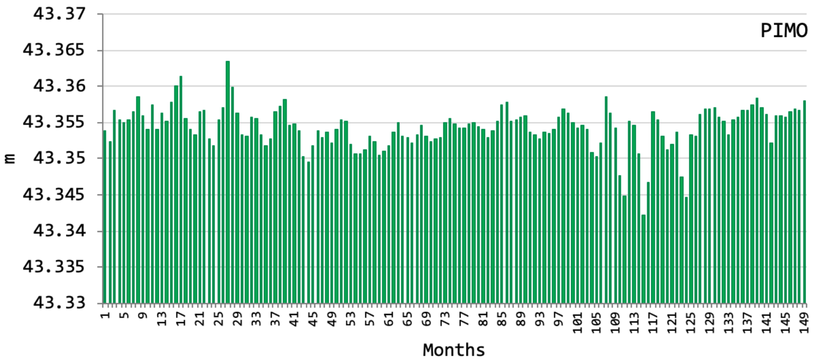

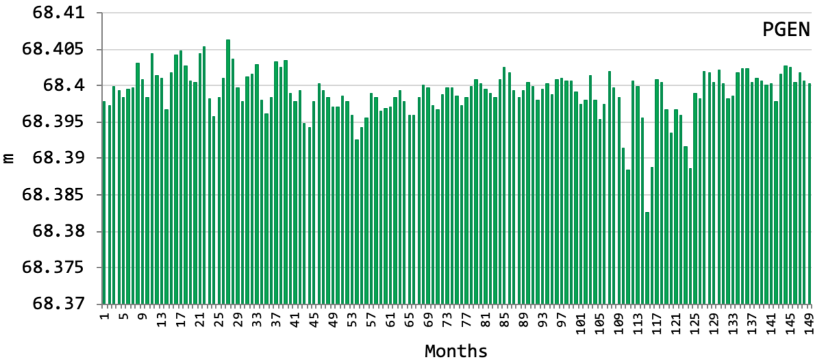

Figure 4.19. Geoid height (in m) variations for sample stations (PIMO and PGEN) from 2002 to 2015 GRACE temporal solutions.

The GRACE temporal models indicate large variations (~5mm to 10mm) from month 106 to 134 (October 2010 – February 2013) for both stations. This is coincident with the 2010-2013 high rainfall period mentioned previously. Limited field information for the areas in the time frame is insufficient to establish that high rainfall periods cause variations in the geoid.

4.4. Recommendations on the treatment of temporal effects on the Philippine Height System

Temporal effects, in the context of a regularly distributed data, can be treated as a time-dependent Geodetic Boundary Value Problem (GBVP) (see Chapter 2, Section 2.3.5) with the deformable solid Earth surface as a boundary surface and gravity and heights as the boundary data. Extensive formulations of the boundary value problem are presented in the texts of Biró (1983), and Heck and Mälzer (1986). Biró's formulation is independent of assumptions associated with the driving mechanisms of internal mass redistributions. Assuming a stationary geocentre, the relationship for the rates of change can be given by,

$$\dot{h} = \dot{H} + \dot{H}_O + \dot{N} \tag{4.10}$$

where, $\dot{h}$ is the rate of the absolute vertical displacement derived from the BVP solution; $\dot{H}$ is the rate of change of the orthometric height; $\dot{H}_O$ is the rate of change of the fundamental datum point; $\dot{N}$ is the rate of change of the geoid heights. For irregularly distributed data, approaches that are data-driven, such as the least squares method used in the computation of the geoid rates, is implementable.

In the realisation of the new Philippine Height System, a framework of fundamental points can be stations with accurate information on GNSS positions and absolute gravity that are corrected for tidal and non-tidal effects. Corrections of permanent tide effects are essential in relating and adjusting geodetic observations with diverse epochs. Systematic distortions in the inferred displacements have been observed in this study's early computations that lack consideration for permanent tide systems. Consideration and consistency of tide systems are necessary if the new Philippine Height System is to be geoid-based and dependent on these fundamental stations.

Given that combined characteristic errors of the height components h, H and N is estimated to be in the range of ~10 mm to ~10 cm (or possibly more), a frequent correction of the geoid model is not practical. The accounting of vertical land motion, however, should be considered at least annually. Though vertical land motion can be detected using InSAR, ground techniques such as precise re-levelling and/or continuous GNSS observations over a dense network still provide the most reliable observations.

4.5. Chapter Summary

Linking the Philippine Height System to the International Height Reference System/Frame involves the understanding of the relationship of the existing height systems/frames with the conventional W_0 value (investigated in Chapter 5) and the understanding of the temporal variations.

This is the first study on hydrological effects to physical monuments and on the geoid of the Philippine Height System. The effects on physical benchmarks were determined by analysing the atmospheric, oceanic and hydrospheric non-tidal loading for selected Philippine Active Geodetic Network (PAGeNet) and École et Observatoire des Sciences de la Terre (EOST) supplementary stations for the period 2008-2015.

Models based on the European Centre for Medium-Range Weather Forecasts (ECMWF) operational model were used to derive height effects due to atmospheric loading. The seasonality in precipitation is shown to produce an average loading effect between -2 mm to 2 mm for PLEG, PPPC and PGEN; and -2.5 mm to 2.5 mm between PIMO, PTGG and PBAT. TVST exhibit an asymmetrical displacement pattern (more compressive than expansive) and KAYT had the largest height displacements of approximately -5 mm to 5 mm. The mechanism for the irregularity may be geographic and geologic in origin due to the volcanic characteristics of KAYT's location.

The dynamic ocean response from the TUGO-m model makes ATMMO an optimal atmospheric and non-tidal loading model for the Philippines. However, it is incompatible with classical ocean circulation models.

Seasonal trends for oceanic non-tidal loading are not as pronounced as those for atmospheric and hydrospheric non-tidal loading. The GLORYS data for the station on the island adjacent to the West Philippine Sea (PPPC) began a steep drop of approximately 5 mm from 2009 which is not the case for ECCO-based models. Higher values (average of 1 mm) of displacement between ECCO and ECCO2 were computed, which may be due to the difference in temporal resolution (Table 4.2). The difference is on the upward trend since 2010.

Hydrospheric non-tidal loading effects through soil moisture were computed using the ERAin, GLDAS, MERRA models. Notable peaks were observed in the years 2010, 2013 and 2015. In general, the linear trend from 2008 to 2015 is downward (around -0.019 mm per year). However, if the 2014 and 2015 oceanic and hydrospheric non-tidal loading are indicators, an upward trend may be emerging.

The signature of heavy rainfall typically consists of ground dilation from atmospheric pressure followed by ground compression from water. This signature is shown clearly in the PIMO station because the rainfall occurrence is concentrated over a distinct period (May 2013 to November 2013).

Estimations through Interferometric Synthetic Aperture Radar (InSAR) confirm the intensity of land motion in the eastern and southern part of the country. Resolution may explain the apparent inconsistency between the predicted uplift in PPPC and the inferred subsidence from Sentinel-1A, and a "cushioning" of magnitudes. Comparing the Sentinel-1A results with previous studies (Raucoules et al., 2013; Rodolfo, 2014; Eco et al., 2018) in a smaller, localised area yield discrepancies of ~2 cm/yr. Some very small areas in Manila, for example were shown to subside ~5 cm/yr. Some areas in Manila, such as areas where PIMO is located, is not subsiding based on long term GNSS information (uplift of ~2 mm/yr observed over 20 years) Despite the computational limitations, the results contribute to the very limited large-scale studies of surface behaviour in the Philippines.

Gravity variations are estimated using the Gravity Recovery and Climate Experiment (GRACE) temporal solutions. Solutions from three independent solution providers Centre for Space Research (CSR), Jet Propulsion Laboratory (JPL), and (German Research Centre for Geosciences) GFZ were investigated. Gravity field solutions from 2002 to 2015 were used for the calculations. Large variations of approximately 5 to 10 mm from month 106 to 134 (October 2010 – February 2013) were noted for both stations. Computations show coincidence to the 2010-2013 high rainfall period. A causality relationship between extreme weather events and geoid variation, however, is inconclusive. Table 4.5 provides a useful summary of known geophysical phenomena affecting the geoid.

Table 4.5. Geophysical phenomena effecting the shape of the geoid. (Jacob et al., 2012)

	Frequency	**Time span for a 1-cm geoid change**	**Observations/models needed (incomplete list)**	**Comments**
Continental hydrology and climate variability	Secular/ Periodic/ Episodic	~50-100 years	Meteorological forcings, GRACE-like missions, LSMs, GCMs	Predicted geoid changes from LSMs and GCMs vary greatly
Groundwater withdrawal	Secular/ Periodic/ Episodic	~30-60 years	Hydrological/meteorological measurements, 3D aquifer-scale models	Will depend on pumping rates and future climate
Glacial isostatic adjustment	Secular	<10 years	Ice history, mantle rheology, ground-based geodesy, GRACE like missions	Use of current model leads to a 1-cm error after 20 years
Ice mass loss	Secular/ Periodic	<10 years	Ground-based geodesy, ice sheet elevations, GRACE-like missions, ice sheet mass balance	Rates are not linear, depends on future climate
Earthquakes	Episodic	Coseismic: instant; Postseismic: 1-10 years	Seismic networks, ground-based geodesy, mantle rheology	Important for only the largest megathrust subduction earthquakes
Volcanic eruptions	Episodic	Instant	Ground-based geodesy, seismic networks	Significant only for cataclysmic events, flank collapse

In a demonstration of the time-varying effects over two proposed International Terrestrial Reference Frame (IHRF) stations, it was shown that conventions on the accounting of these effects are necessary. The last two rows of Table 4.5, for example, needs comprehensive monitoring for the Philippines. Tectonically active countries may experience geoid changes that are large but localised. Local areas affected by earthquakes and volcanic eruptions should be re-observed by repeat campaigns. Very recently (12 January 2020-ongoing), Taal Volcano (the vicinity of KAYT and TVST) erupted. With the eruption came important information that can contribute to future accounting of unpredictable episodic variations.

Given that combined characteristic errors of the height components h, H and N is estimated to be in the range of ~10 mm to ~10 cm (or possibly more), a frequent correction of the national geoid model is not practical. The accounting of vertical land motion and loading effects, however, should be considered at least annually. Though vertical land motion can be detected using satellite methods, ground techniques such as precise re-levelling and/or continuous GNSS observations over a dense network still provide the most reliable observations. Considerations on the treatment of localised effects on IHRF stations needs to be studied if the IHRS/F is to be practical for local applications.

This chapter supports the development of the new Philippine Height System by providing insight on how tropical factors affects PHS benchmarks and the geoid. This chapter also supports NAMRIA's decision making with respect to PHS update frequency and considerations in the crafting of the next phases of the PHS modernisation structure and timeline. New space-borne technologies, such as the GRACE Follow On mission and other upcoming gravity missions, in addition to an increased investment by the Philippines in geodetic infrastructure and field campaigns, provides research opportunities that can build on the results of this study.

Chapter 5: The Philippine Height System and the International Height Reference Frame explores the challenges of relating the PHS to the global reference system for physical heights.

Chapter Five

The Philippine Height System and the International Height Reference System

5.1. The International Height Reference System

For more than a century, height systems have operated with minimal or no integration with each other. Studies on the realisation of a "World Height System" have been well documented in geodetic literature by Rapp & Balasubramania (1992), Burša et al., (1992; 1999; 2007); Gruber, Gerlach, & Haagmans (2012) Ihde et al., (2015) and many others. In 2011, the Global Geodetic Observation System (GGOS) of the International Association of Geodesy (IAG) organised the Global Geodetic Observing System (GGOS) Focus Area 1: Unified Height System, to respond to the growing need for height systems integration. The initiative is motivated by the need for consistent heights in capturing environmental changes that goes beyond administrative boundaries and the development of new geodetic techniques and technologies. The consultations and preliminary studies resulted in an IAG resolution released in the 26th General Assembly of the International Union of Geodesy and Geophysics last July of 2015. The resolution mandates the establishment of the International Height Reference System (IHRS) and its realisation into the International Height Reference Frame (IHRF) for the next four years (International Association of Geodesy, 2015).

According to the GGOS Focus Area 1, the IHRS/F should (GGOS, n.d.),

1. supports geometrical (ellipsoidal) and physical (normal, orthometric, geoidal) heights world-wide with centimetre precision in a global frame;
2. enables the unification of all existing physical height systems (i.e., all geopotential differences shall be referred to one and the same reference equipotential surface with potential W_0); and
3. provides high-accuracy and long-term stability of the vertical coordinates.

The IHRS is defined in terms of potential parameters (Ihde et al., 2015),

$$C(P) = W_0 - W(P) = -\Delta W(P) \quad (5.1)$$

Where W_0 is the global reference potential, $C(P)$ is a geopotential number that represents the difference between W_0 and the potential $W(P)$ at point P (Fig. 5.1. Also See Chapter 2).

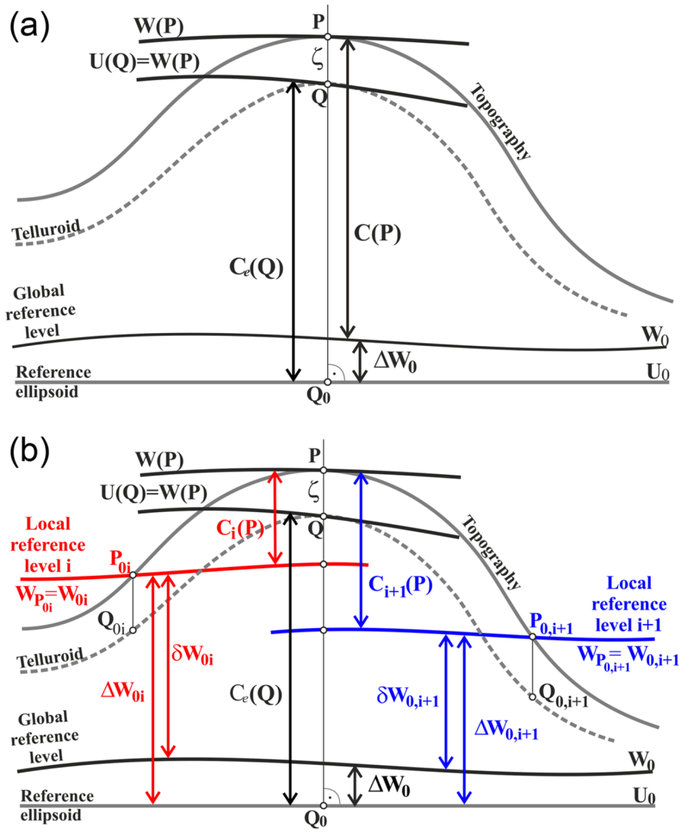

Figure 5.2 a. Potential anomaly within a global height reference system. b. vertical datum parameters for local height systems *i* and *i + 1*. **(Sánchez & Sideris, 2017)**

The reference potential W_{0i} of a local height system with vertical datum i ={1,2,3,…m}, (where the local geopotential number $C_i(P)$ is referred to) is $W_{0i} = W(P_{0i})$ or the potential at local origin point, P_{0i}. The local origin point is usually a fundamental tide gauge where the local mean sea level that realises the local reference surface, is measured from.

In some cases, multiple benchmarks are used to define the local reference potential using the formula,

$$\widehat{W}_{0i} = \frac{1}{K}\sum_{i=1}^{K}[W(P_i) + c(P_i)] \tag{5.2}$$

The local vertical datums and the global vertical datum are related through Vertical datum parameters defined by the relationships $W_0 - W_{0i}$. The choice of the geoid reference potential, W_0, can be arbitrary. The adoption of the IHRS/F , provides the global W_0 value 62636853.4 m^2s^{-2} by convention to support consistency in the relationship among national height systems (Sánchez et al., 2016).

In the Philippines, the traditional establishment of local height systems is independent from W_0 values or gravity field models. Direct or indirect relative measurements from benchmarks with fixed heights have been sufficient for practical determination of heights. Infrastructure between islands such as inter-island bridges are very limited (logistics and transportation mostly rely on modes through sea and air which were perceived to be cheaper that constructing long-distance bridges), thus the motivation for a "centralised" height system was lacking in the past. The absence of such motivation is a factor in the piecemeal development of the Philippine Height System. As mentioned in Chapter 3, the Philippine Height System (PHS) is a collection of multiple local height systems that are realised by utilising mean sea level (MSL) observations at one or more fundamental tide gauges (ideally) gathered over a long period. These local sea level observations were traditionally averaged in attempts to define a levelling surface for the Philippines (Paringit & Paringit, 2015). This method is problematic because it produces an assumption that the sea level at one local height system is the same as the other (Pan & Sjoberg, 1998; Kearseley & Ahmad, 1995) or that the different local height systems that form the PHS are defined similarly.

Most of the large islands (e.g. Mindanao, Iloilo, Palawan) have local vertical datums tied to one or more tide gauges located in the same island. The Luzon island where most of the development is concentrated, is covered by multiple height systems. Some islands have vertical datums that were tied to the tide gauge of another island (e.g. Tablas, Socorro). These datums are still in use but the data and the computations establishing ties cannot be recovered. Inland height systems have several versions and connections from one inland vertical datum to another cannot be identified. Some small, inhabited islands do not have height systems that are practically based on fundamental tide stations. Development on these islands refer heights from "safe" structures, or coast side structures (that may or may not still exist) that are not reached by the high tide.

The manner of development is not surprising considering factors such as the large socioeconomic gaps between islands, changes in the political climate, poor documentation and change management resulting in unsatisfactory quality control, undocumented assumptions and use of poorly verified data over time. These "human factors" were combined with geographical, geological, and environmental factors to create a complex situation that makes a single W_{0i} estimate for the Philippines difficult to interpret. This reality, which is not ideal but is not uncommon, needs to be considered to integrate developing countries that have similar geodetic situations as the Philippines in the development of the IHRS/F. For the aforementioned reasons, the treatment of the Philippine Height System as a regional system consisting of multiple local height systems is proposed.

The determination of geoid heights in the context of the IHRS requires the accounting of the zero degree term. The International Centre for Global Earth Models (ICGEM) computing service (Barthelmes, 2013; Ince et al., 2019) includes the zero degree term in the calculations based on different values of $GM * C_{00}$ of the geopotential model, and GM of the normal potential. The zero degree term is given by the following relationships (Heiskanen & Moritz, 1967),

The zero degree term for the disturbing potential *(T_0)* is,

$$T_0 = \frac{(GM_{GGM} - GM_{GRS80})}{r_P} \tag{5.3}$$

The zero degree term for the geoid *(N)* is,

$$N_0 = \frac{(GM_{GGM} - GM_{GRS80})}{r_P \gamma_{Q_0}} - \frac{W_0 - U_0}{\gamma_{Q_0}} \tag{5.4}$$

And for the quasigeoid *(ζ)*,

$$\zeta_0 = \frac{(GM_{GGM} - GM_{GRS80})}{r_P \gamma_Q} - \frac{W_0 - U_0}{\gamma_Q} \tag{5.5}$$

where GM_{GGM} and GM_{GRS80} are respective model constants for the GGMs and GRS80; r_P is the geocentric radial distance of point P.

5.2. Determination of $\widehat{W}_{0i}$

5.2.1. Approach 1. An approach using orthometric heights and gravity information independent of geoid heights.

Gridoriadis et al., (2014) developed an estimator that uses orthometric heights and gravity information. The advantage of this method is the elimination of terrain modelling errors due to its independence from using geoid heights. The simultaneous estimation of multiple W_{0i} takes Equation 5.2 and yields

$$\widehat{W}_{0i} = \frac{1}{K}\sum_{i=1}^{K}[W(P_i) + \bar{g}_i H(P_i)] \tag{5.6}$$

where $W(P_i)$ is the gravity potential at the levelling benchmark synthesized from a gravitational part of the geoid model's spherical harmonic coefficients and a centrifugal part using the benchmark's known spatial position and the Earth's conventional rotational velocity (Petit & Luzum, 2010). The zero degree term was considered.

This approach is demonstrated in Gridoriadis et al., (2014), Tocho & Vergos (2015), and He et al., (2017) using EGM2008 and EGM2008-derived $W(Pi)$ and g_i values. Equation 5.7 then describes the weighted least-squares estimator with the unknown parameter $\widehat{W}_{0i}$.

$$\widehat{W}_{0i} = \frac{\sum_i p_i [W(P_i) + \bar{g}_i H(P_i)]}{\sum_i p_i} \tag{5.7}$$

where p_i, a benchmark weight factor used to detect the presence of height dependent systematic errors, combined with the residual, $\delta W(P_i)^2$ satisfies,

$$\sum_i p_i \delta W(P_i)^2 = min \tag{5.8}$$

$1/H(P_i)$, $1/H(P_i)^2$ *and* $1/H(P_i)^{0.5}$ are used as p_i in the estimator, and labeled A1.1, A1.2 and A1.3 respectively.

5.2.2. Approach 2. An approach using GNSS/levelling and geoid heights

The second approach combines orthometric heights, ellipsoidal heights and geoid heights in a least squares estimator with unknown parameter $\widehat{W}_{0i}$ given by,

$$\widehat{W}_{0i} = W_0 - \frac{\sum_{i=1}^{K} \frac{1}{g(P_i)} [h(P_i) - H(P_i) - N(P_i)]}{\sum_{i=1}^{K} \frac{1}{g(P_i)^2}} \tag{5.9}$$

The PGM2016.66 and selected global geopotential models (GGM) (for comparative purposes) were used for Approach 2. This method is recommended for geographically isolated areas (such as islands), with heterogenous heights and limited gravity information. The zero degree term was considered. This method was applied to the Hellenic Islands by Kotsakis, Katsambalos and Ampatzidis (2012).

5.2.3. Approach 3. An approach using reobservations of ellipsoidal and orthometric heights and a GGM-derived geoid height change.

The third approach attempts to compute for a "predicted" $\widehat{W}_{0i}$ from reobservations of orthometric and ellipsoidal heights and a GGM-derived geoid height change model. Deriving from Equation 5.9,

$$\widehat{W}_{0i} = W_0 - \bar{g}(\varphi, \lambda) \frac{\sum_{i=1}^{K} [h(P_i)_t - H(P_i)_t - N(P_i)_t]}{K} \tag{5.10}$$

where,

$$h(P_i)_t = h(P_i)_{t_0^h} + \dot{h}(P_i)(t - t_0^h) \tag{5.11}$$

$$H(P_i)_t = H(P_i)_{t_0^h} + \dot{H}(P_i)(t - t_0^H) \tag{5.12}$$

$$N(P_i)_t = N(P_i)_{t_0^h} + \dot{N}(P_i)(t - t_0^N) \tag{5.13}$$

$\dot{h}(P_i)$, $\dot{H}(P_i)$ and $\dot{N}(P_i)$ are ellipsoidal, orthometric and geoid heights change rates. $\dot{h}(P_i)$, $\dot{H}(P_i)$ for the local height systems were computed from observations/reobservations done during the 2007-2010 Philippine Reference System of 1992 (PRS92) project that aimed to fix and upgrade the (new) reference system and 2012-2015 PhilLiDAR Project, with the exception of the Leyte-Samar height system which was observed from 2014 to 2016. $\dot{N}(P_i)$ was derived from the GRACE-based geoid rate model presented in Chapter 4. The static $N(P_i)$ was derived from the PGM2016.66.

5.2.4. Approach 4. A least squares-based approach.

Approach 4 is least squares approach built from observation equations of the form,

$$\begin{aligned} l_P &= h(P)\gamma - C_i(P) - T_i(P) + \Delta W_0 \\ &= \left(1 + f_{0i}(P)\right)\delta\widehat{W}_{0i}(P) + \sum_{\substack{j=1 \\ j \neq i}}^{J} f_{0i}(P)\delta\widehat{W}_{0j}(P) + v_P \end{aligned} \tag{5.14}$$

where l_P represents the observable; v_p denotes the stochastic residual; $T_i(P)$ is the disturbing potential inferred from the national geoid. The terms f_{0i} and f_{0j}, functions of spherical distance between evaluation and integration points, were taken to be zero in this study's computation. Known parameters are gathered on the left side and the unknown parameters are assembled on the right side. An implementation of this method is provided in Sánchez & Sideris (2017).

5.2.5. Estimation Accuracy

The uncertainty of the Earth's gravity field model and the uncertainty of the local vertical datum coordinates affect the accuracy of the $\widehat{W}_{0i}$ estimation (Kotsakis, Katsambalos, & Ampatzidis, 2012).

For Approach 1, assuming $p_i = 1$ error propagation is given by,

$$\sigma_{\widehat{W}_{0i}} = \frac{\sum_i^m (H_i)^2}{m} \sigma_g \tag{5.15}$$

where σ_g is the accuracy of the GGM-derived surface gravity reconstructions as in Filmer et al., (2010).

For Approach 2, the deviation is given by,

$$\sigma_{\widehat{W}_{0i}} = \left(\frac{{\sigma_h}^2 - {\sigma_H}^2 - {\sigma_N}^2}{\sum_{i=1}^{K} \frac{1}{{g_i}^2}} \right)^{1/2} \tag{5.16}$$

where σ_h, σ_H and σ_N are accuracy measures of ellipsoidal, orthometric and geoid heights at each station of the test set. A relative error in the order of 10^{-9} to the estimate of $\widehat{W}_{0i}$ is introduced by the uncertainty of Earth's geocentric gravitational constant. The zero degree term of the GGM affects the accuracy by, $\sigma_{\widehat{W}_{0i}} \approx 0.13$ m^2/s^2.

For Approach 3, the adopted initial observation times, t_0^h, t_0^H, t_0^N are not necessarily equal. This relationship reflects operational issues such as piecemeal reference frame establishment and inconsistent reobservation schedules. Equation 5.6 is modified by using mean gravity $\bar{g}(P_i)$. Developing countries typically do not have the resources to conduct gravity reobservation campaigns nor establish absolute gravity stations. In this limitation, the effects of the change in observed gravity with respect to time is absorbed by an averaging procedure. Ideally, a gravity-height ratio can be computed with co-located gravity and GNSS data that should correspond to $\dot{h}(P_i)$ and approximations of $\dot{H}(P_i)$, in a least squares collocation solution for an optimal combination of heterogenous terrestrial data (Rangelova, 2007). Gravity-height ratios can range from very low (> 0.1uGal/mm) (Appleby, Smith, Wilkinson, Ziebart, & Williams, 2008; Rangelova, 2007) to relatively high (~ 1 uGal/mm) in complicated areas with inferred magmatic activity (Currenti, 2014). A recommendation for the establishment of absolute gravity stations are included in Chapter 6.

For Approach 4, the indirect bias term is negligible if a GGM of $N_{max} \geq 180$ is used for the determination of $T_i(P)$ (Sánchez & Sideris, 2017). This implies that f_{0i} coefficients in Equation 5.11 can be set to equal zero. This results in a simple system where the solution is the weighted mean of $\delta W_{0i}(P)$ values of the stations (Amjadiparvar, Rangelova, & Sideris, 2016; Sánchez & Sideris, 2017).

5.3. Data

Fourteen local height systems were used for this study (Fig. 3.14). The computations are dependent on provided certificates of geodetic control points with orthometric heights, levelling benchmarks, tidal benchmarks and gravity data by the National Mapping and Resource Information Authority (NAMRIA). The certificates were issued through the 2016-0224 and 2016-1011 NAMRIA free-issue licences. The local height systems are consistent with what was made available for previous studies on Philippine vertical datum connectivity (Chapter 3, Section 3.1), with the addition of the Samar-Leyte local height system whose datum was re-established from 2014 to 2016 (Gatchalian, 2016). The local vertical datums corresponding to the provided height systems were defined by primary and secondary tide stations (Chapter 3, Section 3.1).

The local height system in Northern Luzon is defined by two different official versions, 1947-1965 MSL (Paringit, Ventura, & Isada, 2009; Paringit & Paringit, 2015) and 1989-2008 MSL (NAMRIA Coast and Geodetic Survey Department, 2016) both using the Manila South Harbour primary tide station. Upon verification, the orthometric heights were officially tied to the to the later version. Because the distance from the northernmost point of the Luzon island is far from Manila, several tide gauges (Currimao, Port Irene etc.) served as unofficial origins for various levelling sections (Gatchalian, 2016). Information as to which benchmarks are tied to these tide gauges cannot be recovered, thus an assumption of inclusion based on proximity to the fundamental stations was made in the computations. Southern Luzon is fixed using two stations, Manila South Harbour primary tide station and Legaspi primary tide station (1970-1988 MSL (Paringit, Ventura, & Isada, 2009) and 1989-2007 MSL (NAMRIA Coast and Geodetic Survey Department, 2016)). The Davao primary tide station, 1970-1988 MSL, is the official origin for the entirety of Mindanao (Paringit, Ventura, & Isada, 2009; Paringit & Paringit, 2015), though Zamboanga, Cagayan de Oro and Surigao also served as origins. Other large islands like Cebu, Mindoro and Palawan referred their datum to the MSL defined by their respective tide stations (Paringit, Ventura, & Isada, 2009). First order levelling lines are usually located along national roads and second order levelling lines are located along streets within well-developed areas. The orthometric heights used in the proposed system were of the Helmert type.

111 first order GNSS benchmarks were established during the National Resource Management and Development Project (Australian International Development Assistance Bureau , 1987). Additional 223 first order benchmarks were established during the 2007-2010 PRS92 Project (Gatchalian, 2016). 80 GNSS observations were also taken from the PhilLiDAR project (2012-2016). To eliminate errors produced by inconsistent tide systems, the 1983 International Association of Geodesy (IAG) recommended the usage of a zero tide (ZT) system (Ekman, 1989; Mäkinen & Ihde, 2009). According to the IERS Conventions 2010 (Petit & Luzum, 2010), the zero tide as applied to the crust is synonymous with mean tide. NAMRIA certificates provide the data “in WGS84” without specifying the generation. It is important to note that in the IERS conventions, GRS80 is recommended (Petit & Luzum, 2010). The computations in this study were made in line with the IERS recommendations.

Most of the terrestrial gravity data were gathered from 1964 to 1989 (Paringit, Ventura, & Isada, 2009; Lopez, 2014). Upon assessment the 1964-1989 data was not used due to age, quality and lack of documentation and/or unavailability of sources with knowledge on the conduct of the old gravimetric surveys. 87 first order gravity stations were established as of 2016 (Cayapan, 2016).

Table 5.1. Local vertical datums and GNSS/levelling points.

Code	Datum Zone	GNSS/Levelling Points
0	Manila	13
1	Legaspi	5
2	Cebu	7
3	Davao	11
4	San Jose	13
5	Puerto Princesa	5
6	Real	5
7	Dumaguete	16
8	Tagbilaran	7
9	Sta.Ana	13
10	Currimao	76
11	Iloilo	9
12	Balanacan	3
13	Leyte-Samar	48

5.4. Results and Discussion

Estimates of $\widehat{W}_{0i}$ are summarised in Figure 5.2 to 5.6. Units are in m^2/s^2. Summary tables are presented in the Appendix.

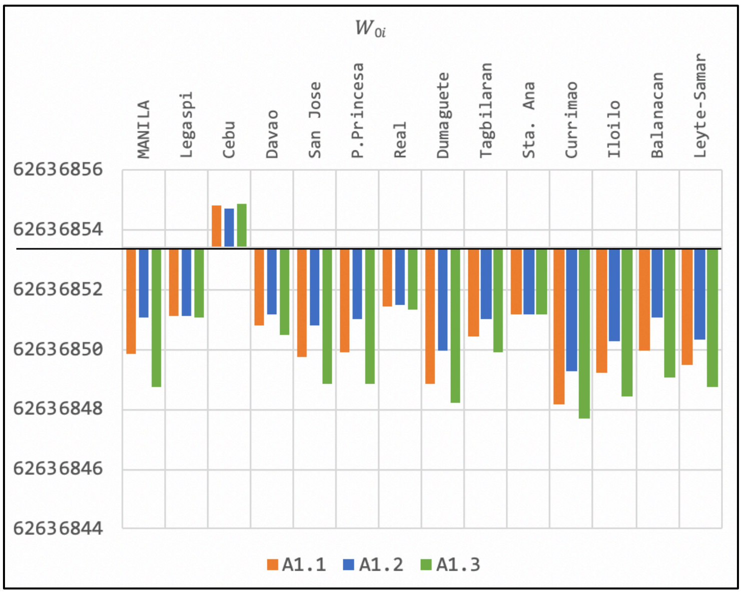

Figure 5.2. $\widehat{W}_{0i}$ in m^2/s^2 computation using Approach 1. Black line reflects the conventional value W_0 = 62636853.4 m^{2}s^{-2}

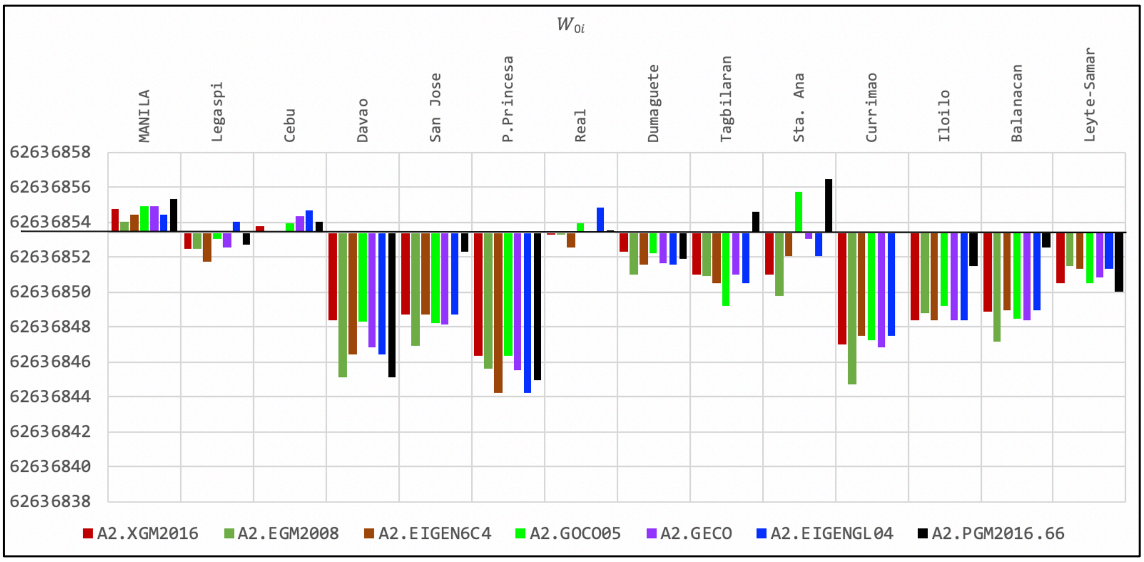

Figure 5.3. $\widehat{W}_{0i}$ in m^2/s^2 computation using Approach 2. Black line reflects the conventional value W_0 = 62636853.4 m^{2}s^{-2}

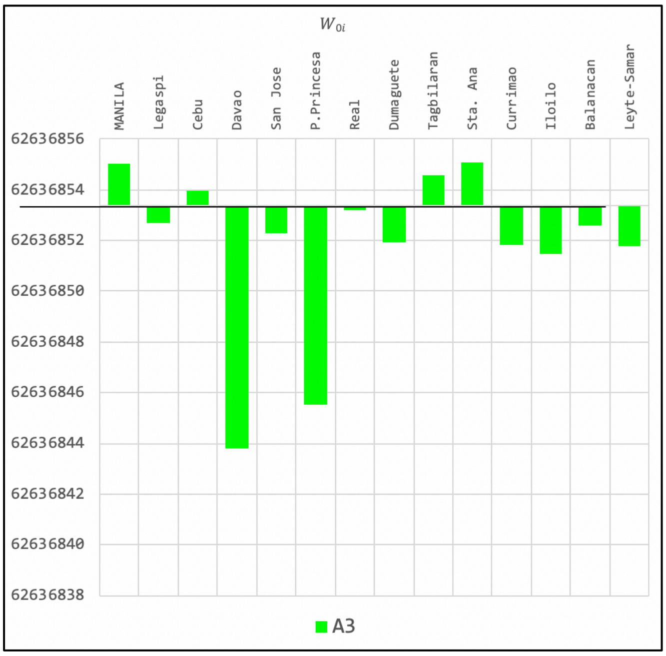

Figure 5.4. $\widehat{W}_{0i}$ in m^2/s^2 computation using Approach 3. Black line reflects the conventional value W_0 = 62636853.4 m^{2}s^{-2}

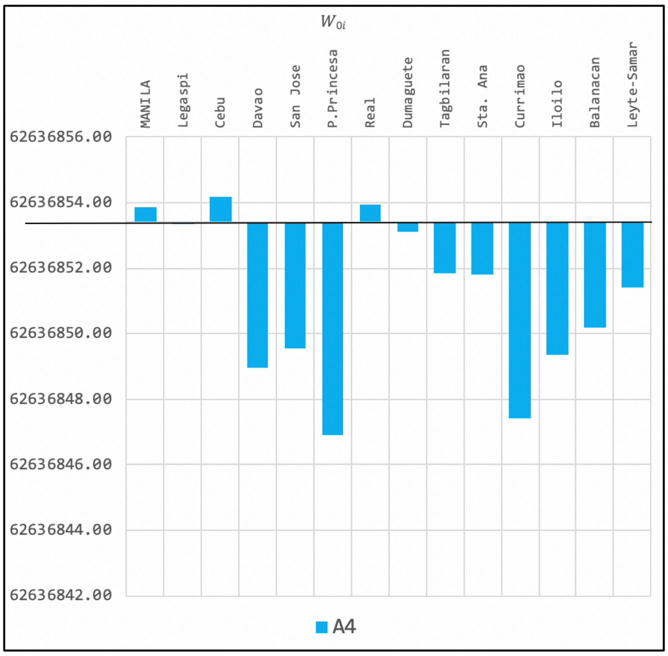

Figure 5.5. $\widehat{W}_{0i}$ in m^2/s^2 computation using Approach 4. Black line reflects the conventional value W_0 = 62636853.4 m^{2}s^{-2}

Results reveal, for the first time, estimations of the local zero-height geopotential levels for the Philippines with respect to the IHRS/F. Differences between vertical datum parameters range from ~ 0.01 m^2/s^2 to ~ 20 m^2/s^2 (inclusive of model errors). The estimation accuracies are similar, being dependent upon the local height system defined, with Legaspi, Cebu, Dumaguete, Iloilo and Davao producing the highest estimation errors. This, in addition to the reasons mentioned at the beginning of this chapter, makes the treatment of the Philippine Height System as a regional system (with multiple $\widehat{W}_{0i}$) preferable. Tables of the values are presented in the Appendix, Tables A.3. to A.8.

Approach 1 produced estimates of $\widehat{W}_{0i}$ with uncertainties (< 0.1 m^2/s^2). This was also observed in other areas, such as Greece, that included test points in mountainous areas (Grigoriadis, Kotsakis, Tziavos, & Vergos, 2014). The approach's independence from using geoid heights limits terrain modelling and associated errors to the potential values in the estimation. Higher differences in the estimation of $\widehat{W}_{0i}$ among the three weighting schemes may indicate height-dependent biases in the dataset used. This is evident for all except Legaspi, Cebu, Davao and Sta Ana. The averaging procedure also makes $\widehat{W}_{0i}$ estimates insensitive to the uncertainty of gravity values. The evaluation of Equation 5.3 and the vertical datum parameter may be biased, however, due to unaccounted systematic errors of the geopotential model that was used in the derivation of $W(P_i)$.

Approach 2 produced estimates of $\widehat{W}_{0i}$ using geoid heights from different GGMs. The estimates produced for Approach 2 contains larger errors relative to Approach 1. These estimates do not accommodate the omission errors produced by unrepresented (due to max degree limitations) residual geoid height signal in the GGMs. Equation 5.8 is also biased because $h - H - N$ is not modelled perfectly.

Figure 5.6 shows a comparison of the $\widehat{W}_{0i}$ estimates using the PGM from Approach 2 and Approach 3.

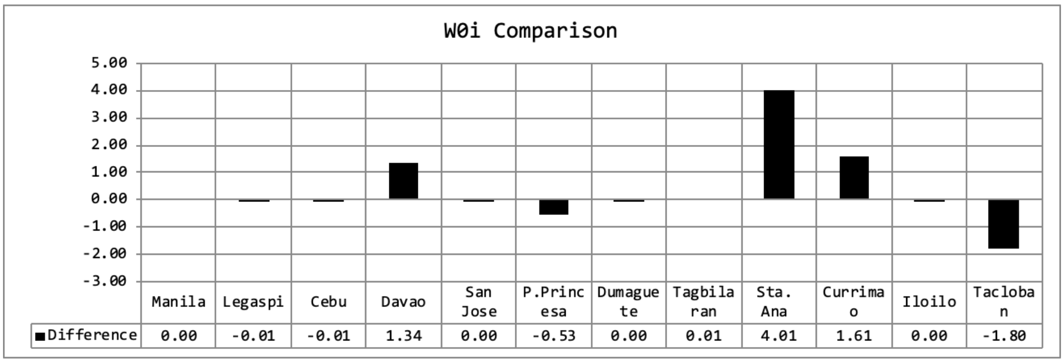

Figure 5.6. Comparison of Approach 2 (PGM2016.66) and Approach 3.

Based on the Figure 5.6, Davao, Sta. Ana, Currimao and Leyte-Samar have estimates that differ by more than 1 m^2/s^2 from Approach 2 (PGM) estimates. This seems to be caused by the time-dependent variations of Equation 5.10's elements. Most points from these areas came from observations in the 1990s and reobservation is not frequent.

Secular and episodic variations in the elements of Approach 3 were absorbed in the linear rates of change, and therefore not separated. This assumption affects the trend in areas that are geodynamically very active in between observations such as Legaspi, Davao and Leyte-Samar. Longer sets of data "dampens" this effect.

The change in gravity with respect to time was absorbed in the averaging procedure. The significance of the computed differences can be found less on the quantification of the values themselves but more on the indication that it provides the authorities in terms of required attention or resource allocation for maintenance and other purposes. Approach 4 performs better in areas where terrestrial gravity anomalies are geographically dense and homogenous (e.g. Manila).

The apriori variance σ_{W0} for the IHRS definition was not taken into account in the estimation of $\widehat{W}_{0i}$. The effect of heteroscedasticity and geographic correlation of errors is not integrated in the computation of $\sigma_{\widehat{W}_{0i}}$. Therefore, care should be taken in interpreting $\sigma_{\widehat{W}_{0i}}$. The accuracy measure is more reflective of the consistency of the heterogenous height data rather than the actual estimation accuracy of W_{0i}.

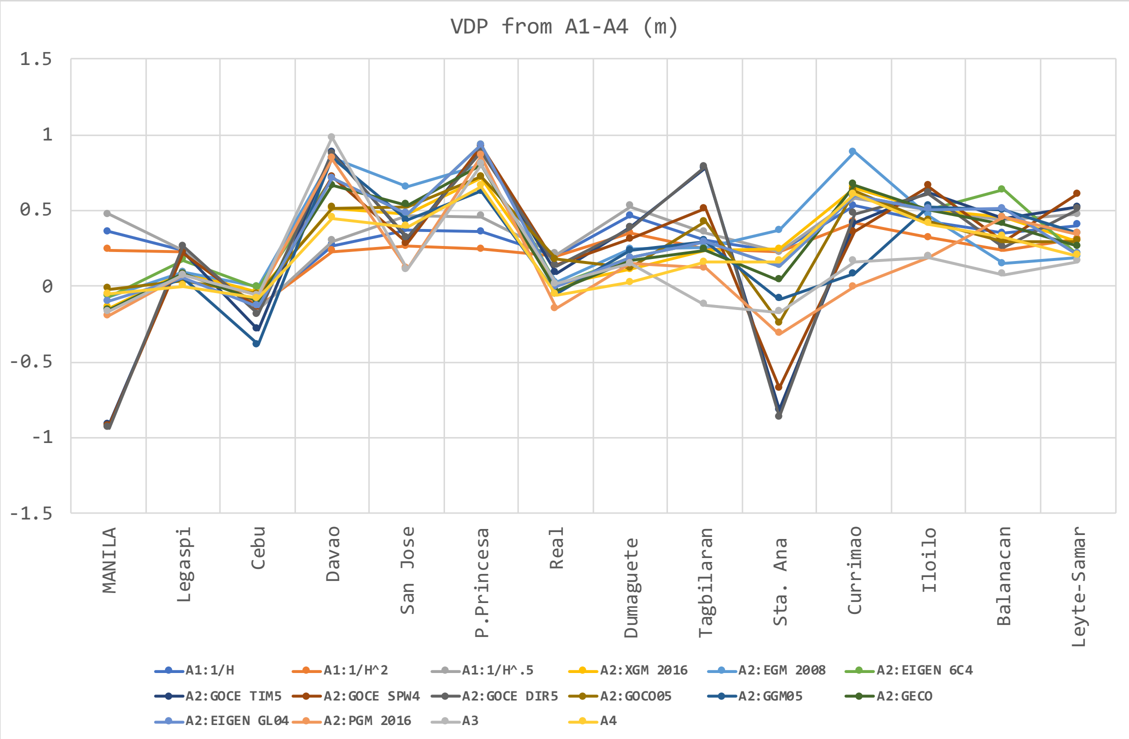

Figure 5.7. Vertical datum parameters (in m) from Approach 1 to Approach 4.

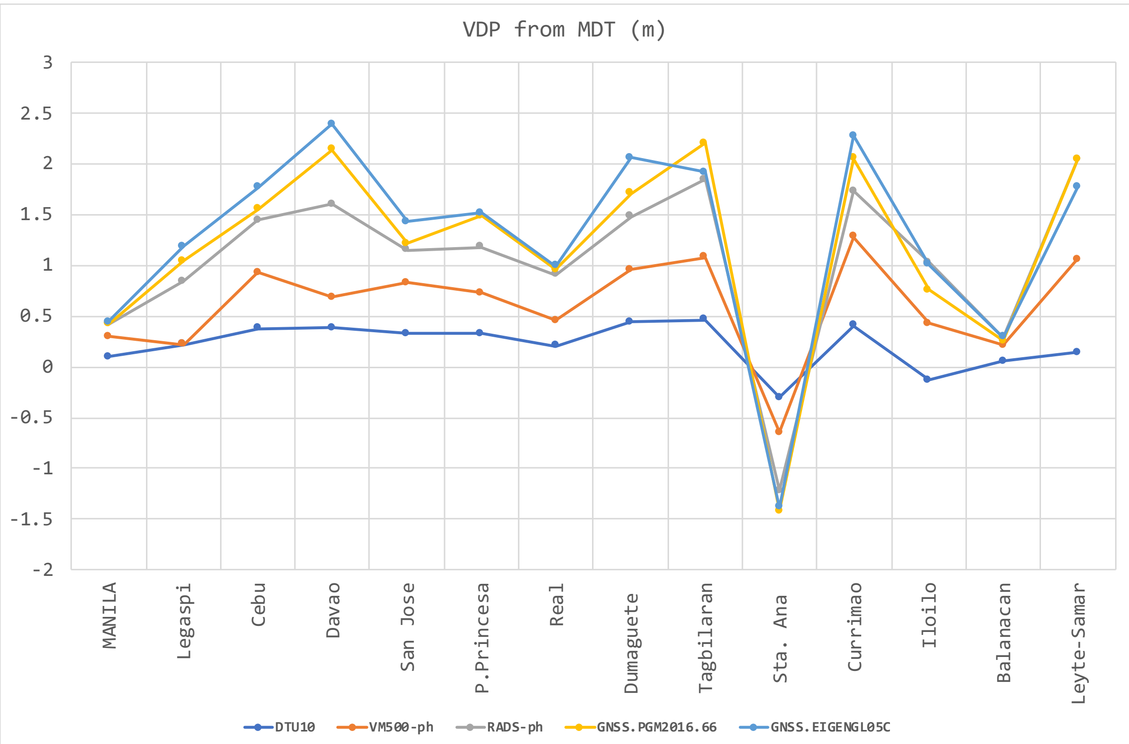

Figure 5.8. Vertical datum parameters (in m) inferred from mean dynamic topography.

Results show large deviations in the computation of $\widehat{W}_{0i}$ using Approach 2 and Approach 3 due to the estimation of geoid heights. Therefore, any of the scenarios from the Approach 1 is recommended for the computation of $\widehat{W}_{0i}$. The selection of the weighting scheme will depend on the number and the location of additional points that will be used in the future.

In Approach 4, the results emphasize the need for a numerical evaluation of the observation equations to be performed at homogenous, high-quality geodetic stations. Reliability of the computations for $\widehat{W}_{0i}$ depends on the consistency of the input epochs, especially the ellipsoidal heights and local geopotential numbers. In addition to the reference stations, observation equations for the evaluation may be formulated in the marine areas surrounding the reference tide gauges of the existing PHS. This is recommended for future study.

Figures 5.7 and 5.8 shows a comparison of vertical datum parameters (in m) from Approach 1 to Approach 4 and the vertical datum parameters inferred from the MDT in Chapter 3, Section 3.1.3. Behavioural agreement is evident except for Cebu, Palawan and Iloilo. The three locations are situated within the Visayas group of islands. It appears that the MDT could be a primary cause of the differences, however, a more comprehensive localised investigation is proposed for definitiveness.

5.5. Chapter Summary

The treatment of the Philippine Height System (PHS) as a regional system consisting of multiple local height systems in relating to the International Height Reference System (IHRS) was proposed and implemented. Estimations of the local zero-height geopotential levels of the twelve local height systems for the Philippines with respect to the IHRS were made for the first time.

Four approaches were implemented. The first approach implemented an estimator that uses orthometric heights and gravity information, independent from geoid heights. Benchmark weight factors were used to detect the presence of height-dependent systematic errors. Approach 1 produced estimates of $\widehat{W}_{0i}$ with uncertainties (< 0.1 m^2/s^2). The approach's independence from using geoid heights limits terrain modelling and associated errors to the potential values in the estimation. Higher differences in the estimation of $\widehat{W}_{0i}$ among the three weighting schemes may indicate height-dependent biases in the dataset used.

The second approach combines orthometric heights, ellipsoidal heights and geoid heights to produce estimates of $\widehat{W}_{0i}$ using geoid heights from different global geopotential models. The estimates produced for Approach 2 includes larger GGM-introduced errors relative to Approach 1.

The third approach attempts to compute for a "predicted" $\widehat{W}_{0i}$ from reobservations of orthometric and ellipsoidal heights and a GGM-derived geoid height change model. Davao, Sta. Ana, Currimao and Leyte-Samar have estimates that are different by more than 1 m^2/s^2 from Approach 2 estimates. Extreme care should be taken in attributing the difference to time-dependent factors. The significance of the computed differences can be found less on the quantification of the values themselves but more on the indication that it provides the authorities in terms of required attention or resource allocation for maintenance and other purposes.

The fourth approach is least squares approach built from observation equations of multiple geodetic data types. A previous implementation can be verified in Sánchez & Sideris (2017).

Of the four approaches, any of the scenarios from Approach 1 is recommended for the computation of $\widehat{W}_{0i}$ because of the relatively smaller deviations that were produced compared to the other approaches. In particular, the author recommends Approach 1.2. which uses a weighting scheme based on $1/H^2$.

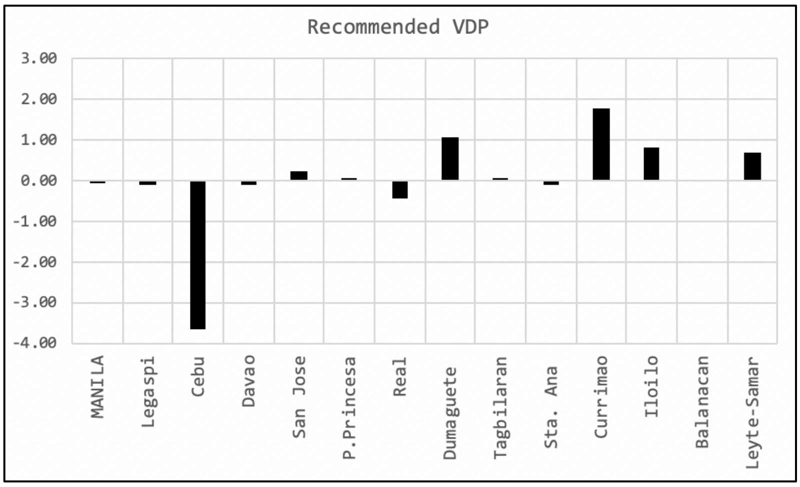

Figure 5.9. Vertical datum parameters (in m) from Approach 1.2 relative to MANILA.

A comparison of vertical datum parameters (in m) from Approach 1 to Approach 4 and the vertical datum parameters inferred from the MDT in Chapter 3 was shown. Behavioural agreement is evident except for Cebu, Palawan and Iloilo. The three locations are situated within the Visayas group of islands. A more comprehensive localised investigation is recommended for definitiveness.

A summary of the conclusions and recommendations of the study is presented in **Chapter 6: Concluding Remarks.**

Chapter Six

Concluding Remarks

This thesis expands the literature available for the Philippine Height System (PHS). The Philippines, as a developing, tropical, archipelagic country is in need of a modern height system to deal with the rapidly changing environment. An ideal modern height system for the Philippines should be accurate (possible sources of errors are known and addressed and informative of temporal variations) and easy to maintain (a gravimetric geoid-based height system of sufficient accuracy). The following research challenges were addressed.

1. *The engineering implications of the new Philippine Geoid Model.*

The newest Philippine Geoid Model (PGM2016.66) was created by Dr Rene Forsberg and his team at DTU Space. It is currently maintained and updated by National Mapping and Resource Information Authority of the Philippines (NAMRIA). The 2016.66 version of the PGM (PGM2016.66) was assessed to provide a quality baseline for managing the progression and limitations of a gravimetric geoid-based height system for the country. The assessment is done by comparing it to selected global geopotential models (GGM) and using GNSS/levelling datasets through nationwide, zonal and localised methods. PGM2016.66 is not yet reliable to be the basis for the Philippine Height System (see Chapter 3, Section 3.4). A thorough assessment, densification (or possibly reestablishment) of the country' heighting assets is desirable. A gravimetric geoid-based height system requires a substantial investment on gravity-related geodetic infrastructure. This is a step in the right direction for a dynamic country such as the Philippines.

Assessing selected GGMs yield significant discrepancies in gravity anomalies from degree 220. Specifically, the direct, timewise and spacewise GOCE models (GO_CONS_GCF_2_DIR_R5, GO_CONS_GCF_2_TIM_R5 and GO_CONS_GCF_2_SPW_R4) exhibit a deterioration of residuals from degree 220. EIGEN-GL04C, which was recommended by the NAMRIA-UP study in 2009 as a possible replacement for the old PGM1991 has RMS that is ~10% larger than EGM2008 from degree 120 up to ~100% from degree 360. It means that for the most recent Philippine terrestrial gravity data, EGM2008 implied a better fit than EIGEN-GL04C (see

Chapter 3, Section 3.3). Combined models show small differences (about 0.5 to 2 metres) in GNSS/levelling geoid heights and GGM-derived geoid heights in about 70% of the assessment points compared to satellite-only models. Though the majority of the points exhibit these relatively small differences, care should be taken in interpreting these as a sufficient measure of GGM performance because of the non-uniform spatial distribution of the assessment points (see Chapter 3, Section 3.3).

Statistical measures show that points clustered in the southern latitudes and eastern longitudes have relatively higher residuals. One explanation is that the frequent geodynamic activity in the area is not accounted for in the relatively long gap between the observations of the orthometric heights and the ellipsoidal heights. For areas near the equator, GGMs overestimate geoid heights. Biases ranging from 80 cm to 95 cm were computed. Zoning was then implemented to cluster points of similar characteristics and contain the analyses to small regions and relatively short baselines. Areas with large geoid height differences (Zones 12 to 14 and 17 to 20 were isolated) (see Table 3.7, Fig. 3.25, 3.26 and 3.27).

To gain an insight on PGM2016.66 performance without these errors, a controlled procedure in establishing an assessment network over a demonstration area was carried out. The campaigns produced two sets of values $N_{GNSS/levelling}$ and $N_{PGM2016.66}$ which are then compared with each other. For this demonstration area, the mean absolute difference of geoid heights between the two sets of values is 1.352 metres with a standard deviation of 0.018 metres (see Chapter 3, Section 3.4).

Because the mean absolute difference and standard deviation is relatively high, a corrector surface model was explored to absorb systematic distortions. To determine which surface model best suits the study area, parametric combinations of spatial interpolation methods were compared over the study area (see Chapter 3, Section 3.4). It is concluded that the local-area PGM with Empirical Bayesian Kriging (EBK) as a corrector surface can be used for third order applications.

It is acknowledged least squares collocation (LSC) is a common approach (Birardi et al., 1995; Lyszkowicz, 2000; Featherstone, 2000; Featherstone & Sproule, 2006) for corrector surfaces. An updated computation using LSC for the whole country, to be published by NAMRIA, is ongoing. Once released officially, the results of the NAMRIA LSC computations will be compared to the results of this study, and the recommendations will be properly reconsidered.

The assessment emphasised the PGM's need for corrector surface models. It is recommended that corrector surface models are realised for each local height system. Once data is available, the contributions of the new GRACE-FO mission is recommended to be evaluated over the Philippines. A thorough records review including the metadata and format, and creation of a well-structured digital central repository for observations are critical. Based on the high residual zones and logistical considerations (e.g. ease of access, manpower), GNSS and levelling reobservation campaigns are recommended in the following order of priority – Zone 20, 17, 18, 19, 12, 13, 14. The densification of the Philippine gravity network in the southern part of the country is also advocated. In addition, an absolute gravity network first proposed in the NAMRIA-UP project is presented for reconsideration (Fig. 6.1).

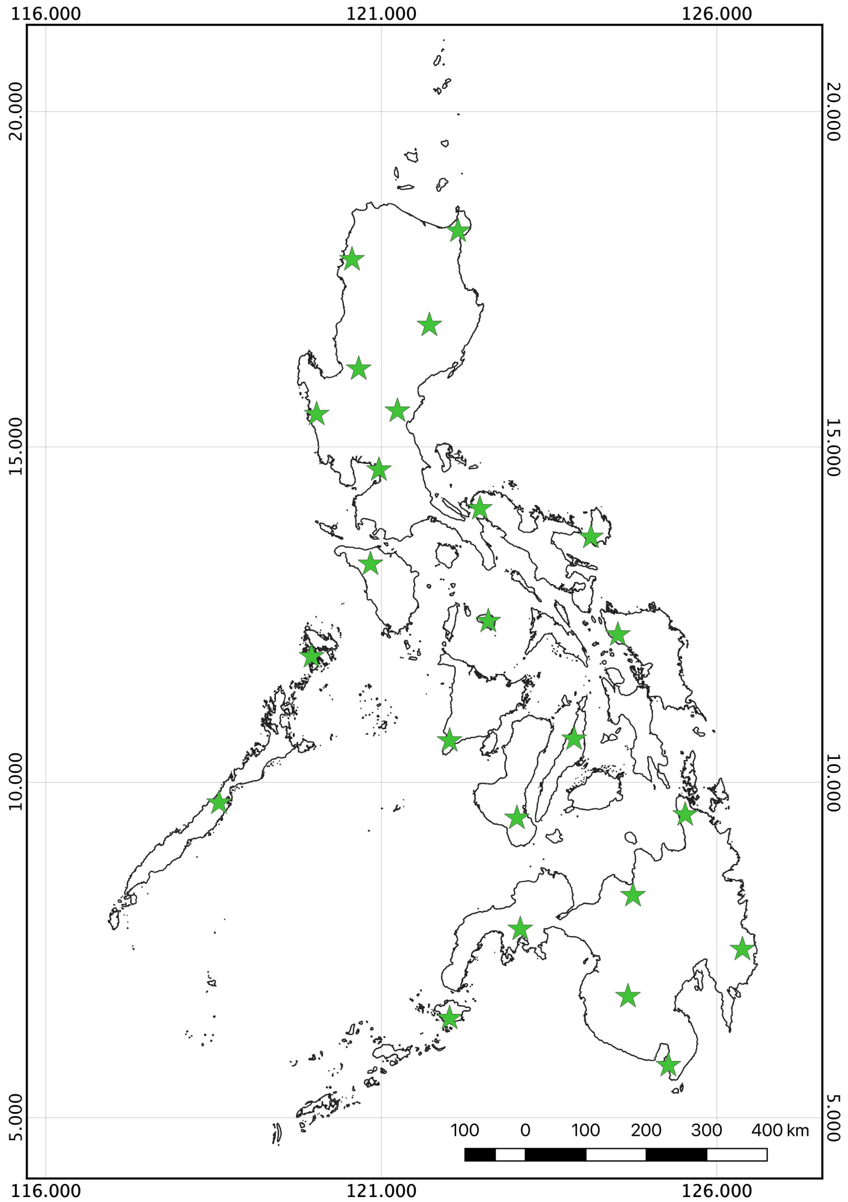

Figure 6.1. Proposed Absolute Gravity Network for the Philippines.

Inconsistencies in the treatment of permanent tide systems can yield discrepancies to up to ~10 cm in corresponding heights, if not treated, especially in the southern part of the Philippines. This reiterates the international community's recommendations of permanent tide treatment for height computations (see Fig. 3.4).

The mean dynamic topography (MDT) was also investigated. DTU10, VM500-ph and RADS-ph were compared with GNSS-geoid MDTs (GNSS-PGM2016.66, GNSS-EIGENGL05C). The largest discrepancies were computed in the Mindanao area (Davao, Cagayan de Oro, General Santos, Calapan, Mambajao, Mati, Pagadian) (see Fig. 3.5, 3.6, 3.7). Satellite altimetry can be used to infer the MDT in areas that do not currently have tide gauge stations (such as isolated islands), but sufficiently precise measurements, at present, is not possible. Among the models, GNSS-PGM2016.66 MDT is best used for such areas.

The shift of emphasis from a levelling-based height system to a GNSS and high-resolution gravimetric geoid-based height system as the most practical next generation heighting solution for the Philippines was explored in this study. For the long term, a geoid-based system is desirable, orthometric heights will still be used and the same orthometric hypotheses is to be conventionally applied in the geoid for consistency. A geoid-based height system would theoretically guarantee that the archipelago is using a consistent reference surface. This provides a reliable solution to the issues caused by isolated reference to local tide gauges.

Vertical coordinates can be assigned with normal heights to avoid dealing with the complexities of the orthometric hypothesis. In doing so, the reference surface would be the quasigeoid and not the geoid. A gridded estimation of the magnitude of the difference in orthometric (Helmert) gravity reductions and the normal (Molodensky) reduction for a pilot area was shown. The differences were observed to be larger in higher elevations, as expected. Conversion to the use of normal heights from the long-preferred orthometric heights would be ideal in the context of the IHRS/F but would create undesired misinterpretation issues in the Philippine geodetic industry.

The modern PHS should be realised with a reference network with precise ITRS/F-based GNSS coordinates, geoid undulations and orthometric heights. It is necessary, however, to emphasize that for high-accuracy, high-precision, localised engineering applications, provisions for geodetic levelling is still desirable. Based on the diagnostic, the reliability of long-term registrations at the tide gauges are not sufficient. However, given NAMRIA's recent densification of the tide gauge network and operational improvement, the ongoing tidal registrations should be protected for future integrity and consistency. The establishment of offshore tide gauge stations is recommended in the future. This will make future geoid/inferred MSL relationships reliable.

In line with the recommendation to continue utilising orthometric heights, campaigns that densify gravity observations must be pursued. The PGM2016.66, though shown to be useable for third-order engineering applications is not yet sufficient as a basis for the new PHS in its current form. For the PGM to be a viable alternative, more gravity data from calibrated instruments (starting from the developed zones for practicality of security and access—NCR, Ilocos, Cebu, Palawan, CDO, Davao, Leyte), is recommended.

2. *Model the variations of the physical benchmarks and the geoid with respect to time and provide insight on its particularities for tropical archipelagos. Secular and episodic variations related to tropical fators were investigated.*

Tropical effects on the benchmarks' displacement are analysed by modelling the tidal and non-tidal loading from 2008 to 2015 for selected Philippine active geodetic stations using rain sensor data, local geologic information and ground validation using the École et Observatoire des Sciences de la Terre (EOST) loading service (see Chapter 4, Section 4.2.1).

The seasonality in precipitation is shown to produce an average non-tidal loading effect between -2 mm to 2 mm for PLEG, PPPC and PGEN; -2.5 mm to 2.5 mm between PIMO, PTGG and PBAT, TVST exhibits an asymmetrical displacement pattern (more compressive than expansive) and KAYT produced the largest height displacements of approximately -5 mm to 5 mm (see Fig. 4.8 to 4.10).

The response of TVST and KAYT to atmospheric non-tidal loading is "irregular". This is due to the stations unique geography. The land cover seasonality of the location of the stations may introduce multipath errors in GNSS computations. The dynamic ocean response from the TUGO-m model suggests that the ATMMO is an optimal model for tropical regions.

Notable peaks were observed in the years 2010, 2013 and 2015 (see Fig. 4.8 to 4.10). These are record-breaking years in terms of typhoons and monsoon occurrences for the

Philippines over the last decade. In general, the linear trend from 2008 to 2015 implies subsidence of around -0.019 mm per year.

Two Philippine stations (PIMO and PGEN) proposed to be included for the realisation of the International Height Reference System were examined. The signature of heavy rainfall situations typically consists of ground dilation or uplift from atmospheric pressure followed by ground compression or subsidence from water. This is shown clearly for PIMO from May 2013 to November 2013 (see Fig. 4.12 and 4.13). The effects of rainfall on the reference frame, often thought of as insignificant, needs to be revisited in the Philippine setting.

Estimations confirm the intensity of land motion in the eastern and southern part of the country. Resolution may explain the apparent inconsistency between the predicted uplift in PPPC and the inferred subsidence from Sentinel-1A, and a "cushioning" of magnitudes (see Fig 4.14). Comparing the Sentinel-1A results with previous studies (Raucoules et al., 2013; Rodolfo, 2014; Eco et al., 2018) in a smaller, localised area yield discrepancies of ~2 cm/yr. Some very small areas in Manila, for example were shown to subside ~5 cm/yr. Some areas in Manila, such as areas where PIMO is located, is not subsiding based on long term GNSS information (uplift of ~2 mm/yr observed over 20 years) Despite the computational limitations, the results contribute to the very limited large-scale studies of surface behaviour in the Philippines.

The effect of tropical hydrology on the geoid is examined by using Gravity Recovery and Climate Experiment (GRACE) temporal models. The GRACE temporal models registered large variations from month 106 to 134 for both stations. This is coincident with the 2010-2013 high rainfall period (see Fig. 4.19). A causality relationship between high rainfall and geoid variation, however, is inconclusive.

The computed secular rates of change are small (max ~0.16 mm/yr) compared to areas with effects from post-glacial rebound (max ~1.5 mm/yr.). GRACE geoid errors exceed the geoid rate estimates produce in this study (see Fig. 4.18). A closer look at seasonal effects is recommended.

Given that combined characteristic errors of the height components h, H and N is estimated to be in the range of ~10 mm to ~10 cm (or possibly more), a frequent correction of the geoid model is not practical. The accounting of vertical land motion, however, should be considered at least annually. Though vertical land motion can be detected using satellite methods, ground techniques such as precise re-levelling and/or continuous GNSS observations over a dense network still provide the most reliable observations.

The Philippine Active Geodetic Network (PAGeNet) relies heavily on manpower for processing and maintenance. For future studies, the optimisation of PAGeNet processes are recommended. A study on the maximisation of newly-established PAGeNet stations is proposed.

3. *Demonstrate relative connectivity between non-landlocked height systems of different geodetic development states and tectonic realms in the context of the International Height Reference System.*

The treatment of the PHS as a regional system consisting of multiple local height systems in relating to the International Height Reference System (IHRS) was proposed and implemented (see Fig. 3.13). Estimations of the local zero-height geopotential levels of the fourteen proposed local height systems for the Philippines with respect to the IHRS were made for the first time.

Four approaches were implemented. The first approach implemented an estimator that uses orthometric heights and gravity information, independent from geoid heights. Benchmark weight factors were used to detect the presence of height-dependent systematic errors. Approach 1 produced estimates of $\widehat{W}_{0i}$ with uncertainties (< 0.1 m^2/s^2). The approach's independence from using geoid heights limits terrain modelling and associated errors to the potential values in the estimation. Higher differences in the estimation of $\widehat{W}_{0i}$ among the three weighting schemes may indicate height-dependent biases in the dataset used (see Fig. 5.2).

The second approach combines orthometric heights, ellipsoidal heights and geoid heights to produce estimates of $\widehat{W}_{0i}$ using geoid heights from different global geopotential models (see Fig. 5.3). The estimates produced for Approach 2 includes larger errors (due to the use of geoid heights) relative to Approach 1.

The third approach attempts to compute for a "predicted" $\widehat{W}_{0i}$ from reobservations of orthometric and ellipsoidal hights and a GGM-derived geoid height change model (see Fig. 5.4). Davao, Sta. Ana, Currimao and Leyte-Samar have estimates that are different by more than 1 m^2/s^2 from Approach 2 estimates. Extreme care should be taken in attributing the difference to time-dependent factors. The significance of the computed differences can be found less on the quantification of the values themselves but more on the indication that it provides the authorities in terms of required attention or resource allocation for maintenance and other purposes.

The results of the fourth approach emphasize the need for a numerical evaluation of the observation equations to be performed at homogenous, high-quality geodetic stations (see Fig. 5.5). Reliability of the computations for $\widehat{W}_{0i}$ depends on the consistency of the input epochs, especially the ellipsoidal heights and local geopotential numbers. In addition to the reference stations, observation equations for the evaluation may be formulated in the marine areas surrounding the reference tide gauges of the existing PHS. This is recommended for future study.

A comparison of vertical datum parameters (in m) from Approach 1 to Approach 4 and the vertical datum parameters inferred from the MDT in Chapter 3 was also shown (see Fig. 5.6). Behavioural agreement is evident except for Cebu, Palawan and Iloilo (see Fig. 5.7 and 5.8). The three locations are situated within the Visayas group of islands. It appears that the MDT could be a primary cause of the differences, however, a more comprehensive localised investigation is proposed for definitiveness.

Of the four approaches, any of the scenarios from Approach 1 is recommended for the computation of $\widehat{W}_{0i}$ because of the relatively smaller deviations that were produced compared to the other approaches. In particular, the author recommends Approach 1.2. which uses a weighting scheme based on $1/H^2$.

Table 6.1. Reference potential values and datum parameters from Approach 1.2 (in m^2s^{-2}).

Approach 1.2	**Datum Parameter**	±	**Reference potential**	±
MANILA	3.529	0.02	62636851.05	0.02
Legaspi	2.309	0.05	62636851.13	0.05
Cebu	-1.404	0.01	62636854.69	0.01
Davao	2.629	0.04	62636851.14	0.04
San Jose	3.672	0.02	62636850.82	0.02
P.Princesa	3.524	0.01	62636850.99	0.01
Real	1.989	0.04	62636851.46	0.04
Dumaguete	4.562	0.04	62636849.97	0.04
Tagbilaran	2.993	0.02	62636850.98	0.02
Sta. Ana	2.242	0.02	62636851.16	0.02
Currimao	5.214	0.04	62636849.25	0.04
Iloilo	4.203	0.06	62636850.24	0.06
Balanacan	3.442	0.03	62636851.05	0.01
Leyte-Samar	3.944	0.04	62636850.34	0.04

The verification of the computed $\widehat{W}_{0i}$ values in a pilot area using re-observed and intensively-corrected height data is the next logical step for research.

Appendix

A.1. Supplementary Notes on the Height Datum Problem

Staring with setting the normal potential of the reference ellipsoid U_0 equal to W_0 through the formula,

$$W_0 = \frac{\mu}{a}\left(\frac{1}{e}\right)\tan^{-1}\frac{e}{\sqrt{1-e^2}} + \frac{1}{3}m_0 = U_0 \tag{A.15}$$

Where a is the semi-major axis of the reference ellipsoid; e is the first eccentricity; and $m_0 = \omega^2 a^3/\mu$.

Sanso and Venutti (2002) summarised the evolution of the height datum problem definition into the following:

a. *Global, single boundary value problem, spherical approximation, single height datum problem.* Recall that Q (refer to Figure 2.1) is defined in the relationship,

$$U_Q = U_0 - (W_P - \delta W). \tag{A.16}$$

Using the linearised U_Q in the equation,

$$\Delta g = g_P - \gamma_Q \cong \frac{\partial T}{\partial h} + \frac{\partial \gamma}{\partial h}\zeta \tag{A.17}$$

to derive the boundary relation,

$$-\frac{\partial T}{\partial h} - \frac{2}{r}T = \Delta g - \frac{2\delta W}{r}. \tag{A.18}$$

Applying the boundary relation to a sphere with radius R, the first harmonic coefficient coincides with the constant kM as defined in the previous sections. The relationship,

$$\delta W = \frac{R}{2}\Delta g_0 = \frac{R}{8\pi}\int \Delta g d\sigma\,, \tag{A.19}$$

is then derived.

The Stokes formula in the solution can be written as,

$$N = \frac{R}{\gamma\, 4\pi} \int \Delta g \left[S(\psi) - \frac{1}{2} \right] d\sigma. \tag{A.20}$$

b. *Global, single boundary value problem, spherical approximation, multiple height datum problem*. This definition arises from the consideration that the boundary value problem is not constrained to a single area in global practice. The problem can then be expressed as

$$T_P = \frac{1}{4\pi} \int S(\psi_{PQ}) \Delta g_Q d\sigma Q - \frac{2}{R} \sum \delta W_i \frac{1}{4\pi} \left[\int_{A_i} S(\psi_{PQ}) d\sigma Q \right] \tag{A.21}$$

on a sphere with radius *R*.

Assuming that in each area, A_i with multiple stations,

$$P_{is} \in A_i \qquad s = 1, \dots, n_i, \qquad i = 1, \dots, n$$

δW_i is estimated by applying a least squares procedure onto the system of observation equations,

$$\begin{aligned} h_{P_{is}} - h_{Q_{is}} = \frac{1}{\gamma} \frac{1}{4\pi} \int S(\psi_{P_{is}Q}) \Delta g_Q d\sigma Q \\ - \frac{2}{R} \sum_k \delta W_k \frac{1}{4\pi} \left[\int_{A_k} S(\psi_{PQ}) d\sigma Q \right] - \frac{1}{\gamma} \delta W_i. \end{aligned} \tag{A.22}$$

The reader is referred to the work of Colombo (Colombo, 1980), Rummel and Teunissen (1988), Heck (1989), Xu & Rummel (1991), Rapp and Balasubramania (1992) among others for practical examples and more information.

c. *Global, single boundary value problem, ellipsoidal approximation, multiple height datum-geodetic spherical approximation*. Sanso and Usai (1995) provided a solution similar to item b but added the change effects of the height system.

d. *Global, mixed boundary value problem, spherical approximation, multiple height datum problem*. Lehman (Lehmann, 2000), in his work, takes into account the difference between the geodetic data on land and ocean in the formulation of the boundary value problem.

e. *Local, single boundary value problem, spherical approximation, multiple height datum problem*. Statistical approaches, such as least squares collocation, are applied to provide solutions for the boundary value problem in local areas. This approach can be used to treat the following equations: For a set of gravity anomaly measurements,

$$P_{ij} \in A_i: \qquad \Delta g_{P_{ij}} = \left(-\frac{\partial T}{\partial r} - \frac{2}{r}T\right)_{P_{ij}} + \frac{2}{r}\delta W_i. \tag{A.23}$$

For GNSS height observations,

$$P_{ij} \in A_i: \qquad \Delta\zeta_{P_{ij}} = \frac{1}{\gamma}T_{P_{is}} - \frac{1}{\gamma}\delta W_i. \tag{A.24}$$

The strength of this approach is the usage of realistic data and modern approaches to geoid determination. The reader is referred to the work of Forsberg (2000).

f. *Local, single boundary value problem, ellipsoidal approximation, dual height datum, geodetic datum problem*. A solution is formulated using a geocentric datum based on the reference ellipsoid E_0, and a local geocentric datum based on the local ellipsoid E_L with levelling data, gravimetric data, geodetic networks data and GNSS data. The 10-step solution is presented in Sanso and Venuti (2002).

	Accuracy Standard	Spacing	Number
Horizontal			
AGS	1 ppm	100km	35 + 1 (shared)
Zero order	1 ppm	70km	65
First order	10 ppm	50km	318
Second order	20 ppm	20 km	2,360
Third order	50 ppm	10km	5,266
Fourth order	100 ppm	5km	29,591
Vertical			
First order	$4\sqrt{K}$ (mm)	1 km (national roads)	20,902
Second order	$8.4\sqrt{K}$ (mm)	0.5 km (city streets)	1,950
Gravity			
First order		50km	87
Second order		20km	1,624
International Collaborations			
IGS sites	4 (PIMO, PTAG, PPPC, PGEN)		
DORIS site	1 (Manille)		
APREF / APRGP	PTAG / All PageNET AGS		
MGM-Net	2 (PLUZ, PMIN)		
REGINA	1 (PTGG)		

Figure A.1. Philippine Survey Standards (Cayapan, 2016)

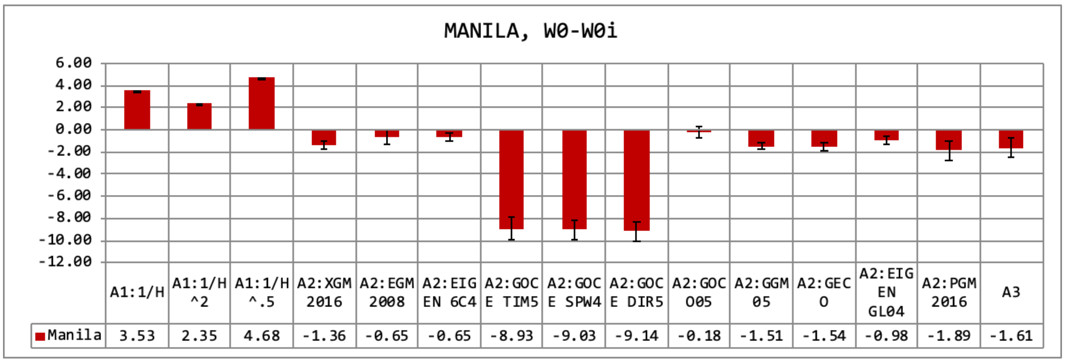

Figure A.2. Manila Vertical Datum Parameters

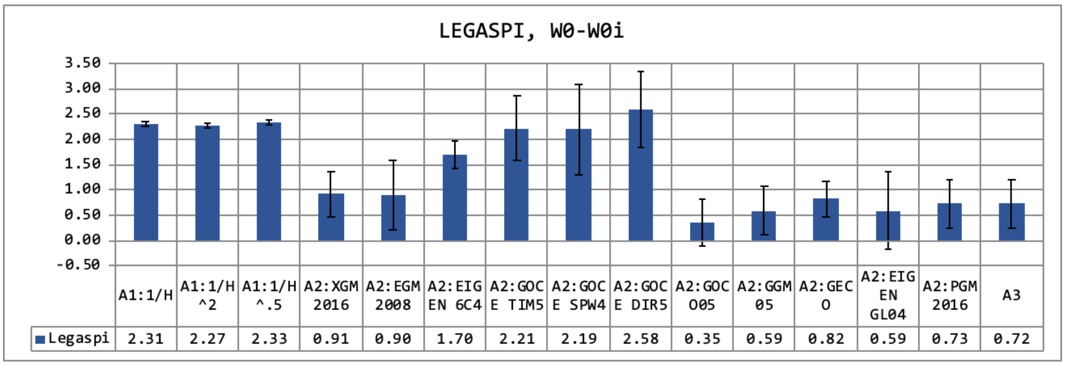

Figure A.3. Legaspi Vertical Datum Parameters

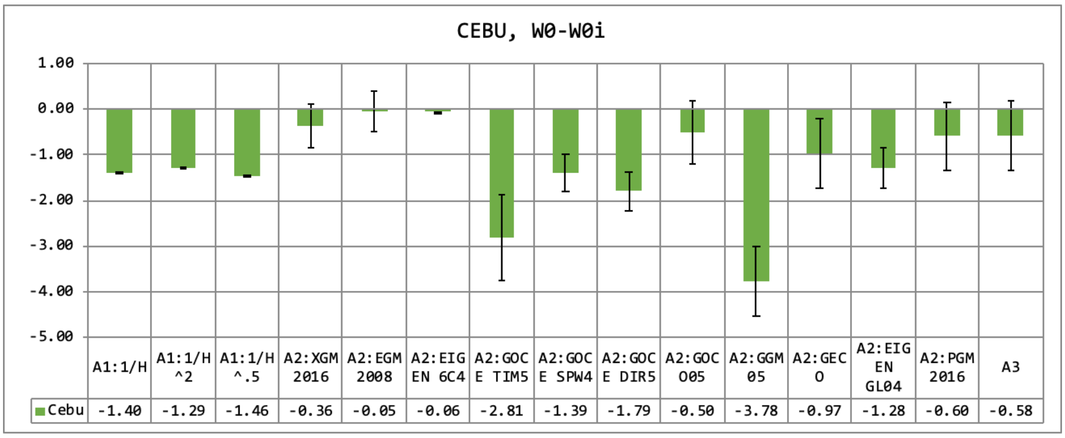

Figure A.4. Cebu Vertical Datum Parameters

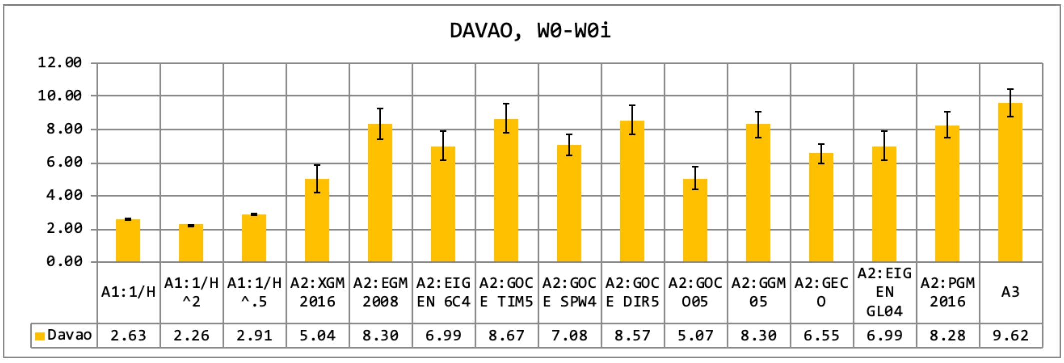

Figure A.5. Davao Vertical Datum Parameters

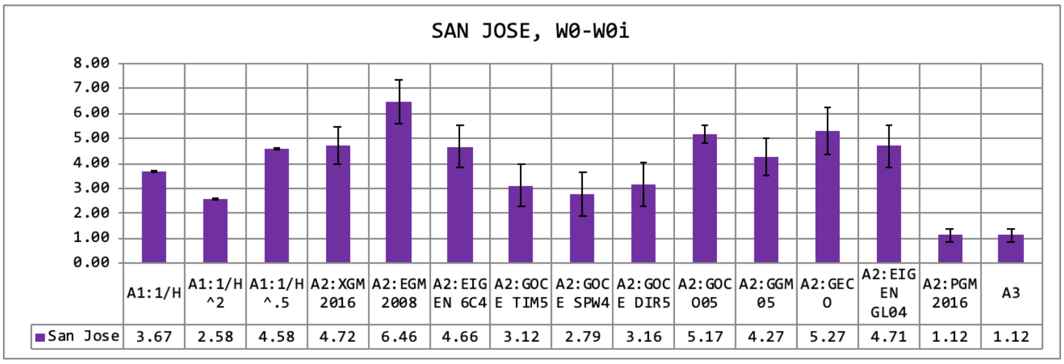

Figure A.6. San Jose Vertical Datum Parameters

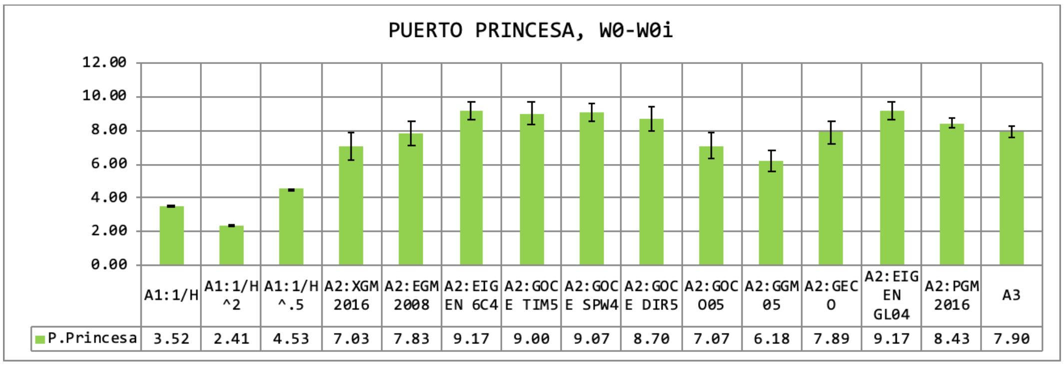

Figure A.7. Puerto Princesa Vertical Datum Parameters

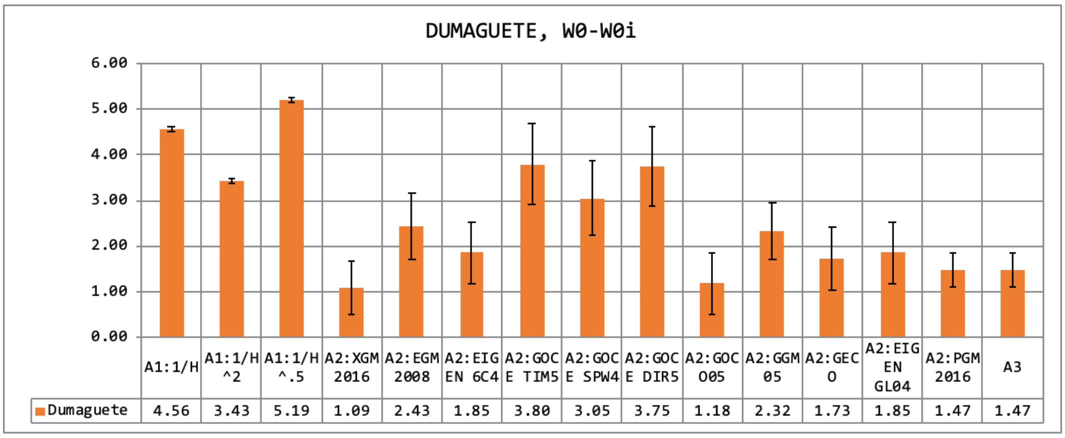

Figure A.8. Dumaguete Vertical Datum Parameters

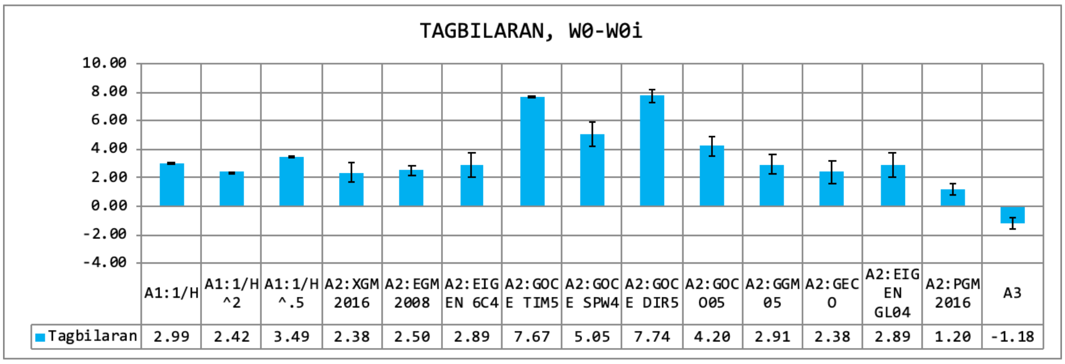

Figure A.9. Tagbilaran Vertical Datum Parameters

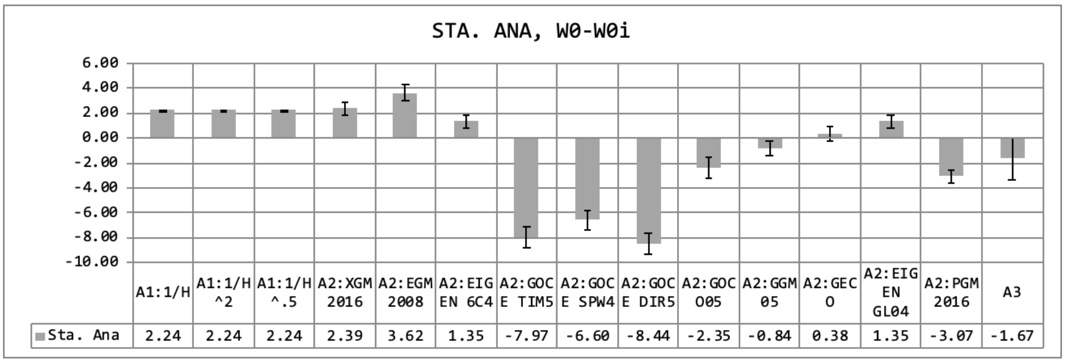

Figure A.10. Sta Ana Vertical Datum Parameters

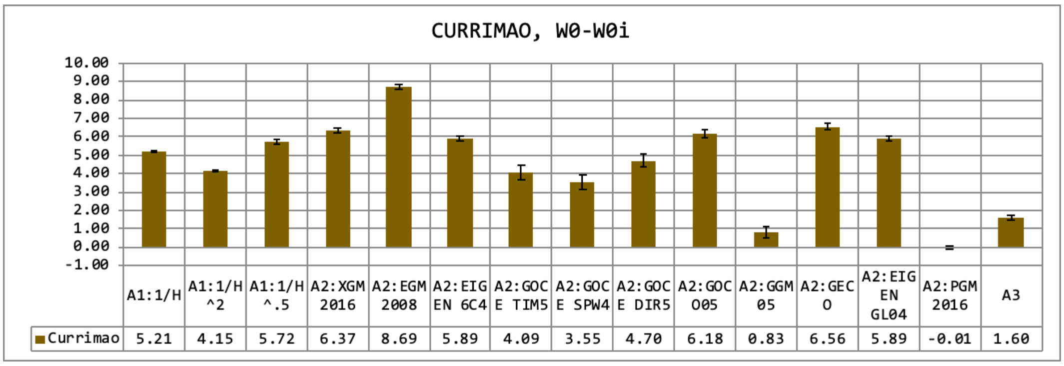

Figure A.11. Currimao Vertical Datum Parameters

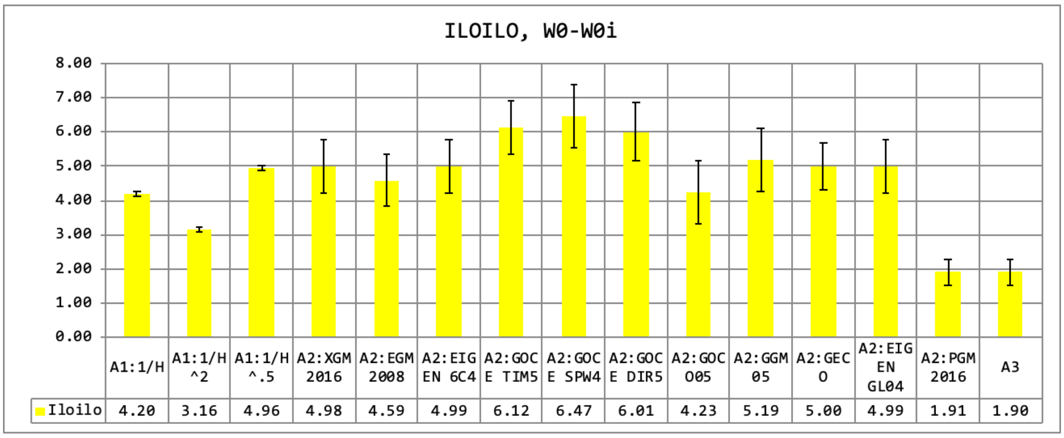

Figure A.12. Iloilo Vertical Datum Parameters

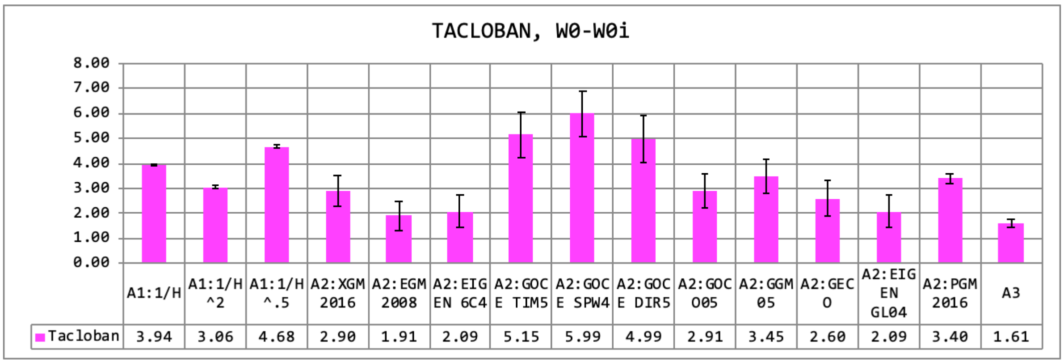

Figure A.13. Tacloban Vertical Datum Parameters

Table A.1. Raw Data for the Guiguinto Fieldwork

Name	h_GB	H_GB	N_T_GB	N_{PGM}_GB	ΔN_GB	(ΔN_GB)_NoTrend
GB001	47.299	4.211	43.088	44.754	1.666	0.066
GB002	45.641	2.456	43.185	44.84	1.655	0.055

GB003	45.090	1.854	43.236	44.896	1.660	0.060
GB004	46.655	3.425	43.230	44.915	1.685	0.085
GB005	46.342	3.21	43.132	44.815	1.683	0.083
GB006	47.253	4.185	43.068	44.738	1.670	0.070
GB007	49.313	6.248	43.065	44.742	1.677	0.077
GB008	45.297	2.149	43.148	44.837	1.689	0.089
GB009	49.779	6.541	43.238	44.93	1.692	0.092
GB010	48.420	5.133	43.287	44.988	1.701	0.101
GB011	49.504	6.25	43.254	45.001	1.747	0.147
GB012	47.461	4.226	43.235	44.909	1.674	0.074
GB013	48.035	4.937	43.098	44.805	1.707	0.107
GB014	50.765	7.714	43.051	44.74	1.689	0.089
GB015	47.133	3.939	43.194	44.896	1.702	0.102
GB016	50.310	6.945	43.365	44.995	1.630	0.030
				mean	1.683	0.083
				st.dev	0.025	0.025

Table A.2. Land Cover Classification Accuracy Table.

Classifier	Overall Accuracy	Kappa Coefficient
Parallelepiped	86.62%	0.84
Minimum Distance	86.69%	0.82
Mahalanobis Distance	78.51%	0.76
Maximum Likelihood	87.13%	0.93
Isodata	69.51%	0.60
Kmeans	68.82%	0.59

Table A.3. $\widehat{W}_{0i}$ in m^2/s^2 computation using Approach 1.

Approach 1	**1/H**	**±**	**(1/H)^2**	**±**	**(1/H)^(1/2)**	
Manila	62636849.87	0.02	62636851.05	0.02	62636848.72	0.03
Legaspi	62636851.09	0.05	62636851.13	0.03	62636851.07	0.05
Cebu	62636854.8	0.01	62636854.69	0.01	62636854.86	0.01
Davao	62636850.77	0.05	62636851.14	0.05	62636850.49	0.06
San Jose	62636849.73	0.02	62636850.82	0.02	62636848.82	0.03
P.Princesa	62636849.88	0.02	62636850.99	0.01	62636848.87	0.02
Dumaguete	62636848.84	0.04	62636849.97	0.04	62636848.21	0.05
Tagbilaran	62636850.41	0.02	62636850.98	0.02	62636849.91	0.03
Sta. Ana	62636851.16	0.02	62636851.16	0.02	62636851.16	0.02
Currimao	62636848.19	0.08	62636849.25	0.04	62636847.68	0.14
Iloilo	62636849.2	0.07	62636850.24	0.06	62636848.44	0.08
Leyte-Samar	62636849.46	0.04	62636850.34	0.04	62636848.72	0.06

Table A.4. $\widehat{W}_{0i}$ in m^2/s^2 computation using Approach 2 (XGM2016, EGM2008, EIGEN-6C4).

Approach 2	**XGM 2016**	±	**EGM 2008**	±	**E6C4**	±
Manila	62636854.76	0.36	62636854.05	0.40	62636854.38	0.39
Legaspi	62636852.49	0.46	62636852.50	0.69	62636851.70	0.27
Cebu	62636853.76	0.48	62636853.45	0.43	62636853.46	0.00
Davao	62636848.36	0.84	62636845.10	0.92	62636846.41	0.87
San Jose	62636848.68	0.78	62636846.94	0.85	62636848.74	0.84
P.Princesa	62636846.37	0.83	62636845.57	0.70	62636844.23	0.55
Dumaguete	62636852.31	0.59	62636850.97	0.73	62636851.55	0.68
Tagbilaran	62636851.02	0.63	62636850.90	0.35	62636850.51	0.82
Sta. Ana	62636851.01	0.50	62636849.78	0.68	62636852.05	0.50
Currimao	62636847.03	0.14	62636844.71	0.13	62636847.51	0.14
Iloilo	62636848.42	0.77	62636848.81	0.77	62636848.41	0.79
Leyte-Samar	62636850.50	0.60	62636851.49	0.58	62636851.31	0.64

Table A.5. $\widehat{W}_{0i}$ in m^2/s^2 computation using Approach 2 (GOCE only models: TIM R5, SPW R4, DIR R5).

Approach 2	**TIM**	±	**SPW**	±	**DIR**	±
Manila	62636862.33	0.98	62636862.43	0.92	62636862.54	0.88
Legaspi	62636851.19	0.64	62636851.21	0.90	62636850.82	0.74
Cebu	62636856.21	0.95	62636854.79	0.40	62636855.19	0.42
Davao	62636844.73	0.86	62636846.32	0.61	62636844.83	0.89
San Jose	62636850.28	0.85	62636850.61	0.86	62636850.24	0.90
P.Princesa	62636844.40	0.66	62636844.33	0.55	62636844.70	0.69
Dumaguete	62636849.60	0.89	62636850.35	0.82	62636849.65	0.86
Tagbilaran	62636845.73	0.09	62636848.35	0.81	62636845.66	0.43
Sta. Ana	62636861.37	0.85	62636860.00	0.78	62636861.84	0.87
Currimao	62636849.31	0.39	62636849.85	0.40	62636848.70	0.37
Iloilo	62636847.28	0.78	62636846.93	0.93	62636847.39	0.84
Leyte-Samar	62636848.25	0.93	62636847.41	0.90	62636848.41	0.95

Table A.6. $\widehat{W}_{0i}$ in m^2/s^2 computation using Approach 2 (GOCO05, GGM05, GECO, EIGEN-GL04, PGM2016).

Approach 2	**GOCO05**	±	**GGM05**	±	**GECO**	±	**EGL04**	±	**PGM**	±
Manila	62636854.91	0.66	62636849.91	0.52	62636854.94	0.30	62636854.38	0.39	62636855.29	0.83
Legaspi	62636853.05	0.45	62636852.81	0.47	62636852.58	0.36	62636853.99	0.78	62636852.67	0.48
Cebu	62636853.90	0.69	62636857.18	0.77	62636854.37	0.78	62636854.68	0.44	62636854.00	0.75
Davao	62636848.33	0.68	62636845.10	0.77	62636846.85	0.62	62636846.41	0.87	62636845.12	0.80
San Jose	62636848.23	0.34	62636849.13	0.73	62636848.13	0.94	62636848.69	0.84	62636852.28	0.23
P.Princesa	62636846.33	0.78	62636847.22	0.68	62636845.51	0.70	62636844.23	0.55	62636844.97	0.32
Dumaguete	62636852.22	0.67	62636851.08	0.62	62636851.67	0.69	62636851.55	0.68	62636851.93	0.37
Tagbilaran	62636849.20	0.66	62636850.49	0.68	62636851.02	0.77	62636850.51	0.82	62636854.60	0.42

Sta. Ana	62636855.75	0.86	62636854.24	0.55	62636853.02	0.57	62636852.05	0.50	62636856.47	0.49
Currimao	62636847.22	0.28	62636852.57	0.31	62636846.84	0.15	62636847.51	0.14	62636853.41	0.10
Iloilo	62636849.17	0.93	62636848.21	0.91	62636848.40	0.69	62636848.41	0.79	62636851.49	0.39
Leyte-Samar	62636850.49	0.68	62636849.95	0.68	62636850.80	0.71	62636851.31	0.64	62636850.00	0.19

Table A.7. $\widehat{W}_{0i}$ in m^2/s^2 computation using Approach 3.

Station	W0	±
Manila	62636855.01	0.83
Legaspi	62636852.68	0.47
Cebu	62636853.98	0.75
Davao	62636843.78	0.80
San Jose	62636852.28	0.24
P.Princesa	62636845.5	0.32
Dumaguete	62636851.93	0.37
Tagbilaran	62636854.58	0.42
Sta. Ana	62636855.07	0.62
Currimao	62636851.8	0.10
Iloilo	62636851.5	0.39
Leyte-Samar	62636851.79	0.19

Table A.8. $\widehat{W}_{0i}$ in m^2/s^2 computation using Approach 4.

Station	W0	±
Manila	62636853.87	0.52
Legaspi	62636853.39	0.21
Cebu	62636854.17	0.02
Davao	62636848.97	0.31
San Jose	62636849.54	0.01
P.Princesa	62636846.91	0.16
Dumaguete	62636853.95	0.36
Tagbilaran	62636853.13	0.08
Sta. Ana	62636851.83	0.47
Currimao	62636851.79	0.11
Iloilo	62636847.43	0.27
Leyte-Samar	62636849.34	0.16

References

Abazu, I. C., Din, A. H., & Omar, K. M. (2017). Mean dynamic topography over Peninsular Malaysian seas using multimission satellite altimetry. *Journal of Applied Remote Sensing*, 11(2):026017.

Adams, J. B., & Gillespie, A. R. (2006). *Remote Sensing of Landscapes with Spectral Images: A Physical Modeling Approach.* Cambridge: Cambridge University Press.

Ahmad, Z., Harvey, B., Kasenda, A., & Kearseley, A. H. (1993). *Contributions to Geoid Evaluations and GPS Heighting.* Sydney: University of New South Wales.

Akaike, H. (1974). A new look at the statistical model identification. *IEEE Transactions on Automatic Control, 19*(6), 716-723.

Akyilmaz, O., Ustun, A., Aydin, C., Arslan, N., Doganalp, S., Guney, C., . . . Yagci, O. (2016). *High Resolution Gravity Field Determination and Monitoring of Regional Mass Variations using Low-Earth Orbit Satellite.* Potsdam: GFZ Data Service.

Allister, N. A., & Featherstone, W. E. (2001). Estimation of Helmert orthometric heights using digital barcode levelling, observed gravity and topographic mass-density data over part of Darling Scarp, Western Australia. *Geomatics Res Australasia, 75*, 25-52.

Amin, H., Sjöberg, L. E., & Bagherbandi, M. (2019). A global vertical datum defined by the conventional geoid potential and the Erth ellipsoid parameters. *Journal of Geodesy*, 93:1943-1961.

Amin, M. (1988). Spatial variations of mean sea level of the North Sea off the coast of Britain. *Continental Shelf Research*, 8:1087-1106.

Amjadiparvar, B., Rangelova, E., & Sideris, M. G. (2016). The GBVP approach for vertical datum unification—recent results in North America. *Journal of Geodesy*, 90(1):45–63.

Amos, M. J., & Featherstone, W. E. (2001). Estimation of Helmert orthomet- ric heights using digital barcode levelling, observed gravity and topographic mass-density data over part of the Darling Scarp, Western Australia. *Geomat Res Australas*, 75:25-52.

Amos, M., & Featherstone, W. E. (2008). Unification of New Zealand's local vertical datums: iterative gravimetric quasigeoid computations. *Journal of Geodesy, 83*(1), 57-68.

Andersen, O. B., & Knudsen, P. (2000). The role of satellite altimetry in gravity field modelling in coastal areas. *Phys. Chem. Earth Part A*, 25(1):17-24.

Andersen, O. B., & Knudsen, P. (2009). DNSC08 mean sea surface and mean dynamic topography models. *Journal of Geophysical Research*, 114:C11001.

Andersen, O. B., & Knudsen, P. (2010). The DTU10 Global Gravity field and mean sea surface – improvements in the Arctic. *IGFS-2.* Fairbanks: DTU Space.

Appleby, G., Smith, V., Wilkinson, M., Ziebart, M., & Williams, S. (2008). Comparison of height anomalies determined from SLR, absolute gravimetry and GPS with high frequency borehole data at Hertmonceux. *Gravity, Geoid and Earth Observation* (pp. 107-113). Crete: Springer.

Ardalan, R., & Grafarend, E. (2004). High resolution geoid computation without applying Stokes's formula case study: high resolution geoid of Iran. *Journal of Geodesy, 78*, 138-156.

Australian International Development Assistance Bureau . (1987). *Natural Resources Management and Development Project - Phase 1.* Manila: Australian International Development Assistance Bureau

Balasubramania, N. (1994). *Definition and Realisation of a Global Vertical Datum.* Columbus: The Ohio State University.

Barthelmes, F. (2013). *Definition of Functionals of the Geopotential and Their Calculation from Spherical Harmonic Models. Theory and Formulas Used by the Calculation Service of the International Centre form Global Earth Models.* Potsdam: GFZ Potsdam.

Barthelmes, F., & Köhler, W. (2016). International Centre for Global Earth Models (ICGEM), The Geodesists Handbook 2016. *Journal of Geodesy, 90*(10), 907-1205.

Bato, V. A., & Nicopior, O. B. (2009). Philippine Soils. Manila: Department of Agriculture.

Bayoud, F. A., & Sideris, M. G. (2003). Two different methodologies for geoid determination from ground and airborne gravity data. *Geophysical Journal International, 155*(3), 914-922.

Beccario, C. (2018, September 12). *Earth*. (Cameron Beccario) Retrieved September 12, 2018, from https://earth.nullschool.net/

Bettadpur, S., Ries, J., Eanes, R., Nagel, P., Pie, N., Poole, S., . . . Save, H. (2015). Evaluation of the GGM05 mean Earth gravity models. *Geophysical Research Abstracts*.

Bingham, R. J., Haines, K., & Lea, D. J. (2014). How well can we measure the ocean's mean dynamic topography from space. *Journal of Geophysical Research*, 119(6):3336-3356.

Birardi, G., Santarsiero, D., Tufillaro, D., & Surace, L. (1995). Setting up Local "Mapping Geoids" with the Aid of GPS/LEV Traverses: Application to the Geoids of Sardinia and Calibra. *Journal of Geodesy*, 70(2):98-109.

Biró, P. (1983). *Time Variation of Heights and Gravity.* Budapest: Akadmia Kiadó.

Blewitt, G., Lavalleé, D., Clarke, P., & Nurutdinov, K. (2001). A new global mode of Earth deformation: seasonal cycle detected. *Science*, 294(5550):2342–2345.

Bomford, G. (1980). *Geodesy.* Oxford: Oxford University Press.

Bos, M. S., & Scherneck, H. G. (2013). Computation of Green's functions for ocean tide loading. *Sciences of Geodesy II*, 1-52.

Boy, J. P., & Chao, B. F. (2005). Precise evaluation of atmospheric loading effects on Earth's time-variable gravity field. *Journal of Geophysical Research, B08412*, 110.

Bressan, D. (2017, September 6). *How Hurricanes Change The Earth's Surface*. (Forbes) Retrieved March 31, 2019, from https://www.forbes.com/sites/davidbressan/2017/09/06/the-impact-of-large-hurricanes-on-earths-surface/#43e204196240

Brockmann, J. M., Zehentner, N., Hock, E., Pail, R., Loth, I., Mayer-Gurr, T., & Schuh, W. D. (2014). EGM_TIM_RL05: An independent geoid with centimeter accuracy purely based on the GOCE mission. *Geophysical Research Letters*, 41(22):8089-8099.

Bruinsma, S. L., Forste, C., Abrikosov, O., Marty, J. C., Rio, M. H., Mulet, S., & Bonvalot, S. (2014). The new ESA satellite-only gravity field model via the direct approach. *Geophysical Research Letters*, 40(14):3607-3612.

Bruinsma, S. L., Marty, J. C., Balmino, G., Biancale, R., Foerste, C., Abrikosov, O., & Neumayer, H. (2010). *GOCE Gravity Field Recovery by Means of the Direct Numerical Method.* Norwijk: ESA Publications Division.

Brutsaert, W. (2005). *Hydrology: An Introduction.* Cambridge: Cambridge University Press.

Burkholder, E. F. (2017). *The 3-D Global Spatial Data Model: Principles and Applications.* Florida: CRC Press.

Burša, M., Kenyon, S., Kouba, J., Müller, A., Radej, K., Vatrt, V., Vítek, V. (1999). Long-term stability of geoidal geopotential from Topex/Poseidon satellite altimetry 1993-1999. *Earth, Moon, Planets*, 84:163-176.

Burša, M., Kenyon, S., Kouba, J., Raděj, K., Vatrt, V., Vojtíšková, M., & Šimek, J. (2002). World Height System Specified by Geopotential at Tide Gauge Stations. *Vertical Reference Systems. International Association of Geodesy Symposia* (p. 124). Berlin: International Association of Geodesy .

Burša, M., Kenyon, S., Kouba, J., Šíma, Z., Vatrt, V., Vojtíšková, M., & Vítek, V. (2007). The geopotential value W0 for specifying the relativistic atomic time scale and a global vertical reference system. *Journal of Geodesy*, 81:103-110.

Burša, M., Kouba, J., Müller, A., Radéj, K., True, S. A., Vatrt, V., & Vojtfskovâ, M. (1998). Determination of geopotential differences between Local Vertical Datums and realization of a World Height System. *Symp ZAG Towards an Integrated Global Geodetic Observing System.* Munich.

Burša, M., Kouba, J., Müller, A., Radéj, K., True, S. A., Vatrt, V., & Vojtfskovâ, M. (1999). Geoidal Geopotential and World Height System. *Studio Geoph. and Geod*, 43:327–337.

Burša, M., Kouba, J., Radej, K., True, S., Vatrt, V., & Vojtíšková, M. (1998). Monitoring geoidal potential on the basis of Topex/Poseidon altimeter data and EGM96. *Geodesy on the move-gravity, geoid, geodynamics and Antartica* (pp. 119:352-358). New York: International Association of Geodesy.

Burša, M., Šíma, Z., & Kostelecky, J. (1992). Determination of the geopotential scale factor from satellite altimetry. *Studia geoph et geod*, 36:101-109.

Calang, M. G. (2017). *The Philippine Disaster Risk Reduction and Management System: A Country Report.* Kobe, Japan: Asia Disaster Reduction Center.

Carrère, L., & Lyard, F. (2003). Modeling the barotropic response of the global ocean to atmospheric wind and pressure forcing – comparisons with observations. *Geophysical Research Letterd, 30*(6), 1275.

Cartwright, D. E., & Crease, J. (1963). A comparison of the geodetic reference levels of England and France by means of the sea surface. *Proc Royal Soc Lon*, 273:558-580.

Cayapan, C. (2016). Philippine Geodetic Infrastructure: Status, Challenges and Future Direction. *FIG Geospatial and GNSS CORS Infrastructure Forum.* Kuala Lumpur.

Cayapan, C. (2017, March 16). *NAMRIA measures displacement of PageNET stations from the 10 February 2017 M6.7 Surigao Earthquake*. (NAMRIA) Retrieved March 31, 2019, from https://www.google.com/url?sa=t&rct=j&q=&esrc=s&source=web&cd=1&cad=rja&uact=8&ved=2ahUKEwjK25CwkKrhAhVYVH0KHR87D-AQFjAAegQIABAB&url=http%3A%2F%2Fwww.namria.gov.ph%2Flist.php%3Fid%3D1126%26alias%3Dnamria-measures-displacement-of-pagenet-stations-from-the-

CCRS. (2010, February 17). *Glossary of remote sensing terms.* (NRCAN) Retrieved March 31, 2019, from http://www.ccrs.nrcan.gc.ca/glossary/index_e.php?id=600

Chen, J. L., Rodell, M., Wilson, C. R., & Famiglietti, J. S. (2005). Low degree spherical harmonic influences on gravity recovery and climate experiment (GRACE) water storage estimates. *Geophys Res Lett*, 32(14):L14405.

Chen, J. L., Wilson, C. R., & Seo, K. W. (2006). Optimised smoothing of Gravity Recovery and Climate Experiment (GRACE) time variale gravity observations. *Journal of Geophysical Research, 111*(B06408).

Chen, Q., Shen, Y., Zhang, X., Chen, W., & Hsu, H. (2015). Tongji-GRACE01: A GRACE-only static gravity field model recovered from GRACE Level-1B data using modified short arc approach. *Advances in Space Research*, 56(5):941-951.

Cheng, M., Tapley, B. D., & Ries, J. C. (2013). Deceleration in the Earth's oblateness. *Journal of Geophysical Research*, 118(2):740–747.

Cheng, Y., & Andersen, O. B. (2010). Improvement in global ocean tide model in shallow water regions. *Poster SV.1-68 45 OSTST.* Lisbon.

Climate Change Commission. (2013). *Project Climate Twin Phoenix*. (CCC) Retrieved March 31, 2019, from http://climate.gov.ph/convergence/adaptation-initiatives/project-climate-twin-phoenix

CNN Philippines. (2016, February 20). *More islands, more fun in the Philippines*. (CNN Philippines) Retrieved June 25, 2018, from http://cnnphilippines.com/videos/2016/02/20/More-islands-more-fun-in-PH.html

Coast and Geodetic Surveys Department. (2016). Tide Gauge Bench Marks of the Philippines. Manila: NAMRIA CGSD.

Coleman, R., Rizos, C., Masters, E. G., & Hirsch, B. (1979). The investigation of the sea surface slope along the north eastern coast of Australia. *Aust J Geod*, 31:686-699.

Colombo, O. L. (1980). *A world vertical network.* Columbus, Ohio: Department of Geodetic Science and Surveying, Ohio State University.

Cruz, E. (2019, October 6). Metro Manila and Davao are sinking. *The Philippine Star*.

Čunderlík, R., & Mikula, K. (2009). Numerical solution of the fixed altimetry-gravimetry BVP using the direct BEM formulation. *Observing our Changing Earth*, 133.

Čunderlík, R., Minarechová, Z., & Mikula, K. (2012). Realization of WHS Based on the Static Gravity Field Observed by GOCE. *Gravity, Geoid and Height Systems.* Venice.

Currenti, G. (2014). Numerical evidence enabling reconciliation of gravity and height changes in volcanic areas. *Geophysical Journal International*, 197:164-173.

Dahle, C., Murböck, M., Flechtner, F., Dobslaw, H., Michalak, G., Neumayer, K. H., . . . Förste, C. (2019). The GFZ GRACE RL06 Monthly Gravity Field Time Series: Processing Details and Quality Assessment. *Remote Sensing*, 11(18): 2116.

Darwin, G. H. (1899). The theory of the figure of the Earth. *Monthly Notices of the Royal Astronomical Society*, 60.

Dayoub, N., Edwards, S. J., & Moore, P. (2012). The Gauss-Listing potential value W0 and its rate from altimetric mean sea level and GRACE. *Journal of Geodesy*, 86(9):681-694.

De Mulder, W., Molenberghs, G., & Verbeke, G. (2018). A Generalization of Inverse Distance Weighting and an Equivalence Relationship to Noise-free Gaussian Process Interpolation Via Riesz Representation Theorem. *Linear and Multilinear Algebra, 66*(5), 1054-1066.

Delgado Blasco, J., Foumelis, M., Stewart, C., & Hooper, A. (2019). Measuring Urban Subsidence in the Rome Metropolitan Area (Italy) with Sentinel-1 SNAP-StaMPS Persistent Scatterer Interferometry. *Journal of Remote Sensing*.

Demianov, G., Sermyagin, R., & Tsybankov, I. (2012). *Global Gravity Field Model GAO2012 [Data set].* Potsdam: GFZ Data Center.

Deng, X., Hua, X., & You, Y. (2013). Transfer of height datum across seas using GPS leveling, gravimetric geoid and corrections based on a polynomial surface. *Computers and Geosciences, 51*, 135-142.

Deodhar, M. J. (2008). *Elementary Engineering Hydrology.* London: Pearson Education.

Dermanis, A. (1984). Kriging and collocation - a comparison. *Manuscripta Geodaetica*, 9(3):159-167.

Dong, D., Dickey, J. O., Chao, Y., & Cheng, M. K. (1997). Geocenter variations caused by atmosphere, ocean and surface ground water. *Geophysical Reseach Lettersd*, 1867-1870.

Dong, D., Yunck, T., & Heflin, M. (2003). Origin of the International Terrestrial Reference Frame. *Journal of Geophysical Research*, 108(B4) 2200.

Dragomir, V. C., Ghitau, D. N., Mihailescu, M. S., & Rotaru, M. G. (2017). *Theory of the Earth's Shape.* New York: Elsevier.

Drewes, H. (2009). Reference Systems, Reference Frames, and the Geodetic Datum - Basic Considerations. *Observing our Changing Earth. Proceedings of the 2007 IAG General Assembly.* Perugia, Italy.

Drewes, H., Kuglitsch, F., Adám, J., & Rózsa, S. (2016). The Geodesist's Handbook. *Journal of Geodesy*, 90:907–1205.

Dziewonski, A. M., & Anderson, D. L. (1981). Preliminary reference Earth model. *Physics of the Earth and Planetary Interiors*, 25(4):297–356.

Eco, R. C., Rodolfo, K. S., Sulapas, J. J., Morales Rivera, A., Lagmay, A. M., & Amelung, F. (2018). Widespread land subsidence in Metro Manila, Philippines and surrounding areas detected by InSAR time-series analysis. *AGU Fall Meeting 2018.* Washington D. C.: American Geophysical Union.

Egbert, G. D., & Erofeeva, L. (2010). Efficient inverse modeling of barotropic ocean tides. *Journal of Atmospheric and Oceanic Technology*, 19.

Ekman, M. (1989). Impacts of geodynamic phenomena on systems of height and gravity. *Bulletin Géodésique*, 63 (2), 281-296.

ENVI. (2006). *ISODATA Classification. ENVI User's Guide.* RSI.

EOST. (2015). *EOST Loading Service*. Retrieved 11 28, 2018, from http://loading.u-strasbg.fr/displ_itrf.php

Erol, B., & Çelik, R. N. (2006). Modelling local GPS/levelling geoid: assessment of inverse distance weighting and geostatistical kriging methods. *Geoinformation Science Journal, 6*(1), 78-83.

European Space Agency. (2018, June). *Software Tool/App - SNAP.* Retrieved from Sentinels: https://sentinels.copernicus.eu/subb

Farahani, H., Hashemi, D. P., Klees, R., Liu, X., Zhao, Q., & Guo, J. (2013). The static gravity field model DGM-1S from GRACE and GOCE data: computation, validation and an analysis of GOCE mission’s added value. *Journal of Geodesy*, 87(9):843-867.

Farrell, W. E. (1972). Deformation of the earth by surface loads. *Rev. Geophys*, 10:761-797.

Featherstone, W. (2001). Absolute and relative testing of gravimetric geoid models using global positioning system and orthometric height data. *Computers and Geosciences, 27*, 807-814.

Featherstone, W. E. (1995). On the use of Australian Geodetic Datums in gravity field determination. *Geomatics Research Australasia*, 62:17-36.

Featherstone, W. E. (1996). An updated explanatiion of the Geocentric Datum of Australia and its effects upon future mapping. *The Australian Surveyor*, 41(2), 121-130.

Featherstone, W. E. (2000). Refinement of a Gravimetric Geoid Using GPS and Levelling Data. *Journal of Surveying Engineering*, 126(2):27-56.

Featherstone, W. E., & Dentith, M. C. (1997). A geodetic approach to gravity reduction for geophysics. *Computers and Geosciences*, 23:1063-1070.

Featherstone, W. E., & Filmer, M. S. (2012). The north-south tilt in the Australian Height Datum is explained by the ocean's mean dynamic topography. *J. Geophys. Res.*, 117:C08035.

Featherstone, W. E., & Kirby, J. (1998). Estimates of the separation between the geoid and the quasigeoid over Australia. *Geomatics Research Australasia*, 68:79-90.

Featherstone, W. E., & Sproule, D. M. (2006). Fitting AusGeoid98 to the Australian Height Datum using GPS-levelling and least squares collocation: Application of a cross-vaidation technique. *Survey Review*, 38(301).

Featherstone, W. E., Dentith, M. C., & Kirby, J. F. (1998). Strategies for the accurate determination of orthometric heights from GPS. *Survey Review*, 34(267), 278-296.

Featherstone, W., & Kuhn, M. (2006). Height Systems and Vertical Datums: a Review in the Australian Context. *Journal of Spatial Science, 51*(1), 21-41.

Fecher, T., Pail, R., & Gruber, T. (2015). Global gravity field modeling based on GOCE and complementary gravity data. *International Journal of Applied Earth Observation and Geoinformation*, 35:120-127.

Ferreira, V. G., & de Freitas, S. R. (2012). An attempt to link the Brazilian height system to a world height system. *Boletin de Cincias Geodsicas, 18*(2), 363-377.

Ferry, N., Remy, E., Brasseur, P., & Maes, C. (2007). The MERCATOR ocean operational analysis / forecast system: assessment and validation of a 11-year reanalysis. *Journal of Marine Systems, 65*(1), 540-560.

Filmer, M. S., Featherstone, W. E., & Kuhn, M. (2010). The effect of EGM2008-based normal, normal-orthometric and Helmert orthometric height systems on the Australian levelling network. *Journal of Geodesy*, 84(8):501-513.

Filmer, M. S., Hughes, C. W., Woodworth, P. L., Featherstone, W. E., & Bingham, R. J. (2018). Comparison between geodetic and oceanographic approaches to estimate mean dynamic topography for vertical datum unification: evaluation at Australian tide gauges. *Journal of Geodesy*, 92(12):1413-1437.

Flechtner, F., Dahle, C., Neumayer, K. H., König, R., Förste, C., Flechtner, F. M., . . . Wickert, J. (2010). *The Release 04 CHAMP and GRACE EIGEN Gravity Field Model.* Berlin: Springer.

Flores, J. F., Balagot, V. F., & Arakawa, H. (1969). Climate of the Philippines. In *World Survey of Climatology, Volume 8: Climates of Northern and Eastern Asia.* Michigan: Elsevier.

Flury, J., & Rummel, R. (2009). On the geoid–quasigeoid separation in mountain areas. *Journal of Geodesy, 83*(9), 829-847.

Forsberg, R. (2000). *Draping of geoids to GPS observations.* Johor, Malaysia: IGeS Geoid School.

Forsberg, R., Olesen, A. V., Gatchalian, R., & Ortiz, C. C. (2014). *Geoid Model of the Philippines from Airborne and Surface Gravity.* Taguig: National Mapping and Resource Information Authority.

Förste, C., & Bruinsma, S. L. (2016). *EIGEN-6S4: A time-variable satellite-only gravity field model to d/o 300 based on LAGEOS, GRACE and GOCE data from the collaboration of GFZ Potsdam and GRGS Toulouse.* Potsdam: GFZ Data Center.

Förste, C., Bruinsma, S. L., Abrikosov, O., Lemoine, J.-M., Marty, J. C., Flechtner, F., Biancale, R. (2014). *EIGEN-6C4 The latest combined global gravity field model including GOCE data up to degree and order 2190 of GFZ Potsdam and GRGS Toulouse.* Potsdam: GFZ Data Services.

Förste, C., Bruinsma, S. L., Flechtner, F., Marty, J. C., Lemoine, J. M., Dahle, C., Balmino, G. (2012). *A preliminary update of the Direct approach GOCE Processing and a new release of EIGEN-6C.* San Francisco.

Förste, C., Bruinsma, S. L., Shako, R., Marty, J. C., Flechtner, F., Abrikosov, O., Balmino, G. (2011). EIGEN-6 - A new combined global gravity field model including GOCE data from the collaboration of GFZ-Potsdam and GRGS-Toulouse. *Geophysical Research Abstracts*.

Förste, C., Flechtner, F., Schmidt, R., König, R., Meyer, U., Stubenvoll, R., Lemoine, J. M. (2006). A mean global gravity field model from the combination of satellite mission and altimetry/gravimetry surface gravity data. *Geophysical Research Abstracts*.

Förste, C., Flechtner, F., Schmidt, R., Meyer, U., Stubenvoll, R., Barthelmes, F., Raimondo, J. C. (2005). A New High Resolution Global Gravity Field Model Derived From Combination of GRACE and CHAMP Mission and Altimetry/Gravimetry Surface Gravity Data. *Poster presented at EGU General Assembly 2005.* Vienna: EGU.

Förste, C., Flechtner, F., Schmidt, R., Stubenvoll, R., Rothacher, M., Kusche, J., Meyer, U. (2008). EIGEN-GL05C - A new global combined high-resolution GRACE-based gravity field model of the GFZ-GRGS cooperation. *Geophysical Research Abstracts*, 10.

Fotopoulos, G., Kotsakis, C., Sideris, & M. (2003). How accurately can we determine orthometric height differences fro GPS and geoid data? *Journal of Survey Engineering, 129*, 1-10.

Gatchalian, R. (2016, August 6). Status of the Philippine Height System.

Gatchalian, R., Forsberg, R., & Olesen, A. (2017). *PGM2016: A new Geoid Model for the Philippines.* Taguig: NAMRIA.

Gatti, A., Reguzzoni, M., Migliaccio, F., & Sanso, F. (2014). *Space-wise grids of gravity gradients from GOCE data at nominal satellite altitude.* Paris: GFZ.

Gegout, P., Boy, J. P., Hinderer, J., & Ferhat, G. (2008). Modeling and Observation of Loading Contribution to Time-Variable GPS Sites Positions. *Gravity, Geoid and Earth Observation: IAG Commission 2: Gravity Field* (pp. 651-659). Crete: International Association of Geodesy.

Gervasio, F. (1967). Age and Nature of Orogenesis in the Philippines. *Tectonophysics, 4*(1), 379-402.

GGOS. (n.d.). (GGOS) Retrieved March 07, 2019, from http://www.ggos.org/en/focus-areas/unified-height-system/objectives/

Gilardoni, M., Reguzzoni, M., & Sampietro, D. (2016). GECO: a global gravity model by locally combining GOCE data and EGM2008. *Studia Geophysica et Geodaetica*, 60:228-247.

Goiginger, H., Höck, E., Rieser, D., Mayer-Gürr, T., Maier, A., Krauss, S., . . . Kusche, J. (2011). *The combined satellite-only global gravity field model GOCO02S.* Vienna.

Goldstein, R. M., & Werner, C. L. (1998). Radar interferogram filtering for geophysical applications. *Geophysical Research Letters*, 4035-4038.

Gomarasca, M. (2009, February 18). *Basics of Geomatics.* Milan: Springer. Retrieved March 31, 2019, from http://geog.hkbu.edu.hk/virtuallabs/rs/classification3.htm

Grafarend, E. W. (1989). The geoid and the gravimetric boundary value problem. In *Report 18 Trita. Geod.* Stockholm: The Royal Institute of Technology Stockholm Department of Geodesy.

Grafarend, E. W., & Ardalan, A. A. (1999). World geodetic datum 2000. *Journal of Geodesy, 73*(11), 611-623.

Grigoriadis, V. N., Kotsakis, C., Tziavos, I. N., & Vergos, G. S. (2012). Estimation of the reference geopotential value for the local vertical datum of continental Greece using EGM08 and GPS/leveling data. *Proceedings of the IAG Symposium Gravity, Geoid and Height Systems 2012.* Venice.

Grigoriadis, V. N., Kotsakis, C., Tziavos, I. N., & Vergos, G. S. (2014). Estimation of the reference geopotential value for the local vertical datum of continental Greece using EGM08 and

GPS/leveling data. *Proceedings of the IAG Symposium Gravity, Geoid and Height Systems 2012.* Venice.

Gruber, T. (2009). Evaluation of the EGM2008 gravity field by means of GPS-levelling and sea surface topography solutions. *Newton's Bull Bur Gravimétrique Int (BGI)/Int Geoid Service (IGes), 4*, 3-17.

Gruber, T. (2013). Overview of HSU study and preliminary roadmap for height system unification. *Tide Gauge Unification Workshop for Sea Level and Ocean Modelling.* Noordwijk.

Gruber, T., Gerlach, C., & Haagmans, R. (2012). Intercontinental Height Datum Connection with GOCE and GPS-Levelling Data. *Journal of Geodetic Science, 2*(4), 270-280.

Gruber, T., Visser, P. N., Ackermann, C., & Hosse, M. (2011). Validation of GOCE gravity field models by means of orbit residuals and geoid computations. *Journal of Geodesy, 85*, 845-860.

Hayford, J. F. (2018). *A Textbook of Geodetic Astronomy.* Minnesota, USA: Chizine Publication.

He, L., Chu, Y., & Yu, N. (2017). Evaluation of the geopotential value W0LVD of China. *Geodesy and Geodynamics, 2017*, 1-5.

Heck, B. (1989). Acontribution to the scalar free boundary value problem of physical geodesy. *Manuscripta Geodaetica, 14*(2), 87-99.

Heck, B. (1995). *Rechenverfahren und Auswertemodelle der Landesver- messung.* Heidelberg: Herbert Wichmann Verlag.

Heck, B., & Mälzer, H. (1986). On some problems connected with the determination of recent vertical crustal movements from repeated levelling and gravity measurements. *Tectonophysics*, 299-305.

Heiskanen, W. A., & Moritz, H. (1967). *Physical Geodesy.* San Francisco, USA: Freeman.

Helmert, F. R. (1890). *Die Schwerkraft im Hochgebirge, Insbesondere in den Tyroler Alpen.* Berlin, Germany: Veröff. Königl. Preuss Geod .

Hendershott, M. (n.d.). *Lecture 1: Introduction to Ocean Tides.* Woods Hole: Woods Hole Oceanographic Institution .

Herceg, M., Knudsen, P., & Tscherning, C. C. (2012). GOCE Data for Local Geoid Enhancement. *Gravity Geoid and Height Systems.* Venice.

Hermann, H. (1861). *On the general theory of the movement of fluids.* Göttingen, Germany: Dieterische University Buchdruckerei.

Hijmans, R. J., Cameron, S. E., Parra, J. L., Jones, P. G., & A, J. (2005). Very high resolution interpolated climate surfaces for global land areas. *International Journal of Climatology, 25*, 1965-1978.

Hirt, C., Gruber, T., & & Featherstone, W. E. (2011). Evaluation of the first GOCE static gravity field models using terrestrial gravity, vertical deflections and EGM2008 quasigeoid heights. *Journal of Geodesy, 85*(10), 723-740.

Hirt, C., Marti, U., Bürki, B., & Featherstone, W. E. (2010). Assessment of EGM2008 in Europe using accurate astrogeodetic vertical deflections and omission error estimates from SRTM/DTM2006.0 residual terrain model data. *Journal of Geophysical Research*, 115:B10.

Hirth, C. (2011). Assessment of EGM2008 over Germany using accurate quasigeoid heights fro vertical deflections, GCG05 and GPS levelling. *Zeitschrift für Geodäsie, 136*(3).

Hirvonen, R. A. (1960). *New theory of the gravimetric geodesy.* Helsinki: Publ. Isost. Inst. Int. Assoc. Geodesy.

Hoffmann-Wellenhoff, B., & Moritz, H. (2005). *Physical Geodesy.* New York: Springer.

Holdahl, S. R. (1979). Height systems for North America. *Proceedings of the First International Conference on the Redefinition of the North American Geodetic Vertical Control Network* (pp. 128-142). Fort Clayton: US Department of Commerce.

Huber, M., Hummelbrunner, W., Raggam, J., Small, D., & Kosmann, D. (2004). Technical Aspects of Envisat ASAR Geocoding Capability at DLR. *Proceedings of the 2004 Envisat & ERS Symposium (ESA SP-572).* Salzburg: ERS.

IBTrACS. (2018). Global Typhoon Tracks 1969-2011. Asheville: National Centers for Environmental Information.

IERS. (1996). *IERS Conventions 1996.* Paris: International Earth Rotation Service.

Ihde, J., & Sanchez, L. (2005). A unified global height reference system as a basis for the IGGOS. *Journal of Geodynamics, 40*, 400-413.

Ihde, J., Barzaghi, R., Marti, U., Sánchez, L., Sideris, M. D., Foerste, C., Pail, R. (2015). Report of the Ad-hoc Group on an International Height Reference System (IHRS). In *IAG Reports 2011-2015.* International Association of Geodesy.

Ihde, J., Sánchez, L., Bargzaghi, R., Drewes, H., Foerste, C., Gruber, T., Sideris, M. (2017). Definition and Proposed Realization of the International Height Reference System (IHRS). *Surv Geophys*.

Ince, E. S., Barthelmes, F., Reißland, S., Elger, K., Förste, C., Flechtner, F., & Schuh, H. (2019). ICGEM – 15 years of successful collection and distribution of global gravitational models, associated services and future plans. *Earth System Science Data*, 11(647-674).

International Association of Geodesy. (1984). IAG Resolutions adopted at the XVIII General Assembly of the IUGG in Hamburg, August 1983. *Bulletin Geodesique*, 58(3).

International Association of Geodesy. (2015, July). *IAG Resolution (No. 1) for the definition and the realization of an International Height Reference System (IHRS).* Retrieved March 7, 2019, from https://ihrs.dgfi.tum.de/fileadmin/JWG_2011/IAG_Resolutions_2015.pdf

International Earth Reference Service. (2017). *Coordinates of the Pole*. Retrieved May 17, 2018, from https://hpiers.obspm.fr/eop-pc/earthor/polmot/pm.html#filtered-pole

Jäggi, A., Beutler, G., Meyer, U., Prange, L., Dach, R., & Mervart, L. (2012). AIUB-GRACE02S: Status of GRACE Gravity Field Recovery Using the Celestial Mechanics Approach. *IAG Scientific Assembly 2009.* Buenos Aires: International Association of Geodesy.

Jäggi, A., Meyer, U., Beutler, G., Prange, L., Dach, R., & Mervart, L. (2011). *AIUB-GRACE03S: A static gravity field model computed with simultaneously solved-for time variations from 6 years of GRACE data using the Celestial Mechanics Approach.*

Jacob, T., Wahr, J., Gross, R., Swenson, S., & Geruo, A. (2012). Estimating geoid height change in North America: past, present and future. *Journal of Geodesy*, 86(5), 337-358.

Jayne, S. R. (2006). Circulation of the North Atlantic Ocean from altimetry and the Grace Recovery and Climate Recovery Experiment. *Journal of Geophysical Research*, C3:C03005.

Jekeli, C. (1981). *Alternative methods to smooth the Earth's gravity field.* Columbus: Department of Geodetic Science and Surveying, Ohio State University.

Jekeli, C. (1999). An analysis of vertical defections derived from high-degree spherical harmonic models. *Journal of Geodesy*, 73:10-22.

Jekeli, C. (2000). *Heights, The Geopotential, and Vertical Datums.* Columbus: Department of Geodetic Science, The Ohio State University.

Jensen, H. (1950). Formulas for the astronomical correction to the precise levelling. *Bulletin Géodésique*, 17(1):267-277.

Johnson, A. (2006). *Plane and Geodetic Surveying: The Management of Control Networks.* London: CRC Press.

Juanico, M. (1987). *Physical Geography.* Manila: Goodwill Trading.

Kasenda, A. (2009). *High Precision Geoid for Modernisation of Height Systems in Indonesia.* Sydney: The University of New South Wales.

Kearseley, A. H., & Ahmad, Z. (1995). Problems with geoid evaluations in Southeast Asia. *Gravity and Geoid: Joint Symposium of the International Gravity Commission, 113*, 435-439.

Kenyeres, A. (2016). GPS/leveling. *Encyclopedia of Geodesy*.

Khazrei, S. M., Nafisi, V., Amiri-Simkooei, A. R., & Asgari, A. (2017). Combination of GPS and leveling observations and geoid models using least-squares variance component estimation. *Journal of Surveying Engineering*, 143(2).

King, R. W., & Bock, Y. (2008). *Documentation for the GAMIT processing software.* Cambridge: Massachusetts Institute of Technology.

Kintanar, R. L. (1984). *Climate of the Philippines.* Manila: PAGASA.

Knudsen, P., Andersen, O., Khan, S. A., & Høyer, J. (2001). Ocean tide effects on GRACE gravimetry. *Gravity, Geoid and Geodynamics 2000*, 159-164.

König, R., Fagiolini, E., Raimondo, J., & Vei, M. (2016). A Non-tidal Atmospheric Loading Model: On Its Quality and Impacts on Orbit Determination and C20 from SLR. *International Symposium on Earth and Environmental Sciences for Future Generations* (p. 147). Switzerland: Springer.

Kotsakis, C., Katsambalos, K., & Ampatzidis, D. (2012). Estimation of the zero-height geopotential level W0LVD in a local vertical datum from inversion of co-located GPS, levelling and geoid heights: a case study in the Hellenic islands. *Journal of Geodesy, 86*, 423-439.

Krakiwsky, E., & Wells, D. (1971). *Coordinate Systems in Geodesy.* New Brunswick: University of New Brunswick.

Kreemer, C., Blewitt, G., & Klein, E. C. (2014). A geodetic plate motion and global strain rate model. *Geochemistry, Geophysics, Geosystems, 15*, 3849-3889.

Krivoruchko, K. (2012). Empirical bayesian kriging implemented in ArcGIS geostatistical analyst. *ArcUser, 15*, 6-10.

Kuhn, M., Featherstone, W. E., & Kirby, J. F. (2009). Complete spherical Bouguer gravity animalies over Australia. *Australian Journal of Earth Sciences*, 56(2):213-223.

Kusche, J., Schmidt, R., Petrovic, S., & Rietbroek, R. (2009). Decorrelated GRACE time-variable gravity solutions by GFZ, and their validation using a hydrological model. *Journal of Geodesy, 83*(10), 903-913.

Lagmay, A. M., Tejada, M. L., Peña, R., Aurelio, M. A., David, S., & Billedo, E. (2009). New definition of Philippine Plate boundaries and implications to the Philippine Mobile Belt. *Journal of the Geological Society of the Philippines, 64*(1), 17-30.

Lambrou, E. (2012). Accurate Geoid Height Differences Computation from GNSS Data and Modern Astrogeodetic Observations. *Gravity, Geoid and Height Systems.* Venice.

Ledersteger, K. (1955). *Der schwereverlauf in den Lotlinien und die Berechnung der wahren Geoidschwere.* Helsinki: Finnish Geodetic Institute.

Lehmann, R. (2000). Altimetry-gravimetry problems with free vertical datum. *Journal of Geodesy, 74*(3-4), 327-334.

Lemoine, F. G., Kenyon, S. C., Factor, J. K., Trimmer, R. G., Pavlis, N. K., Chinn, D. S., Olson, T. R. (1998). *The Development of the Joint NASA GSFC and the National IMagery and Mapping Agency (NIMA) Geopotential Model EGM96.* Greenbelt, Md: Goddard Space Flight Center.

Letellier, T. (2004). *Etude des ondes de marée sur les plateaux continentaux. Thèse doctorale.* Toulouse: Université de Toulouse III.

Lin, L. (2013). Orthometric height improvement in Tainan City using RTK GPS and local geoid corrector surface models. *Journal of Surveying Engineering, 140*(1), 35-43.

Linsley, R., Kohler, M., & Paulhus, J. (1958). *Hydrology for Engineers.* New York: McGraw-Hill.

Lopez, E. (2014). *PRS92: Implementation Issues and Recommendations.* Manila: National Mapping and Resource Information Authority.

Lyard, L., Lefevre, L., Letellier, T., & Francis, O. (2006). Modelling the global ocean tides: insights from FES2004. *Ocean Dynamics*, 56(416).

Lydolph, P. E. (1985). *The Climate of the Earth.* Maryland: Rowman & Littlefield.

Lyszkowicz, A. (2000). Improvement of the Quasigeoid Model in Poland by GPS and Levelling Data. *Artificial Satellites*, 35(1):3-8.

Mader, K. (1954). *Die orthometrische Schwerekorrektion des Präzisions-Nivellements in den Hohen Tauern.* Vienna, Austria: Österreichische Zeitschrift für Vermessungswesen.

Mäkinen, J. &. (2009). The Permanent Tide In Height Systems. *Observing our Changing Earth. International Association of Geodesy Symposia, vol 133.* (pp. 81-87). Berlin: Springer.

Mäkinen, J., & Ihde, J. (2009). The permanent tide in height systems. *IAG Symposium Series, 133*, 81-87.

Marti, U., & Schlatter, A. (2002). Höhenreferenzsysteme und -rahmen. *Vermessung, Photogrammetrie, Kulturtechnik, 1*, 8-12.

Martinec, Z. (1998). Boundary value problems for gravimetric determination of precise geoid. In *Lecture Notes in Earth Sciences.* Germany: Springer Verlag.

Mather, R. S. (1975). On the evaluation of stationary sea surface topography using geodetic techniques. *Bull. Geod*, 115(1):65-82.

Matheron, G. (1963). Princiopoles of Geostatistics. *Economic Geology*, 58(8): 1246-1266.

Mayer-Gürr, T., Eicker, A., & Ilk, K. H. (2006). ITG-GRACE02s: a GRACE gravity field derived from short arcs of the satellite's orbit. *Proceedings of the First Symposium of International Gravity Field Service.* Istanbul: International Gravity Field Service.

Mayer-Gürr, T., Eicker, A., & Ilk, K. H. (2007). *ITG-Grace03 Gravity Field Model.* Bonn: Universität Bonn.

Mayer-Gürr, T., Kurtenbach, E., & Eicker, A. (2010). *ITG-Grace2010 Gravity Field Model.* Bonn: Universität Bonn.

Mayer-Gürr, T., Pail, R., Gruber, T., Fecher, T., Rexer, M., Schuh, W. D., Jäggi, A. (2015). *The combined satellite gravity field model GOCO05s.* Vienna: GFZ.

Mayer-Gürr, T., Rieser, D., Höck, E., Brockmann, J. M., Schuh, W. D., Krasbutter, I., Gruber, T. (2012). *The new combined satellite only model GOCO03s.* Venice.

Mayer-Gürr, T., Zehentner, N., Klinger, B., & Kvas, A. (2014). *ITSG-Grace2014: a new GRACE gravity field release computed in Graz.* Potsdam: GFZ Data Services.

McCarthy, D. D., & Petit, G. (2004). *IERS Conventions 2003. IERS Technical Note No. 32.* Frankfurt: Verlag des Bundesamtes für Kartographic und Geodäsie.

McGuffie, K., & Henderseon-Sellers, A. (2005). *A Climate Modelling Primer.* New York: John Wiley & Sons.

Menemenlis, D., Fukumori, I., & Lee, T. (2005). Using Green's functions to calibrate an ocean general circulation model. *Mon. Weather Rev.*, 133:1224-1240.

Meneses, S. F., & Paringit, E. (2009). Gravimetric geoid determination by using terrestrial and satellite-derived data. *Proceedings of the Asian Conference on Remote Sensing 2009.* Beijing.

Meyer, T., Roman, D., & Zilkoski, D. (2004). What does height really mean? Part I: Introduction. *Surveying and Land Information Science, 63*(4), 223-233.

Mines and Geosciences Bureau. (2004). *Geology and Mineral Resource of the Philippine - Volume I.* Manila: Department of Environment and Natural Resources.

Moffatt, M. (2017, March 29). *An Introduction to Akaike's Information Criterion (AIC)*. (ThoughtCo) Retrieved February 9, 2018, from https://www.thoughtco.com/introduction-to-akaikes-information-criterion-1145956

Mohr, P., Newell, D., & Taylor, B. (2014). CODATA Recommended Values of the Fundamental Physical Constants: 2014. *Reviews of Modern Physics, 88*.

Molodenskij, M. S., Eremeev, V. F., & Yurkina, M. I. (1962). *Methods for study of the external gravitational field and figure of the Earth. Translated from Russian by the Israel program for scientific translations.* Washington, D.C.: Office of Technical Services Department of Commerce.

Moritz, H. (2000). Geodetic reference system 1980 (repub. with corrections). *Journal of Geodesy*, 74:128-133.

Moritz, H., & Mueller, I. (1987). *Earth rotation - theory and observation.* New York: Ungar.

NAMRIA Coast and Geodetic Survey Department. (1987). *13 May 1987 Letter on MSL observations for the PSMSL.* Manila: National Mapping and Resource Information Authority.

NAMRIA Coast and Geodetic Survey Department. (1988). *22 January 1988 Letter on MSL Observations to the PSMSL.* Manila: National Mapping and Resource Information Authority.

NAMRIA Coast and Geodetic Survey Department. (2003). *21 October 2003 Letter on MSL Observations to the PSMSL.* Manila: National Mapping and Resource Information Authority.

NAMRIA Coast and Geodetic Survey Department. (2016). *Mean Sea Level of Tide Stations.* Manila: NAMRIA Coast and Geodetic Survey Department.

National Geodetic Survey. (1998). *Geodetic Glossary.* Rockville, Maryland: National Oceanic and Atmospheric Administration.

National Imagery and Mapping Agency. (1997). *Department of Defense World Geodetic System 1984.* St. Louis: National Imagery and Mapping Agency.

National Mapping and Resource Information Authority. (2016). Interferometric Synthetic Aperture Radar Digital Elevation Model. Taguig: NAMRIA.

National Mapping and Resource Information Authority. (2017, September 27). *NAMRIA Geoportal*. (NAMRIA) Retrieved March 31, 2019, from http://www.geoportal.gov.ph/viewer/

National Mapping and Resource Information Authority. (2018). *Hydrography, Physical Oceanography and Nautical Charting.* Retrieved October 12, 2018, from http://www.namria.gov.ph/about.aspx

National Oceanic and Atmospheric Administration. (2000). *Tide and Current Glossary.* Maryland: U.S. Department of Commerce. Retrieved from https://tidesandcurrents.noaa.gov/publications/glossary2.pdf

National Oceanography Centre. (2016, October 10). *Permanent Service for Mean Sea Level (PSMSL)*. (National Oceanography Centre) Retrieved 3 29, 2019, from https://www.psmsl.org/data/

National Statistical Coordination Board. (2010). *A View of the Philippines*. (NSCB) Retrieved March 5, 2015, from http://www.nscb.gov.ph/view/geography.asp

Natural Resources Canada. (2017, January 26). *Height Reference System Modernization.* Retrieved June 27, 2018, from http://www.nrcan.gc.ca/earth-sciences/geomatics/geodetic-reference-systems/9054

Niethammer, T. (1932). *Nivellement und Schwere als Mittel zur Berechnung wahrer Meereshöhen.* Berne: Schweizerische Geodätische Kommission.

NIMA. (1997). *Department of Defense World Geodetic System 1984.* Bethesda, Maryland: National Imagery and Mapping Agency.

Oberheide, J., Hagan, M. E., Richmond, A. D., & Forbes, J. M. (2015). Dynamical Meteorology. Atmospheric Tides. *Encyclopedia of Atmospheric Sciences*, 287-297.

Odumosu, J. O., Ajayi, O. G., Idowu, F. F., & Adesina, E. A. (2018). Evaluation of the various orthometric height systems and the Nigerian scenario – A case study of Lagos State. *Journal of King Saud University - Engineering Sciences*, 46-53.

Pail, R., Albertella, A., Rieser, D., Brockmann, J. M., Schuh, W., & Savcenko, R. (2014). Satellite gravity models and their use for estimating mean ocean circulation. *Earth on the Edge: Science for a Sustainable Planet* (pp. 275-281). Melbourne: International Association of Geodesy.

Pail, R., Fecher, T., Barnes, D., Factor, J., Holmes, S., Gruber, T., & Philipp, Z. (2017). The experimental gravity field model XGM2016. . *GFZ Data Services*.

Pail, R., Goiginger, H., Schuh, W. D., Höck, E., Brockmann, J. M., Fecher, T., Rieser, D. (2010). Combined satellite gravity field model GOCO01S derived from GOCE and GRACE. *Geophysical Research Letters*, 37(20).

Pan, M., & Sjoberg, L. (1998). Unification of vertical datums by GPS and gravimetric geoid models with application to Fennoscandia. *Journal of Geodesy, 72*(2), 64-70.

Papanikolaou, T. D., & Papadopoulos, N. (2015). High-frequency analysis of Earth gravity field models based on terrestrial gravity and GPS/levelling data: a case study in Greece. *Journal of Geodetic Science, 5*, 67-79.

Paringit, E. C., Balicanta, L. P., & Sarmiento, C. J. (2015, February). Survey requirements for river flood assessment and spatial planning. *Coordinates Magazine*.

Paringit, E. C., Ventura, D., & Isada, J. G. (2009). Research and Development in Support of the Implementation of the Philippine Reference System of 1992: Results and Recommendations. *Proceedings of the 7th FIG Regional Conference.* Hanoi.

Paringit, M. C., & Paringit, E. C. (2015). Vertical Datum Unification in the Philippines from Analysis of Tide Stations. *International Journal of Geomatics and Geosciences, 6*(2), 1464-1474.

PASCO Corporation. (2004). *Earthquake Impact Reduction Study for Metropolitan Manila.* Manila: JICA, MMDA and PHIVOLCS.

Pavlis, N. K., Chinn, D. S., Cox, C. M., Lemoine, F. G., & Smith, D. E. (2000). *Geopotential Model Improvement Using POCM_4B Dynamic Ocean Topography Information: PGM2000A.* Maryland: NASA Goddard Space Flight Center.

Pavlis, N. K., Holmes, S. A., Kenyon, S. C., & Factor, J. K. (2012). The development and evaluation of the Earth Gravitational Model 2008 (EGM2008). *Journal of Geophysical Research: Solid Earth (1978-2012)*, 117(B4).

Penna, N. T., Featherstone, W. E., Gazeaux, J., & Bingham, R. J. (2013). The apparent British sea slope is caused by systematic errors in the levelling-based vertical datum. *Geophysical Journal International*, 194:772-786.

Perez, R. T., Feir, R. B., Carandang, E., & Gonzalez, E. B. (1996). Potential impacts of sea level rise on the coastal resources of Manila Bay: a preliminary vulnerability assessment. *Climate Change Vulnerability and Adaptation in Asia and the Pacific.* Manila.

Petit, G., & Luzum, B. (2010). IERS Conventions. In *IERS Technical Note No. 36* (p. 179). Frankfurt: Verlag des Bundesamts fur Kartographie and Geodasie.

Philippine Institute for Development Studies. (2005, February). Basics on Philippine Climatology. *Economic Issue of the Day*.

Pizzetti, P. (1894). Sull' espressione della gravitá alla superficie del geoide supposto ellisoidico. *Atti. Accad. Nazl. Lincei, Rend, Classe Sci. Fis. Mat. Nat.*, 5(3): 166-172.

Pizzetti, P. (1913). *Principi della teoria meccanica della figura dei pianeti.* Pisa.

Poutanen, M., Vermeer, M., & Mäkinen, J. (1996). The permanent tide in GPS positioning. *Journal of Geodesy*, 70:499-504.

Prange, L. (2010). *Global Gravity Field Determination Using the GPS Measurements Made Onboard the Low Earth Orbiting Satellite CHAMP.* Schweizerische Geodätische Kommission.

Pruppacher, H. R., & Klett, J. D. (1997). *Microphysics of Clouds and Precipitation.* Berlin: Springer.

Pugh, D. T. (1987). *Tides, surges and mean sea level: a handbook for engineers and scientists.* Chichester: Wiley.

Pugh, D., & Woodworth, P. (2014). *Sea-Level Science: Understanding Tides, Surges, Tsunamis and Mean Sea-Levelo Changes.* Cambridge: Cambridge University Press.

Rangelova, E. V. (2007). *A Dynamic Geoid Model for Canada.* Calgary: University of Calgary.

Rangelova, E., van der Wal, W., & Sideris, M. G. (2007). Numerical models of the rates of change of the geoid and orthometric heights over Canada. *Dynamic Planet, 130*, 563-570.

Rapp, R. (1994). Separation between reference surfaces of selected vertical datums. *Bulletin Géodésique, 69*(1), 26-31.

Rapp, R. H. (1961). *The orthometric heights (M.Sc. Thesis).* Columbus: Ohio State University.

Rapp, R. H. (1995). *Equatorial radius estimates from TOPEX altimeter data.* Munich: University FAF.

Rapp, R. H., & Balasubramania, N. (1992). *A conceptual formulation of a world height system.* Columbus, Ohio: Department of Geodetic Science and Surveying, Ohio State University.

Rapp, R., & Pavlis, N. (1991). OSU89A/B Potential Coefficient Models. *Determination of the Geoid. International Association of Geodesy Symposia book series (IAG SYMPOSIA, volume 106)* (pp. 7-9). Columbus: International Association of Geodesy.

Raucoules, D., Cozannet, G. L., Wöppelmann, G., Michele, M. D., Gravelle, M., Daag, A. S., & Marcos, M. (2013). High nonlinear urban ground motion in Manila (Philippines) from 1993 to 2010 observed by DInSAR: Implications for sea-level measurement. *Remote Sensing of Environment*, 139:386-397.

Ray, R. D., & Ponte, R. M. (2003). Barometric tides from ECMWF operational analyses. *Annales. Geophysicae*, 21:1897-1910.

Reddy, P. J. (2005). *A Text Book of Hydrology.* New Delhi: Firewall Media.

Reigber, C., Casper, R., & Päffgen, W. (1999). The CHAMP Geopotential Mission. *IAA 2nd International Symposium on Small Satellites for Earth Observation* (pp. 25-28). Berlin: IAA.

Reigber, C., Jochmann, H., Wünsch, J., Petrovic, S., Schwintzer, P., Barthelmes, F., Wickert, J. (2004). *Earth Gravity Field and Seasonal Variability from CHAMP.* Berlin: Springer.

Reigber, C., Schmidt, R., Flechtner, F., König, R., Meyer, U., Neumayer, K.-H., . . . Zhu, S. Y. (2005). An Earth gravity field model complete to degree and order 150 from GRACE: EIGEN-GRACE02S. *Journal of Geodynamics*, 39(1):1-10.

Reyes, R. B., Nagai, M., Kamiya, Y., Tipdecho, T., & Ninsawat, S. (2014). Effect of sea level rise in the validation of geopotential/geoid models in Metro Manila, Philippines. *Survey Review, 47*(342), 211-219.

Richards, J. A. (2013). *Remote Sensing Digital Image Analysis: An Introduction.* Berlin: Springer-Verlag Berlin Heidelberg.

Ridgeway, K. R., Dunn, J. R., & Wilkin, J. L. (2002). Ocean interpolation by four-dimensional weighted least squares application to the waters around Australasia. *Journal of Atmos Ocean Tech*, 19(9):1357-1375.

Rienecker, M. M., Suarez, M. J., Gelaro, R., Todling, R., Bacmeister, J., Liu, E., . . . da Silva, A. (2011). MERRA: NASA's Modern-Era Retrospective Analysis for Research and Applications. *Journal of Climate, 24*, 3624-3648.

Ries, J. C., Bettadpur, S., Poole, S., & Richter, T. (2011). *Mean Background Gravity Fields for GRACE Processing.* Austin.

Ries, J., Bettadpur, S., Eanes, R., Kang, Z., Ko, U., McCullough, C., Tapley, B. (2015). *The Combined Gravity Model GGM05C.* Potsdam: GFZ Data Services.

Rio, M. H., Mulet, S., & Picot, N. (2014). Beyond GOCE for the ocean circulation estimate: synergetic use of altimetry, gravimetry, and in situ data provides new insight into geostropic and Ekman currents. *Geophysical Research Letters*, 41(24):8918-8925.

Rizos, C. (2015). *Vertical Reference Frames in Practice: Time Dependence and Transformations.* Singapore: International Federation of Surveyors.

Rodell, M., Houser, P. R., Jambor, U., Gottschalck, J., Mitchell, K., Meng, C. J., . . . Toll, D. (2004). The Global Land Data Assimilation System. *Bull. Amer. Meteor. Soc., 85*(3), 381-394.

Rodolfo, K. (2014). On the geological hazards that threaten existing and proposed reclamations of Manila Bay. *Philippine Science Letters*, 7:228-240.

Roman, D. R., & Li, X. (2015). Dynamic heights in the Great Lakes using OPUS projects. *American Geophysical Union Fall Meeting 2015.* San Francisco.

Rudenko, S., Dettmering, D., Esselborn, S., Schöne, T., Förste, C., Lemoine, J.-M., . . . Neumayer, K.-H. (2014). Influence of time variable geopotential models on precise orbits of altimetry satellites, global and regional mean sea level trends. *Advances in Space Research*, 54(1):92-118.

Rummel, R., & Teunissen, P. (1988). Height datum definition, height datum connection and the role of the geodetic boundary value problem. *Bulletin Géodésique, 62*(4), 477-498.

Rummel, R., Gruber, T., Ihde, J., Liebsch, G., Rulke, A., Schafer, U., . . . Hughes, C. (2014). *Height System Unification with GOCE.* Munich: International Association of Geodesy.

Sanchez, L. (2006). Strategy to establish a global vertical reference system. *Geodetic Reference Frames: IAG Symposium 2006, 134*, 273-278.

Sánchez, L. (2007). Definition and realisation of the SIRGAS vertical reference system within a globally unified height system. *Dyn Planet Monit Underst Geod Oceanogr Tools*, 130:638-645.

Sánchez, L. (2013). Towards a vertical datum standardisation under the umbrella of Global Geodetic Observing System. *Journal of Geodetic Science*, 2(4):325-342.

Sánchez, L., & Sideris, M. (2017). Vertical datum unification for the International Height Reference System (IHRS). *Geophysical Journal International, 209*, 570-586.

Sánchez, L., Cunderlík, R., Dayoub, N., Mikula, K., Minarechová, Z., Síma, Z., Vojísková, M. (2016). A conventional value for the geoid reference potential W0. *Journal of Geodesy, 90*(9), 815-835.

Sánchez, L., Denker, H., Pail, R., Lieb, V., Huang, J., Roman, D., Luz, R. (2017). A first approximation to the International Height Reference Frame (IHRF). *Proceedings of the Joint Scientific Assembly of the International Association of Geodesy and the International Association of Seismology and Physics of the Earth's Interior (IAG-IASPEI 2017).* Kobe.

Sansò F. (2018) The Analysis of the Geodetic Boundary Value Problem: State and Perspectives. In: Freeden W., Nashed M. (eds) *Handbook of Mathematical Geodesy. Geosystems Mathematics*. Birkhäuser, Cham

Sansò, F., & Usai, S. (1995). Height datum and local geodetic datums in the theory of geodetic boundary value problems. *Allgemeine Vermessung- Nachrichten, 102*(8-9), 343-355.

Sansó, F., & Venuti, G. (2002). The height datum/geodetic datum problem. *Geophysical Journal International, 149*(3), 768-775.

Santos, M., Vaníček, P., Featherstone, W. E., Kingdon, R., Ellmann, A., & Martin, B. A. (2006). The relation between rigorous and Helmert's definition of orthometric heights. *Journal of Geodesy, 80*(12), 691-704.

Sarmiento, C. J., & Paringit, E. C. (2013). A watershed characterization method for hydrological simulations. *Proceedings of the 34th Asian Conference on Remote Sensing.* Bali.

Sarmiento, C. J., Castro, P. P., & Gonzalez, R. M. (2012). Remote Sensing and GIS in Inflow Estimation for Reservoir Operations: Magat Dam, Philippines. *Remote Sensing and Hydrology*, 325-328.

Sarmiento, C. J., Gonzalez, R. M., Castro, P. P., & Ayson, R. V. (2010). Remote Sensing and GIS in inflow estimation: the Magat Reservoir, Philippines experience (RSAP-092). *100 Years ISPRS: Advancing Remote Sensing Science*, 227-232.

Sarmiento, C. J., Macapinlac, O. T., Sempio, J. N., & Simbulan, G. (2013). Development and implementation of a web-based GIS tool for the Pasig river system management. *Proceedings of the 12th Southeast Asian Survey Congress: Geospatial Cooperation Towards a Sustainable Future.* Manila.

Sarmiento, C. J., Paringit, E. C., Balicanta, L. P., & Cruz, C. (2014). *DREAM Data Acquisition Component Manual.* Quezon City: UP Training Center for Applied Geodesy and Phogrammetry.

Sarmiento, C. J., Rizos, C., & Roberts, C. A. (2018). Time-variable satellite gravity models application for the development of an archipelagic geoid-based height system. *Proceedings of the 2018 IEEE 14th International Colloquium on Signal Processing & Its Applications (CSPA)*.

Sarmiento, C. J., Sempio, J. N., & Paringit, E. C. (2013). Geomatics in hydrological simulations: the Iligan experience . *Proceedings of the 2nd Philippine Geomatics Symposium.* Manila.

Sasgen, I., Martinez, Z., & Fleming, K. (2007). Wiener optimal filtering of GRACE data. *Stud. Geophys. Geod., 50*(4), 499-508.

Save, H., Bettadpur, S., & Tapley, B. D. (2016). High resolution CSR GRACE RL05 mascons. *J. Geophys. Res. Solid Earth*, 121.

Saxena, S. (2016, 2 20). *Ocean levels in the Philippines rising at 5 times the global average*. Retrieved 3 29, 2019, from https://arstechnica.com/science/2016/02/ocean-levels-in-the-philippines-rising-at-five-times-the-global-average/

Schall, J., Eicker, A., & Kusche, J. (2014). The ITG-Goce02 gravity field model from GOCE orbit and gradiometer data based on the short arc approach. *Journal of Geodesy*, 88(4):403-409.

Scharroo, R., Leuliette, E. W., Lillibridge, J. L., Byrne, D., Naeije, M. C., & Mitchum, G. T. (2012). RADS: Consistent multi-mission products. *Proc. of the Symposium on 20 Years of Progress in Radar Altimetry* (pp. SP-710). Venice: Eur. Space Agency Spec. Publ.

Scherneck, H. G. (1991). A parametrized solid Earth tide mode and ocean loading effects for global geodetic base-line measurements. *Geophys. J. Int*, 106(3):677-694.

Schowengerdt, R. (2007). *Remote Sensing: Models and Methods for Image Processing.* Oxford: Elsevier.

Schrama, E. J., & Visser, P. N. (2007). Accuracy assessment of the monthly GRACE geoids based upon a simulation. *Journal of Geodesy, 81*, 67-80.

Schrama, E. J., Wouters, B., & Lavallée, D. A. (2007). Signal and noise in Gravity Recovery and Climate Experiment (GRACE) observed surface mass variations. *Journal of Geophysical Reserch, 112*(B8).

Sempio, J. N., Sarmiento, C. J., & Paringit, E. C. (2013). he effects of the changing landscape along the Mandulog River to lowland flood risk. *roceedings of the 2nd Philippine Geomatics Symposium.* Manila.

Seo, K. W., Wilson, C. R., Famiglietti, J. S., Chen, J. L., & Rodell, M. (2006). Terrestrial water mass load changes from Gravity Recovery and Climate Experiment (GRACE). *Water Resources Research, 42*(W05417).

Smith, O. (2017, August 22). *Britain most coastline than Brazil - but which country has the most seaside?* (The Telegraph) Retrieved June 25, 2018, from https://www.telegraph.co.uk/travel/maps-and-graphics/countries-with-longest-coastlines/

Somigliana, C. (1929). Teoria Generale del Campo Gravitazionale Dell'ellisoide di Rotazione. *Memorie della Societ Astronomia Italiana, 4*(425).

Somigliana, C. (1930). Sul campo gravitazionale esterno del geoide ellisoidico. *Atti. Accad. Nazl. Lincei, Rend., Classe Sci. Fis. Mat. Nat.*, 5(11): 237-243.

Sośnica, K. (2014). *Determination of Precise Satellite Orbits and Geodetic Parameters using Satellite Laser Ranging.* Bern: University of Bern.

Steven, M. D., & Clark, J. A. (2013). *Applications of Remote Sensing in Agriculture.* Nottingham: Elsevier.

Stokes, G. G., 1849. *On the variation of gravity at the surface of the Earth*. Translations of Cambridge Phil. Sco. 8; Coll. Works, 2, Cambridge.

Taniguchi, M. (2012). *Subsurface Hydrological Responses to Land Cover and Land Use Changes.* Nara: Springer Science & Business Media.

Tapley, B. D., Bettadpur, S., Watkins, M., & Reigber, C. (2004). The gravity recovery and climate experiment: Mission overview and early results. *Geophysical Research Letters*, 31(9).

Tapley, B. D., Chambers, D. P., Bettadpur, S., & Ries, J. C. (2003). Large scale ocean circulation from the GRACE GGM01 Geoid. *Geophysical Research Letters*, 20(22).

Tapley, B. D., Flechtner, F., Bettadpur, S., & Watkins, M. M. (2013). The status and future prospect for GRACE after the first decade. *Eos Trans., Vol Fall Meet. Suppl*.

Tapley, B., Ries, J., Bettadpur, S., Chambers, D., Cheng, M., Condi, F., Wang, F. (2005). GGM02 - An improved Earth gravity field model from GRACE. *Journal of Geodesy*.

Tenzer, R., Vaníček, P., Santos, M., Featherstone, W. E., & Kuhn, M. (2005). The rigorous determination of orthometric heights. *Journal of Geodesy*, 79(2005):82-92.

Tenzer, R., Vatrt, V., Abdalla, A., & Dayoub, N. (2011). Assessment of the LVD offsets for the normal-orthometric heights and different permanent tide systems—a case study of New Zealand. *Applied Geomatics, 3*, 1-8.

Teunissen, P., & Mentenbruck, O. (2017). *Springer Handbook of Global Navigation Satellite Systems.* Cham: Springer Nature.

Thomson, D. B. (1978). *Introduction to Geodetic Astronomy.* New Brunswick: Unniversity of New Brunswick.

Tiangco, P., & Papa, L. (2006). *PCGIAP-Data Integration Philippine Country Report.* Taguig: National Mapping and Resource Information Authority.

Tocho, C., & Vergos, G. S. (2015). Estimation of the geopotential value W0 for the local vertical datum of Argentina using EGM2008 and GPS/levelling data. *IAG 150 years*, 271-279.

Torge, W. (2001). *Geodesy.* Berlin: Walter de Gruyter.

Torge, W., & Müller, J. (2012). *Geodesy.* Hannover, Germany: De Gruyter.

Tregoning, P., Watson, C., Ramillien, G., McQueen, H., & Zhang, J. (2009). Detecting hydrologic deformation using GRACE and GPS. *Geophysical Research Letters*, 36:L15401.

Tscherning, C. C., Forsberg, R., & Knudsen, P. (1992). The GRAVSOFT package for geoid determination. *Continued Workshop on the European Geoid.*

UNAVCO. (2014, March 3). *Borehole Strainmeters*. (UNAVCO) Retrieved March 31, 2019, from https://www.unavco.org/instrumentation/geophysical/borehole/bsm/bsm.html

United Nations Development Programme. (2015). *Project ReBUILD: Resilience Capacity Building for Cities and Municipalities to Reduce Disaster Risks from Climate Change and Natural Hazards (Phase 1)*. (UNDP Philippines) Retrieved March 31, 2019, from http://www.ph.undp.org/content/philippines/en/home/operations/projects/environment_and_energy/Project-ReBUILD.html

United Nations Economic and Social Commission for Asia and the Pacific. (2009). Country Report on Surveying and Mapping in the Philippines. *18th United Nations Regional Cartographic Conference for Asia and the Pacific.* Bangkok.

United States Geological Survey. (1999). *Energy Resources Program*. (USGS) Retrieved September 10, 2018, from https://energy.usgs.gov/OilGas/AssessmentsData/WorldPetroleumAssessment/WorldGeologicMaps.aspx#pacific_gis

UP Resilience Institute. (2019, February 19). *Nationwide Operational Assessment of Hazards (NOAH)*. (UP NOAH) Retrieved February 19, 2019, from http://noah.up.edu.ph/#/

UP Risk Institute. (2019, February 19). *Nationwide Operational Assessment of Hazards (NOAH)*. (UP NOAH) Retrieved February 19, 2019, from http://noah.up.edu.ph/#/

UP Training Center for Applied Geodesy and Photogrammetry. (2009). *Assessment of the PRS92 Geodetic Control Network and Development of Recommended Guidelines for Primary Geodetic Control, Tidal and Geopotential Surveys.* Quezon City: UP TCAGP.

UP Training Center for Applied Geodesy and Photogrammetry. (2009). *Validation of Global Geopotential Model (GGM)-Derived Geoidal Heights.* Quezon City: UP TCAGP.

UP Training Center for Applied Geodesy and Photogrammetry. (2013). *DREAM and Phil-LiDAR 1*. (DOST) Retrieved March 31, 2019, from https://dream.upd.edu.ph/about/phil-lidar-1/

van Dam, T., & Ray, R. (2010, October). *S1 and S2 Atmospheric Tide Loading Effects for Geodetic Applications*. Retrieved from S1 and S2 Atmospheric Tide Loading Calculator: https://geophy.uni.lu/atmosphere/tide-loading-calculator/

van Dam, T., & Wahr, J. (1987). Displacements of the Earth's surface due to atmospheric loading: Effects on Gravity and Baseline Measurements. *J. Geophys. Res*, 92:1281-1286.

van Dam, T., Collilieux, X., & Wuite, J. (2012). Nontidal ocean loading: amplitudes and potential effects in GPS height time series. *Journal of Geodesy*, 86:1043–1057.

van Gysen, H., & Coleman, R. (1997). On the satellite altimeter crossover problem. *Journal of Geodesy*, 71(2):83–96.

Vaníček, P. (1976). *Physical Geodesy.* New Brunswick: University of New Brunswick.

Vanícék, P., & Krakiwsky, E. J. (1986). *Geodesy, The Concepts.* North Holland: Elsevier.

Vaníček, P., Huang, J., Novák, P., Pagiatakis, S., Véronneau, M., & Martinec, Z. (1999). Determination of the boundary values for the Stokes-Helmert problem. *Journal of Geodesy, 73*(4), 180-192.

Vaníček, P., Novák, P., & Martinek, Z. (2000). Geoid, topography and the Bouguer plate or shell. *Journal of Geodesy, 2001*(75), 210-215.

Vergos, G. S., Grigoriadis, V. N., Tziavos, I. N., & Kotsakis, C. (2014). Evaluation of GOCE/GRACE global geopotential models over Greece with collocated GPS/Levelling observations and local gravity data. *IAG Symposia Series, 141*, 85-92.

Vermeer, M. (2003). The Elusive Stationary Geoid. *Space Science Reviews, 108*, 283-292.

Véronneau, M., & Huang, J. (2016). The Canadian Geodetic Vertical Datum of 2013 (CGVD2013). *GEOMATICA, 70*(1), 9-19.

Vianna, M. L., Menezes, V. V., & Chambers, D. P. (2007). A high resolution satellite-only GRACE-based mean dynamic topography of the South Atlantic Ocean. *Geophysical Research Letters*, 34(24).

Wahr, J., Molenaar, M., & Bryan, F. (1998). Time variability of the Earth's gravity field: Hydrology and oceanic effects and their possible detection using GRACE. *Journal of Geophysical Research, 103*(B12), 30,205-30,229.

Wang, Y. (2001). GSFC00 mean sea surface, gravity anomaly, and vertical gravity gradient from satellite altimeter data. *J. Geophys. Res.*, 106(31):167–174.

Wang Y.M. (2016) Geodetic Boundary Value Problems. *In: Grafarend E. (eds) Encyclopedia of Geodesy*. Springer, Cham

Watkins, M. M., & Eanes, R. J. (1997). Observations of tidally coherent diurnal and semidiurnal variations in the geocenter. *Geophysical Research Letters*, 24(17):2231-2234.

Watkins, M., Yuan, D., Kuang, D., Bertiger, W., Kim, M., & Kruizinga, G. (2005). GRACE harmonic and mascon solutions at JPL. *AGU Fall Meeting Abstracts.* American Geophysical Union.

Weigelt, M., van Dam, T., Jäggi, A., Prange, L., Tourian, M. J., Keller, W., & Sneeuw, N. (2013). Time-variable gravity signal in Greenland revealed by high-low satellite-to-satellite tracking. *Journal of Geophysical Research*, 118(7):3848-3859.

Wells, J. T., & Coleman, J. M. (1981). Periodic mudflat progradation, northeastern coast of South America: a hypothesis. *Journal of Sedimentary Research*, 51(4):1069–1075.

Werth, S., Güntner, A., Schmidt, R., & Kusche, J. (2009). Evaluation of GRACE filter tools from a hydrological perspective. *Geophysical Journal International, 179*(3), 1499-1515.

Widerhold, P. R. (1997). *Water Vapor Measurement.* Florida: CRC Press.

Williams, S. D., & Penna, N. T. (2011). Non-tidal ocean loading effects on geodetic GPS heights. *Geophysical Research Letters*, 38(9).

Wohl, E., Barros, A., Brunsell, N., Chappell, N. A., Coe, M., Giambelluca, T., . . . Ogden, F. (2012). The hydrology of the humid tropics. *Nature Climate Change, 2*(2012), 655-662.

Woodworth, P. L., Gravelle, M., Marcos, M., Wöppelman, G., & Hughes, C. (2015). The status of measurement of the Mediterranean mean dynamic topography by geodetic techniques. *Journal of Geodesy*, 89(8):811-827.

Woodworth, P. L., Hughes, C. W., Bingham, R. J., & Gruber, T. (2012). Towards worldwide height system unification using ocean information. *Journal of Geodetic Science*, 2(4):302-318.

Wu, X., Ray, J., & van Dam, T. (2012). Geocenter motion and its geodetic and geophysical implications. *Journal of Geodynamics*, 2012(58):44–61.

Wunsch, C., Iskandarani, M., Haidvogel, D., & Hughes, R. (1997). Dynamics of the long-period tides. *Progress in Oceanography, 40*, 81-108.

Xu, P., & Rummel, R. (1991). A quality investigation of global vertical datum connection. In *Publications on Geodesy 34,.* Delft, The Netherlands: Netherlands Geodetic Commission.

Yi, W., Rummel, R., & Gruber, T. (2013). Gravity field contribution analysis of GOCE gravitational gradient components. *Studia Geophysica et Geodaetica*, 57(2):174-202.

Zhou, H., Luo, Z., Zhou, Z., Li, Q., Zhong, B., & Hsu, H. (2016). *A new time series of GRACE monthly gravity field models: HUST-Grace2016.* Potsdam: GFZ Data Services.

Ziebart, M., Iliffe, J., Cross, P., Forsberg, R., Strykowski, G., & Tscherning, C. (2004). Great Britain's GPS height corrector surface. *Proceedings of the ION GNSS* (pp. 203-210). Institute of Navigation.